UNIVERSIDAD DE LA RIOJA

TESIS DOCTORAL

Título
Design, Synthesis, Photochemical and Biological Evaluation of Novel Photoactive Molecular Switches
Autor/es
David Martínez López
Director/es
Diego Sampedro Ruiz y Pedro José Campos García
Facultad
Facultad de Ciencia y Tecnología
Titulación
Departamento
Química
Curso Académico

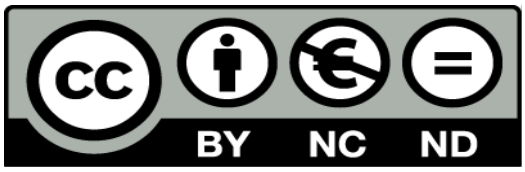

publicaciones.unirioja.es
E-mail: publicaciones@unirioja.es

UNIVERSIDAD DE LA RIOJA

Facultad de Ciencia y Tecnología

Departamento de Química

Área de Química Orgánica

Grupo de Fotoquímica Orgánica

TESIS DOCTORAL

DESIGN, SYNTHESIS, PHOTOCHEMICAL AND BIOLOGICAL EVALUATION OF NOVEL PHOTOACTIVE MOLECULAR SWITCHES

Memoria presentada en la Universidad de La Rioja
para optar al grado de Doctor en Química por:

David Martínez López

Junio 2019

Facultad de Ciencia y Tecnología

Departamento de Química

Área de Química Orgánica

Grupo de Fotoquímica Orgánica

D. DIEGO SAMPEDRO RUIZ, Profesor Titular de Química Orgánica del Departamento de Química de la Universidad de La Rioja,

y D. PEDRO JOSÉ CAMPOS GARCÍA, Catedrático de Química Orgánica del Departamento de Química de la Universidad de La Rioja.

CERTIFICAN:

Que la presente memoria, titulada "Design, synthesis, photochemical and biological evaluation of novel photoactive molecular switches", ha sido realizada en el Departamento de Química de La Universidad de La Rioja bajo su dirección por el Licenciado en Química D. DAVID MARTÍNEZ LÓPEZ y autorizan su presentación para que sea calificada como Tesis Doctoral.

Logroño, Junio de 2019

Fdo. Diego Sampedro Ruiz

Fdo. Pedro J. Campos García

Finalmente una etapa acaba, en la que hace unos años ni me imaginaba que pudiera ni siquiera empezar. Por ello, en primer lugar me gustaría agradecer a mis directores de tesis, **Diego** y **Pedro** por haberme dado una gran acogida en el grupo de investigación desde el principio, así como por el apoyo que me han brindado en los buenos y malos momentos, además del esfuerzo que han aportado para la realización de esta memoria.

A **Miguel Ángel**, además de uno de mis jefes, un amigo más con el que he compartido alegrías, penas y alguna que otra cerveza… Por todo ello, una persona imprescindible que la tesis ha puesto en mi vida y de la cual quiero seguir aprendiendo por mucho tiempo.

De la misma manera, para que una tesis sea más fácil de llevar, es imprescindible que en este largo camino se tengan tan buenos compañeros de laboratorio como los míos. En este caso, agradecer a **Raúl** tanto por los buenos momentos, como por el apoyo técnico siempre que he necesitado. A **Elena** y **Eduardo** por hacerme más ameno el día a día, sobre todo en los que lo veía todo negro y siempre al final, me sacaban una sonrisa. También agradecer a **Cris** (mi calculadora), sin la que hubiera sido imposible realizar esta tesis doctoral, pero reconocerle sobre todo su amabilidad en todo momento. Tampoco me quiero olvidar de los antiguos compañeros, en especial de **Marina** ya que fue la que me enseñó a desenvolverme en el laboratorio, aunque el primer día la mojé entera.

Qué decir de los quibi-buitres, gracias a todos ellos (**Iris A., Ismael, Xhenti, Paula, Malicia, Pablo, Claudio y Nuria**) por los ratos divertidos en el laboratorio, y sobre todo por los viernes de pinchopote. A pesar de estar en el otro lado de la química, también he tenido buenos compañeros inorgánicos (**Mattia, María G., María R., Quinti, Mónica, Raquel, Patri, Manso y Jesús**) gracias a todos ellos por los jueves de "Impass" que hemos pasado juntos.

No me puedo olvidar de ninguna manera del PAS, en especial de **Nines** por todas las conversaciones y risas que hemos tenido en el masas durante tantos años.

También agradecer a todos **mis amigos** por hacerme siempre desconectar, y a la vez interesarse por mis experimentos. Dedicar también un agradecimiento especial a **Patri** por realizar la portada de esta Tesis Doctoral.

I am really grateful to **Prof. Andrew Woolley** for allowing me be part of his lab team for 4 months. He provided me all the support needed to carry out my research work.

Moreover, I would like to flag his kindness at all times with any member of his group, creating an excellent working atmosphere.

Also, I would like to thank **Debbie** and **June** for checking the grammar of this thesis.

Aparte de toda la gente que he conocido durante la realización de este trabajo, debo de agradecer **a mis padres y mi hermana** por todo el apoyo, ánimo y cariño que me han dado durante tantos años (no solo los de la tesis) siendo imprescindibles y necesarios para convertirme en la persona que soy hoy en día.

Por último y no menos importante, agradecer a **Nora** por estar todos los días a mi lado compartiendo este camino que iniciamos ya hace unos cuantos años juntos. No se me ocurre mejor compañera para compartir mi vida.

En último lugar, agradecer a las entidades financiadores por el apoyo económico prestado para la realización de este trabajo. En especial, me gustaría agradecer a la **Universidad de La Rioja** por el contrato predoctoral FPI-UR y las ayudas a tesis doctorales (ATUR), así como al **Ministerio de Ciencia e Innovación** por los proyectos CTQ2011-24800, CTQ2014-59650-P y CTQ2017-87372-P.

ABSTRACT

This doctoral thesis is mainly focused on the study of new families of molecular switches based on *E*/*Z* isomerism. Specifically, it is evaluated their photophysical and photochemical properties, and how they can be tuned by slight modifications in their structure.

This thesis is divided into different chapters. First, a brief introduction is presented, which deals with a short overview of the history of photochemistry, followed by the explanation of some fundamental basis about photochemistry, which will be applied throughout this thesis.

In the second chapter, the most important types of molecular switches that have been developed up until now are introduced. Moreover, it is presented how light has been applied in biological systems to activate or deactivate a specific biological function. Then, the objectives of this work (Chapter 3) are described.

In Chapter 4, it is studied a new family of molecular photoswitches based on arylidene-hydantoins together with their synthesis, photochemical and photophysical studies. Moreover, their irradiation using different sources to check the effect on the photostationary state is commented. Furthermore, the experimental data obtained are explained by a careful computational study.

In Chapter 5, the study of new derivatives based on PSB-retinal is presented. Moreover, it is compared the photoswitching process of this family of switches by means of different electronic states (singlet or triplet state). Furthermore, it is explored how through a slight modification, it is possible to change some relevant chemical properties such as the water solubility and the absorption wavelength. Moreover, it is described the attachment of a photoswitch to a more complex system, such as a peptide. The photochemical study of the cross-linked peptide is performed, as well as how its biological activity changes after the irradiation.

In Chapter 6 it is described the synthesis, photochemical properties and cytotoxic evaluation of a novel family of photoactive molecules based on metronidazole. Rational modifications are done to match the requirements needed to apply these derivatives in biological systems.

Finally, in Chapter 7 it is described the synthesis and study of new derivatives which belong to a new and almost unexplored family of molecular switches based on Donor and Acceptor Stenhouse Adducts (DASAs). Furthermore, a new strategy is proposed to red-shift the absorption wavelength of these new derivatives.

RESUMEN

Esta tesis doctoral se centra en el estudio de nuevas familias de interruptores moleculares basados en isomería *E*/*Z*. En concreto, se han estudiado sus propiedades fotofísicas y fotoquímicas, además de cómo se pueden ajustar mediante pequeñas modificaciones en la estructura.

Esta tesis se divide en distintos capítulos. Primero, se presenta una introducción que empieza con un breve resumen de la historia de la fotoquímica, seguido de la explicación de algunos aspectos fundamentales que se emplearán a lo largo de esta tesis.

En el segundo capítulo, se detallan los distintos tipos de interruptores moleculares más importantes y que han sido estudiados hasta ahora. Además, se presenta como se puede utilizar la luz en sistemas biológicos para activar o desactivar una determinada función. A continuación, se centran los objetivos de este trabajo.

En el cuarto capítulo, se describe una nueva familia de interruptores moleculares basados en la hidantoína, así como su síntesis y propiedades fotoquímicas y fotofísicas. Al mismo tiempo, se muestra la irradiación de estos interruptores utilizando distintas fuentes de luz para comprobar como afecta al estado fotoestacionario. Finalmente, se analizarán los datos experimentales gracias a un minucioso estudio computacional.

En el quinto capítulo, se profundiza en el estudio de nuevos derivados basados en la base de Schiff protonada del retinal. Además, se compara la fotoisomerización de estos derivados a través de distintos estados electrónicos (singlete o triplete). Aparte de esto, se estudia como mediante una pequeña modificación en la estructura es posible cambiar las propiedades químicas y fotofísicas, como por ejemplo la solubilidad en agua o la longitud de onda de absorción. También, se realiza el anclaje de uno de estos interruptores en un sistema más complejo como es un péptido, realizando el estudio fotoquímico del sistema péptido-interruptor, así como el cambio en su actividad biológica una vez irradiado.

En el sexto capítulo, se describe la síntesis, las propiedades fotoquímicas, así como la citotoxicidad de una nueva familia de moléculas fotoactivas basadas en el metronidazol. Además, se realizan nuevas modificaciones en la estructura para aumentar su citotoxicidad y cumplir los requisitos necesarios para utilizar estos derivados en sistemas biológicos.

Para acabar, en el capítulo 7, se describe la síntesis y el estudio de nuevos derivados pertenecientes a una nueva y casi inexplorada familia de interruptores moleculares conocidos como *"Donor and Acceptor Stenhouse Adducts".* Además, se propone una nueva estrategia para desplazar al rojo la longitud de onda de absorción de estos derivados.

ABBREVIATIONS AND ACRONYMS

Å	angstrom
ATP	adenosine triphosphate
Boc	*tert*-butyloxycarbonil
BODIPY	boron-dipyrromethene
BR	Bacteriorhodopsin
BzDO	1,4-benzodioxane
^{13}C NMR	carbon nuclear magnetic resonance
ca.	approximately
CA-4	combretastatin A-4
CASSCF	complete active space -self-consistent field
CASPT2	complete active space-perturbation theory of second order
ChR	Channelrhodopsin
d	doublet (in NMR spectroscopy)
DASAs	Donor Acceptor Stenhouse Adducts
dd	doublet of doublets (in NMR spectroscopy)
DFT	density functional theory

DIEA	diisopropyl ethyl amine
DMF	dimethylformamide
DNA	Deoxyribonucleic acid
EDT	2-[2-(bis(carboxymethyl)amino)ethyl-(carboxymethyl)amino]ethanoic acid
E_T	triplet energy
M	molarity
max.	maximum
MS	mass spectrometry
Ep	moles of photons absorbed x cm^{-2} x s^{-1}
ES (+)	electrospray in positive ion mode
ESPT	excited-state proton transfer
eV	electron volt
f	oscillator strength
F (λ)	F factor
FC	Franck-Condon
FP	fluorenylidene-pyrroline
fs	femtosecond

GC/MS	gas chromatography/mass spectrometry
GFP	green fluorescent protein
HBTU	*O*-(Benzotriazol-1-yl)-*N*,*N*,*N'*,*N'*-tetramethyluronium hexafluorophosphate
^{1}H NMR	proton nuclear magnetic resonance
HPLC	High Performance Liquid Chromatography
HR	Halorhodopsin
Hz	hertz
hυ	light, photons, irradiation
IP	indanylidene-pyrroline
IR	infrared light
ISC	intersystem crossing
J	joule
kcal	kilocalories
LEDs	light-emitting diodes
M	molarity
MALDI	matriz-assisted laser desorption ionization
Me	methyl

MEP	minimum energy path
min.	minute
MLCT	metal ligand charge transfer
NAIP	*N*-alkylated indanylidene-pyrroline
NAFP	*N*-alkylated fluorenylidene-pyrroline
nm	nanometer (10^{-9} meters)
NMR	nuclear magnetic resonance
OD	Optical Density
PCM	Polarizable continuum model
PDT	Photodynamic therapy
Ph	Phenyl
ppm	parts-per-million
PSB	protonated Schiff base
PSS	photostationary state
q	quatriplet (in NMR spectroscopy)
ROS	reactive oxygen species
RT	room temperature
s	singlet (in NMR spectroscopy)

S_0	ground state
S_n	singlet excited state
t	triplet (in NMR spectroscopy)
T_n	triplet excited state
TCEP	tris(2-carboxyethyl)phosphine
td	triplet of doublets (in NMR spectrocopy)
TFA	trifluoroacetic acid
THF	tetrahydrofuran
TIS	triisopropyl silane
TLC	thin layer chromatography
Tris (buffer)	tris(hydroxymethyl)aminomethane
UV-Vis	ultraviolet-visible
Δ	heat; increase
δ	chemical shift
ε	molar extinction coefficient, molar absorptivity
λ	wavelength
Φ	quantum yield

1. Introduction.

1. Brief history of photochemistry.

It is known since ancient times that sunlight plays a key role in the life on Earth. The sun is the world´s largest energy provider, being the driving force of our life. Unfortunately, we do not know yet how to take full advantage of this endless source of energy,[1] although many efforts have been directed to face this challenge over the last decades.[2,3]

Sunlight is involved in many processes, photosynthesis being the most important one.[4] Through this process, different living organisms turn light into chemical energy (Scheme 1.1).[5] This energy is used by many organisms (plants, algae and many species of bacteria) to carry out their vital needs, allowing its survival over the years.

$$6\ CO_2\ (g) + 6\ H_2O\ (l) \xrightarrow{h\nu} C_6H_{12}O_6\ (s) + 6\ O_2\ (g)$$

Scheme 1.1. Photochemical reaction involved in photosynthesis.

All the photochemical changes that were observed prior 1817 such as photofading, photosynthesis or blackening of silver halides were rationalized qualitatively.[6] The quantitative approach of photochemistry went hand in hand with Grotthus and Draper in the beginning of the 19th century, when they stated the first law of photochemistry: *only that light which is absorbed by a system can cause chemical change.*[7]

Transformations caused by the exposure to light have attracted a great interest, but they were not explored until the 19th century due to the lack of experimental techniques. As an example, Trommsdorff explored the photoreaction of α-santonin crystals in 1834, which lead to a color change under the exposure to sunlight.[8] Moreover, the first attempts to relate the color of organic compounds to their structure date back to the mid-19th century, due to the importance of organic dyes in the chemical industry.

---

[1] Council, N. R., *The Sun to the Earth -- and Beyond: A Decadal Research Strategy in Solar and Space Physics*. The National Academies Press: Washington, DC, 2003; p 196.
[2] Hammarström, L., Overview: Capturing the Sun for Energy Production *AMBIO* **2012,** *41*, 103-107.
[3] Melis, A., Photosynthesis-to-fuels: from sunlight to hydrogen, isoprene, and botryococcene production *Energy Environ. Sci.* **2012,** *5*, 5531-5539.
[4] Esser, P.; Pohlmann, B.; Scharf, H.-D., The Photochemical Synthesis of Fine Chemicals with Sunlight *Angew. Chem. Int. Ed.* **1994,** *33*, 2009-2023.
[5] S. Singhal, G.; Renger, G.; Sopory, S.; Irrgang, K. D.; Govindjee, G., The Basic Photosynthetic Process. In *Concepts in Photobiology: Photosynthesis and Photomorphogenesis*, Kluwer Academic Publishers: Boston, 1999.
[6] Rohatgi-Mukherjee, K. K., Fundamentals of Photochemistry. John Wiley & Sons: New Delhi, 1978.
[7] Von Grotthuss, T., Auszug aus vier Abhandlungen Physikalisch-chemischen Inhalts *Annalen der Physik* **1819,** *61*, 50-74.
[8] Trommsdorff, H., Ueber Santonin *Ann. Pharm.* **1834,** *11*, 190-207.

After that time the photochemistry started to develop, increasing the studies in which light was used as reagent. For instance, the first photochemical kinetic study was developed by Bunsen and Roscoe in the 1850s. They studied the formation of hydrogen chloride from its components. Moreover, they also found that the progress of the reaction was proportional to the light intensity and time of irradiation.[9, 10]

Later, Giacomo Luigi Ciamician, who is known as the father of the modern photochemistry due to its relevant contribution reported his first articles on photochemistry, which were about the reduction of quinone to hydroquinone and the reduction of nitrobenzene.[11, 12] Moreover, he was aware of the necessity of using solar light instead of fossil fuels as a source of energy, a hundred years ago.[13]

In the context of this thesis, it should be remarked that the first geometric photoisomerization of olefins was reported by William Henry Perkin in 1881. He investigated the transformation of *trans*-2-hydroxycinnamic acid into its *cis*-isomer after exposure to sunlight (Figure 1.1).[14]

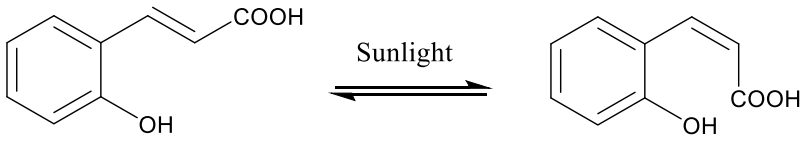

Figure 1.1. Photoisomerization process of *trans*-2-hydroxycinnamic acid.

Nowadays, organic photochemistry has turned into a powerful synthetic tool for organic chemist.[15,16] Due to the interaction between matter and light, it may be used to prepare different reaction products that could not be afforded by thermal activation.

Therefore, photochemistry could be defined as the branch of chemistry concerned with the chemical effects of light (from UV to far IR). Thus, light could be seen as an efficient way to apply energy into a molecular system.

---

[9] Bunsen, R.; Roscoe Henry, E.; Stokes George, G., XVII. Photo-chemical researches.—Part I. Measurement of the chemical action of light *Phil. Trans. R. Soc. Chem.* **1857,** *147*, 355-380.

[10] Bunsen Robert, W.; Roscoe Henry, E.; Stokes George, G., I. Photo-chemical researches.—Part II. Phenomena of photo-chemical induction *Proc. R. Soc.* **1857,** *8*, 326-330.

[11] Ciamician, G., Su una trasformazione del chinone in idrochinone *Gazz. Chim. Ital.* **1886,** *16*, 111-112.

[12] Ciamician, G., Sull'azione della luce solare sul nitroben-zol in soluzione *Gazz. Chim. Ital.* **1886,** *16*, 536-537.

[13] Ciamician, G., The Photochemistry of the Future *Science* **1912,** *36*, 385-394.

[14] Perkin, W. H., On the isomeric acids obtained from coumarin and the ethers of hydride of salicyl *J. Chem. Soc., Trans.* **1881,** *39*, 409-452.

[15] Albini, A.; Fagnoni, M., *Handbook of Synthetic Photochemistry*. Wiley-VCH: Weinheim, 2010.

[16] Hoffmann, N., Photochemical Reactions as Key Steps in Organic Synthesis *Chem. Rev.* **2008,** *108*, 1052-103.

In this thesis the interaction between an organic molecule and different types of light affording diverse reactivities, depending on the chromophore under study, will be described.

2. Physical basis.

2.1. Electromagnetic radiation.

The electromagnetic spectrum is divided into different regions, which correspond to different energies. In Figure 1.2, it is shown that the electromagnetic spectrum covers a wide range, since it comprises from radio waves to gamma radiation. However, the radiation used in photochemistry to carry out any type of reaction involves a very small region of the electromagnetic spectrum, which goes from 200 to 700 nm. This part of the spectrum is further divided into different regions: ultraviolet (10-400 nm) and visible light (400-700 nm). This last range is usually desirable for photobiological purposes because it is not harmful to living organisms, and it penetrates deeper into human body than UV-light (Figure 1.2).

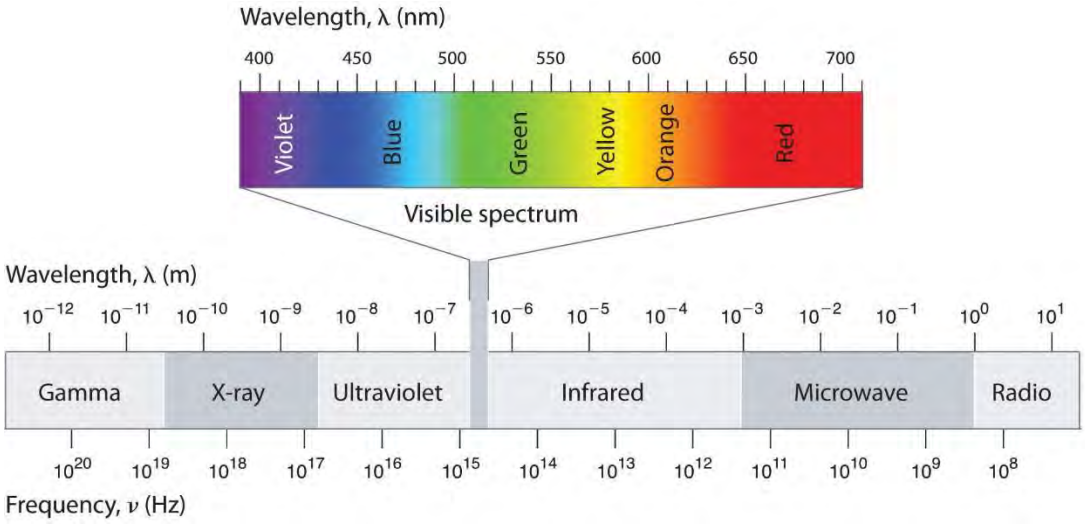

Figure 1.2. Electromagnetic spectrum, highlighting the useful region in photochemistry.[17]

Photochemistry was deeply developed when modern physics established that light was irradiated in discrete quanta, called photons, which had an energy proportional to the frequency of the light. This energy was quantified by Max Planck in 1900, when he discovered the Planck´s constant, being fundamental to quantify the energy of a photon (Equation 1.1).[18]

$$E = \frac{hc}{\lambda}$$

Equation 1.1

[17] https://chem.libretexts.org/
[18] Planck, M., *The theory of heat radiation*. P. Blakiston's Son & Co: Philadelphia, 1914.

Where h is the Planck´s constant, c the speed of light and λ the light wavelength.

Then, in the period of 1908-1913, Johannes Stark and Albert Einstein, independently, formulated the second law of photochemistry: *For every quantum of light that is absorbed, one molecule of substrate reacts*.

2.2. Franck-Condon principle.

When a molecule is excited by the absorption of one photon from its ground state, a vertical transition occurs to get an upper energy level. This electron movement takes place very fast, so the nuclei has not enough time to be rearranged due to its larger mass. Therefore, it is assumed that the structure is fixed during the transition (Figure 1.3).[19]

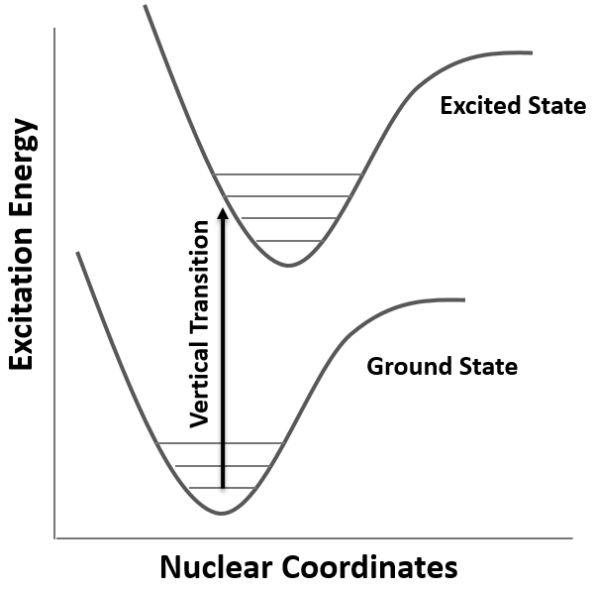

Figure 1.3. Representation of Franck-Condon transition.[20]

So, this principle states that an electronic transition is most likely to occur without changes in the positions of the nuclei in the molecular entity and its environment. The resulting state is called a Franck–Condon state, and the transition involved, a vertical transition.[21]

[19] Mustroph, H., Potential-Energy Surfaces, the Born–Oppenheimer Approximations, and the Franck–Condon Principle: Back to the Roots *ChemPhysChem* **2016,** *17*, 2616-2629.
[20] García-Iriepa, C. Design, Synthesis and Computational Study of Photoactive Molecular Devices. PhD. Thesis, University of Alcalá de Henares, Madrid, 2016.
[21] McNaught, A. D.; Wilkinson, A., *IUPAC compendium of chemical terminology*. Blackwell: Oxford, 1997.

2.2.1. Nature of electronic transitions in organic compounds.

In organic molecules, there are two main types of electronic transitions depending on the character of the orbital in which the electron involved in the process is placed.

- n-π^* transition occurs in organic molecules which present heteroatoms with unshared pair electrons in its structure.
- π-π^* transition occurs when an electron situated in the π bonding orbital of the molecule is involved in the excitation. This transition takes place in unsaturated compounds such as aromatic compounds, alkenes or carbonyl compounds among others.

The nature of both transitions is completely different, since the π-π^* allowed transition is more probable to happen, so it has a bigger oscillator strength (*f*). In contrast, the n-π^* transition is "forbidden" by symmetry considerations, thus the intensity of this band is much lower.

2.3. Excitation pathways.

The excitation of a molecule is based on the electronic transition from its ground state (S_0) to an upper energy level (S_n). When the molecule is in its ground state, it shows some specific properties such as bond length, energy content or charge distribution. These properties are related to the electronic distribution present in the molecule. Therefore, when exciting a molecule to another state, the electronic distribution becomes different as well as its energy content and geometry.

The excitation of a molecule can be afforded by different ways, depending on the mechanism followed throughout the irradiation.

2.3.1. Direct irradiation.

The simplest way of generating an excited state is the absorption of a photon with the appropriate energy. This absorption promotes an electron from its ground state to an excited state through an allowed transition. It is required that the energy gap between both states and the energy of the photon absorbed to be equal.

In this process, one or more excited states can be populated through a S_0-S_n allowed transition, leading to different singlet states (no unpaired electrons, its overall spin quantum number is zero). One of those states is usually the responsible for the photoreaction, but through a non-radiative process called intersystem crossing (ISC), the triplet state (two unpaired electrons, its overall spin quantum number is one) can be also populated, which can lead to a different photoreactivity.

2.3.2. Indirect irradiation.

Other types of irradiations are based on getting a molecule in its excited state without absorbing light by itself. The main processes of indirect irradiation are based on the energy transfer photosensitization[22] and photoinduced electron transfer (Figure 1.4).[23] These processes have been widely used in organic chemistry, [24] but in this thesis, we will focus on the energy transfer photosensitization.

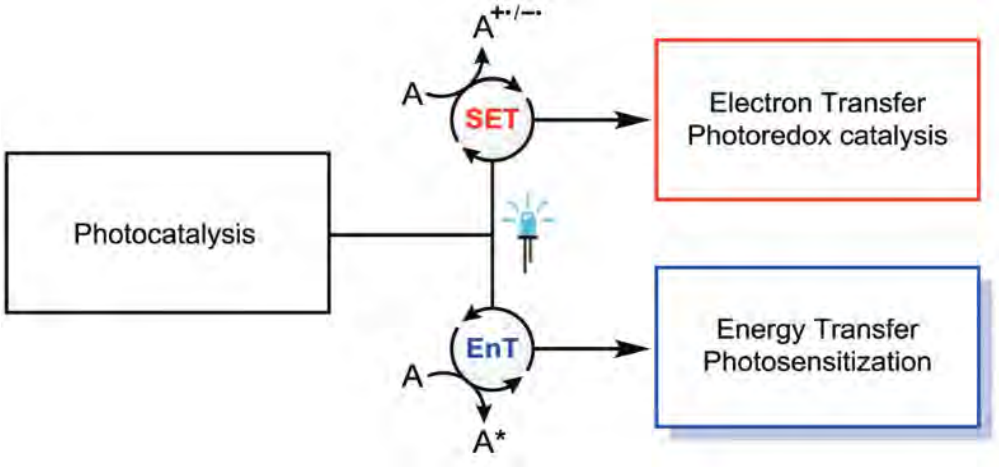

Figure 1.4. Representation of two possible indirect irradiations.[25]

2.3.2.1. Energy transfer photosensitization.

Photosensitization is the process whereby a photophysical or photochemical change occurs in one molecule as the result of light absorption of another.[26]

Most of the organic molecules present triplet states of high energy, but the ISC between the singlet (S_1) and the triplet state (T_1) is not favored due to its inefficient spin-orbit coupling, which entails the quantum yield of this processing being very low, preventing this process taking place. It is of great importance that sensitization is a well-used method in organic photochemistry to generate excited organic molecules in their corresponding triplet states.

[22] Zhao, J.; Wu, W.; Sun, J.; Guo, S., Triplet photosensitizers: from molecular design to applications *Chem. Soc. Rev.* **2013,** *42*, 5323-5351.
[23] Prier, C. K.; Rankic, D. A.; MacMillan, D. W. C., Visible Light Photoredox Catalysis with Transition Metal Complexes: Applications in Organic Synthesis *Chem. Rev.* **2013,** *113*, 5322-5363.
[24] Zhou, Q.-Q.; Zou, Y.-Q.; Lu, L.-Q.; Xiao, W.-J., Visible-Light-Induced Organic Photochemical Reactions through Energy-Transfer Pathways *Angew. Chem. Int. Ed.* **2019,** *58*, 1586-1604.
[25] Strieth-Kalthoff, F.; James, M. J.; Teders, M.; Pitzer, L.; Glorius, F., Energy transfer catalysis mediated by visible light: principles, applications, directions *Chem. Soc. Rev.* **2018,** *47*, 7190-7202.
[26] Wardle, B., *Principles and applications of photochemistry*. Wiley: Hoboken, N.J., 2009.

In these processes, the molecule under study is initially in its ground state and it reaches its excited triplet state [A*(T_1)] through an energy transfer from another molecule in its excited triplet state, called sensitizer [S*(T_1)] (Figure 1.5). Therefore, triplet-triplet energy transfer allows for the indirect production of molecules in the triplet, which are unable of being produced by direct irradiation. It should be noted that, through this methodology, only triplet states could be populated due to the conservation of the spin momentum, as the energy transfer takes place with spin conservation.

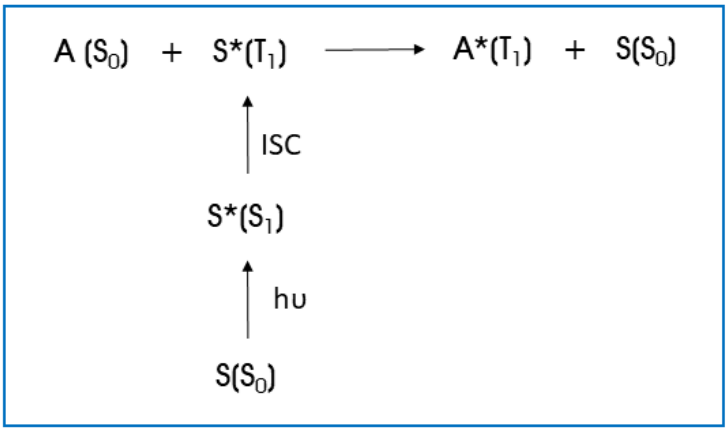

Figure 1.5. Schematic representation of a sensitized process.

The sensitizer must meet some requirements to carry out successfully a sensitized reaction, which are described below:

- The triplet energy of the sensitizer must be high enough to allow for the triplet-triplet energy transfer with the molecule. In case of being lower, the photoreaction will not take place.
- The lifetime of the triplet state of the sensitizer should be long enough to transfer the energy to the ground state reactant molecule.
- The ISC between the singlet and triplet state should be fast, in order to minimize the appearance of competitive deactivation process. The quantum yield of the ISC should be around 1 ($\Phi_{ISC}=1$). Ketones usually have a small gap between the singlet and triplet state, increasing the quantum yield of the ISC, this fact makes them usually good photosensitizers.
- It should be nonreactive towards the molecule under study to avoid undesired side reactions.

2.4. Relaxation decay.

After the absorption of one photon by a molecule, it leads to an excited state which can be deactivated by different processes. These processes can be categorized

in two types of relaxation processes depending on how the molecule returns to the ground state. These pathways are known as photophysical and photochemical processes.

2.4.1. Photophysical processes.

When a molecule is deactivated by photophysical processes, no changes will be found in the structure when it returns to the ground state. These pathways are well represented in the Jablonski diagram (Figure 1.6). They are further divided into radiative or non-radiative processes, depending on whether the emission of a photon takes place or not during the decay, respectively.

The radiative processes are based on the emission of a photon from different states. When the emission occurs from a singlet state, it leads to fluorescence. On the contrary, when the emission involves a triplet state, which has been formed through an intersystem crossing (ISC), phosphorescence takes place. It should be noted that both processes take place from the last vibrational state of the corresponding electronic level.

Furthermore, the non-radiative processes are based on the deactivation of an excited state through vibrational relaxation (VR) in the same excited state. Moreover, it can also take place between vibrational levels of different excited states whether their energy is similar, this process is known as internal conversion (IC).

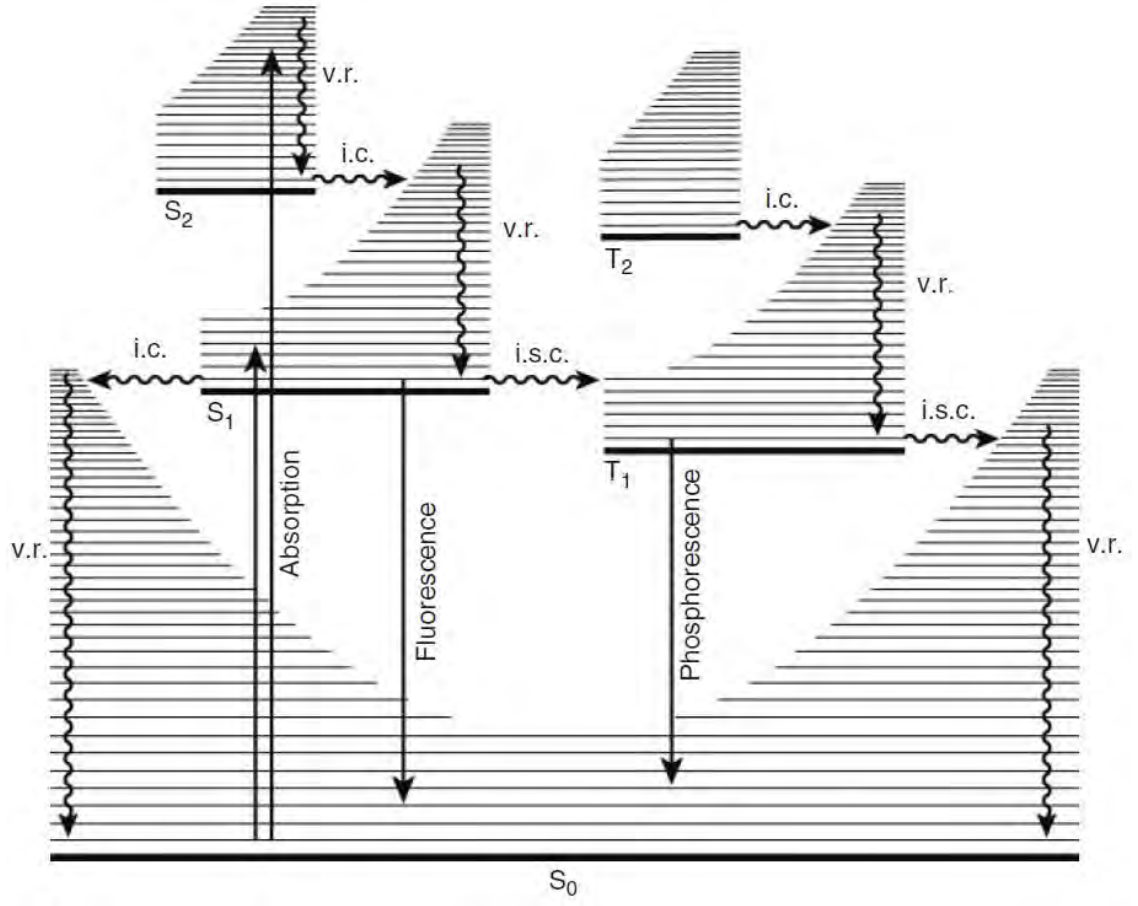

Figure 1.6. Jablonski diagram representation. [27]

2.4.2. Photochemical processes.

This pathway involves that the excited state can decay to the ground state by bringing forth a new molecule. Thus, photochemistry has turned into a powerful synthetic tool for organic chemists.[28]

Briefly, the photochemical reactions can be divided into different groups, depending on which type of transformation occurs, such as additions,[29] photocleavage,[30] photosubstitution[31] or *E*/*Z* isomerization.[32]

---

[27] Balzani, V.; Ceroni, P.; Juris, A., Light Absorption and Excited-State Deactivation. In *Photochemistry and photophysics : concepts, research, applications*, Wiley-VCH: Weinheim, Germany, 2014.
[28] See ref. 16.
[29] Anker Jørgensen, K., Cycloaddition Reactions in Organic Synthesis. 2001; Vol. 34, pp 301-327.
[30] Kellett, M. A.; Whitten, D. G., Electron-transfer photofragmentation reactions: analogies and divergences of the reactivity of ditertiary amines as compared with aminoalcohols *J. Am. Chem. Soc.* **1989,** *111*, 2314-2316.
[31] Mizuno, K., Photochemistry of aromatic compounds. In *Photochemistry: Volume 40*, The Royal Society of Chemistry: 2012; Vol. 40, pp 106-145.
[32] García-Iriepa, C.; Marazzi, M.; Frutos, L. M.; Sampedro, D., E/Z Photochemical switches: syntheses, properties and applications *RSC Adv.* **2013,** *3*, 6241-6266.

The isomerization of a double bond involves a change in its shape. When a double bond capable of isomerizing is irradiated it reaches an excited state in which its double bond losses the planarity. In fact, a twist close to 90° in its excited state is usually found. The excess of energy in the molecule is dissipated through rotation of the bond in the ground state. This rotation can take place in the same direction resulting in a new isomer, or go back, leading to the thermally stable isomer (Figure 1.7).

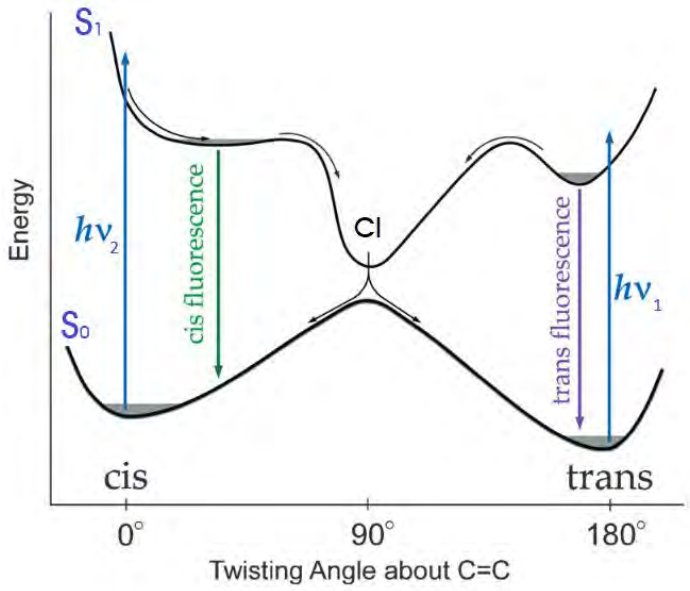

Figure 1.7. Potential energy surfaces of S_0 and S_1 involved in an *E*/*Z* photoisomerization.

In Figure 1.7 is shown a typical potential energy surface of a molecular switch based on *E*/*Z* isomerism. Throughout this thesis different chromophores will be explored as efficient photoswitches, and how their photophysical and photochemical properties can be easily modified by making slight changes in the structure. Moreover, the importance of the nature of the excited state which is involved in the photoreaction will be demonstrated.

2. Literature review.

1. Molecular machines.

A molecular machine could be defined as "*an assembly of a distinct number of molecular components that are designed to perform machine like movements (output) as a result of an appropriate external stimulation (input)*".[1] In other words, they turn any type of energy (depending on the input used) into mechanical forces and motions. Moreover, among all the possible inputs to make a molecular machine work, light energy is considered as the best input to operate these molecular machines.

There are many molecular machines in nature,[2] and specifically in our bodies, which are responsible for controlling many biological and essential functions such as the transportation of cations,[3] the synthesis of ATP,[4] or the muscle motion.[5]

During the last three decades, chemists have been inspired by nature to design and synthesize artificial molecular machines in order to emulate those which exist in the macroscopic world.[6,7] Due to the high relevance acquired by these systems in our society, three pioneers in the artificial molecular machines, Jean Pierre Sauvage,[8] Sir J. Fraser Stoddart,[9] and Ben L. Feringa[10] were awarded the 2016 Nobel Prize in Chemistry recognizing their achievements in this field.[11]

Currently, as it will be detailed in the next section, the molecular devices most studied are molecular switches. Throughout this thesis several substrates will be evaluated as efficient molecular switches. Therefore, it is expected to get an effective switching between both states being able to produce a reasonably ratio of each state, depending

[1] Balzani, V.; Credi, A.; Raymo, F. M.; Stoddart, J. F., Artificial Molecular Machines *Angew. Chem. Int. Ed.* **2000,** *39*, 3348-3391.
[2] Goodsell, D. S., *Our Molecular Nature: The Body's Motors, Machines and Messages* Springer-Verlag: New York, 1996.
[3] Subramaniam, S.; Henderson, R., Molecular mechanism of vectorial proton translocation by bacteriorhodopsin *Nature* **2000,** *406*, 653.
[4] Noji, H.; Yasuda, R.; Yoshida, M.; Kinosita, K., Direct observation of the rotation of F1-ATPase *Nature* **1997,** *386*, 299-302.
[5] Finer, J. T.; Simmons, R. M.; Spudich, J. A., Single myosin molecule mechanics: piconewton forces and nanometre steps *Nature* **1994,** *368*, 113-119.
[6] Erbas-Cakmak, S.; Leigh, D. A.; McTernan, C. T.; Nussbaumer, A. L., Artificial Molecular Machines *Chem. Rev.* **2015,** *115*, 10081-10206.
[7] Browne, W. R.; Feringa, B. L., Making molecular machines work *Nat. Nanotechnol.* **2006,** *1*, 25.
[8] Sauvage, J.-P., From Chemical Topology to Molecular Machines (Nobel Lecture) *Angew. Chem. Int. Ed.* **2017,** *56*, 11080-11093.
[9] Stoddart, J. F., Mechanically Interlocked Molecules (MIMs)—Molecular Shuttles, Switches, and Machines (Nobel Lecture) *Angew. Chem. Int. Ed.* **2017,** *56*, 11094-11125.
[10] Feringa, B. L., The Art of Building Small: From Molecular Switches to Motors (Nobel Lecture) *Angew. Chem. Int. Ed.* **2017,** *56*, 11060-11078.
[11] Leigh, D. A., Genesis of the Nanomachines: The 2016 Nobel Prize in Chemistry *Angew. Chem. Int. Ed.* **2016,** *55*, 14506-14508.

on the stimulus applied. For this purpose, the synthesis, characterization and photochemical study of different chromophores will be evaluated.

1.1. Molecular switches.

A molecular switch is a molecule that can be reversibly interchanged between at least two thermally stable states with the aid of an external stimulus. The conversion between different states could be controlled changing the input used. In Figure 2.1, it is represented schematically a simple molecular switch.

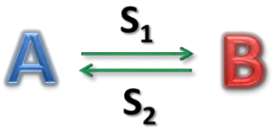

Figure 2.1. Schematic representation of a bistable molecular switch.

In the Figure above, a bistable system is shown in which A and B represent two different states. The interconversion between both states must occur only when the stimulus is present. Both states show different features, such as energy content and chemical and physical properties, since each state can represent totally different molecules. Therefore, it is essential to carry out a prior study to design a specific molecular switch, depending on which is the application to control.

1.2. How to activate a molecular switch.

Different stimuli can be applied to induce the molecular movements necessary to activate or deactivate a molecular switch. Therefore, they can be divided into different groups depending on the input used to control the process.

1.2.1. Electrochemical switches.

The switching of these molecules is controlled by applying different electric potentials which cause diverse oxidation/reduction reactions. Depending on the electric potential applied, the forward and back-reaction can take place. Therefore, these molecular switches show a reversible switching. They have been widely used, for instance, in supramolecular chemistry.[12, 13]

[12] Korybut-Daszkiewicz, B.; Więckowska, A.; Bilewicz, R.; Domagała, S.; Woźniak, K., An Electrochemically Controlled Molecular Shuttle *Angew. Chem. Int. Ed.* **2004,** *43*, 1668-1672.
[13] Kaifer, A.; Gómez-Kaifer, M., Electrochemical Switching. In *Supramolecular Electrochemistry*, WILEY-VCH: 2007.

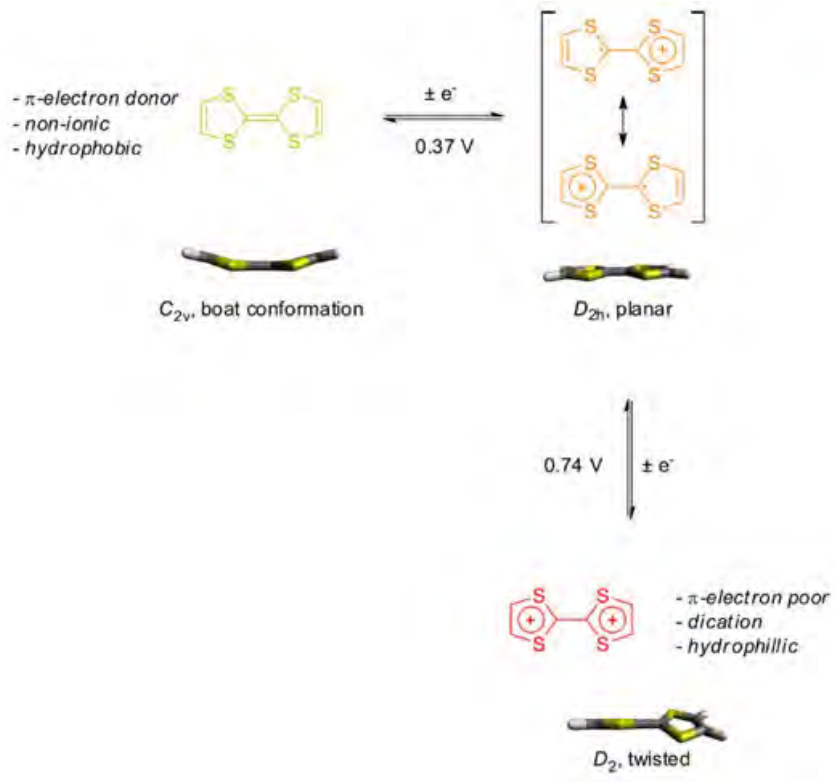

Figure 2.2. Electroswitching of a tetrathiafulvalene system. [14]

In Figure 2.2 a tetrathiafulvalene system is shown,[15] which might be the most popular redox system, due to the stability shown towards decomposition.[16] This feature is difficult to find in other electrochemical molecular switches.

1.2.2. Chemical switches.

These molecules are activated by the energy expelled in the reaction. Therefore, in each cycle it is necessary to add a new reagent to continue the process. For instance, a conformational change can be easily achieved by changing the pH of the medium (Figure 2.3).[17]

[14] Bissell, R. A.; Córdova, E.; Kaifer, A. E.; Stoddart, J. F., A chemically and electrochemically switchable molecular shuttle *Nature* **1994,** *369*, 133-137.
[15] Schröder, H. V.; Schalley, C. A., Tetrathiafulvalene – a redox-switchable building block to control motion in mechanically interlocked molecules *Beilstein J. Org. Chem.* **2018,** *14*, 2163-2185.
[16] Ashton, P. R.; Balzani, V.; Becher, J.; Credi, A.; Fyfe, M. C. T.; Mattersteig, G.; Menzer, S.; Nielsen, M. B.; Raymo, F. M.; Stoddart, J. F.; Venturi, M.; Williams, D. J., A Three-Pole Supramolecular Switch *J. Am. Chem. Soc.* **1999,** *121*, 3951-3957.
[17] Okamoto, I.; Terashima, M.; Masu, H.; Nabeta, M.; Ono, K.; Morita, N.; Katagiri, K.; Azumaya, I.; Tamura, O., Acid-induced conformational alteration of cis-preferential aromatic amides bearing N-methyl-N-(2-pyridyl) moiety *Tetrahedron* **2011,** *67*, 8536-8543.

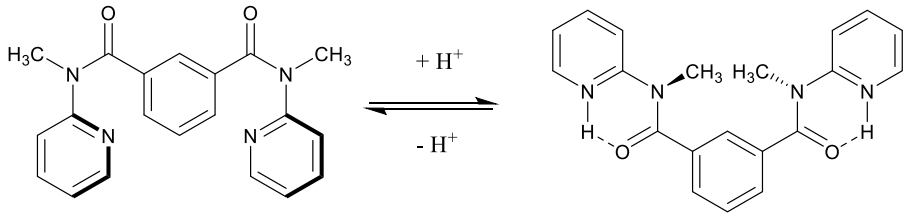

Figure 2.3. Chemical switch based on a conformational change induced by adding acid.[18]

These switches are well applied by nature to control many processes.[19] For instance, changing the pH can also lead to a conformational change in a substrate controlling the *trans*-membrane permeability.[20]

The main disadvantage of these synthetic molecular switches is the accumulation of side products due to the necessity of adding a new reagent in each cycle.[21] Nature has solved this problem by creating different secretion channels to expel the undesired products, avoiding the accumulation of toxic substances.

1.2.3. Photoswitches.

The input needed to activate these switches is the light. Therefore, when irradiating a photoswitch, it has to absorb light and it must lead to a photochemical reaction. But, as it was said in the introduction, other mechanisms could be used to activate a molecule photochemically without irradiating it directly. These mechanisms are based on single electron transfer and energy transfer (see introduction for further details).

1.2.3.1. Advantages of light.

Molecular switches activated by light have suffered a widespread in the last years in relation to other types of switches,[22, 23] due to the benefits offered by light. The main advantages of using light energy to activate these switches are:

[18] Okamoto, I.; Nabeta, M.; Minami, T.; Nakashima, A.; Morita, N.; Takeya, T.; Masu, H.; Azumaya, I.; Tamura, O., Acid-induced conformational switching of aromatic N-methyl-N-(2-pyridyl)amides *Tetrahedron Lett.* **2007,** *48*, 573-577.
[19] Knipe, P. C.; Thompson, S.; Hamilton, A. D., Ion-mediated conformational switches *Chem. Sci.* **2015,** *6*, 1630-1639.
[20] Hu, F.; Luo, W.; Hong, M., Mechanisms of Proton Conduction and Gating in Influenza M2 Proton Channels from Solid-State NMR *Science* **2010,** *330*, 505.
[21] Tatum, L. A.; Foy, J. T.; Aprahamian, I., Waste Management of Chemically Activated Switches: Using a Photoacid To Eliminate Accumulation of Side Products *J. Am. Chem. Soc.* **2014,** *136*, 17438-17441.
[22] Feringa, B. L.; Browne, W. R., *Molecular Switches*. Wiley-VCH: 2011; Vol. 1.
[23] Bléger, D.; Hecht, S., Visible-Light-Activated Molecular Switches *Angew. Chem. Int. Ed.* **2015,** *54*, 11338-11349.

- Light is a clean source of energy since it does not generate any wastage, which is a critical issue in chemical switches.
- It shows a high temporal and spatial resolution that makes it very selective.
- The provider of energy can be switched *on* and *off* immediately.

All these advantages, together with the huge development of powerful and versatile sources of light, have contributed to the widespread use of light as an energy source. For instance, the development of Hg lamps in the 20th century involved an increase in the number of photochemical studies, since this type of emitting light was the most widely used in photochemistry until the last decade. These types of lamps produce a wide range emission, from high-UV radiation to far visible light.

Moreover, the growth of new sources of light such as lasers have contributed to the development of new techniques that have been widely used to study photochemical reactions, such as flash photolysis[24] and pump-probe spectroscopy.[25]

[24] Novak, J. R.; Windsor, M. W.; Porter, G., Laser photolysis and spectroscopy: a new technique for the study of rapid reactions in the nanosecond time range *Proc. R. Soc. Lond. A. Math. Phys. Sci.* **1968,** *308*, 95-110.

[25] Beeby, A., Pump-Probe Laser Spectroscopy. In *An Introduction to Laser Spectroscopy: Second Edition*, Andrews, D. L.; Demidov, A. A., Eds. Springer US: Boston, MA, 2002; pp 105-137.

2. Using light as a source of energy in biological applications.

Since 1970s, the use of light to control biological functions has aroused a lot of interest in different research fields due to its advantages. For example, Francis Crick realized the necessity of controlling one type of cells while leaving the rest unaltered. He thought that light could be a good tool to manage this issue. Once more, scientists were inspired by nature to develop different techniques to control biological processes (Figure 2.4).[26] Moreover, it has been tried many times to explore this issue, and in the following, the strategies shown in Figure 2.4 will be explained.

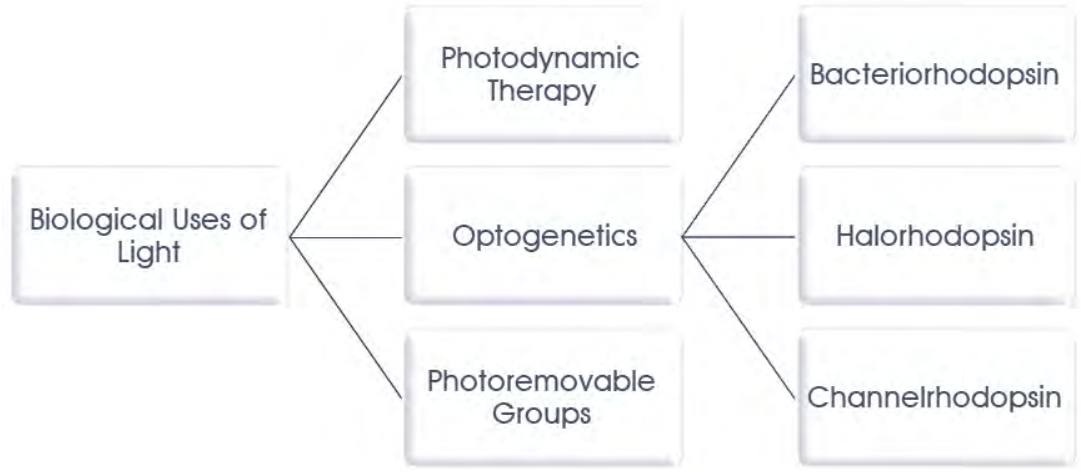

Figure 2.4. Scheme of different approaches of using light with biological purposes.

As it can be seen in the figure above, different approaches with biological purposes are addressed. The main difference between them is the strategy used to resolve the biological issue under study.

2.1. Photodynamic therapy (PDT).

The PDT is based on the use of the energy of photons to irradiate a photoresponsive drug known as photosensitizer (see introduction for further details), which leads to the formation of a cytotoxic agent. In this therapy, the sensitizer can react with the oxygen forming reactive oxygen species (ROS), such as anion radicals, hydroxyl radicals and hydrogen peroxides (Type I in Figure 2.5), although the strategy most used is the formation of singlet oxygen (Type II in Figure 2.5), which kills nearby cells.[27]

[26] Daniell, M. D.; Hill, J. S., A History of Photodynamic Therapy *ANZ J. Surg.* **1991,** *61*, 340-348.
[27] Schiff, L. J.; Eisenberg, W. C.; Dziuba, J.; Taylor, K.; Moore, S. J., Cytotoxic Effects of Singlet Oxygen *Environ. Health Perspect.* **1987,** *76*, 199-203.

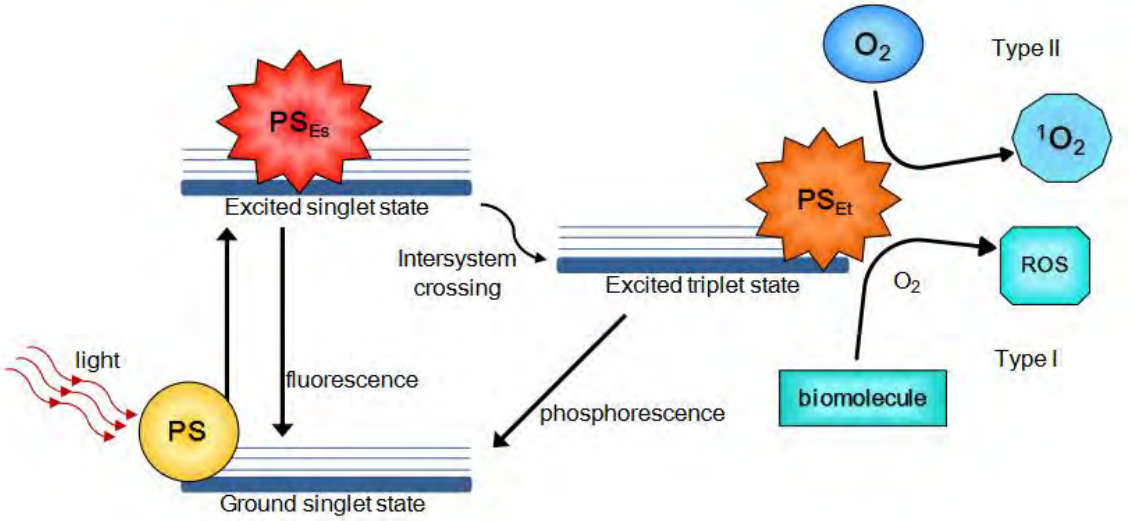

Figure 2.5. Schematic ways of the production of different cytotoxic agents by PDT.[28]

These two types of reactions can occur simultaneously; depending on the sensitizer used, one pathway or the other will be favored. In this therapy, the activation wavelength of the sensitizer should be above 700 nm to allow deeper penetration of light. In this way it could reach the target tissues, since many endogenous molecules, such as hemoglobin, present a strong absorption below 700 nm, acting as a light filter. Therefore, many structures have been designed to use them as effective photosensitizers in PDT therapy. Most of these structures are based on phtalocyanines, phenothiazines or anthraquinones among others (Figure 2.6).[29]

[28] Calixto, G.; Bernegossi, J.; de Freitas, L.; Fontana, C.; Chorilli, M., Nanotechnology-Based Drug Delivery Systems for Photodynamic Therapy of Cancer: A Review *Molecules* **2016,** *21*, 342.
[29] Ormond, A. B.; Freeman, H. S., Dye Sensitizers for Photodynamic Therapy *Materials* **2013,** *6*, 817.

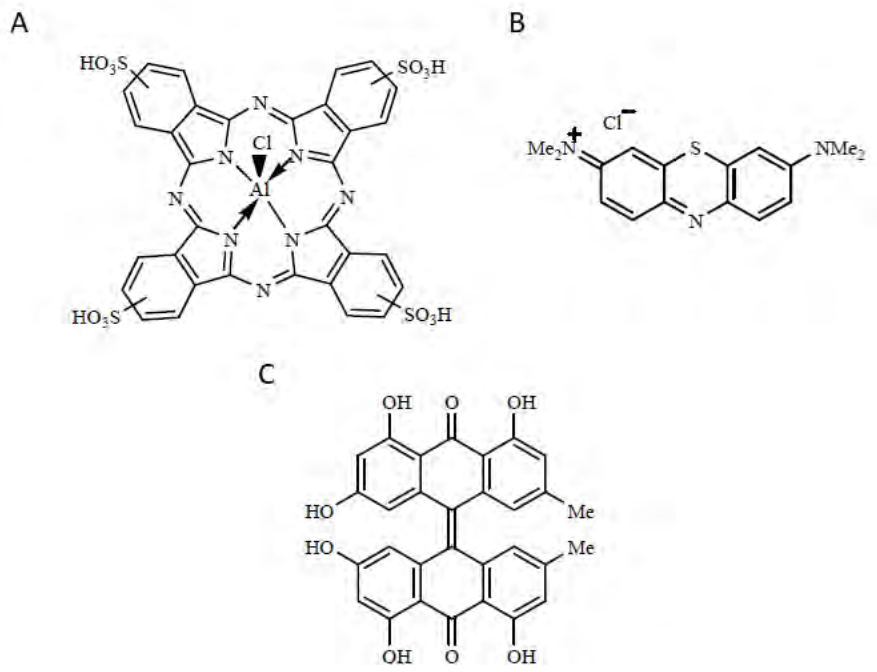

Figure 2.6. Structures of some examples used as photosensitizers in PDT.

The first examples of the use of PDT in clinical practice took place at the beginning of the 20th century.[30] PDT has been widely used against infections, specially it has been demonstrated that Gram (+) bacteria are relatively easy to kill by PDT.[31] For instance, PDT has been used in the treatment of skin maladies such as psoriasis, rosacea and other benign diseases.[32] Moreover, PDT has been used to form cytotoxic agents, and so it has also been used in the treatment of other serious diseases such as cancer. It should be noted that several factors are relevant to evaluate the effectiveness of the use of PDT as antitumor therapy: the type, concentration and location of the tumor, its level of oxygenation and when the light should be applied.[33] It has been found that the active oxygen species formed by PDT can lead to the tumor destruction by mainly three methods:[34]

- It can kill tumor cells directly.
- It affects the tumor vasculature avoiding its dissemination.

[30] Raab, O., Ueber die wirkung fluoreszierenden stoffe auf infusorien *Z Biol.* **1900,** *39*, 524-526.
[31] Sharma, S. K.; Mroz, P.; Dai, T.; Huang, Y.-Y.; St Denis, T. G.; Hamblin, M. R., Photodynamic Therapy for Cancer and for Infections: What Is the Difference? *Isr. J. Chem.* **2012,** *52*, 691-705.
[32] Kim, M.; Jung, H. Y.; Park, H. J., Topical PDT in the Treatment of Benign Skin Diseases: Principles and New Applications *Int. J. Mol. Sci.* **2015,** *16*, 23259.
[33] Dolmans, D. E. J. G. J.; Fukumura, D.; Jain, R. K., Photodynamic therapy for cancer *Nat. Rev. Cancer* **2003,** *3*, 380.
[34] Dougherty, T. J.; Gomer, C. J.; Henderson, B. W.; Jori, G.; Kessel, D.; Korbelik, M.; Moan, J.; Peng, Q., Photodynamic therapy *J. Natl. Cancer Inst.* **1998,** *90*, 889-905.

- It can activate an immune response against cancer cells.

These different approaches can take place independently, or simultaneously. But several limitations of PDT have been found in the treatment of cancer, such as the inability to treat solid or non well-oxygenated tumors. Moreover, deep tumors cannot be treated by PDT due to the low tissue penetration of visible light.[35] Finally, PDT is a localized treatment since the currently available technology does not allow the irradiation of the whole body with the appropriate light intensity.[36]

2.2. Optogenetics.

Another approach was developed in the mid-20th century known as optogenetics. In the last 50 years it has been found that some microorganisms produce several light-gated proteins which control the ions flow through the cell membrane. The first example was discovered in 1971, it being found that bacteriorhodopsin (BR) could act as an ion pump when it was activated with visible light (Figure 2.7).[37]

Later, another photoresponsive protein was discovered. Halorhodopsin (HR) was found to be a specific light-driven chlorine pump present in archaea. When halorhodopsin is irradiated with green or yellow light, it allows the penetration of chlorine ions into the cell (Figure 2.7).[38]

Finally, in 2002 it was described another member of this family of proteins. In green algae the channelrhodopsin protein (ChR) is present, which permits the passage of cations across the membrane when it is activated with blue light (Figure 2.7).[39] It also controls the movement of the green algae towards light, this phenomenon is also known as phototaxis.

[35] Huang, Z.; Xu, H.; Meyers, A. D.; Musani, A. I.; Wang, L.; Tagg, R.; Barqawi, A. B.; Chen, Y. K., Photodynamic Therapy for Treatment of Solid Tumors — Potential and Technical Challenges *Technol. Cancer Res. Treat.* **2008,** *7*, 309-320.
[36] Brown, S. B.; Brown, E. A.; Walker, I., The present and future role of photodynamic therapy in cancer treatment *Lancet Oncol.* **2004,** *5*, 497-508.
[37] Oesterhelt, D.; Stoeckenius, W., Rhodopsin-like Protein from the Purple Membrane of Halobacterium halobium *Nat. New Biol.* **1971,** *233*, 149.
[38] Matsuno-Yagi, A.; Mukohata, Y., Two possible roles of bacteriorhodopsin; a comparative study of strains of Halobacterium halobium differing in pigmentation *Biochem. Biophys. Res. Commun.* **1977,** *78*, 237-243.
[39] Nagel, G.; Ollig, D.; Fuhrmann, M.; Kateriya, S.; Musti, A. M.; Bamberg, E.; Hegemann, P., Channelrhodopsin-1: A Light-Gated Proton Channel in Green Algae *Science* **2002,** *296*, 2395-2398.

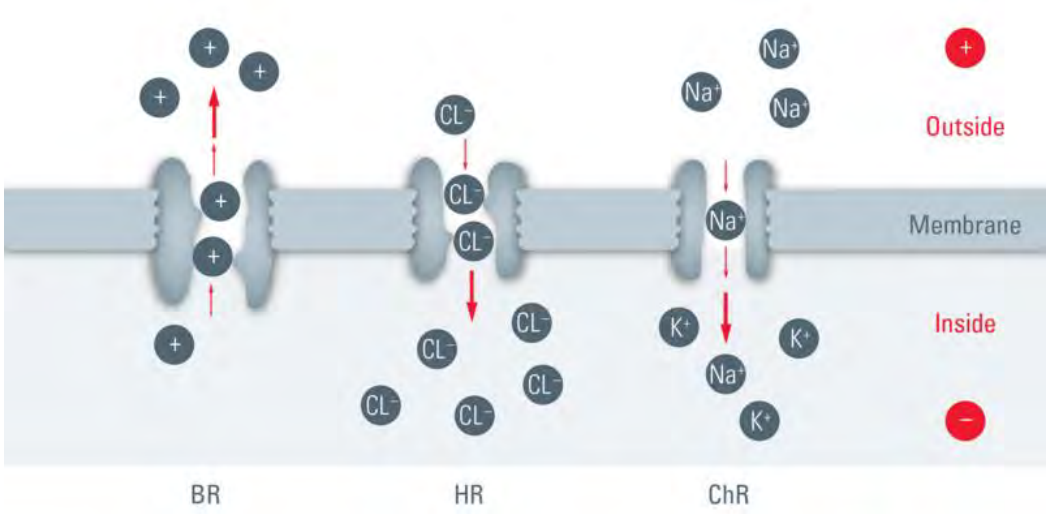

Figure 2.7. Light-gated proteins.[40]

All these findings were helpful to develop what it is known today as optogenetics, a new technique that combines genetic engineering with light, and it is used to control the activity or inactivity of some specific cells, specially neurons.

Therefore, the aim of these techniques is to create neurons able to express exogenous photosensitive proteins making them responsive to light (opsins), taking as reference the bacterial photosensitive proteins addressed before. When a light-sensitive opsin is expressed, the cell membrane suffers an alteration of membrane ion permeability when it is illuminated.

Several studies have described how to deliver light into the genetically modified neurons to activate them. For this purpose, lasers are a good option since they produce light in a very narrow band, increasing the selectivity. Moreover, they can be implanted in a fiber optic to reach deeper zones of the brain. The laser most used in optogenetics is a diode pumped solid state laser with a maximum power of 100 mW.[41]

Another method could be the use of light-emitting diodes (LEDs). They could be very useful due to their low cost and their emission can be easily tuned using different colors.[42]

[40] https://www.leica-microsystems.com/science-lab/optogenetics/
[41] Adamantidis, A. R.; Zhang, F.; Aravanis, A. M.; Deisseroth, K.; de Lecea, L., Neural substrates of awakening probed with optogenetic control of hypocretin neurons *Nature* **2007,** *450*, 420.
[42] Lammel, S.; Tye, K. M.; Warden, M. R., Progress in understanding mood disorders: optogenetic dissection of neural circuits *Genes Brain Behav.* **2014,** *13*, 38-51.

Due to its great applicability in neuroscience, optogenetics had an enormous impact in the scientific community, becoming "the method of the year" in 2010.[43]

2.3. Photoremovable protecting groups.

Photocages are molecules that are covalently linked to a target molecule to inhibit its action. After the exposure of these molecules towards light, a photoreaction occurs, and the target molecule recovers its activity. This kind of molecules are of great interest in biological applications (Figure 2.8). [44]

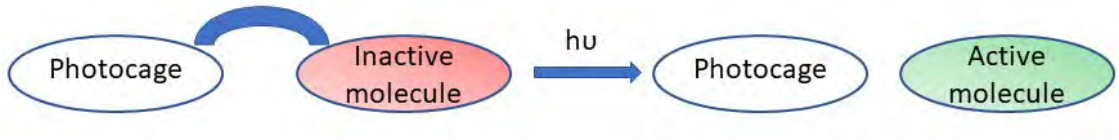

Figure 2.8. General performance of a photocage.

There are many chemical groups that can be released by the irradiation with light, such as phenazyl,[45] coumarin derivatives[46] or metal-containing groups[47] amongst others. This confers a high spatial and temporal control over many chemicals due to the benefits given by light.

The main drawback of this strategy, to be applied in a biological application, is that most of the photoremovable groups are only active under UV light, which does not penetrate deeply into tissues. Moreover, this energetic light can cause phototoxicity.[48]

Therefore, many efforts have been applied to find photoremovable groups which could be cleaved under far-visible light (>600 nm). The most studied group to achieve this goal is the use of boron-dipyrromethene group (BODIPY) as photocage.[49] Moreover, it

[43] Mahmoudi, P.; Veladi, H.; Pakdel, F. G., Optogenetics, Tools and Applications in Neurobiology *J. Med. Signals Sens.* **2017,** *7*, 71-79.
[44] Klán, P.; Šolomek, T.; Bochet, C. G.; Blanc, A.; Givens, R.; Rubina, M.; Popik, V.; Kostikov, A.; Wirz, J., Photoremovable Protecting Groups in Chemistry and Biology: Reaction Mechanisms and Efficacy *Chem. Rev.* **2013,** *113*, 119-191.
[45] Sheehan, J. C.; Umezawa, K., Phenacyl photosensitive blocking groups *J. Org. Chem.* **1973,** *38*, 3771-3774.
[46] Givens, R. S.; Matuszewski, B., Photochemistry of phosphate esters: an efficient method for the generation of electrophiles *J. Am. Chem. Soc.* **1984,** *106*, 6860-6861.
[47] Haas, K. L.; Franz, K. J., Application of Metal Coordination Chemistry To Explore and Manipulate Cell Biology *Chem. Rev.* **2009,** *109*, 4921-4960.
[48] Kim, K.; Park, H.; Lim, K.-M., Phototoxicity: Its Mechanism and Animal Alternative Test Methods *Toxicol Res.* **2015,** *31*, 97-104.
[49] Goswami, P. P.; Syed, A.; Beck, C. L.; Albright, T. R.; Mahoney, K. M.; Unash, R.; Smith, E. A.; Winter, A. H., BODIPY-Derived Photoremovable Protecting Groups Unmasked with Green Light *J. Am. Chem. Soc.* **2015,** *137*, 3783-3786.

has been described as the easiness to tune the absorption wavelength of these derivatives containing a BODIPY moiety from 500 to 750 nm (Figure 2.9).

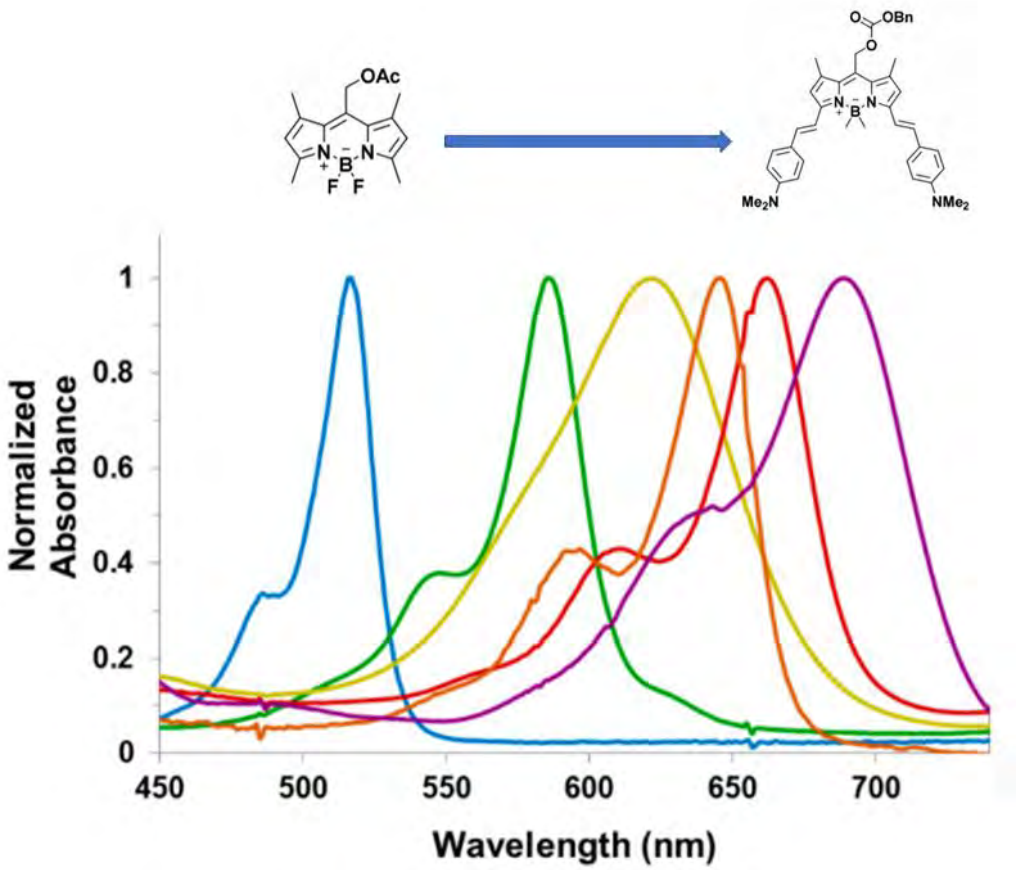

Figure 2.9. Absorption bands of different photocages based on BODIPY. [50]

To sum up, it has been showed how light can be used to induce and control some biological functions through different strategies. Furthermore, it will be described in the following section how light can control different molecular switches, of which some are responsible for a specific biological activity.

[50] Peterson, J. A.; Wijesooriya, C.; Gehrmann, E. J.; Mahoney, K. M.; Goswami, P. P.; Albright, T. R.; Syed, A.; Dutton, A. S.; Smith, E. A.; Winter, A. H., Family of BODIPY Photocages Cleaved by Single Photons of Visible/Near-Infrared Light *J. Am. Chem. Soc.* **2018,** *140*, 7343-7346.

3. Types of molecular switches activated by light.

So far, many structures have been developed that can be used as efficient photoswitches. They can be divided into different groups depending on which reaction is involved in the photochemical process. The two most important are those in which the key step is the photoisomerization of a double bond (C=N, C=C, N=N)[51] or a photorearrangement.[52]

In Figure 2.10, an overview is presented of the different systems than can be photoswitchable between two states (Figure 2.10).

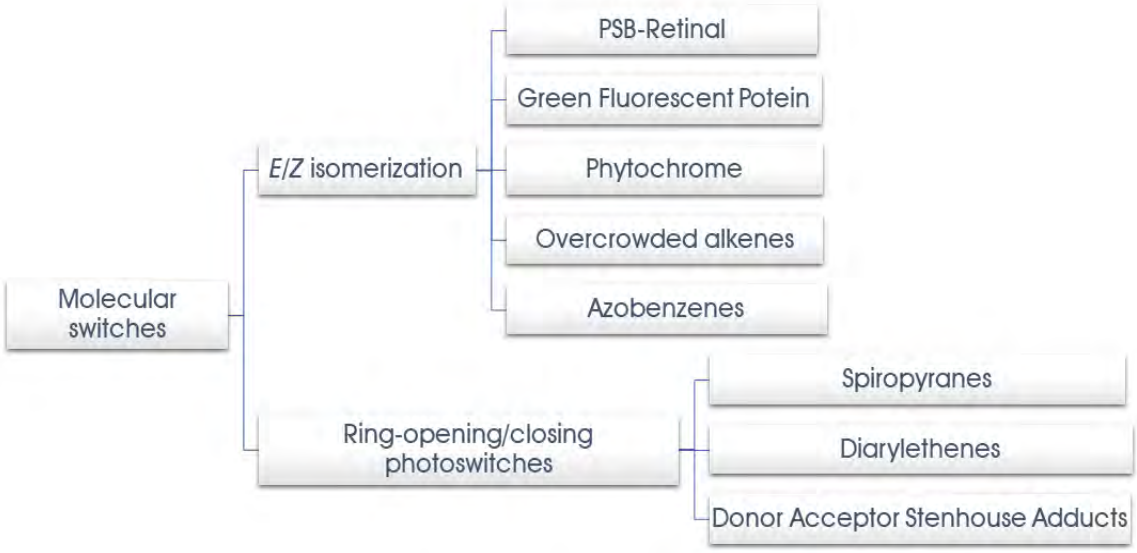

Figure 2.10. Scheme of the most important photoswitches.

3.1. *E/Z* isomerization based molecular switches.

As it was mentioned before, many biological processes in nature start with a simple isomerization of a double bond when it is exposed to light. The most important examples are 1) the responsible of vision, in which the rhodopsin chromophore experiments an *Z/E* isomerization when it is irradiated, 2) the presence of luminescence in different organisms, such as the green fluorescent protein and 3) photoreceptor proteins as the phytochrome.[53] All these natural molecules have inspired us to design different chromophores trying to maintain the extraordinary properties that they show in nature.

[51] García-Iriepa, C.; Marazzi, M.; Frutos, L. M.; Sampedro, D., E/Z Photochemical switches: syntheses, properties and applications *RSC Adv.* **2013,** *3*, 6241-6266.
[52] Wegner, H. A., *Molecular Switches*. John Wiley & Sons, Ltd: 2012; Vol. 51, p 2281.
[53] Gozem, S.; Luk, H.; Schapiro, I.; Olivucci, M., Theory and Simulation of the Ultrafast Double-Bond Isomerization of Biological Chromophores *Chem. Rev.* **2017,** *117*.

3.1.1. Protonated Schiff base (PSB) of the retinal.

Firstly, one of the most important examples in nature of a molecular motor is the retinal chromophore of rhodopsin which experiments a photoisomerization of one of its double bonds from the *cis*-isomer to the *trans*-form (Figure 2.11). This process exhibits a high efficiency *in vivo* reaching a value of 0.67 quantum yield.[54] This photoisomerization takes place when the chromophore absorbs visible light, initiating the process of vision.[55]

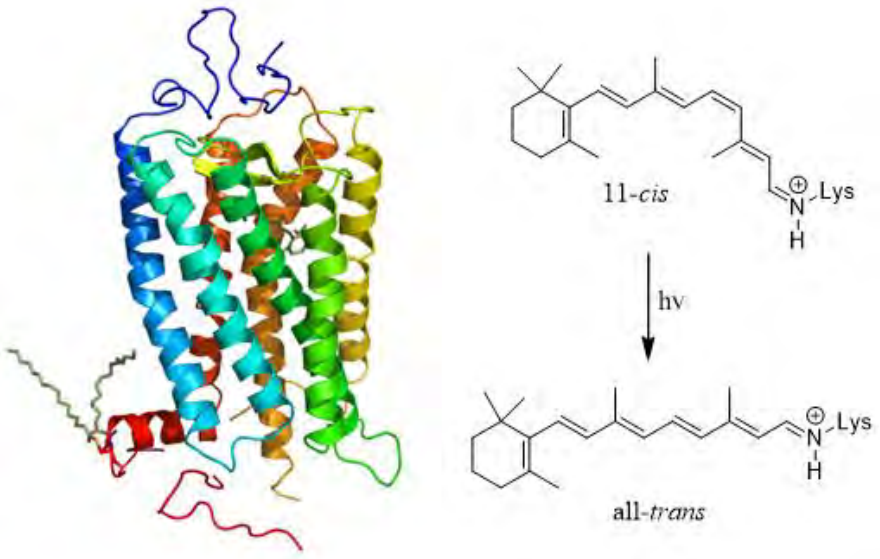

Figure 2.11. Rhodopsin and its chromophore (a protonated Schiff base of retinal).

This simple change forces the rest of the protein to be reorganized generating an electric impulse that reaches the brain, which initiates the visual transduction process.[56] Moreover, the natural chromophore photoisomerizes very fastly and effectively due to the geometrical constraints made by the protein surrounding.

For this reason, many efforts have been put on the design and synthesis of new derivatives based on non-natural protonated Schiff base (PSB) able to keep in solution the good properties of the protein-embedded chromophore. Therefore, these new prototypes should share some structural characteristics with the natural structure such as an extended conjugation and the presence of an iminic bond. To decide which structure could be the best option to study, several computational studies were carried out prior to the synthesis

[54] Dartnall, H. J. A., The photosensitivities of visual pigments in the presence of hydroxylamine *Vision Res.* **1968,** *8*, 339-358.
[55] Kandori, H.; Shichida, Y.; Yoshizawa, T., Photoisomerization in Rhodopsin *Biochemistry* **2001,** *66*, 1197-209.
[56] McBee, J. K.; Palczewski, K.; Baehr, W.; Pepperberg, D. R., Confronting Complexity: the Interlink of Phototransduction and Retinoid Metabolism in the Vertebrate Retina *Prog. Retin. Eye Res.* **2001,** *20*, 469-529.

of the target molecules.[57, 58] After these studies, some structures were selected such as indanylidene-pyrrolines, fluorenylidene-pyrrolines and benzylidene-pyrrolines, and these will be explained in the following section.

3.1.1.1. Indanylidene-pyrrolines (IP).

The general structure of this kind of molecular switches is shown in Figure 2.12. As it can be seen, these new prototypes present a Schiff base function as the natural chromophore, but it is included in a pyrrolidine ring in order to reduce its degrees of freedom, trying to simulate the protein surrounding. Moreover, these derivatives included an *N*-alkylated pyrroline (NAIP) moiety as the natural retinal chromophore.

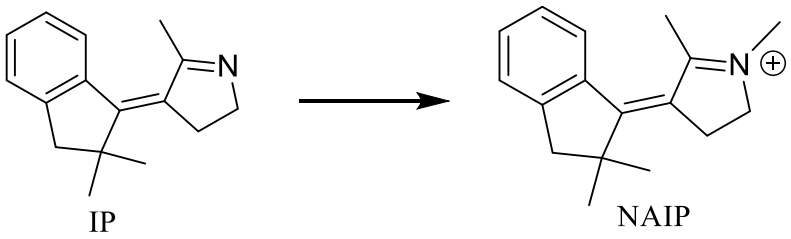

Figure 2.12. *N*-alkylated indanylidene-pyrroline Schiff bases.

These derivatives have been shown to isomerize very fastly, completing each photoswitching from *E* to *Z*-isomer in picoseconds.[59] This is in good agreement with a reaction path in which there are no intermediates, as it happens in the natural chromophore (Figure 2.13).

[57] Lumento, F.; Zanirato, V.; Fusi, S.; Busi, E.; Latterini, L.; Elisei, F.; Sinicropi, A.; Andruniów, T.; Ferré, N.; Basosi, R.; Olivucci, M., Quantum Chemical Modeling and Preparation of a Biomimetic Photochemical Switch *Angew. Chem. Int. Ed.* **2007,** *46*, 414-420.

[58] Sampedro, D.; Migani, A.; Pepi, A.; Busi, E.; Basosi, R.; Latterini, L.; Elisei, F.; Fusi, S.; Ponticelli, F.; Zanirato, V.; Olivucci, M., Design and Photochemical Characterization of a Biomimetic Light-Driven Z/E Switcher *J. Am. Chem. Soc.* **2004,** *126*, 9349-9359.

[59] Sinicropi, A.; Martin, E.; Ryazantsev, M.; Helbing, J.; Briand, J.; Sharma, D.; Léonard, J.; Haacke, S.; Cannizzo, A.; Chergui, M.; Zanirato, V.; Fusi, S.; Santoro, F.; Basosi, R.; Ferré, N.; Olivucci, M., An artificial molecular switch that mimics the visual pigment and completes its photocycle in picoseconds *PNAS* **2008,** *105*, 17642-17647.

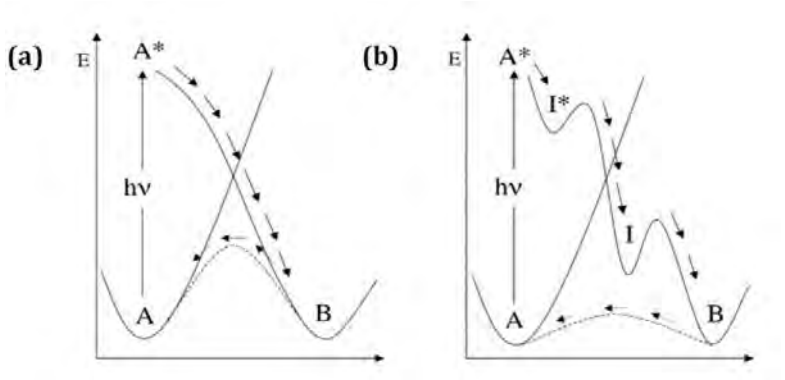

Figure 2.13. (a) Reaction coordinate for an efficient molecular switch. (b) Reaction coordinate for an inefficient molecular switch.[60]

Besides, it should be noted that these photoswitches show a high thermal stability, therefore both isomers are not interconverted at room temperature. Although these systems show good properties to be considered as efficient molecular switches, other properties needed to be improved as the absorption wavelength. These compounds absorb at 350 nm, in the near UV-region. Consequently, these molecular switches could not be applied in any biological application.

3.1.1.2. Fluorenylidene-pyrrolines (FP).

Further, trying to resolve the disadvantages addressed in the prior design, fluorenylidene-pyrrolines were synthesized. These photoswitches are very similar to the indanylidene-pyrrolines reported before (Figure 2.14).

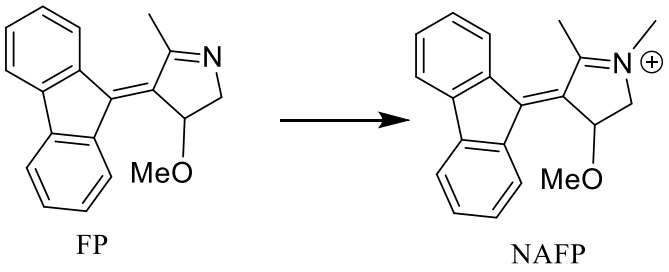

Figure 2.14. *N*-alkylated fluorenylidene-pyrroline Schiff bases.

As it is shown, the conjugation was extended adding a new phenyl group into the chromophore to red-shift the absorption wavelength of these new derivatives. Specifically, they show a clear absorption in the visible region, around 400 nm (Figure 2.15). This

[60] Blanco-Lomas, M. Design, Synthesis and Computational Study of Photoactive Molecular Devices. PhD. Thesis, University of La Rioja, Logroño, 2012.

achievement constituted a clear improvement over previous results, since it increased the applicability of these switches.

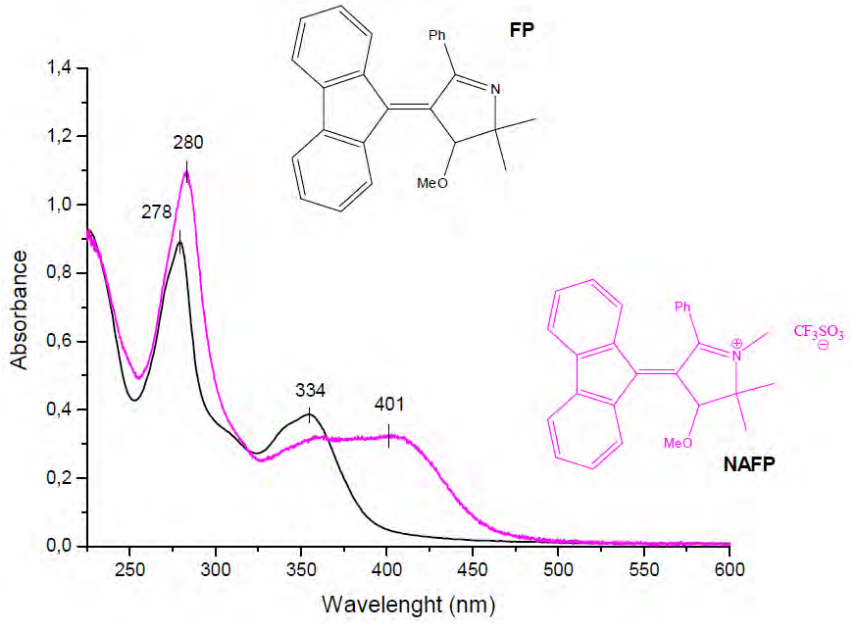

Figure 2.15. Comparison of the UV-Vis spectra of a derivative of a FP and a NAFP. [61]

Moreover, the quantum yield measured for NAFP derivatives was around 0.5, which is very close to the one shown for the natural chromophore *in vivo* (0.67). This behavior is also agreeable with a photoisomerization path without intermediates.

Regarding the stability of these photoswitches, they showed a high-thermal and photochemical stability.

3.1.1.3. Dibenzylidene-pyrrolines.

Another structure was reported trying to go further in the synthesis of new derivatives based on the PSB-retinal. As it is observed in Figure 2.16, the dibenzylidene-pyrrolines were designed from the benzylidene-pyrrolidines in order to improve their photophysical properties.

[61] Rivado-Casas, L.; Sampedro, D.; Campos, P. J.; Fusi, S.; Zanirato, V.; Olivucci, M., Fluorenylidene–Pyrroline Biomimetic Light-Driven Molecular Switches *J. Org. Chem.* **2009,** *74,* 4666-4674.

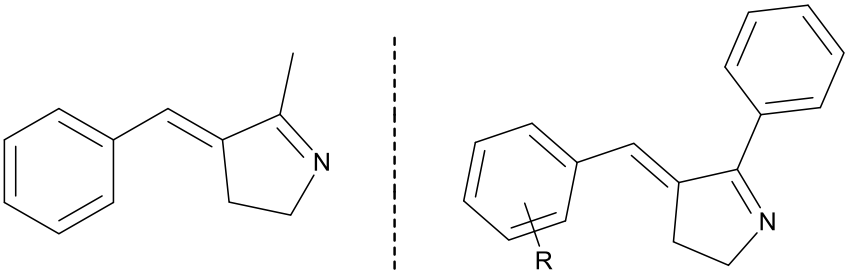

Figure 2.16. General structure of benzylidene-pyrroline and dibenzylidene-pyrroline.

As in other photoswitches, when the π conjugated system is expanded, a red-shift absorption usually takes place. Moreover, many derivatives based on dibenzylidene-pyrroline were synthesized changing the properties of the R group (Figure 2.16). It was observed that the absorption wavelength was very dependent on the electronic properties of the R group.[62] Therefore, the UV-Vis spectrum could be tuned easily using electron-donating or electron-withdrawing groups in the structure. In addition, the photostationary state (PSS) for these photoswitches could be controlled, expanding the applicability of these compounds for biological applications as it will be shown in Section 4.

Furthermore, good photochemical and photophysical properties were found in these molecular switches based on PSB-retinal. Therefore, this structure will be used as a pattern to develop new *N*-quaternized photoswitches in Chapter 5.

3.1.2. Green Fluorescent protein (GFP) chromophore.

In nature, there are some proteins which exhibit fluorescent; they are known as "fluorescent proteins". In this group, one of the most important proteins is the green fluorescent protein; it was found in *Aequorea victoria* jellyfish (Figure 2.17). Its role is to transduce by energy transfer the blue chemiluminescence of another protein, aequorin, into green fluorescence light.[63] Its chromophore can also experiment with a photoisomerization process (*Z*/*E*), decreasing the efficiency of the luminescence. It was reported for the first time in 1992,[64] and since then many studies of different GFP

[62] Blanco-Lomas, M.; Campos, P. J.; Sampedro, D., Synthesis and Photoisomerization of Rhodopsin-Based Molecular Switches *Eur. J. Org. Chem.* **2012,** *2012*, 6328-6334.
[63] Yang, F.; Moss, L. G.; Phillips, G. N., The molecular structure of green fluorescent protein *Nature Biotechnol.* **1996,** *14*, 1246-1251.
[64] Prasher, D. C.; Eckenrode, V. K.; Ward, W. W.; Prendergast, F. G.; Cormier, M. J., Primary structure of the Aequorea victoria green-fluorescent protein *Gene* **1992,** *111*, 229-233.

derivatives have been reported due to its high applicability, as for example in bioimaging.[65]

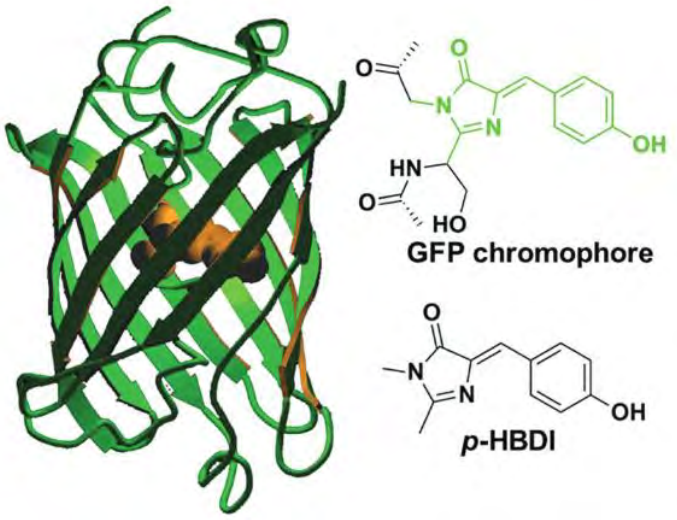

Figure 2.17. Green fluorescent protein (GFP) and its chromophore (*p*-HBDI).[66]

Due to the discovery and development of GFP, Osamu Shimomura,[67] Martin Chalfie[68] and Roger Y. Tsien[69] were awarded the 2008 Nobel Prize in Chemistry.

The GFP chromophore shown in Figure 2.17 is formed *in situ* through autocatalytic cyclization and dehydration/oxidation processes of the three-peptide sequence Ser_{65}-Tyr_{66}-Gly_{67} resulting in *p*-HBDI chromophore (Figure 2.17).[70] The chromophore moiety, *p*-HBDI is responsible for emitting green fluorescence through an excited-state proton transfer (ESPT) when it is embedded in the protein, resulting in a very fluorescent anion (Figure 2.18).[71]

[65] Gutiérrez, S.; Martínez-López, D.; Morón, M.; Sucunza, D.; Sampedro, D.; Domingo, A.; Salgado, A.; Vaquero, J. J., Highly Fluorescent Green Fluorescent Protein Chromophore Analogues Made by Decorating the Imidazolone Ring *Chem. Eur. J.* **2015,** *21*, 18758-18763.
[66] Deng, H.; Zhu, X., Emission enhancement and application of synthetic green fluorescent protein chromophore analogs *Mater. Chem. Front.* **2017,** *1*, 619-629.
[67] Shimomura, O., Discovery of Green Fluorescent Protein (GFP) (Nobel Lecture) *Angew. Chem. Int. Ed.* **2009,** *48*, 5590-5602.
[68] Chalfie, M., GFP: Lighting Up Life (Nobel Lecture) *Angew. Chem. Int. Ed.* **2009,** *48*, 5603-5611.
[69] Tsien, R. Y., Constructing and Exploiting the Fluorescent Protein Paintbox (Nobel Lecture) *Angew. Chem. Int. Ed.* **2009,** *48*, 5612-5626.
[70] Heim, R.; Prasher, D. C.; Tsien, R. Y., Wavelength mutations and posttranslational autoxidation of green fluorescent protein *PNAS* **1994,** *91*, 12501-12504.
[71] Morin, J. G.; Hastings, J. W., Energy transfer in a bioluminescent system *J. Cell. Physiol.* **1971,** *77*, 313-318.

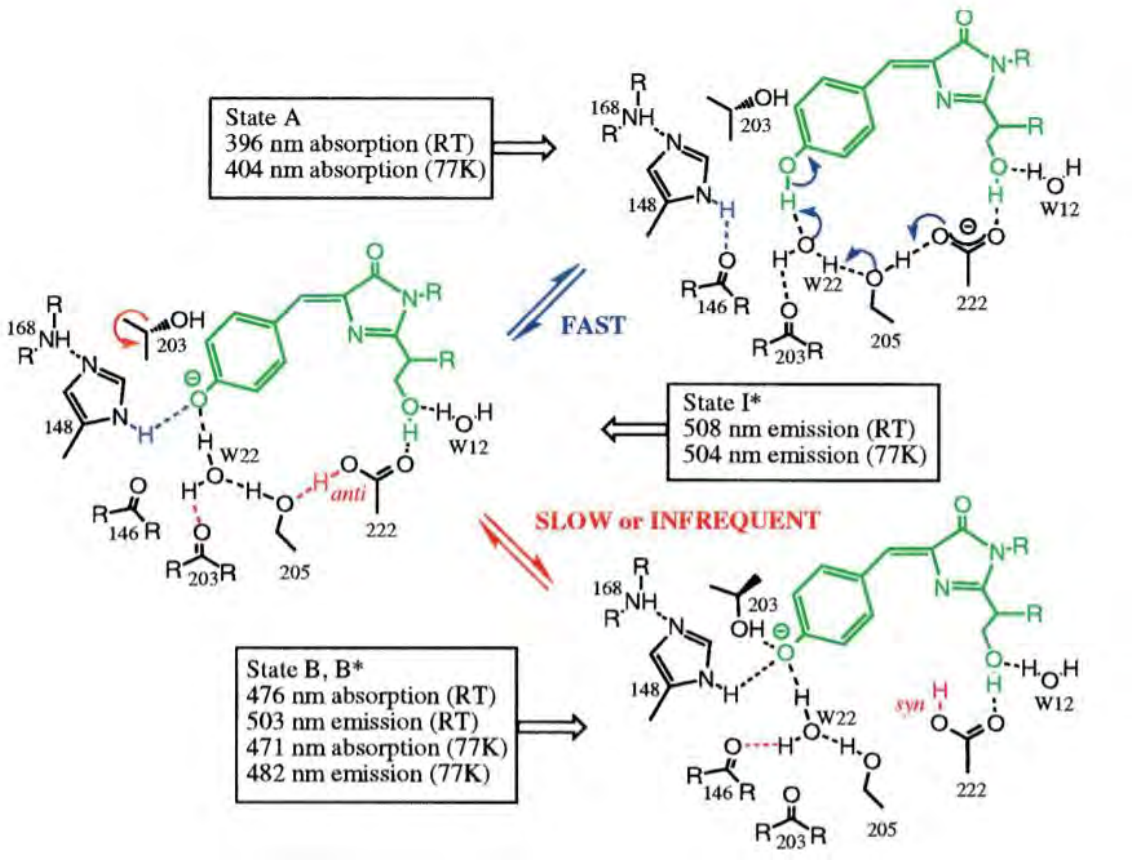

Figure 2.18. Formation of a fluorescent species by an excited-state proton transfer.[72]

However, when *p*-HBDI is isolated, the fluorescence decreases dramatically in solution at room temperature (RT).[73] Many studies have revealed that the excited state of *p*-HBDI also decays to the ground state through non-radiative processes when it is not fixed to the protein, resulting in a *Z/E* photoisomerization (Figure 2.19), which leads to the reduction of the fluorescence quantum yield.[74]

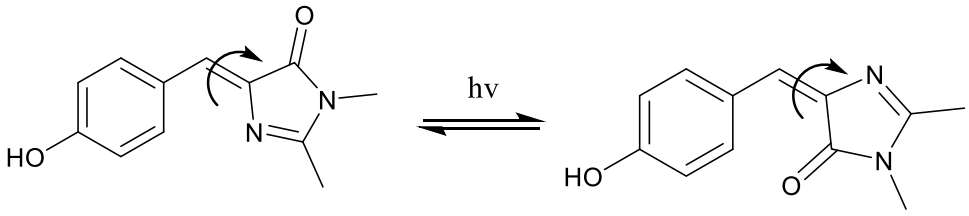

Figure 2.19. Photoisomerization process of the GFP chromophore.

[72] Brejc, K.; Sixma, T. K.; Kitts, P. A.; Kain, S. R.; Tsien, R. Y.; Ormö, M.; Remington, S. J., Structural basis for dual excitation and photoisomerization of the *Aequorea victoria* green fluorescent protein *PNAS* **1997,** *94*, 2306-2311.

[73] Baldridge, A.; Samanta, S. R.; Jayaraj, N.; Ramamurthy, V.; Tolbert, L. M., Activation of Fluorescent Protein Chromophores by Encapsulation *J. Am. Chem. Soc.* **2010,** *132*, 1498-1499.

[74] Voliani, V.; Bizzarri, R.; Nifosì, R.; Abbruzzetti, S.; Grandi, E.; Viappiani, C.; Beltram, F., Cis–Trans Photoisomerization of Fluorescent-Protein Chromophores *J. Phys. Chem. B* **2008,** *112*, 10714-10722.

Many studies have been performed to synthesize fluorescent GFP analogues. For instance, one strategy was used by Kevin Burgess and co-workers who tried to constrain the structure to mimic the protein surrounding. For this purpose, they designed and synthesized the molecule which is detailed in Figure 2.20.

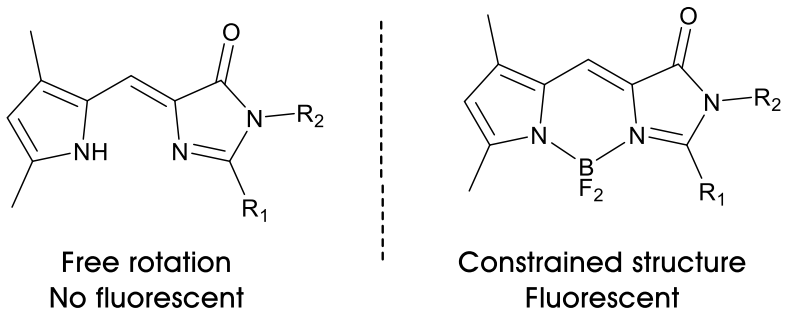

Figure 2.20. Structure to enhance the fluorescence of GFP derivatives.

Through this strategy, many highly fluorescent GFP chromophore derivatives have been described.[75]

Apart from the good fluorescent properties of GFP analogues, it also inspired scientists to design new biomimetic molecular switches based on the GFP-chromophore. For this reason, Sampedro and co-workers designed new oxazolone-based photoswitches.[76] These derivatives were based on the structure shown in Figure 2.21.

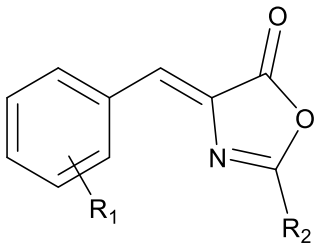

Figure 2.21. General structure of oxazolone-based molecular switches.

These GFP analogues showed an efficient and fast photoswitching, moreover their photophysical properties could be tuned easily changing the R_1 group pointed out in Figure 2.21, as well as the isomer mixture in its PSS. This fact allowed for a very precise control of the main isomer in the equilibrium; this could be helpful to fulfil the requirements needed for a specific application. These photoswitches showed a high thermal and photochemical stability. The main disadvantage of these photoswitches is the solvolysis

[75] Wu, L.; Burgess, K., Syntheses of Highly Fluorescent GFP-Chromophore Analogues *J. Am. Chem. Soc.* **2008,** *130,* 4089-4096.
[76] Blanco-Lomas, M.; Campos, P. J.; Sampedro, D., Benzylidene-Oxazolones as Molecular Photoswitches *Org. Lett.* **2012,** *14,* 4334-4337.

when they are dissolved in a nucleophilic solvent such as methanol, what could prevent the use of them in some applications.

3.1.3. Phytochromes.

This is another biomolecule in which the photoisomerization of a double bond has a huge relevance on its function. They are photoreceptors present in plants, bacteria or fungi.[77] Phytochrome is a protein in which its photoactive part is formed by a bilin chromophore; the photoisomerization of its C=C double bond takes place under the exposure to light (Figure 2.22A). Then, this simple change induces the rest of the protein to be reorganized activating its biological response.[78]

The photoactive part of phytochrome was used as the inspiration to design new possible molecular switches based on this protein. The new designed core used as pattern is a benzalpyrrolinone (Figure 2.22).

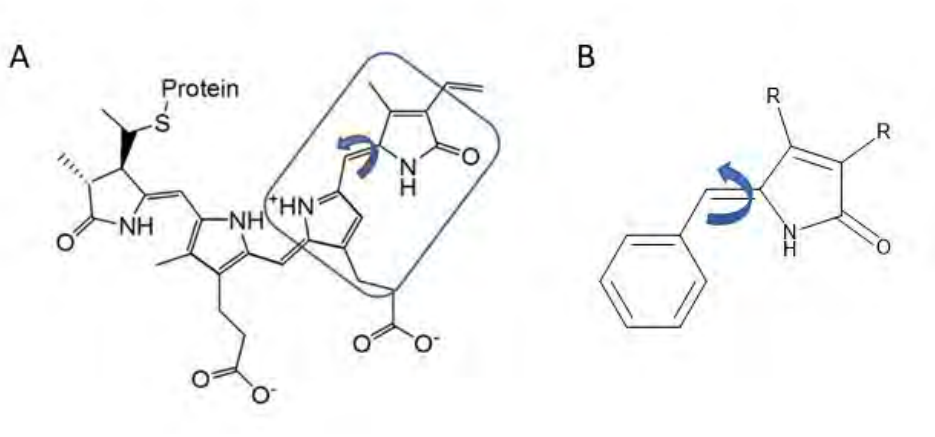

Figure 2.22. A) Phytochrome chromophore and B) phytochrome-based molecular switches.

As we can observe in Figure 2.22, the phytochrome *in vivo* presents four linked rings and several C=C double bonds, one of which is capable of isomerizing. Therefore, in order to simplify the structure in the new prototypes there is just one pyrrolinone. In these photoswitches, the most stable form is the *Z*-isomer. Moreover, the photochemical and photophysical properties can be easily tuned adding different substituents in the phenyl

[77] Quail, P.; Boylan, M.; Parks, B.; Short, T.; Xu, Y.; Wagner, D., Phytochromes: photosensory perception and signal transduction *Science* **1995,** *268*, 675-680.
[78] Chen, M.; Chory, J., Phytochrome signaling mechanisms and the control of plant development *Trends Cell Biol.* **2011,** *21*, 664-671.

ring.[79] Furthermore, phytochrome-based molecular switches showed an efficient and fast photoswitching.

3.1.4. Overcrowded alkenes.

These kind of photoswitches have drawn much attention in the last two decades. They consist of two halves, that can be considered the stator and the rotor part of a molecular motor. These two parts are connected by a central olefinic moiety (axle) (Figure 23). Ben Feringa was essential in the discovery and development of them.[80] The main idea of these molecules is the presence of a C=C double bond (axle), in which the substituents present in the photoswitch should be bulky enough to provide a huge steric hindrance. The axle and the substituents are in the same plane, but depending on the size of the substituents, they can be deviated from the planarity, resulting in a helical structure (Figure 2.23).

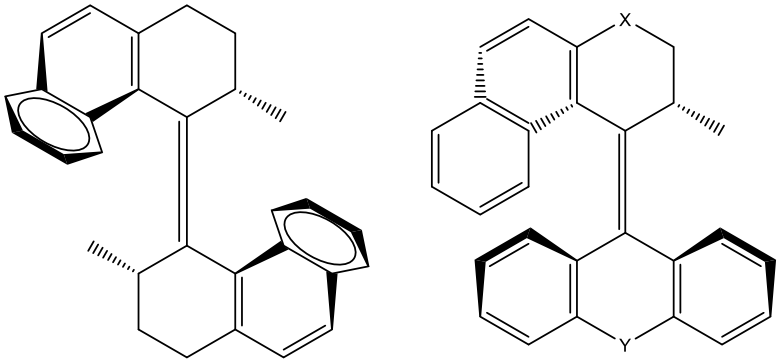

Figure 2.23. First and second generations of light-driven overcrowded alkenes.

As it is observed in Figure 2.23, that the first-generation compounds have the same substituents in both halves (rotor and stator) and two stereocenters. In contrast, in the second-generation these two halves present different substituents and just one stereocenter, and different heteroatoms could be introduced into the structure (X and Y in Figure 2.23).

The mechanism of first-generation light-driven molecular switches is detailed in the Figure 2.24.

[79] García-Iriepa, C.; Ernst, H. A.; Liang, Y.; Unterreiner, A.-N.; Frutos, L. M.; Sampedro, D., Study of Model Systems for Bilirubin and Bilin Chromophores: Determination and Modification of Thermal and Photochemical Properties *J. Org. Chem.* **2016,** *81*, 6292-6302.
[80] Feringa, B. L., In Control of Motion: From Molecular Switches to Molecular Motors *Acc. Chem. Res.* **2001,** *34*, 504-513.

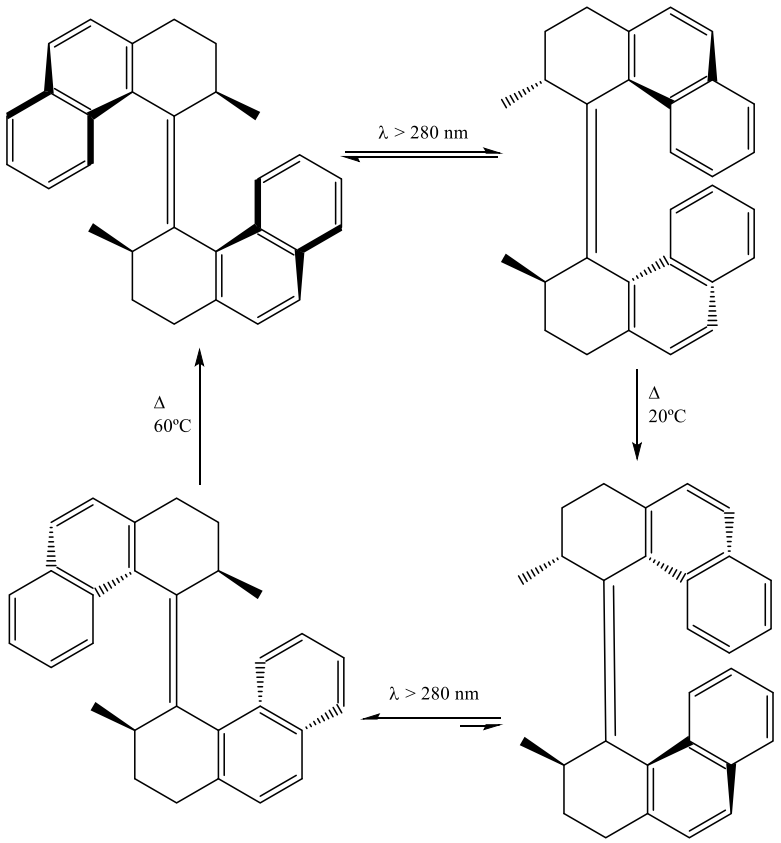

Figure 2.24. Photochemical and thermal isomerization processes during the 360º unidirectional rotary cycle of the first generation of overcrowded alkenes.[81]

This movement is unidirectional due to the presence of quiral atoms and helicity. Firstly, the stable *trans*-isomer in which all the substituents are in the axial position (Figure 2.24, top left) absorbs light to produce the isomerization of the double bond generating the unstable *cis*-isomer, producing a large steric hindrance in the molecule. Then, the energy content of the molecule decreases due to a thermally induced helix inversion changing the orientation of the substituents. Afterwards in the third step, another photochemical isomerization *cis*/*trans* takes place generating an unstable isomer due to the orientation of the substituents and finally, a thermal helix inversion takes place to recover the most stable form.

In the Figure 2.25 the free energy variation is described schematically for each step in the cycle.

[81] ter Wiel, M. K. J.; van Delden, R. A.; Meetsma, A.; Feringa, B. L., Light-Driven Molecular Motors: Stepwise Thermal Helix Inversion during Unidirectional Rotation of Sterically Overcrowded Biphenanthrylidenes *J. Am. Chem. Soc.* **2005,** *127*, 14208-14222.

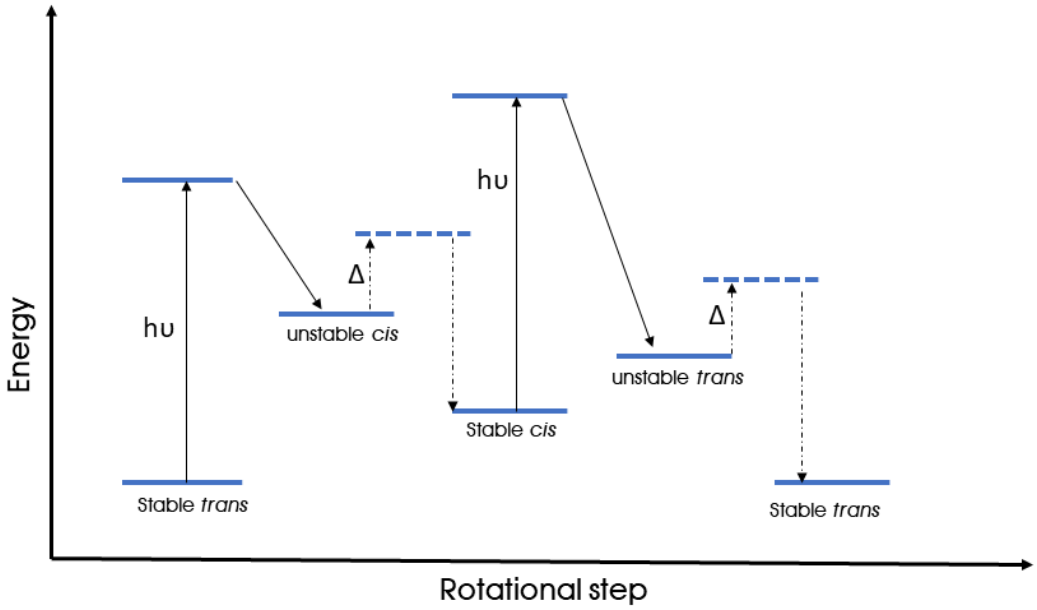

Figure 2.25. Free-energy profile of the rotary cycle of the first generation of overcrowded alkenes.

It should be noted that the photochemical processes happen very fast, in the range of picoseconds.[82] But, the thermal reactions are very slow, due to the energy barriers involved. So, the speed to complete a cycle is determined by the thermal steps.

Many efforts have been made to increase the speed of the thermal steps. Most of those efforts were directed to design new molecules in which the thermal energy barrier would be minimized.

The best strategy to achieve this goal was to replace the six-membered rings present in the rotor and stator with five-membered rings, this simple change leads to a 10^9 fold acceleration of the process.[83] Through the introduction of heteroatoms in the second-generation of photoswitches, a faster thermal process is achieved, although to a minor extent than in five-membered rings cores.

As we can observe, the properties of these photoswitches are very dependent on the substituents present in the molecule, altering the velocity of the process. Therefore, a full set of unidirectional activated motors with rotary motions speeds ranging from hours to microseconds were achieved. Many applications have been reported for these

[82] Zijlstra, R. W. J.; van Duijnen, P. T.; Feringa, B. L.; Steffen, T.; Duppen, K.; Wiersma, D. A., Excited-State Dynamics of Tetraphenylethylene: Ultrafast Stokes Shift, Isomerization, and Charge Separation *J. Phys. Chem. A* **1997,** *101*, 9828-9836.
[83] ter Wiel, M. K. J.; van Delden, R. A.; Meetsma, A.; Feringa, B. L., Increased Speed of Rotation for the Smallest Light-Driven Molecular Motor *J. Am. Chem. Soc.* **2003,** *125*, 15076-15086.

molecular motors, such as the control of dynamic functions,[84, 85] photoactive polymers[86] or applied on the surface of gold nanoparticles.[87]

3.1.5. Azobenzenes.

This core has been known since the middle of the 19th century due to their use in the chemical industry, since the main application of azo compounds was their use as dyes.[88] But it was not until the last part of the 20th century, when the photochemistry of azobenzene was under revision.[89]

In the field of molecular switches, this core is the most important one due to the large number of synthesis, properties and applications that have been reported up until now. Therefore, it is the most studied system until now.

Azobenzenes take as pattern a N=N double bond capable of isomerizing under the exposure to light (Figure 2.26).

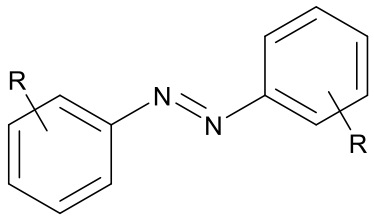

Figure 2.26. General structure of azobenzene photoswitches.

Many efforts have been devoted to the discovery of new, easy and efficient syntheses of this core. In addition, versatile syntheses are needed due to the importance of the substituents on the phenyl ring to regulate their photochemical and photophysical properties, as it will be seen later.[90] In most cases, after the synthesis of these derivatives, only the *trans*-isomer is found in the reaction mixture.

---

[84] van Leeuwen, T.; Lubbe, A. S.; Štacko, P.; Wezenberg, S. J.; Feringa, B. L., Dynamic control of function by light-driven molecular motors *Nat. Rev. Chem.* **2017,** *1*, 0096.

[85] Štacko, P.; Kistemaker, J. C. M.; van Leeuwen, T.; Chang, M.-C.; Otten, E.; Feringa, B. L., Locked synchronous rotor motion in a molecular motor *Science* **2017,** *356*, 964-968.

[86] Liang, W.-J.; Yu, J.-J.; Zhang, Q.; Ma, C.-S.; Shi, Z.-T.; Qu, D.-H., Photo-driven morphological transformations of supramolecular polymers actuated by an overcrowded alkene switch *Polym. Chem.* **2018,** *9*, 4808-4812.

[87] van Delden, R. A.; ter Wiel, M. K. J.; Pollard, M. M.; Vicario, J.; Koumura, N.; Feringa, B. L., Unidirectional molecular motor on a gold surface *Nature* **2005,** *437*, 1337.

[88] Noble, A., III. Zur Geschichte des Azobenzols und des Benzidins *Justus Liebigs Ann. Chem.* **1856,** *98*, 253-256.

[89] Griffiths, J., II. Photochemistry of azobenzene and its derivatives *Chem. Soc. Rev.* **1972,** *1*, 481-493.

[90] Merino, E., Synthesis of azobenzenes: the coloured pieces of molecular materials *Chem. Soc. Rev.* **2011,** *40*, 3835-3853.

When azobenzene-based molecular switches absorbs UV-visible light, a photoisomerization process takes place (Figure 2.27).

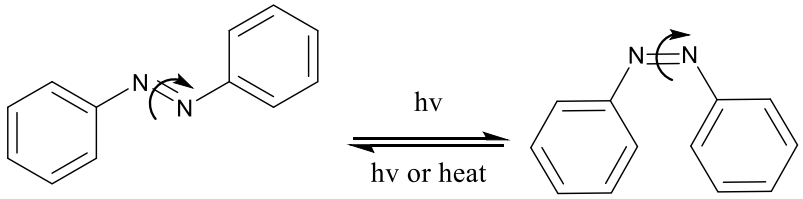

trans-isomer *cis*-isomer

Figure 2.27. Isomerization process of unsubstituted azobenzene photoswitch.

The UV-Vis spectrum of unsubstituted *trans*-azobenzene displays two absorption bands, the most intense band is related to an allowed π-π* transition centered at 320 nm, but it also displays another one due to a forbidden n-π* transition in the visible region (430 nm). These derivatives show a fast and efficient *E*/*Z* isomerization that can be controlled with different irradiation wavelengths. Moreover, the thermal-back reaction usually occurs at room temperature, although, like other photochemical properties, are very dependent on the chemical differences of the molecule, ranging from microseconds up to days.

The isomerization mechanism has been subject to research for a long time, as multiple pathways have been invoked to explain experimental observations.[91] These pathways are based on rotation, inversion, concerted inversion or inversion-assisted rotation as it has been reported (Figure 2.28). But, it is hard to delimit the isomerization in one specific pathway, since it is very dependent on the experimental conditions. Therefore, it is very probable that all the pathways would be correct and they could take place at the same time.

[91] Fujino, T.; Arzhantsev, S. Y.; Tahara, T., Femtosecond Time-Resolved Fluorescence Study of Photoisomerization of trans-Azobenzene *J. Phys. Chem. A* **2001,** *105*, 8123-8129.

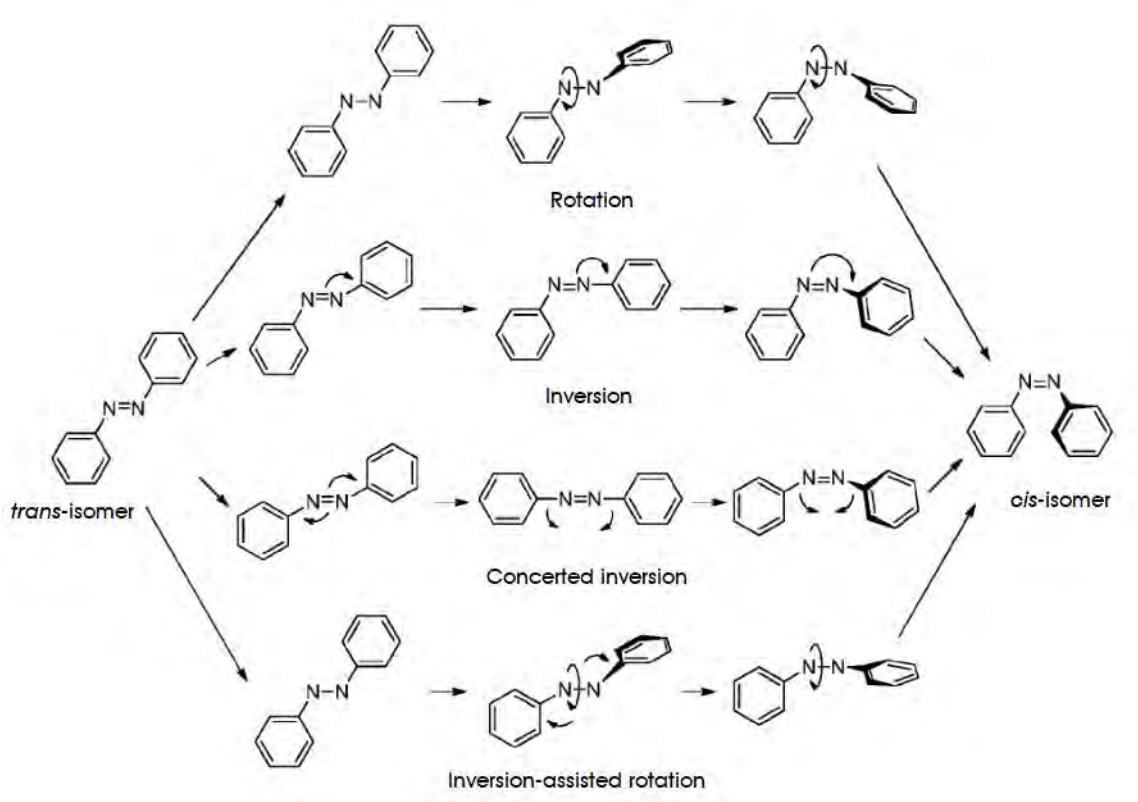

Figure 2.28. Different isomerization pathways for azobenzene photoswitches. [92]

Azobenzene derivatives have been the most widely used class of photoswitch for the control of biomolecules. As it has been mentioned before, biological applications require the use of non-damaging light, so different approaches were undertaken to design new far-red photoswitches. As in other photoswitches, the properties of azobenzenes are highly determined by the electronical properties of the substituents which are placed on the phenyl rings. For instance, two essential properties to apply these photoswitches in biomolecules are the absorption wavelength and the half-life time of the photoisomer.

The first strategy in the design of azobenzenes to be applied in biological systems was the presence of a donor substituent in each phenyl ring or a push-pull system. Push-pull azobenzenes are so-called because one phenyl ring is substituted with an electron donating group, while the other ring is substituted with an electron withdrawing group. This type of substitution confers a strong charge transfer character into the π- π* transition, consequently, a red-shift absorption occurs overlapping the n-π* and π- π* transitions. In general, as the wavelength of maximum absorbance of the thermally stable isomer red

[92] Bandara, H. M. D.; Burdette, S. C., Photoisomerization in different classes of azobenzene *Chem. Soc. Rev.* **2012,** *41*, 1809-1825.

shifts, the thermal half-life of the *cis*-isomer shortens.[93] So, it could be difficult to find a far-red azobenzene-based molecular switch because the thermal-back reaction would be so fast that the photoisomer could not be detected. Therefore, it would prevent the use of these derivatives on the photocontrol of biological properties.

Moreover, when an azobenzene is dissolved in a strong acid solution, one proton is placed on one nitrogen atom of the azo moiety resulting in a derivative called azonium ion. This kind of molecular switch shows a huge red-shift absorption, but the thermal-back reaction is also very fast (typically in microseconds),[94] so the photoisomer can only be detected by flash photolysis spectroscopy.

To adress this problem, a new derivative was designed by Prof. Woolley and colleagues to evaluate the characteristics of the azonium ion. This photoswitch consisted of a tetraorthomethoxy derivative with a piperazine substituent in the *para* positions of both phenyl rings. The presence of the methoxy groups stabilizes the azonium ion by resonance and forming H-bonding between the hydrogen in the azo bond and the *ortho* methoxy group (Figure 2.29).

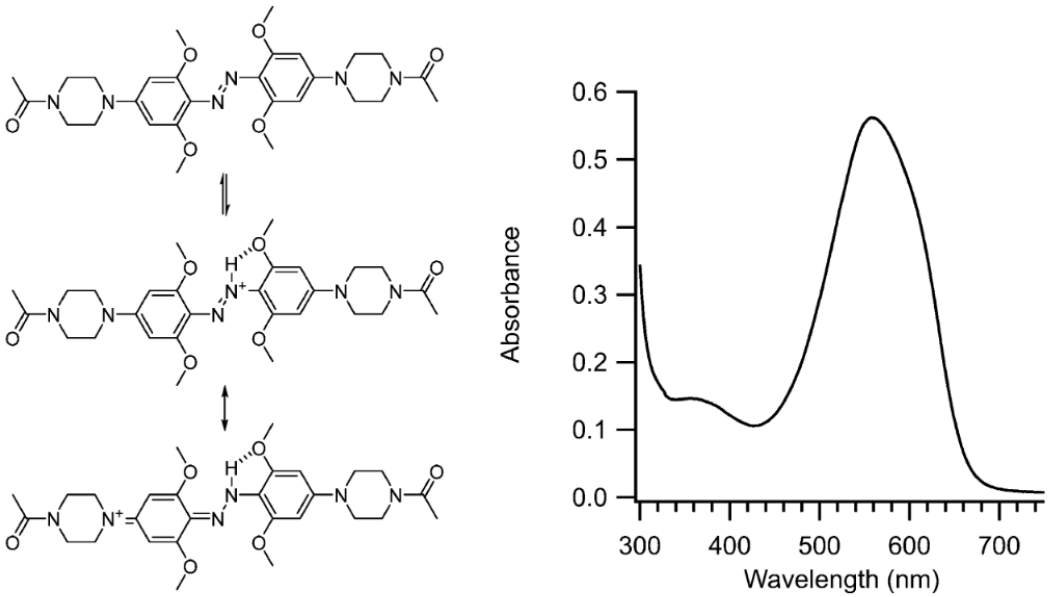

Figure 2.29. Tetraorthomethoxy azobenzene and its UV-Vis spectrum. [95]

[93] Beharry, A. A.; Woolley, G. A., Azobenzene photoswitches for biomolecules *Chem. Soc. Rev.* **2011,** *40*, 4422-4437.

[94] Sanchez, A. M.; Barra, M.; de Rossi, R. H., On the Mechanism of the Acid/Base-Catalyzed Thermal Cis−Trans Isomerization of Methyl Orange *J. Org. Chem.* **1999,** *64*, 1604-1609.

[95] Samanta, S.; Babalhavaeji, A.; Dong, M.-x.; Woolley, G. A., Photoswitching of ortho-Substituted Azonium Ions by Red Light in Whole Blood *Angew. Chem. Int. Ed.* **2013,** *52*, 14127-14130.

Surprisingly, the azonium ion was formed under physiological pH and a thermal relaxation half-life of seconds was achieved, a million times slower than that of a typical azonium ion. Therefore, the use of long wavelength to irradiate this compound could generate large fractions of the photoisomer. Thus, this azobenzene-based molecular switch fulfils the most important requirements to be applied in biological uses.

But it should be noted that the main drawback of azobenzene-based molecular switches to be applied in biological systems is their possible reduction under physiological conditions, which could prevent their use *in vivo*.[96] This fact occurs due to the presence of glutathione in animal cells, which is a short peptide able to break down the azo bond. Therefore, many efforts were applied to design new azobenzenes which are not reduced by glutathione.[97]

3.2. Ring opening/closing photoswitches.

These photoswitches are based on a reversible process of two distinct forms by absorption of different colors. This range of molecules undergo photoswitchable behavior as ring-opening/closing. This change in the molecule leads to a huge red-shift of the absorption bands of both forms; this phenomenon is known as photochromism.[98,99]

Several photoswitchable structures experiment this process. Therefore, in the following, the most important ones will be described.

3.2.1. Diarylethenes

Photochromic diarylethenes have been widely studied due to their good photoswitchable properties in their open-ring and closed-ring forms. These molecules are known to undergo reversible intramolecular pericyclic reactions. The general structure and the photoisomerization process is depicted in the figure below.

[96] Boulègue, C.; Löweneck, M.; Renner, C.; Moroder, L., Redox Potential of Azobenzene as an Amino Acid Residue in Peptides *ChemBioChem* **2007,** *8*, 591-594.
[97] See ref. 93.
[98] Brown, G. H., *Photochromism*. Wiley: New York, 1971.
[99] Irie, M.; Yokoyama, Y.; Seki, T., *New Frontiers in Photochromism*. Springer Japan: Tokio, 2013.

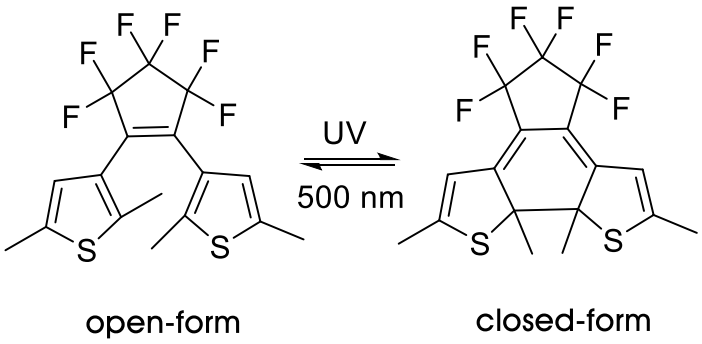

Figure 2.30. General structure of diarylethene-based molecular switches.

As it is observed, when the sample is under the effect of UV-light, a ring-closing reaction takes place, but when the resulting product is under the exposure to visible light, the opposite reaction occurs, recovering the initial isomer.

This simple structure meets the requirements needed to be a photochromic system, since the open-form absorbs in the UV region (λ_{max}=300 nm), whereas the absorption band of the closed-form is placed in the visible region (λ_{max}=500 nm).[100] Moreover, the closed-form is usually stable at high temperatures, so the process is just reversible by light. This structure has been used as a pattern to develop new diarylethene-based molecular switches, because the photochemical / photophysical properties can be easily tuned changing the substituents present in the molecule.

Therefore, many efforts were directed to the displacement of the absorption wavelength of the closed-form to lower energies. The first attempt to get this goal was the introduction of electron-donating groups in the aryl moieties (Figure 2.31).

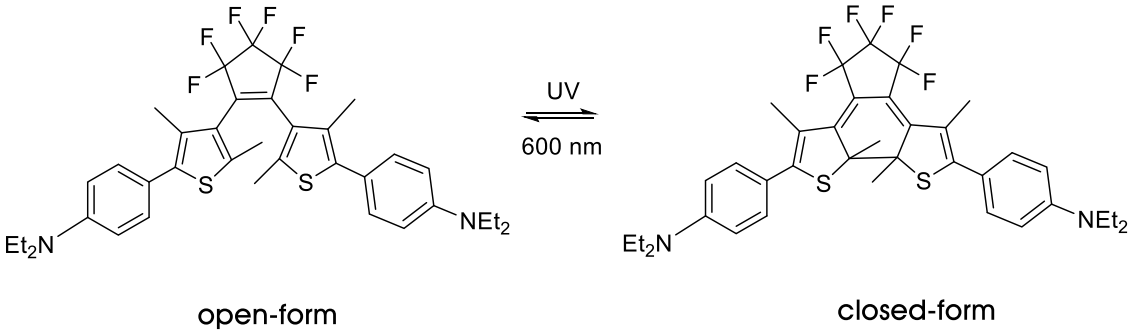

Figure 2.31. Reversible photocyclization of diarylethene-based molecular switches. [101]

[100] Kobatake, S.; Yamada, T.; Uchida, K.; Kato, N.; Irie, M., Photochromism of 1,2-Bis(2,5-dimethyl-3-thienyl)perfluoro- cyclopentene in a Single Crystalline Phase *J. Am. Chem. Soc.* **1999,** *121*, 2380-2386.
[101] Irie, M.; Mohri, M., Thermally irreversible photochromic systems. Reversible photocyclization of diarylethene derivatives *J. Org. Chem.* **1988,** *53*, 803-808.

Through this strategy, it was possible to red-shift the absorption band around 100 nm. Thus, the introduction of a diethylamino group in *para* positions of the phenyl rings yielded an absorption band centered at 600 nm. But this is not the only property that can be changed by introducing electron-donating groups. For instance, by adding this kind of substituent the quantum yield of cyclization increases. In contrast, the ring opening quantum yield is highly decreased. This is considered to be due to the extent of the π conjugation as, when the temperature is increased, the quantum yield of this process is enhanced. This occurs since when the temperature is higher, the phenyl ring rotation is greater, consequently the extension of the π conjugation is suppressed to some extent.[102]

Moreover, electron-withdrawing groups have been introduced in the structure of these photoswitches. Apart from changing the UV-Vis absorption, they also decrease the thermal stability of the closed-state.[103] It should be noted that all derivatives based on diarylethenes present a high fatigue resistance.[104]

3.2.2. Spiropyrans.

This is an important photochromic system able to change its color under the influence of activating light. It has been known since the early 20th century,[105] but it was not until the 1920s that their reversible thermochromic properties were reported.[106] Afterwards, their photochromic behavior started to be subject of study.[107]

The photochromic behavior of these derivatives lies in the presence of a C_{spiro}-O bond that can be photoreleased under UV-light, resulting in a zwitterionic molecule with an extended conjugation, which absorbs in the visible region (λ_{max}>500 nm) (Figure 2.32).

[102] Irie, M.; Sakemura, K.; Okinaka, M.; Uchida, K., Photochromism of Dithienylethenes with Electron-Donating Substituents *J. Org. Chem.* **1995,** *60*, 8305-8309.
[103] Gilat, S. L.; Kawai, S. H.; Lehn, J.-M., Light-Triggered Molecular Devices: Photochemical Switching Of optical and Electrochemical Properties in Molecular Wire Type Diarylethene Species *Chem. Eur. J.* **1995,** *1*, 275-284.
[104] Irie, M., Diarylethenes for Memories and Switches *Chem. Rev.* **2000,** *100*, 1685-1716.
[105] Decker, H.; v. Fellenberg, T., Zur Begründung der Oxoniumtheorie *Liebigs Ann. Chem.* **1909,** *364*, 1-44.
[106] Dilthey, W.; Berres, C.; Hölterhoff, E.; Wübken, H., Beitrag Zur Kenntnis der Spiro-di-benzopyrane (Heteropolare Kohlenstoffverbindungen. IV) *J. Prakt. Chem.* **1926,** *114*, 179-198.
[107] Hirshberg, Y.; Fischer, E., Photochromism and reversible multiple internal transitions in some spiropyrans at low temperatures. Part I *J. Chem. Soc.* **1954**, 297-303.

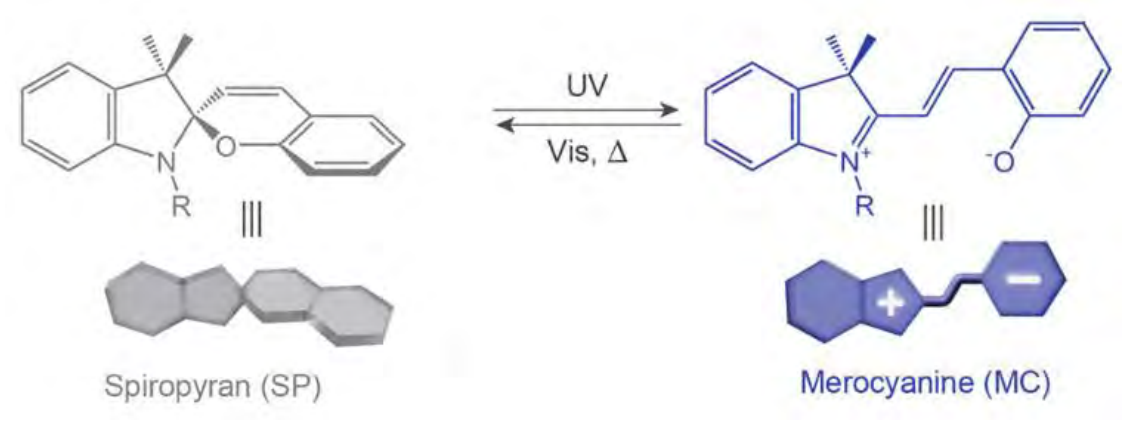

Figure 2.32. General structure of spiropyran and its reversible photochemical process. [108]

As it is shown in the figure above, the structure is formed by an indoline group linked to a chromene moiety by a spiro joint. Many derivatives have been synthesized using the method reported by Wizinger in 1940, which consists of the condensation of methylene bases with o-hydroxy aromatic aldehydes.[109]

The isomerization shown in Figure 2.32 involves a huge change in the structure, apart from a large change in its polarity. Therefore, this fact affects directly to the difference in the solubility of both forms. It should be noted that this equilibrium can be displaced either thermally or photochemically by different types of light.

As with other photoswitches detailed before, the properties of these derivatives could be tuned easily by changing the substituents present in the structure. For instance, the derivative which displays a nitro group in the 6-position of the benzopyran moiety could be remarkable. It presents an absorption band centered at 560 nm and the equilibrium is very displaced to the formation of the merocyanine form.[110] This equilibrium could also be controlled by means of external agents as the solvent, due to the differences in the polarity of both forms. The zwitterionic form will be favored in polar solvents by the stabilization made by hydrogen bonds between the solvent and the merocyanine form.[111]

[108] Klajn, R., Spiropyran-based dynamic materials *Chem. Soc. Rev.* **2014,** *43*, 148-184.
[109] Wizinger, R.; Wenning, H., Über intramolekulare Ionisation *Helv. Chim. Acta* **1940,** *23*, 247-271.
[110] Chibisov, A. K.; Görner, H., Photoprocesses in Spiropyran-Derived Merocyanines *J. Phys. Chem. A* **1997,** *101*, 4305-4312.
[111] E. Wetzler, D.; F. Aramendía, P.; Laura Japas, M.; Fernández-Prini, R., Spectroscopy and thermal decay of a photomerocyanine in mixtures of polar and nonpolar solvents *Phys. Chem. Chem. Phys.* **1999,** *1*, 4955-4959.

3.2.3. Donor acceptor Stenhouse adducts (DASAs).

These novel derivatives are the most recent photochromic molecular switches that have been reported up until now. The first generation of these photoswitches were reported by Read de Alaniz in 2014,[112] which was based on a push-pull system since there are two different parts, a donor and an acceptor group that are linked through a triene chain (Figure 2.33).

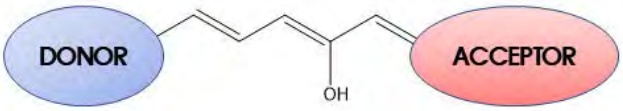

Figure 2.33. General structure of a donor acceptor Stenhouse adduct.

The form that is shown in Figure 2.33 is strongly colored in solution, so it presents an absorption band in the visible region. When it is under exposure of visible light, it results in a colorless solution. Therefore, the photochemical process in these photoswitches involves a negative photochromic process (Figure 2.34).

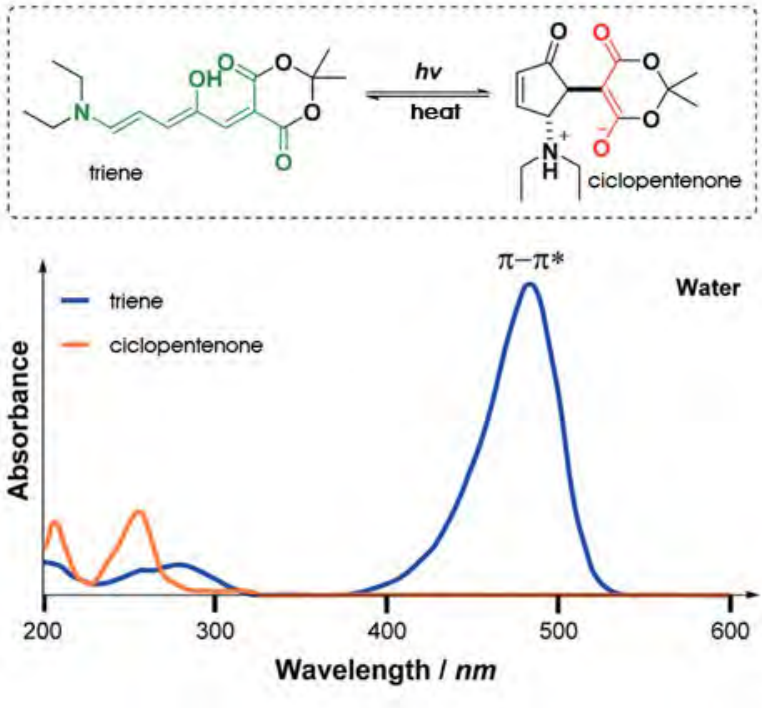

Figure 2.34. Photocyclization of DASAs derivatives and their absorption bands.[113]

[112] Helmy, S.; Oh, S.; Leibfarth, F. A.; Hawker, C. J.; Read de Alaniz, J., Design and Synthesis of Donor–Acceptor Stenhouse Adducts: A Visible Light Photoswitch Derived from Furfural *J. Org. Chem.* **2014,** *79*, 11316-11329.

[113] Lerch, M. M.; Szymanski, W.; Feringa, B. L., The (photo)chemistry of Stenhouse photoswitches: guiding principles and system design *Chem. Soc. Rev.* **2018,** *47*, 1910-1937.

As it is observed, the triene-form presents a large absorption band in the visible region. In contrast, when it is irradiated a photochemical reaction occurs, leading to a cyclic form breaking the conjugation seen in the triene, which absorbs UV light. This process is reversible; when the zwitterionic form is heated in a specific solvent, the triene is recovered.

There are three generations based on DASAs up to now. The only difference between the first and second generation depends on the donor group used, which is essential to determine the properties shown by these derivatives. For instance, different amines were used as donor groups; the first generation of these photoswitches was based on the use of aliphatic amines. On the contrary, the second generation derivatives used cyclic and aromatic amines (Figure 2.35).

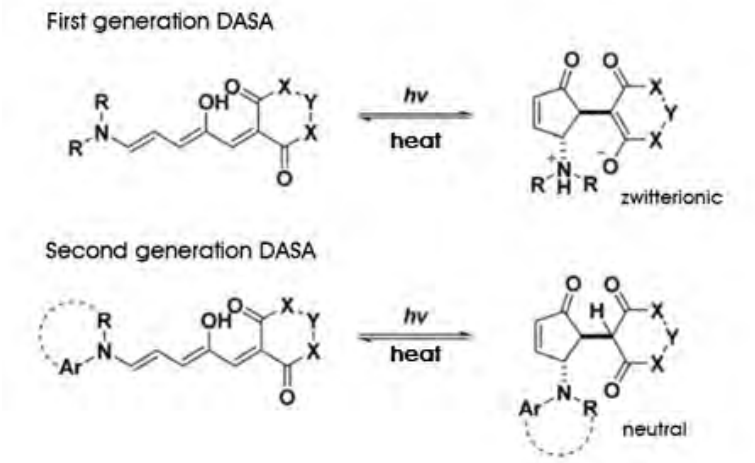

Figure 2.35. Classification of different DASA derivatives depending on the donor used.

Recently, a third generation has emerged resulting in new diverse DASA derivatives, in which the structural changes to the carbon acid acceptor facilitate the ring-opening reaction with electron deficient amine donors.[114]

In this kind of photoswitches, the UV-Vis absorption band can be easily tuned changing the donor and acceptor groups reaching near infrared absorption. For instance, the effect of changing the acceptor group was tested by Read de Alaniz; when it increased the ability to accept electron density, the absorption band red-shifted (Figure 2.36).

[114] Hemmer, J. R.; Page, Z. A.; Clark, K. D.; Stricker, F.; Dolinski, N. D.; Hawker, C. J.; Read de Alaniz, J., Controlling Dark Equilibria and Enhancing Donor–Acceptor Stenhouse Adduct Photoswitching Properties through Carbon Acid Design *J. Am. Chem. Soc.* **2018,** *140*, 10425-10429.

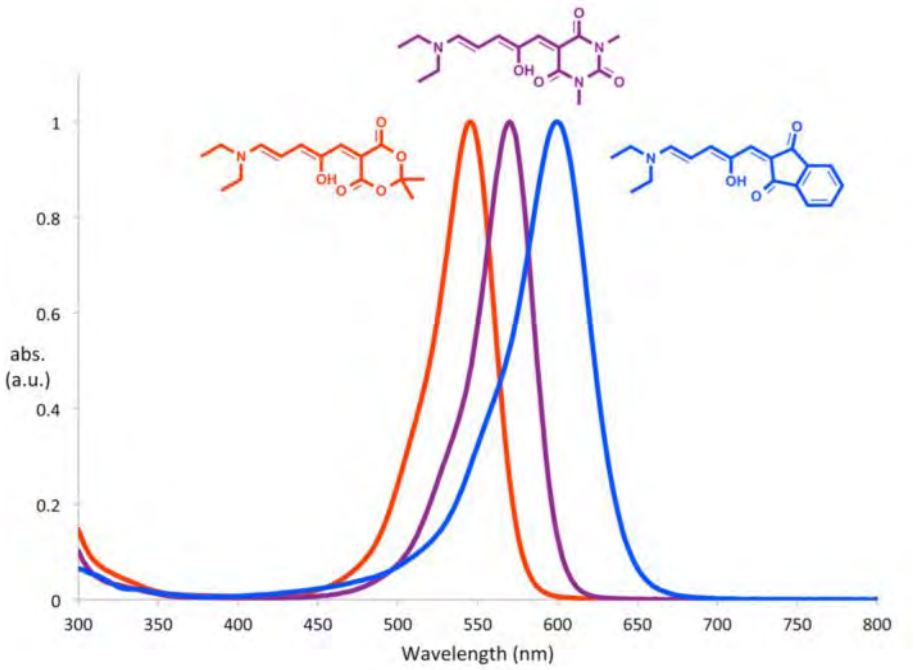

Figure 2.36. Effect on the UV-Vis spectrum by changing the acceptor group. [115]

Moreover, the same experiment was carried out changing the donor group using amines with different ability of donating electron density. As it can be seen in Figure 2.37, when an electron-rich amine is used as a donor group, the absorption band suffers a bathochromic shift, reaching intense absorption bands in the near-infrared region.

[115] See ref. 112.

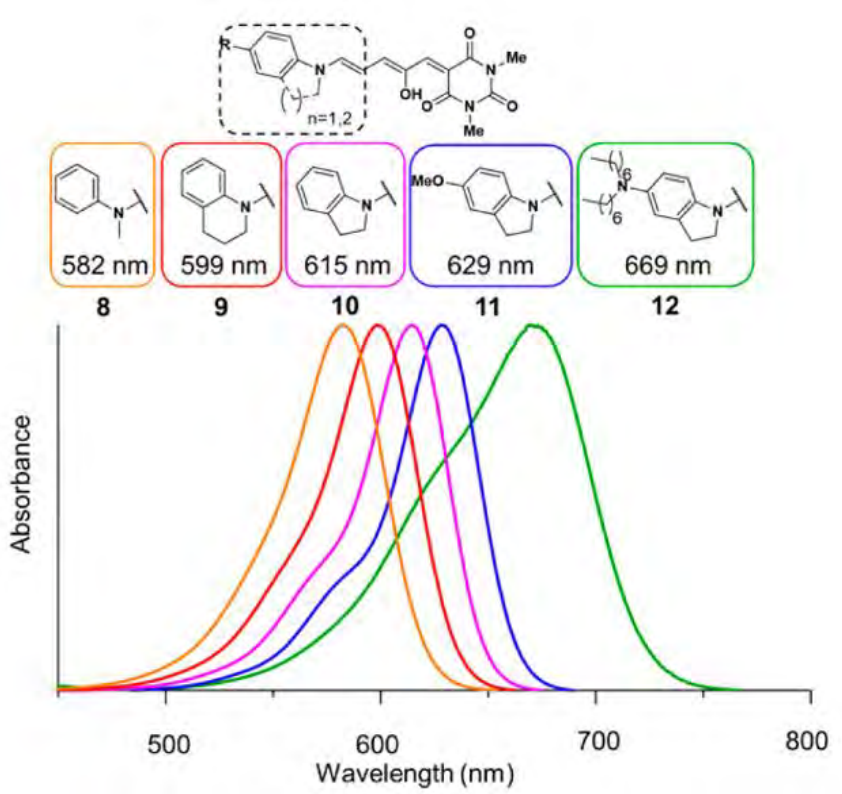

Figure 2.37. Effect on the UV-Vis spectrum changing the donor group. [116]

As it has been demonstrated, the UV-Vis spectra of these derivatives are easily tunable and different long wavelengths could be used to carry out the photocyclization process. The mechanism of this photoswitching process is not totally clear, since not many reports have been published up to now. The most accepted mechanism consists of several steps (Figure 2.38).

[116] Hemmer, J. R.; Poelma, S. O.; Treat, N.; Page, Z. A.; Dolinski, N. D.; Diaz, Y. J.; Tomlinson, W.; Clark, K. D.; Hooper, J. P.; Hawker, C.; Read de Alaniz, J., Tunable Visible and Near Infrared Photoswitches *J. Am. Chem. Soc.* **2016,** *138*, 13960-13966.

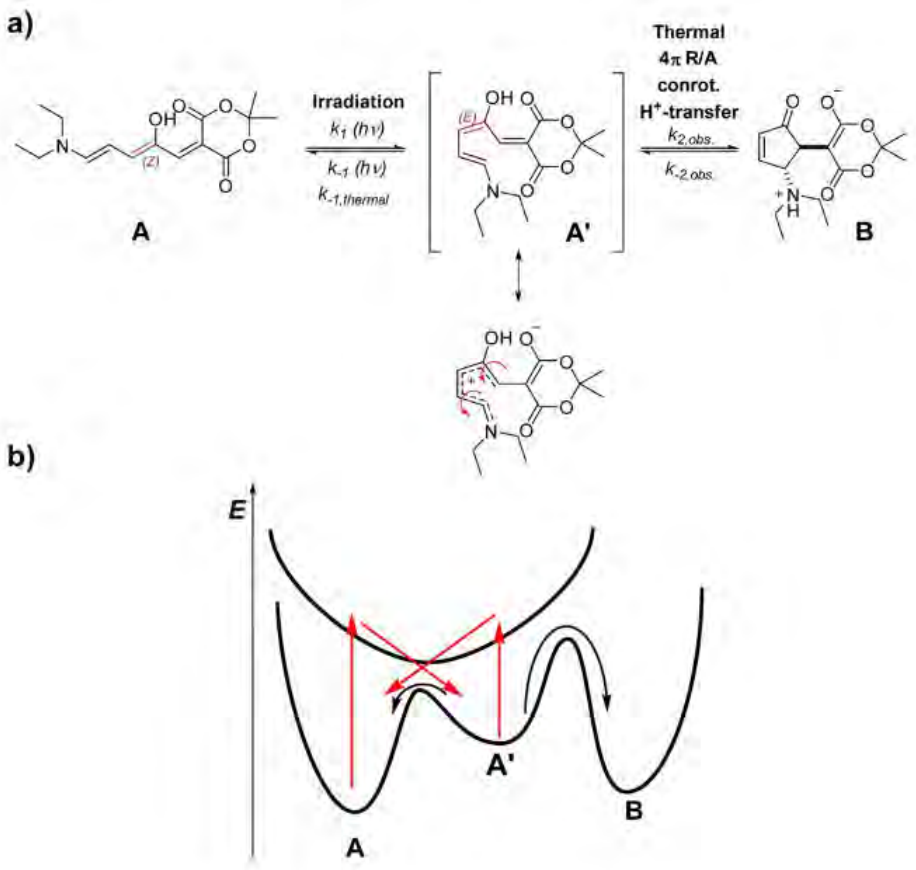

Figure 2.38. Isomerization mechanism on DASA derivatives. [117]

First, a photoisomerization *Z-E* is carried out throughout the absorption of a photon. Then, a conrotatory thermally allowed 4π-electrocyclization occurs to result in compound B.[118]

Promising features and applications are expected for this kind of molecular switches. As in spiropyran-based photoswitches, in these derivatives a very large conformation change occurs and a huge difference in solubility between both forms was found.

[117] Lerch, M. M.; Wezenberg, S. J.; Szymanski, W.; Feringa, B. L., Unraveling the Photoswitching Mechanism in Donor–Acceptor Stenhouse Adducts *J. Am. Chem. Soc.* **2016,** *138*, 6344-6347.
[118] See ref. 113.

4. Applications.

Once it has been described how different structures can work as efficient molecular switches, in the following, several functions will be detailed, that can be controlled by them.

4.1. Photoswitchable peptides.

The incorporation of photoswitches into peptides is a research field that is acquiring a very large relevance lately, since it could allow us to control the peptide conformation and consequently, its function.

For this purpose, several approaches can be evaluated as was described by Renner and Moroder (Figure 2.39).

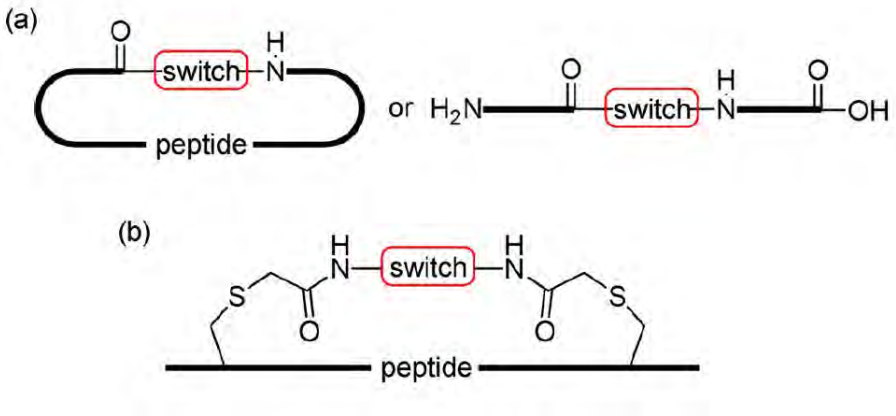

Figure 2.39. Different pathways to photocontrol a peptide. [119]

As is shown in Figure 2.39, the photoswitch could be incorporated into peptides using different strategies: (a) into the backbone of the peptide chain, which can be linear or cyclic peptides or (b) throughout the sulfur atoms of two cysteines to result in a cross-linked peptide.

4.1.1. Photoresponsive switches into the backbone peptide.

One of the first examples of photoregulation of a cyclic peptide conformation by the introduction of an azobenzene unit was reported by Chmielewsky in 1995. It was demonstrated that the azobenzene in its *cis*-isomer facilitates a β-turn conformation.[120]

[119] Renner, C.; Moroder, L., Azobenzene as Conformational Switch in Model Peptides *ChemBioChem* **2006,** *7*, 868-878.
[120] Ulysse, L.; Cubillos, J.; Chmielewski, J., Photoregulation of cyclic peptide conformation *J. Am. Chem. Soc.* **1995,** *117*, 8466-8467.

This conformation is present in many peptides with amazing biological functions such as peptide hormones.[121]

For instance, it was evaluated the photocontrol of a decapeptide called somatostatin, which regulates several hormonal functions such as the cell growth. When the azobenzene was in *trans* configuration, the peptide conformation was inactive, but when it was irradiated with light, the conformational structure changed adopting a β-turn conformation, getting its biological activity because an enhanced affinity for the receptors over the *trans*-form was found.[122]

Azobenzenes have also been introduced into linear peptides; it is well known that the conformation adapted by a peptide is determined by the interactions between the side chains such as hydrogen bondings (Figure 2.40).

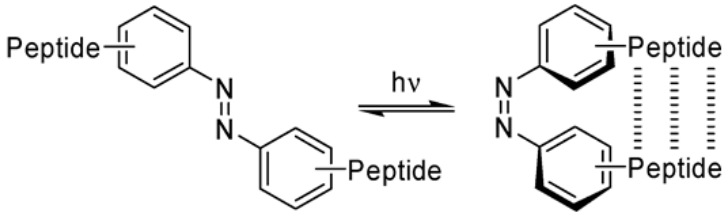

Figure 2.40. Enhancement of the peptide-peptide interaction after an isomerization process. [123]

Through this strategy a peptide can be folded to a β-hairpin structure. This conformation implies two adjacent antiparallel peptide strands which are stabilized by the action of an azobenzene unit. Moreover, this conformation could be established by a reversible process.

4.2.1. Cross-linked peptides.

The α-helix is the classic secondary structure of a peptide, it is essential in many peptides or proteins to maintain its biological activity. For instance, many efforts have

[121] Rose, G. D.; Glerasch, L. M.; Smith, J. A., Turns in Peptides and Proteins. In *Advances in Protein Chemistry*, Anfinsen, C. B.; Edsall, J. T.; Richards, F. M., Eds. Academic Press: 1985; Vol. 37, pp 1-109.
[122] Ulysse Jr., L. G.; Chmielewski, J., A Light-Activated β-Turn Scaffold within a Somatostatin Analog: NMR Structure and Biological Activity *Chem. Biol. Drug Des.* **2006,** *67*, 127-136.
[123] Aemissegger, A.; Kräutler, V.; van Gunsteren, W. F.; Hilvert, D., A Photoinducible β-Hairpin *J. Am. Chem. Soc.* **2005,** *127*, 2929-2936.

been made to stabilize it.[124] In this way, it could enhance the biological function of the peptide.

The inspection of new molecules able to be attached into a peptide chain has increased over the years. For this purpose, the peptide must contain two cysteine residues that are cross-linked by different types of molecular switches. For example, Sampedro, in collaboration with Woolley, attached a PSB-retinal based molecular switch to photocontrol the secondary structure of a model peptide (Figure 2.41).

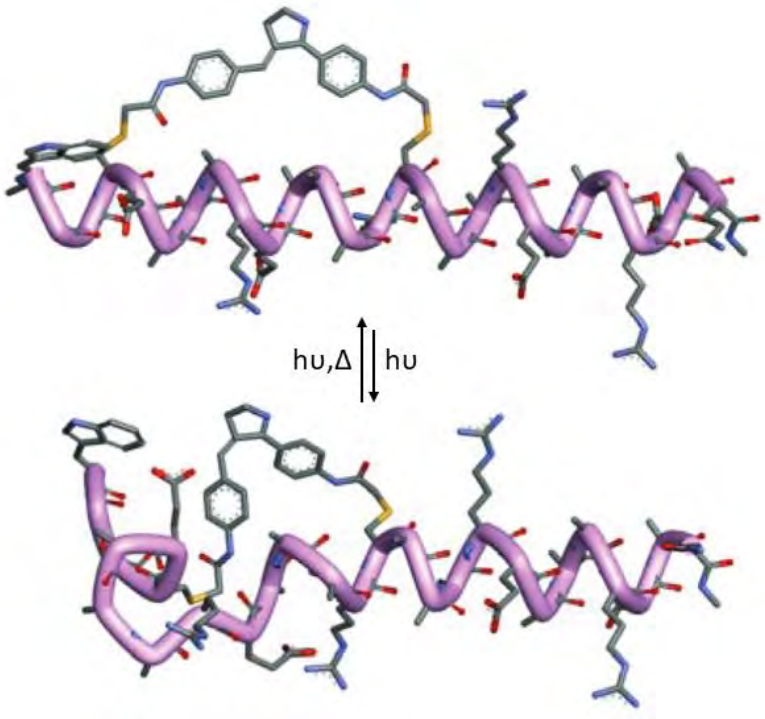

Figure 2.41. Conformational change of a peptide due to the isomerization of a photoswitch based on PSB-retinal. [125]

As is observed in Figure 2.41, a reversible photocontrol over α-helix folding was achieved by the isomerization of the photoswitch. Throughout the use of PSB-retinal based molecular switch, a very large conformational change was achieved in the peptide chain. In detail, using this kind of photoswitch, a 10 Å change in the end-to-end distance can be obtained upon isomerization.

[124] Forood, B.; Feliciano, E. J.; Nambiar, K. P., Stabilization of alpha-helical structures in short peptides via end capping *PNAS* **1993,** *90*, 838-842.
[125] Blanco-Lomas, M.; Samanta, S.; Campos, P. J.; Woolley, G. A.; Sampedro, D., Reversible Photocontrol of Peptide Conformation with a Rhodopsin-like Photoswitch *J. Am. Chem. Soc.* **2012,** *134*, 6960-6963.

This system was used to determine the high influence of the surrounding on the photoswitching process in this type of molecular switches.[126]

Other photoswitches have been widely used on the photocontrol of peptides; indeed azobenzenes are the most widely used in this field.[127] They have been used to photocontrol the function of many peptides.[128] For instance, Prof. Woolley designed an azobenzene able to be attached into a peptide through two cysteine residues. The peptide in its α-helix conformation was very fluorescent but when it was irradiated with the appropriate light and the isomerization of the azo bond took place, a notable fluorescence decrease was found (Figure 2.42).

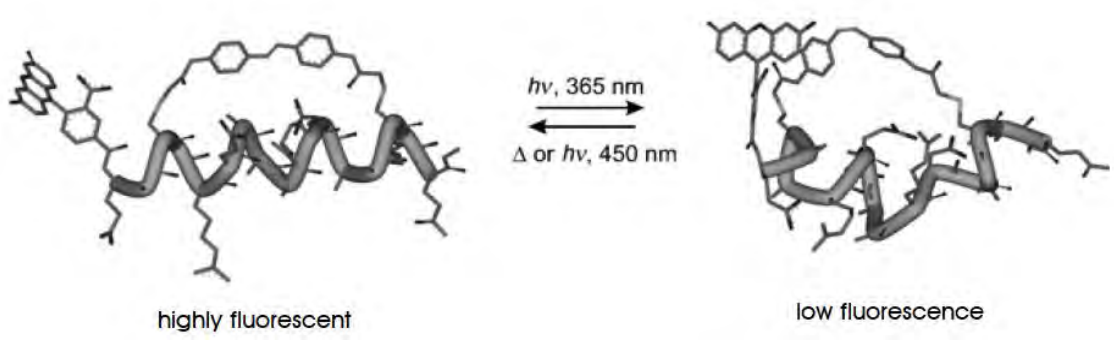

Figure 2.42. Photocontrol of the fluorescence of a peptide by the use of a molecular switch. [129]

4.2. Photopharmacology.

Most of the medical treatments used are non-specific, since they are based on the use of a bioactive compounds, which can interact with the whole body and not only with the target, as was described in PDT (Section 2.1). Therefore, the use of this approach could be the main reason for many side effects. Photopharmacology is an emerging strategy to activate or deactivate a drug by light, [130] providing a high selectivity to sort out the problems related to the lack of specificity of medical treatments.

---

[126] García-Iriepa, C.; Gueye, M.; Léonard, J.; Martínez-López, D.; Campos, P. J.; Frutos, L. M.; Sampedro, D.; Marazzi, M., A biomimetic molecular switch at work: coupling photoisomerization dynamics to peptide structural rearrangement *Phys. Chem. Chem. Phys.* **2016,** *18*, 6742-6753.

[127] Kumita, J. R.; Smart, O. S.; Woolley, G. A., Photo-control of helix content in a short peptide *PNAS* **2000,** *97*, 3803-3808.

[128] Szymański, W.; Beierle, J. M.; Kistemaker, H. A. V.; Velema, W. A.; Feringa, B. L., Reversible Photocontrol of Biological Systems by the Incorporation of Molecular Photoswitches *Chem. Rev.* **2013,** *113*, 6114-6178.

[129] Beharry, A. A.; Wong, L.; Tropepe, V.; Woolley, G. A., Fluorescence Imaging of Azobenzene Photoswitching In Vivo *Angew. Chem. Int. Ed.* **2011,** *50*, 1325-1327.

[130] Broichhagen, J.; Frank, J. A.; Trauner, D., A Roadmap to Success in Photopharmacology *Acc. Chem. Res.* **2015,** *48*, 1947-1960.

The aim of photopharmacology is to control the action of a bioactive compound in a specific zone during a limited period of time (Figure 2.43). For this purpose, different drugs have been designed that can be activated by means of external agents. It has been proved that the most appropriate external input to activate/deactivate a drug is the use of light due to the numerous benefits detailed in Section 1.2.3.1.

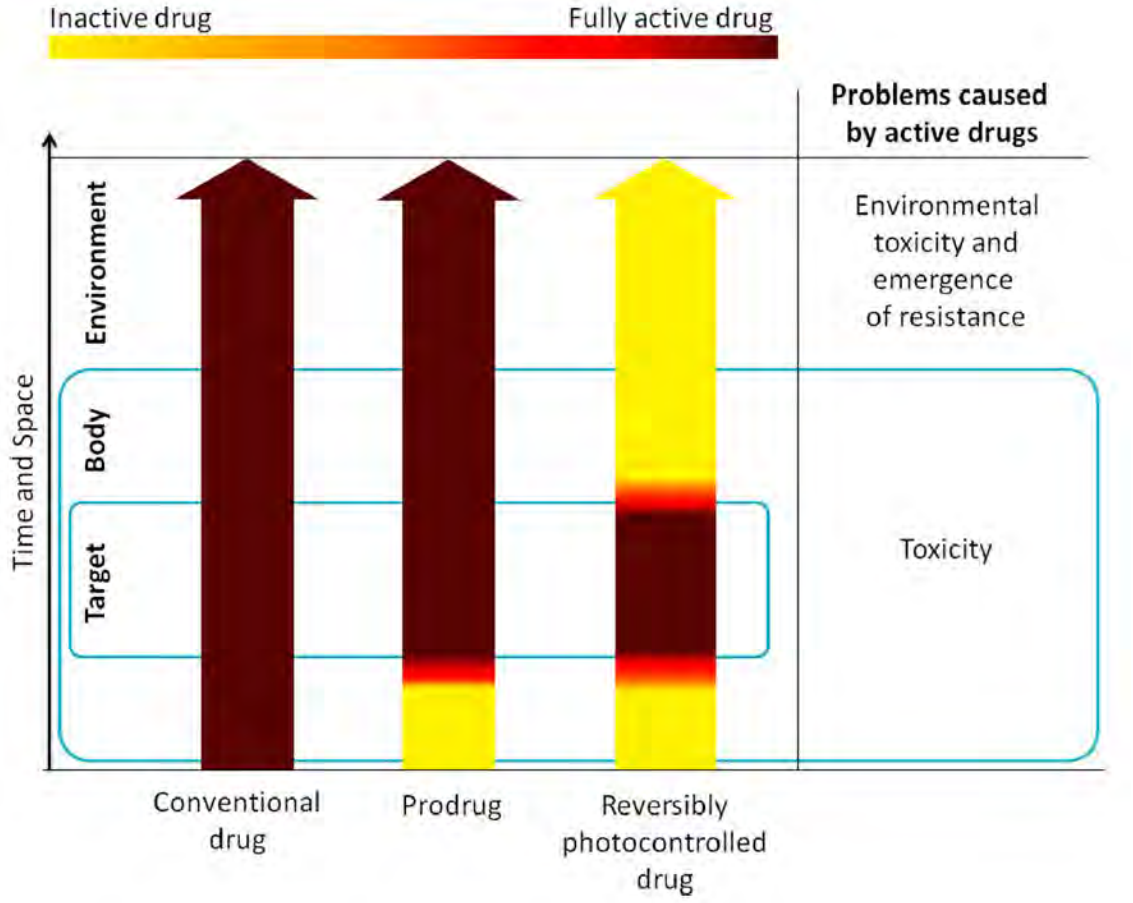

Figure 2.43. Drug activity over time and space for a conventional drug, a prodrug, and a reversibly photocontrolled drug. [131]

As is shown in Figure 2.43, the use of photocontrollable drugs instead of other drugs is of great importance, as by using this methodology the therapeutic effects will be focused and enhanced on the affected area.

One way to design pharmacological agents is to introduce a photoswitchable moiety in bioactive compounds. Thus, it would be possible to change the structure of an active derivative upon irradiation with light. So, through the use of photoswitches this process can be reversible photochemically.

[131] Velema, W. A.; Szymanski, W.; Feringa, B. L., Photopharmacology: Beyond Proof of Principle *J. Am. Chem. Soc.* **2014,** *136*, 2178-2191.

4.2.1. Aspects to design an efficient photoswitchable drug.

Many efforts have been made to the design, synthesis and study of new derivatives based on the azobenzene core, since as it was said before, they are the most widely studied system in this field. To get an efficient photoswitchable drug, several properties should be evaluated.

- Pharmacological activity.

When a photoswitchable unit is introduced into a bioactive compound, it should be evaluated to note if the designed compounds retain the biological activity. If the compound loses its natural activity, a rational design is carried out to enhance the interaction between the molecule and its target.[132] Generally, when an active compound is modified to make it photoresponsive, a decrease in the pharmacological activity occurs. So, it is very important to carry out a prior study based on affinity calculations or X-ray analysis to check how the active part responsible for the bioactivity interacts with the target. Ideally, once these studies are completed, a photoswitchable drug is designed which would lead to a very large change after the isomerization to prevent the interaction of one isomer with the target (Figure 2.44).

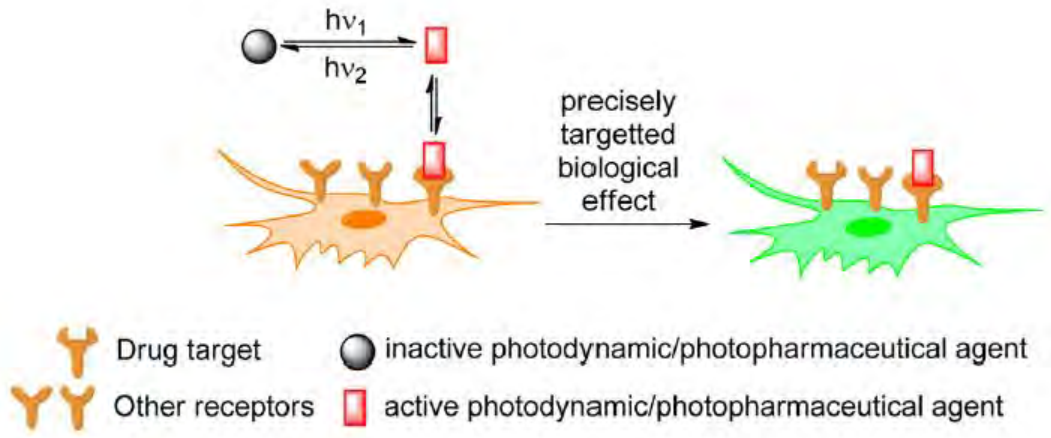

Figure 2.44. Light-induced structural change of a pharmaceutical agent.[133]

- Wavelength.

This is an essential property to be rationalized due to its high importance. This wavelength must promote, for instance, the isomerization of a double bond. Moreover, as it has been said before, the main reasons for using long irradiation wavelengths are the

[132] Jorgensen, W. L., Efficient Drug Lead Discovery and Optimization *Acc. Chem. Res.* **2009,** *42,* 724-733.
[133] See ref. 131.

use of non-damaging light and the wavelength dependent on the depth of tissue penetration.

The useful irradiation wavelength in pharmacotherapy goes from 600 nm to 1200 nm, and this region of the spectrum is termed "*therapeutical spectral window*". As mentioned before, many efforts have been made to get compounds with high absorption bands in this spectral window. Recently, two-photon absorption processes are being performed to enable the use of near-IR light.[134]

- Photostationary state.

This property is essential to be evaluated, since it is not very common to transform quantitatively the *trans*-stable isomer into the *cis*-form when a photoswitch is irradiated.[135] The isomer ratio in the PSS determines the difference in the therapeutic activity that can be observed. In other words, if the PSS is totally displaced to the less stable isomer, with this one being the biologically active isomer, upon irradiation the effect will be dramatically enhanced. So, the aim of many works is to "turn *off*/*on*" the effect of a drug by certain types of light, this way it would be possible to activate the biological effect of a photoresponsive drug.

- Half-life of the photoisomer.

As it has been discussed before, this property can be tuned easily by changing the substituents present, for instance, in the azobenzene core. Moreover, in each specific application is desired a specific half-life of the thermodynamically unstable isomer. Therefore, through this strategy can be achieved the requirements needed to use a photoswitch in an application. For example, if the photoswitchable drug gets its therapeutic activity after irradiation, it must retain its activity for the essential time within body, and then it will deactivate itself, minimizing the side effects.

4.2.2. Photoswitchable moieties applied in photopharmacology.

Hereunder, several applications will be detailed, which are controlled by the use of light to effectively activate/deactivate the therapeutic effect.[136] Azobenzenes are usually employed to induce the structural change in the therapeutic agent due to its well-known good properties.

---

[134] Bort, G.; Gallavardin, T.; Ogden, D.; Dalko, P. I., From One-Photon to Two-Photon Probes: "Caged" Compounds, Actuators, and Photoswitches *Angew. Chem. Int. Ed.* **2013,** *52*, 4526-4537.

[135] Bléger, D.; Schwarz, J.; Brouwer, A. M.; Hecht, S., o-Fluoroazobenzenes as Readily Synthesized Photoswitches Offering Nearly Quantitative Two-Way Isomerization with Visible Light *J. Am. Chem. Soc.* **2012,** *134*, 20597-20600.

[136] Hüll, K.; Morstein, J.; Trauner, D., In Vivo Photopharmacology *Chem. Rev.* **2018,** *118*, 10710-10747.

4.2.2.1. Photocontrol of antibacterial properties.

The increasing resistance of bacteria to antimicrobials is a serious problem that should be dealt with due to the overuse and misuse of antibiotics. For this reason, photopharmacology addresses this issue to use the light as an efficient tool to delimit the action of these bioactive compounds.

In our research group, several photoswitchable moieties capable of controlling the antimicrobial properties by light have been developed. In these derivatives, different antimicrobial agents were used such as ciprofloxacin and nalidixic acid. These antimicrobial agents were modified to include different photoactive moieties in their structure, which were based on phytochrome and hydantoin-based molecular switches that will be described in this thesis in Chapter 4.[137]

These derivatives demonstrated that the optical control of antibacterial properties could be achieved through the use of photopharmacology. The main drawback of these photodrugs to be applied was that their absorption wavelength was centered at 400 nm, so it was not placed in the therapeutical spectral window.[138]

In the same field, improved compounds based on azobenzene core were reported by Feringa, who for the first time achieved the use of green and violet light to photocontrol the antibacterial activity *in vivo*. But it should be remarked that he reported the photodrug shown in Figure 2.45, which presented a huge red absorption band (*ca.* 650 nm), moreover after its irradiation with red light an 8-fold difference in activity was found between both isomers.[139]

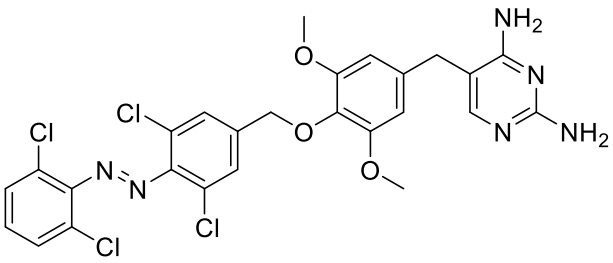

Figure 2.45. Far-red photoswitchable molecule with antibacterial properties.

[137] Martínez-López, D.; Yu, M.-L.; García-Iriepa, C.; Campos, P. J.; Frutos, L. M.; Golen, J. A.; Rasapalli, S.; Sampedro, D., Hydantoin-Based Molecular Photoswitches *J. Org. Chem.* **2015,** *80*, 3929-3939.
[138] Contreras-García, E.; Martínez-López, D.; Alonso, C. A.; Lozano, C.; Torres, C.; Rodríguez, M. A.; Campos, P. J.; Sampedro, D., Optical Control of Antimicrobial Activity in Quinolone Derivatives *Eur. J. Org. Chem.* **2017,** *2017*, 4719-4725.
[139] Wegener, M.; Hansen, M. J.; Driessen, A. J. M.; Szymanski, W.; Feringa, B. L., Photocontrol of Antibacterial Activity: Shifting from UV to Red Light Activation *J. Am. Chem. Soc.* **2017,** *139*, 17979-17986.

4.2.2.2. Photocontrol of cytotoxic activity.

Cancer is one of the most aggressive diseases in our times. The treatments designed to fight against cancer are non-specific and very dangerous for healthy cells. Therefore, the use of photopharmacology could be a good choice to address this problem.

Many researchers are working on the use of light to localize the chemotherapeutic effect in our body (Figure 2.46), thus reducing the side effects of chemotherapeutic treatments.

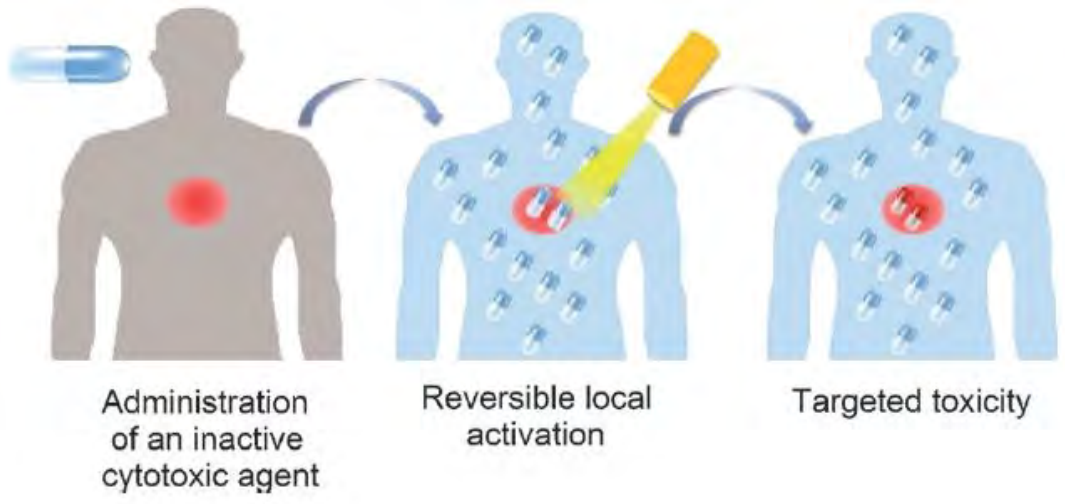

Figure 2.46. Local activation of a photoswitchable drug.[140]

In past years, new photoswitchable drugs with potent anticancer activity have been reported. For this purpose, a new cytotoxic Pt (II) complex has been designed with a photoswitch as ligand. This ligand is based on diarylethene structure; therefore, the activity of the whole complex is determined by the open/close form of the photoswitchable moiety (Figure 2.47).[141]

[140] Szymanski, W.; Ourailidou, M. E.; Velema, W. A.; Dekker, F. J.; Feringa, B. L., Light-Controlled Histone Deacetylase (HDAC) Inhibitors: Towards Photopharmacological Chemotherapy *Chem. Eur. J.* **2015,** *21*, 16517-16524.

[141] Presa, A.; Brissos, R. F.; Caballero, A. B.; Borilovic, I.; Korrodi-Gregório, L.; Pérez-Tomás, R.; Roubeau, O.; Gamez, P., Photoswitching the Cytotoxic Properties of Platinum(II) Compounds *Angew. Chem. Int. Ed.* **2015,** *54*, 4561-4565.

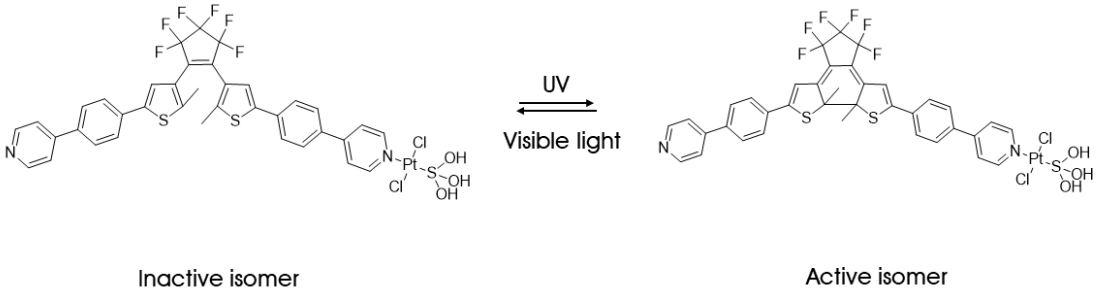

Figure 2.47. Photoswitchable drug based on diarylethene structure.

Other photoswitchable moieties such as azobenzenes were used to photocontrol the anticancer activity. For instance, chemotherapeutic agents such as proteasome inhibitors are widely used as a non-specific treatment against cancer.[142] By the introduction an azobenzene in the structure (Figure 2.48), it was possible to modulate the cytotoxicity of the photodrug by light.[143]

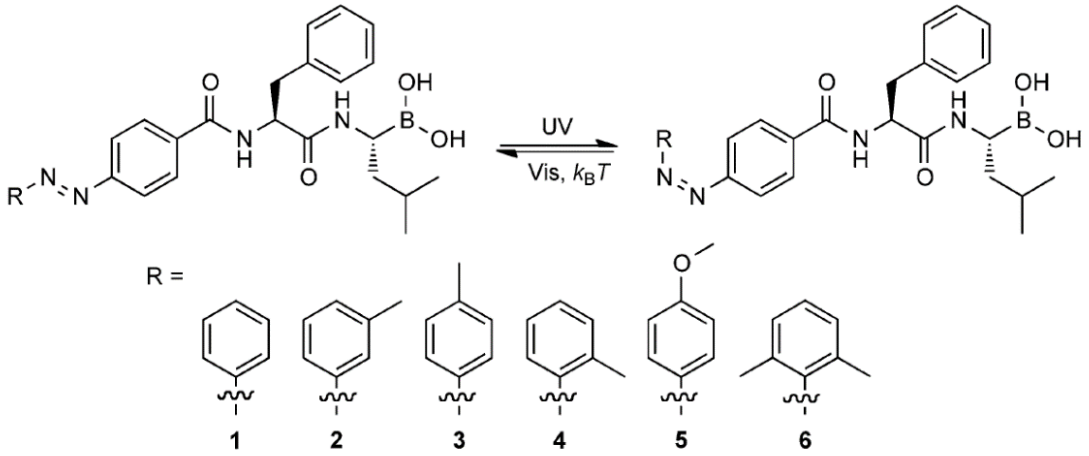

Figure 2.48. Photoswitchable cytotoxic agents based on the azobenzene core.

4.2.2.3. Photoswitches for ion channels.

Ion channels control many neuronal functions that are usually activated by ATP. The creation of new light-sensitive ion channels have been studied by the use of photoswitchable tethered ligands.

[142] Orlowski, R. Z.; Stinchcombe, T. E.; Mitchell, B. S.; Shea, T. C.; Baldwin, A. S.; Stahl, S.; Adams, J.; Esseltine, D.-L.; Elliott, P. J.; Pien, C. S.; Guerciolini, R.; Anderson, J. K.; Depcik-Smith, N. D.; Bhagat, R.; Lehman, M. J.; Novick, S. C.; O'Connor, O. A.; Soignet, S. L., Phase I Trial of the Proteasome Inhibitor PS-341 in Patients With Refractory Hematologic Malignancies *J. Clin. Oncol.* **2002,** *20*, 4420-4427.
[143] Hansen, M. J.; Velema, W. A.; de Bruin, G.; Overkleeft, H. S.; Szymanski, W.; Feringa, B. L., Proteasome Inhibitors with Photocontrolled Activity *ChemBioChem* **2014,** *15*, 2053-2057.

For that purpose, an azobenzene system was developed which enables rapid and selective optical control of nociception (the sense of pain). This designed system blocks the voltage-gated ion channels in its thermally stable state, but not in its *cis*-form (Figure 2.49). This approach can be used to photocontrol the pain.[144]

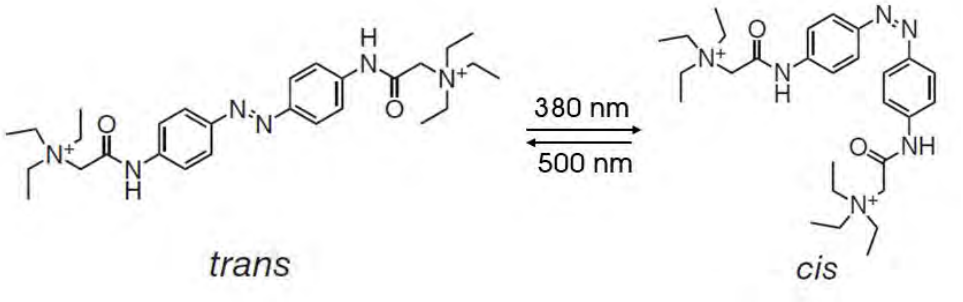

Figure 2.49. Photoswitchable drug able to control voltage-gated ion channels.

[144] Mourot, A.; Fehrentz, T.; Le Feuvre, Y.; Smith, C. M.; Herold, C.; Dalkara, D.; Nagy, F.; Trauner, D.; Kramer, R. H., Rapid optical control of nociception with an ion-channel photoswitch *Nat. Methods* **2012,** *9*, 396.

3. Objectives

The project of this doctoral thesis will try to delve into the development of new and efficient molecular switches with relevant properties, either chemical, photochemical or even biological.

In detail, the aims of this doctoral thesis are highlighted below:

- Firstly, the rational design, synthesis and characterization of novel molecular switches based on diverse chromophores such as hydantoin, PSB-retinal, metronidazole and DASAs derivatives will be approached.
- Then, studying the photophysical and photochemical properties of the synthesized derivatives. This study will include, among others:
  - The study of the photoswitching process through either singlet or triplet state.
  - The evaluation of the influence of the irradiation wavelength on the photoisomerization process.
  - The study of the thermal stability of the photoisomer.
  - The analysis of the efficiency of the isomerization process.
- Moreover, tuning these properties by modifying the electronic properties of the substituents present in the chromophore in order to red-shift the absorption wavelength.
- Furthermore, rationalizing all the experimental data by computational calculations.

In respect of using new photoswitches with biological purposes, some new aims can be outlined:

- The attachment of a photoswitch into a peptide with potent biological activity to photocontrol its secondary structure.
- The synthesis of new photodrugs able to photocontrol a biological activity.

4. Hydantoin-based molecular switches.

The design, study and characterization of new prototypes for using them as molecular switches is a highly important field to research. The photophysical and photochemical properties of a photoswitch are very dependent on which structure is based on their cores.[1] So we should choose the most appropriate core, depending on which application will give the best outcome of the work.[2,3]

As presented previously in the objectives, in this chapter we will describe several derivatives which take the hydantoin core as a pattern to prepare switches based on 5-aryliden-hydantoins.

5-aryliden-hydantoins have attracted the attention of the scientific community over many years due to their biological activity, since several studies have highlighted their properties as anticancer[4] or antibiotic drugs.[5] Apart from their biological properties, their capacity as UV absorbers in the cosmetic industry has also been reported.[6]

Although these derivatives are quite similar to other molecular switches reported before, specifically those which were based on the green fluorescent protein (GFP),[7] no-one explored their behavior as efficient photoswitches before. In Figure 4.1 the structure of both types of molecular switches is shown, in which the imidazoline unit has been replaced by an imidazolinone moiety.

[1] Ritterson, R. S.; Kuchenbecker, K. M.; Michalik, M.; Kortemme, T., Design of a Photoswitchable Cadherin *J. Am. Chem. Soc.* **2013,** *135*, 12516-12519.
[2] Wegner, H. A., *Molecular Switches*. 2012; Vol. 51, p 2281.
[3] Szymański, W.; Beierle, J. M.; Kistemaker, H. A. V.; Velema, W. A.; Feringa, B. L., Reversible Photocontrol of Biological Systems by the Incorporation of Molecular Photoswitches *Chem. Rev.* **2013,** *113*, 6114-6178.
[4] El-Deeb, I. M.; Bayoumi, S. M.; El-Sherbeny, M. A.; Abdel-Aziz, A. A. M., Synthesis and antitumor evaluation of novel cyclic arylsulfonylureas: ADME-T and pharmacophore prediction *Eur. J. Med. Chem.* **2010,** *45*, 2516-2530.
[5] Handzlik, J.; Szymańska, E.; Alibert, S.; Chevalier, J.; Otrębska, E.; Pękala, E.; Pagès, J.-M.; Kieć-Kononowicz, K., Search for new tools to combat Gram-negative resistant bacteria among amine derivatives of 5-arylidenehydantoin *Bioorg. Med. Chem.* **2013,** *21*, 135-145.
[6] Takano, S.; Kobayashi, T., Development of Novel UV Absorbent Synthesis and Screening *J. Cosmet. Sci.* **1993,** *26*, 262-268.
[7] Pakhomov, A. A.; Martynov, V. I., GFP Family: Structural Insights into Spectral Tuning *Cell Chem. Biol.* **2008,** *15*, 755-764.

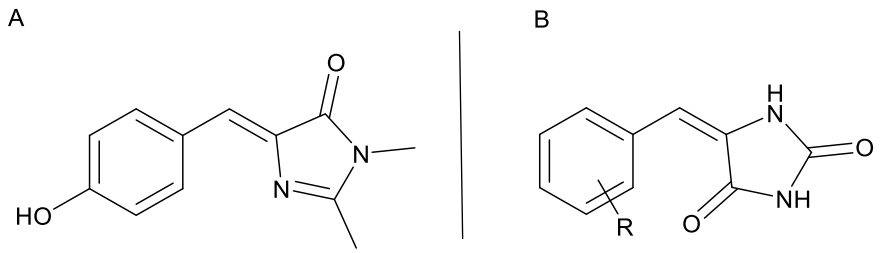

Figure 4.1. A) GFP chromophore. B) Hydantoin-based molecular switches.

Many differences exist between both structures, so it should be noted that the derivatives based on GFP chromophore present an imine bond that may greatly influence the photochemical behavior of the whole chromophore (Figure 4.1A). [8] Therefore, properties totally different with respect to absorption wavelength, PSS (photostationary state), chemical and photochemical stability or solubility, should be expected for the compounds shown in Figure 4.1.

This part of my thesis is mainly focused on the synthesis of a new family of photoswitches based on hydantoin, the study of their photophysical properties, as well as their photochemical behavior. Indeed, the process under study will be mainly the photoisomerization of the central C=C double bond of this new family of photoswitches (Figure 4.2).

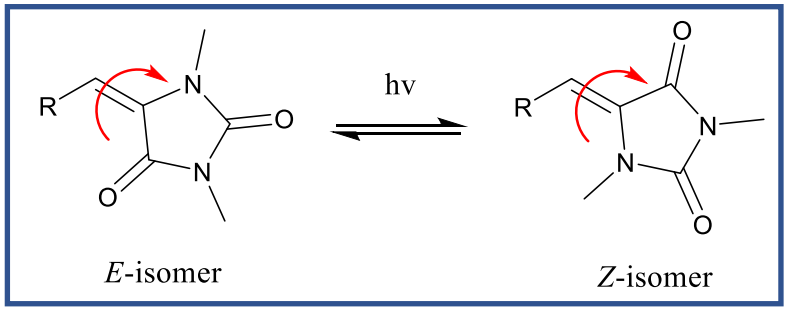

Figure 4.2. Photoisomerization process of hydantoin-based molecular switches.

In addition, after the experimental evaluation, some theoretical calculations will be presented to understand and rationalize their behavior.

[8] Blanco-Lomas, M.; Funes-Ardoiz, I.; Campos, P. J.; Sampedro, D., Oxazolone-Based Photoswitches: Synthesis and Properties *Eur. J. Org. Chem.* **2013,** *2013*, 6611-6618.

1. Synthesis of hydantoin-based molecular switches.

The synthesis of 5-aryliden-hydantoins is well-known since 1899,[9] but no efficient synthesis of these derivatives was known until Hoffman and Wheeler reported the condensation between hydantoin and benzaldehyde in acidic conditions.[10]

In this thesis, two methods were used to synthesize hydantoin-based molecular switches (Scheme 4.1).

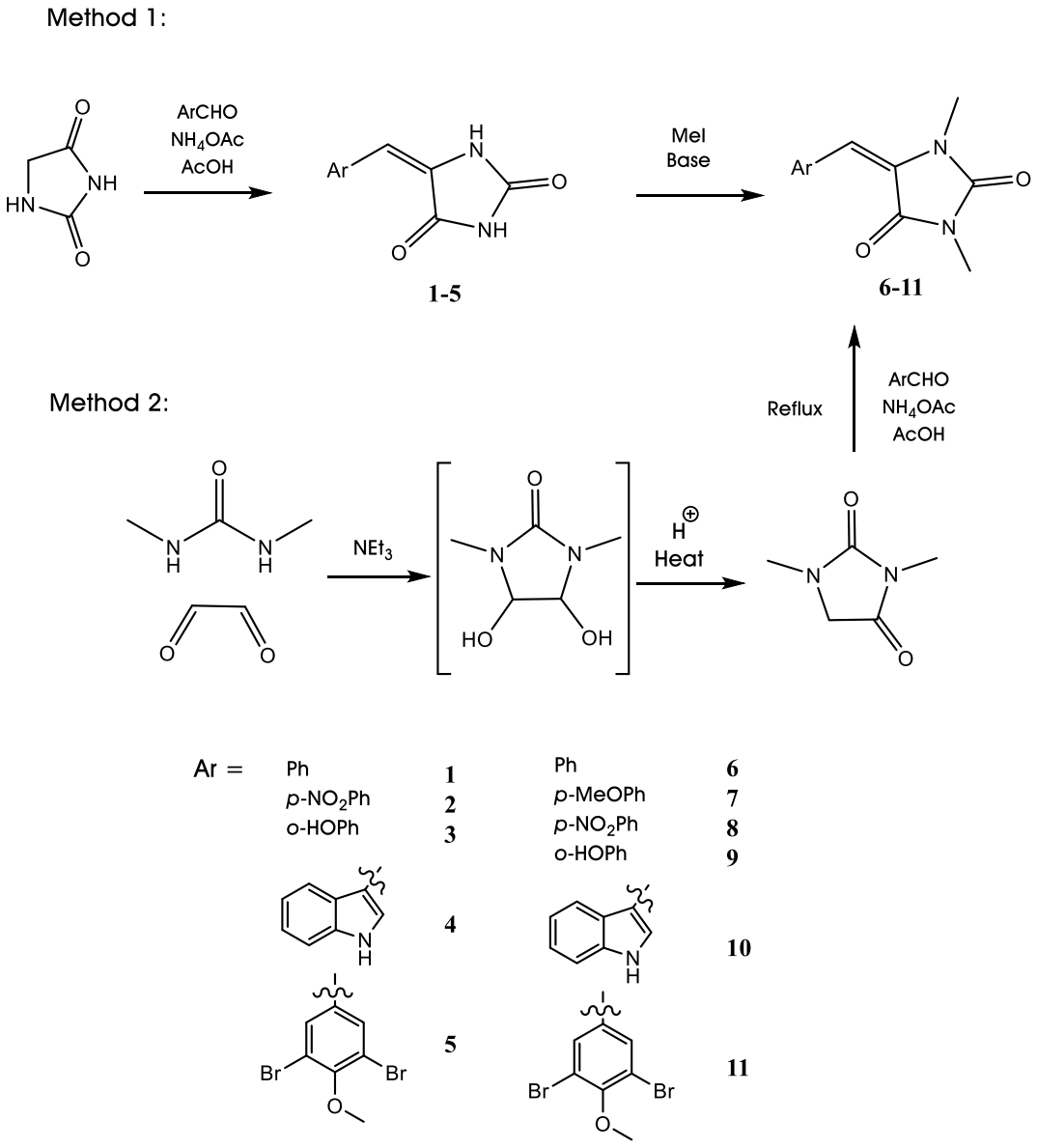

Scheme 4.1. General synthesis of **1-11.**

[9] Ruhemann, S.; Cunnington, A. V., Studies of the acids of the acetylene series *J. Chem. Soc., Trans.* **1899,** *75*, 954-963.
[10] Wheeler, H.; Hoffman, C., Synthesis of Phenylalanine and Tyrosine *Am. Chem. J.* **1911,** *45*, 368-383.

On the one hand, the first method was based on the classical conditions that were reported by Hoffman and Wheeler. The condensation between the hydantoin moiety and an aromatic aldehyde took place under acidic conditions and, in this case, acetic acid was used in the presence of ammonium acetate to carry out the reaction.[11] On the other hand, the first step in method 2 was to synthesize dimethyl hydantoin, and then, the condensation with an aldehyde was performed.

Both methods combined with easy synthesis and good yields in a few steps. Therefore, they can both be considered as good options to prepare 5-aryliden-hydantoins. It should be noted that in the common step in which the double bond is formed, the reactivity of the aromatic aldehyde used in the reaction had negligible effects on the reaction, since the main impact on the yields for both methods came from the first step in method 2 (see section 4.1).

Using any of those methods, the only isomer detected by ^{1}H NMR was the one in which the double bond is in *E*-configuration, since it is more stable than the *Z*-isomer. To confirm this point, some crystals of **7** were obtained to analyze its X-ray structure (Figure 4.3) (see Appendix B for further details).

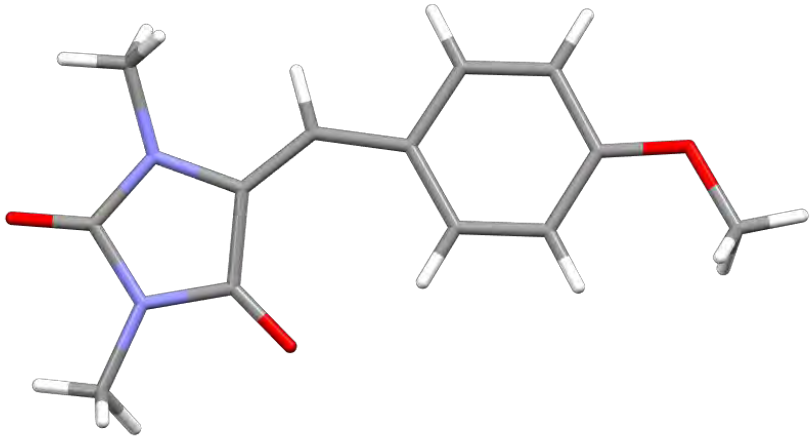

Figure 4.3. X-ray structure of **7**.

The purification of compounds **1-11** was performed following two different methodologies. One set includes compounds **1-5**, in which the nitrogen atoms in the hydantoin scaffold are not methylated. This fact makes them very insoluble in common organic solvents, so the purification could be achieved by just washing the reaction crude with dichloromethane since all the undesired compounds were very soluble in this solvent.

[11] Johnson, T. B.; Nicolet, B. H., Hydantoins: The Alkilation of 2-thio-4-benzalhydantoin *J. Am. Chem. Soc.* **1912,** *34*, 1048-1054.

Moreover, these compounds could be purified by column chromatography using as eluent mixtures of ethyl acetate/hexane in silica gel to afford **1**-**5** with yields ranging from 70% to 90% using both ways of purification. In contrast, compounds **6**-**11**, in which the hydantoin moiety is methylated, making them very soluble in mostly all organic solvents, purification could only be done by column chromatography in silica gel using different eluent mixtures of ethyl acetate/hexane to yield the final compounds.

To sum up, both methods were successful to synthesize 5-aryliden-hydantoins, but if we compare them, evidently method 1 is more practical for several reasons. It has fewer steps in the synthetic route, the purification is faster and easier in the case of washing the crude with dichloromethane, and finally the reaction yields are greater than the ones achieved by method 2.

2. Photochemical study.

In every photochemical reaction, the reacting molecule must contain a chromophore which is the responsible for absorbing light. At the beginning, the molecule is in the ground state S_0 and it must absorb one photon with the appropriate energy to be promoted to an excited state (S_1, S_2 or S_3…) through an allowed singlet-singlet transition. Once the molecule is in an excited singlet state, it can decay to the ground state giving a photoreaction (*E*/*Z* photoisomerization in our case) or through an intersystem crossing (ISC, a non-radiative process) to form a triplet state (T_n) being responsible for the photoreaction (See introduction for further details).[12]

In this section, a set of experiments will be shown to fully characterize a family of molecular switches. For instance, the photophysical properties will be addressed. In addition, the UV-Vis spectrum and the transitions involved will be rationalized. Also, the irradiation of the photoswitches using different sources of light to check the influence of external factors on the PSS will be described. Moreover, the nature of the electronic state involved in the photoreaction will also be subject of study, as well as the efficiency of the photoswitching process through measuring the isomerization quantum yield.

2.1. Absorption and emission properties.

Firstly, in order to perform a photochemical study, we must know which kind of electromagnetic radiation is absorbed by the molecule under investigation. Thus, it is compulsory to record a UV-Vis spectrum of a diluted solution. Once the UV-Vis spectrum is measured, we can choose the appropriate light source to induce the photoreaction. In case the emission of the light source does not fit with the UV-Vis spectrum of the compound, no photoreaction will take place as there will be no interaction between the light and the sample.

As we have just remarked the importance of the absorbance wavelength to perform a photochemical study, UV-Vis spectra of compounds **1-11** were recorded in mixtures of CH_2Cl_2/MeOH (1:1) due to the low solubility of compounds **1-5** in each solvent independently. All the experiments were performed in identical conditions using the same solvent mixture and solutions of a concentration around 5E-5 M.

The different photophysical properties such as the absorption wavelength and the molar extinction coefficients in CH_2Cl_2/MeOH (1:1) are shown in Table 4.1.

[12] Turro, N. J.; Ramamurthy, V.; Scaiano, J. C., *Principles of molecular photochemistry : an introduction*. University Science Books: Sansolito (CA), 2009.

Compound	λ_{max}	ε ($M^{-1}cm^{-1}$)
1	317	20471
2	353	15854
3	340	15200
4	367	11835
5	321	22605
6	309	12316
7	333	16346
8	339	11816
9	326	12077
10	373	13610
11	316	8710

Table 4.1[13]

In all cases, a strong absorption band between 320 and 370 nm appeared, but as was expected, the absorbance depended largely on the substituent in the aromatic ring. Substitution directly affects the electronic properties of the chromophore, tuning its behavior.

It was observed that a noticeable red-shift in the absorption wavelength occurred when changing the substituent in the phenyl ring. A bathochromic effect happened when an electron withdrawing (**2**) or an electron donating (**3**) group was introduced in the chromophore comparing them with the photoswitch, in which there is no substituent in the phenyl ring (**1**) (Figure 4.4). Indeed, it has been demonstrated that in this kind of molecular switches, the photophysical properties were highly determined by the electronic properties of the photoswitch.

[13] Data are referring to *E*-isomer.

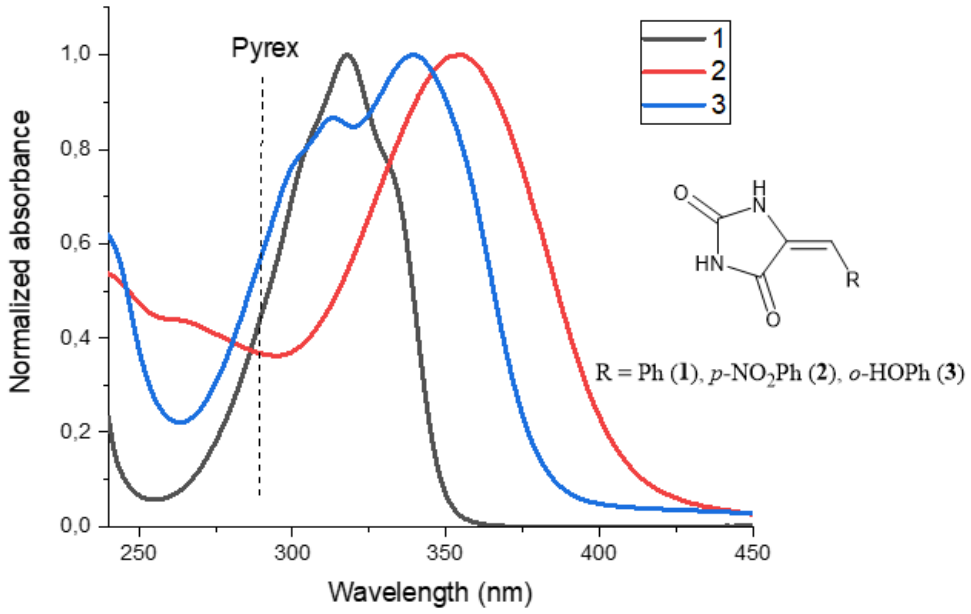

Figure 4.4. UV-Vis spectra of **1**, **2** and **3**.

Analyzing Table 4.1, a greater red-shift was observed in **4** and **10** owing to the increase of the conjugation of the chromophore because the phenyl ring was changed by an indole group (Figure 4.5).

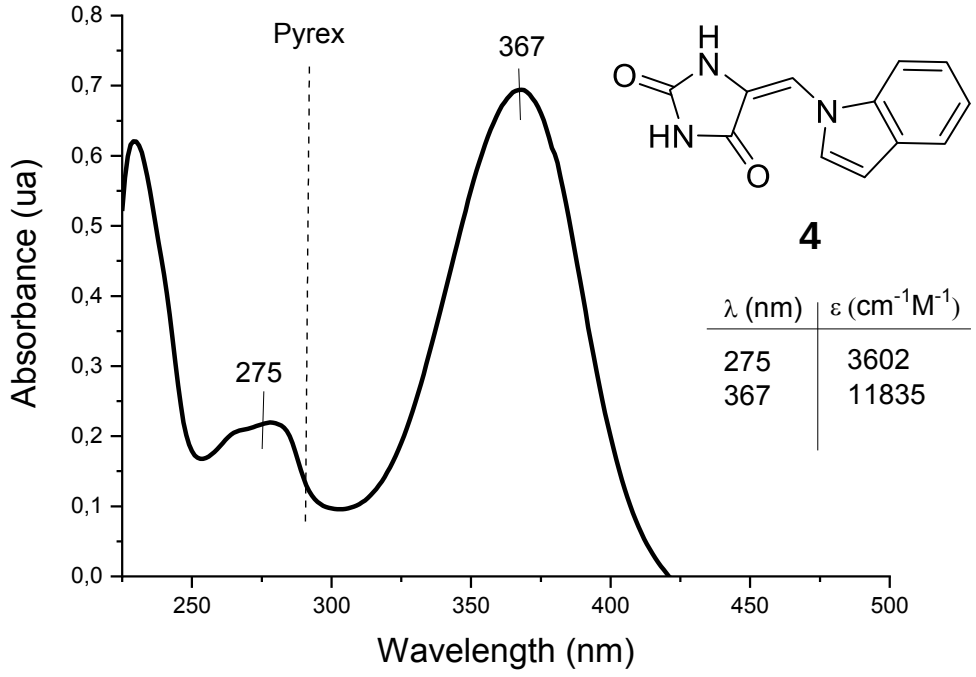

Figure 4.5. UV-Vis spectrum of **4**.

Finally, after studying the outcome of dimethylation of the hydantoin moiety, it was concluded that it had a minor effect on the absorption spectra of these compounds. A small blue-shift of around 10 nm was found when comparing 5-arylinden-hydantoins (**1-5**) with their analogues 1,3-dimethyl-5-arylinden-hydantoins (**6-11**) (Table 1.2).

To complete this study, the effect of the solvent on the UV-Vis spectra for these compounds was also evaluated. Several solvents with different properties were tested such as acetonitrile, chloroform and DMSO. No significant changes were found in the spectra recorded for each solvent. Therefore, it was concluded that the solvent and its polarity had no effect on the photophysical properties of this family of photoswitches.

Once it has been studied on how to excite these molecules, it is important to explore the possible deactivation pathways that can interfere in the efficiency of the switching of these molecules, as the excited state formed could be deactivated through other processes such as fluorescence instead of the isomerization of its double bond.

The emission and excitation processes of two representative photoswitches (**2** and **7**) were measured (Figure 4.6 and 4.7). The corresponding solutions were prepared in CH_2Cl_2/MeOH (1:1) with a concentration of 5E-5 M. The experiments were carried out in a spectrofluorimeter.

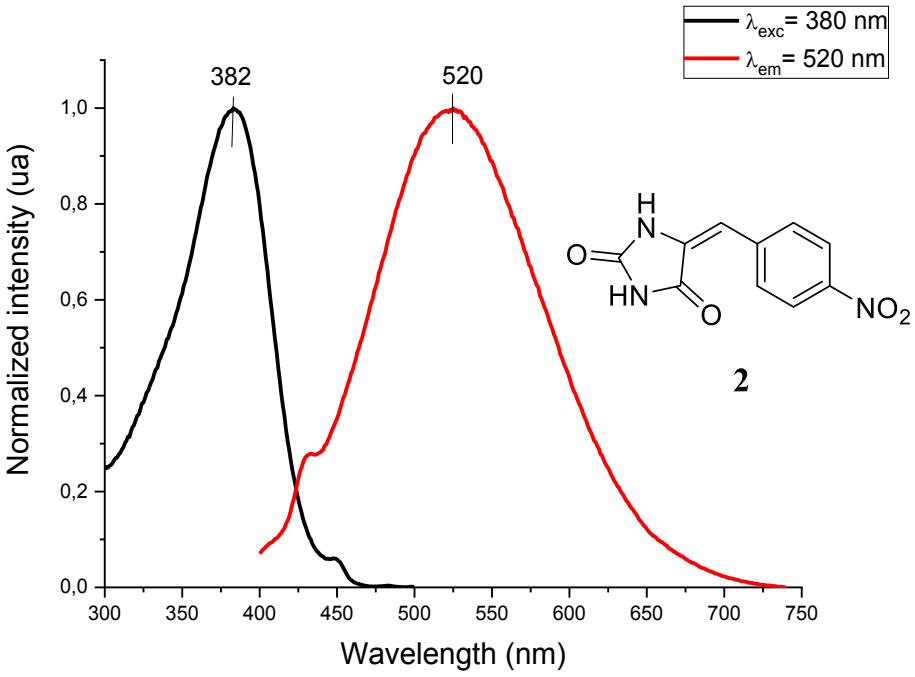

Figure 4.6. Luminescence spectrum of **2**.

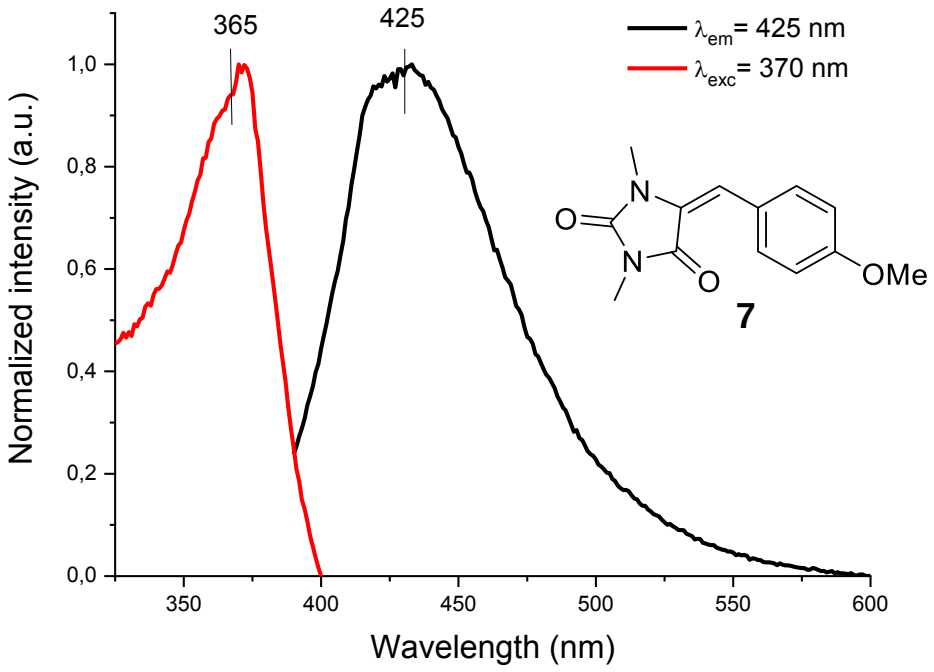

Figure 4.7. Luminescence spectrum of **7**.

A similar emission pattern was found for **2** and **7**, as a single weak emission band was found for them. All the excitation wavelengths led to the same emissive state, therefore the emission properties of these compounds were related to one excited state (singlet state, S_n). In the case of **7**, the emission was located at 425 nm (Figure 4.7). In contrast, in compound **2** the band was centered at 520 nm (Figure 4.6). These bands were related with a fluorescence process in which the excited molecule decays to the ground state through the emission of light. A bigger Stokes shift was found in the case of **2** (140 nm) than in compound **7** (60 nm). The Stokes shift points out qualitatively the structural differences between the molecule in its ground state and in its excited state. This means that **2** was more distorted in its excited state than **7**. Nevertheless, in both cases, the emission quantum yield was below the apparatus threshold, which in this case was fixed on $\phi_{em} < 1\%$.

Therefore, it is concluded that, the low fluorescence quantum yields obtained, indicates that the radiative deactivation of the excited state was not a competitive pathway. For this reason, these compounds could be efficient photoswitches since they do not waste the light energy in other processes beyond photoisomerization.

Once potential radiative processes were discarded after the excitation of these photoswitches, its photoreactivity upon irradiation was explored.

2.2. Nature of the electronic excited state.

The photoreactivity of an organic molecule is determined by the multiplicity of the excited state which is involved in the photoreaction. Hence, it is very relevant to know which type of excited state is involved in the photoisomerization. Doing so, we could control the reactivity and explore different reaction pathways. Moreover, if the photoreaction takes place through a triplet state, external factors such as the oxygen in solution could lead to different reaction rates, which means that, for instance, the irradiation should be performed using deoxygenated solvents.

Hence, in this part of my thesis I will show how to determine which kind of electronic state (singlet or triplet) is responsible for the photoisomerization due to the importance pointed out before. These experiments were based on the irradiation of a photoswitch in the presence of different triplet quenchers such as *cis*-piperylene (it has a triplet energy of 57 kcal/mol) or a solution saturated with oxygen. It is well known that molecular oxygen is a triplet quencher because in its ground state it is a low energy triplet, which reacts deactivating the triplet state of another molecule leading to molecular oxygen in two excited triplet states (E_{T1} = 22.8 kcal/mol and E_{T2} = 37.9 kcal/mol).[14]

Both experiments should be compared with a deoxygenated solution of the same photoswitch. In case the photoisomerization takes place through a triplet state, we would obtain different isomerization rates as aforementioned.

Hence, three solutions of **7** (due to their good photophysical properties that will be described in the following section) at the same concentration (0.05M) were prepared in $CDCl_3$ These conditions were chosen because they were suitable for following the reaction by ^1H NMR. The first sample was prepared bubbling air during at least 20 minutes throughout the NMR tube. To the second one, 5 equivalents of *cis*–piperylene were added and the solution was deoxygenated bubbling argon through the solution for 20 minutes. The third sample was just deoxygenated, using the same way as aforementioned.

Once the three samples were prepared, they were irradiated in several Pyrex NMR tubes using a 125-W medium pressure Hg lamp to carry out the photoisomerization (Figure 4.8). All samples were irradiated simultaneously, and they were followed measuring the isomers ratio at different times by ^1H NMR.[15]

[14] Montalti, M.; Credi, A.; Prodi, L.; Gandolfi, M., *Handbook of Photochemistry, 3rd ed.* CRC Press: Boca Raton, 2006.
[15] Skoog, D. A., *Principios de Análisis Instrumental*. Mc-Graw Hill: Madrid, 2000.

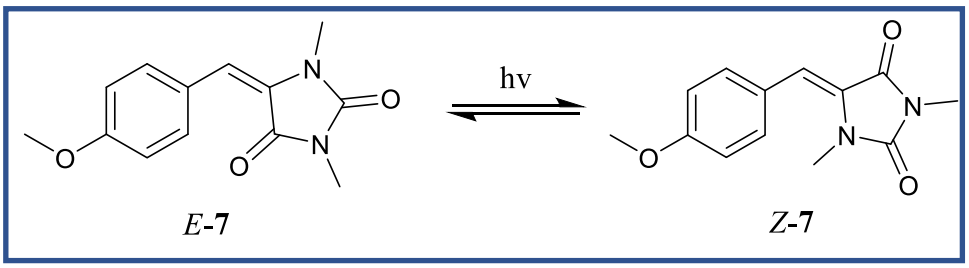

Figure 4.8. Isomerization process of photoswitch **7**.

Time (min)	Sample 1 % *Z*-isomer	Sample 2 % *Z*-isomer	Sample 3 % *Z*-isomer
2	4	5	4
13	48	51	47
18	59	57	59

Table 4.2

Analyzing the results given in Table 4.2, it is observed that at each irradiation time, almost the same isomers ratio was obtained in the mixture for each sample. Thus, the isomerization rate was similar in all samples tested. Indeed, the minimal differences on the results may be attributed to the experimental error of the technique used, which in this case it was ^{1}H NMR. It is concluded that the presence of several quenchers had no significant effect on the isomerization process, what it means is that the nature of the electronic excited state involved in the photoisomerization of 5-aryliden-hydantoins was not a triplet state, but a singlet one.

2.3. Photoisomerization.

When irradiating a molecule many processes can occur; light can induce different molecular movements or even reactions to result in other products. The aim of this section is to study the rotation of the central C=C double bond shown in Figure 4.2 to obtain the corresponding *Z* or *E*-isomer using light.

Thereupon, the behavior of these derivatives towards irradiation using different sources of light will be described, so the intensity and the emission bands will be totally different in each case. This fact could affect directly the relative absorption of both isomers, altering the isomers ratio in the PSS mixture. Indeed, it will be evaluated how it could be able to alter the photochemical properties of these switches using an external input.

2.3.1. Irradiation of photoswitches using a 125-W medium-pressure Hg lamp.

From the values obtained in the previous section, a 125-W medium-pressure Hg lamp was selected for irradiating all compounds. This lamp emits light in a wide range of the spectra, from high energetic UV-light to far visible-light. Thus, during the irradiation a Pyrex filter was used to avoid the radiation below 290 nm, since this kind of irradiation is very powerful, and it could produce undesired side reactions.

Following the irradiation, we used ^{1}H NMR so that it would be easy to follow the photoisomerization through the different chemical shifts that may appear for the *E* and *Z*-isomers, specially the vinylic hydrogen (Figure 4.9). Therefore, the irradiation process was followed at different intervals of time until the photostationary state was reached. Finally, just integrating the ^{1}H NMR signals corresponding to each isomer would show the isomers ratio present in the mixture. The other possible method to follow the irradiation process is using thin layer chromatography (TLC) because *E* and *Z*-isomers present different R_f values; although TLC is not quantitative. This is the main drawback of this method to follow an isomerization, as it would not exactly show the isomers ratio or when the PSS has been reached.

In Figure 4.9, it is observed that the signals corresponding to the *E*-isomer (red spectrum) decreased along the irradiation; on the contrary another group of signals appeared corresponding to the *Z*-isomer (blue spectrum).

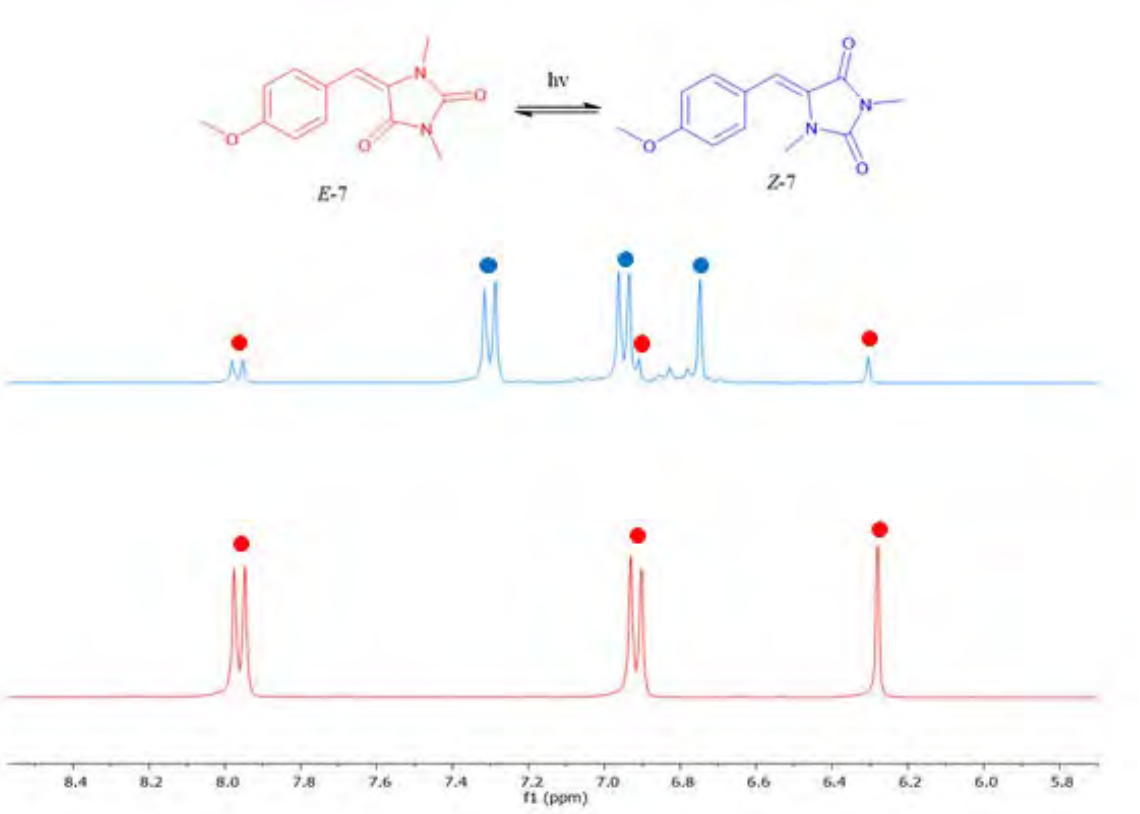

Figure 4.9. NMR signals of both isomers.

For this reason, all the experiments were carried out in different Pyrex NMR tubes and 0.05 M solutions were prepared in different deuterated solvents. For compounds **1**-**5**, the irradiation was followed in DMSO-d^6 due to the low solubility of the switches in other organic solvents. In contrast, the solutions of **6**-**11** were prepared in $CDCl_3$ or CD_3CN. The same results were obtained using any deuterated solvent because in this kind of switches, their photophysical or photochemical properties did not depend on the solvent used (Section 2.1).

As we can see in Figure 4.9, two distinct signals appear for compound **7** at 6.28 (***E*-7**) and 6.71ppm (***Z*-7**). Typically, in this family of photoswitches and with the irradiation conditions described above, the PSS required about 45 minutes to be reached (Figure 4.10A and B).

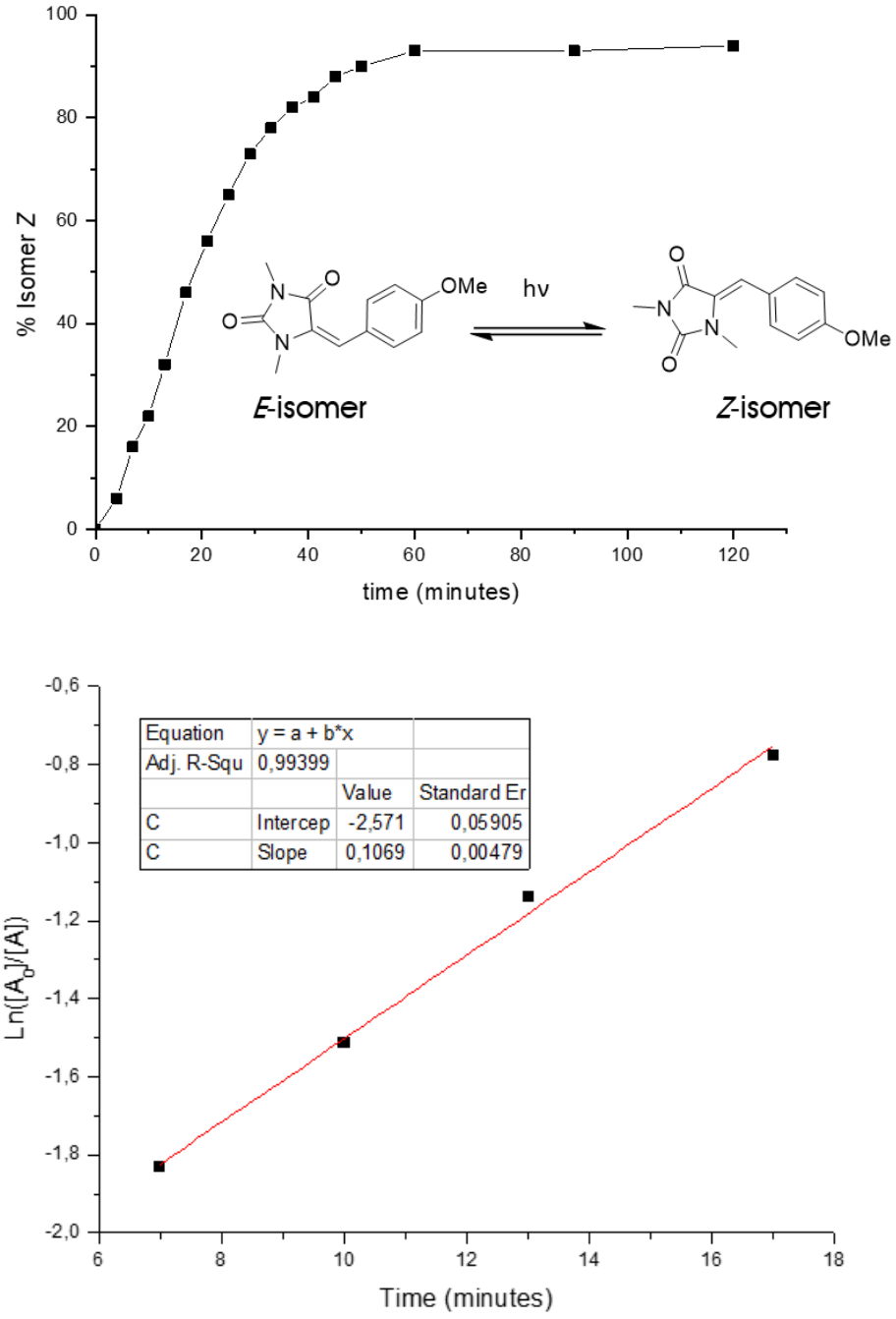

Figure 4.10. Kinetic study of **7**.

The photoisomerization kinetics was studied for compound **7** due to their good photoswitching properties; a solution of 0.05 M in $CDCl_3$ was irradiated under the conditions detailed before. In the same way as other experiments, the irradiation procedure was followed by ^1H NMR. In this case, each 5 minutes, the composition of the mixture was measured to determine the isomers ratio at short irradiation time intervals. Using the first points, when the composition of the mixture was enriched in the *E*-isomer and the absorption of *Z*-isomer was negligible, we obtained a value for the kinetic constant of the photoisomerization for the process *E* to *Z*-isomer of 2.57 s^{-1} (Figure 4.10B).

Therefore, it was determined that under these conditions, a fast photoisomerization took place.

The composition of the PSS under these conditions for compounds **1-11** is shown in Table 4.3.

Compound	PSS	
	E-isomer (%)	*Z*-isomer (%)
1	100	0
2	64	36
3	86	14
4	89	11
5	0	100
6	100	0
7	5	95
8	69	31
9	88	12
10	45	55
11	100	0

Table 4.3.

No side reactions were found after 4 hours of irradiation using a 125-W medium-pressure Hg lamp. It should be noted that despite the fact that the PSS was reached after irradiating 45 minutes, both isomers were continuously absorbing light and reacting in a dynamic equilibrium the rest of the time indicating their good photostability.

Analyzing Table 4.3, we can see totally different mixtures reached depending on the substituents of the aromatic ring. This is due to the fact that the PSS is highly dependent on mainly three factors:

- The relative absorption of both isomers.
- The relative stability of both isomers.
- The topology of the potential energy surfaces.

Other factors can also directly affect the PSS, as for example the quantum yields of the forward *(E → Z)* and backward *(Z → E)* reactions. In turn, these quantum yields are highly dependent on the relative absorption of both isomers and the shape of the potential energy surfaces. So, it is very difficult to provide a quantitative rationale of the PSS because it is dependent on all these factors simultaneously.

In detail, it should be noted that the irradiation of 5 and 7 led to a complete change in the configuration of its double bonds, reaching quantitatively the *Z*-isomer from the *E*-form. This excellent feature is not very common in *E*/*Z* photoswitches, although it is a desired property.[16] For this reason, some studies have been reported trying to accomplish this feature in arylazopyrazoles,[17,18] o-fluoroazobenzenes[19] or hemithioindigos.[20]

On the contrary, under the same conditions, compounds **1**, **6** and **11** did not photoisomerize, but by simply removing the Pyrex filter and using a filter made of quartz, the photoisomerization took place. For these compounds, the irradiation was carried out in different quartz NMR tubes using the same lamp as before, a 125-W medium-pressure Hg lamp. In these cases, the isomerization took place because the relative absorption of both isomers changed since different light was absorbed by the samples. Under these different conditions, the PSSs reached are shown in Table 4.4.

Compound	PSS Pyrex filter		PSS quartz filter	
	E-isomer (%)	*Z*-isomer (%)	*E*-isomer (%)	*Z*-isomer (%)
1	No photoisomerization		79	21
6			61	39
11			54	46

Table 4.4.

This finding takes on special relevance because the photoswitching could be activated just changing an external factor such as a filter, without modifying the source of light.

To understand this behavior, the purification of ***Z*-1** was performed. The isolation of the photoisomer (***Z*-1**) was carried out by column chromatography on silica gel using as

[16] García-Iriepa, C.; Marazzi, M.; Frutos, L. M.; Sampedro, D., E/Z Photochemical switches: syntheses, properties and applications *RSC Adv.* **2013,** *3*, 6241-6266.
[17] Weston, C. E.; Richardson, R. D.; Haycock, P. R.; White, A. J. P.; Fuchter, M. J., Arylazopyrazoles: Azoheteroarene Photoswitches Offering Quantitative Isomerization and Long Thermal Half-Lives *J. Am. Chem. Soc.* **2014,** *136*, 11878-11881.
[18] Calbo, J.; Weston, C. E.; White, A. J. P.; Rzepa, H. S.; Contreras-García, J.; Fuchter, M. J., Tuning Azoheteroarene Photoswitch Performance through Heteroaryl Design *J. Am. Chem. Soc.* **2017,** *139*, 1261-1274.
[19] Bléger, D.; Schwarz, J.; Brouwer, A. M.; Hecht, S., o-Fluoroazobenzenes as Readily Synthesized Photoswitches Offering Nearly Quantitative Two-Way Isomerization with Visible Light *J. Am. Chem. Soc.* **2012,** *134*, 20597-20600.
[20] Zweig, J. E.; Newhouse, T. R., Isomer-Specific Hydrogen Bonding as a Design Principle for Bidirectionally Quantitative and Redshifted Hemithioindigo Photoswitches *J. Am. Chem. Soc.* **2017,** *139*, 10956-10959.

eluent a mixture of hexane/ethyl acetate (1:1). Once the purification was carried out, the UV-Vis spectra of both isomers were compared at the same concentration (Figure 4.11).

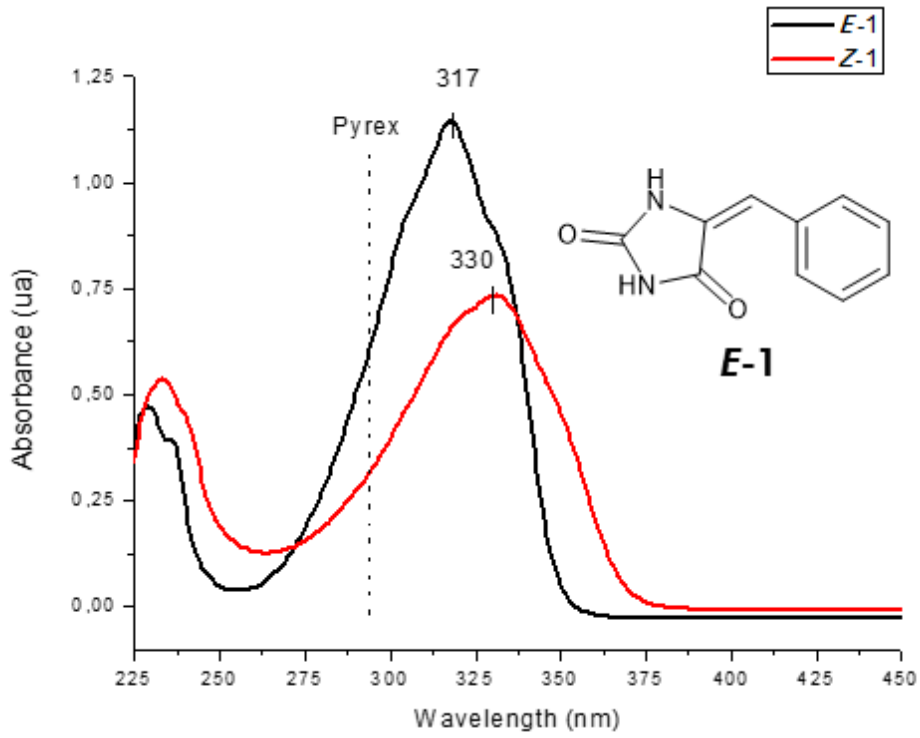

Figure 4.11. UV-Vis spectra of both isomers of **1**.

As Figure 4.11 shows the *Z*-isomer of **1** featured a tail at longer wavelengths, for this reason when a Pyrex filter was used, the *Z*-isomer preferably absorbed the irradiation and the isomerization *Z* → *E* was favored. In this context, although the isomerization could take place using a Pyrex filter, the back reaction was faster, therefore the *Z*-isomer in the irradiation mixture could not be detected. However, when the Pyrex filter was removed and the irradiation was carried out using a quartz filter, the whole absorption band was affected by light and the competitive back reaction was not that effective. This fact led to the PSS showed in Table 4.4.

To confirm all these results, if the *Z*-isomer is irradiated using a Pyrex filter, the reversion should take place photochemically. Then, a simple experiment was performed as we can see in Figure 4.12. For this purpose, a solution of pure ***E*-1** was irradiated in DMSO-d^6 using a quartz filter to promote the forward isomerization. Once the PSS was reached, a Pyrex filter was used to test if the reversion takes place photochemically in the same sample, reaching the starting situation.

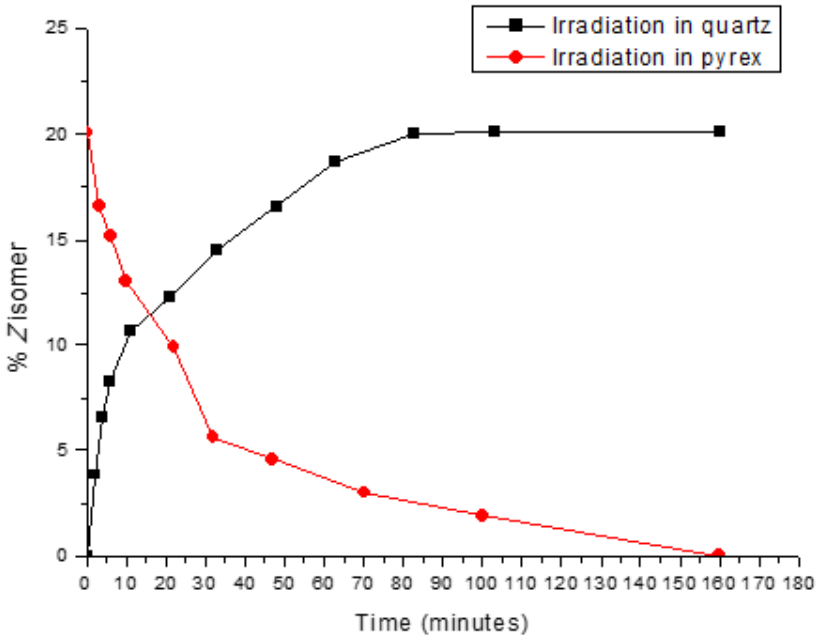

Figure 4.12. Irradiation of **1** using different filters.

As has been confirmed in the previous experiment, the PSS can be altered by external factors by using one filter or another.

2.3.2. Irradiation of photoswitches using a photoreactor.

Regarding the PSS of other compounds shown in Table 4.3, in the case of photoswitches **2-4** in which after irradiation, the mixture was enriched on the thermally stable *E*-isomer, should be also highlighted.

It was tried to increase the *Z*-isomer ratio in the irradiation mixture by changing the light source. For this purpose, a photoreactor with an emission band centered at 350 nm (14 lamps x 8W/lamp) was used. To carry out these experiments, **2-4** was chosen to perform the irradiation, since they present neat absorptions in the 350 nm region (Figure 4.13).

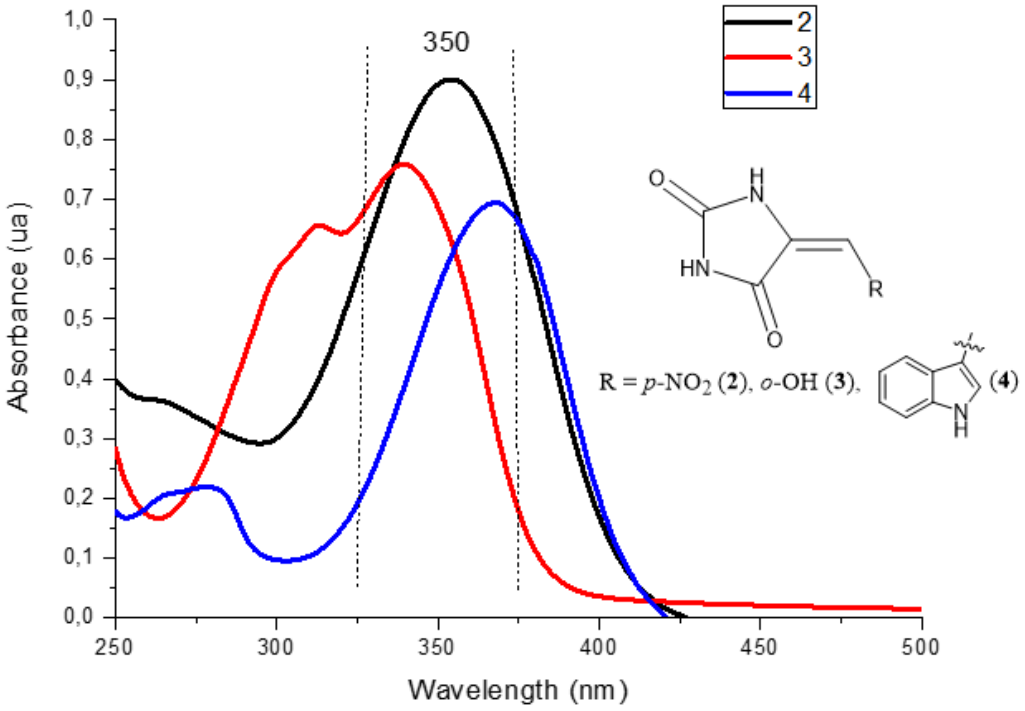

Figure 4.13. UV-Vis spectra of **2**, **3** and **4**.

The values of the PSS reached in each case are shown in Table 4.5. As it is shown, the use of these irradiation conditions caused different PSS increasing the amount of the *Z* isomer in the mixture, especially in compound **4**, due to the change on the relative absorption of both isomers, as aforementioned. These facts gave an especial relevance to this family of photoswitches, as the PSS could also be easily modified by another external agent (the filter and the light source used).

Compound	PSS medium pressure Hg lamp		PSS photoreactor at 350nm	
	E-isomer (%)	*Z*-isomer (%)	*E*-isomer (%)	*Z*-isomer (%)
2	64	36	53	47
3	86	14	48	52
4	89	11	22	78

Table 4.5.

2.3.3. Irradiation of photoswitches using monochromatic light.

Given the importance of the light source used in the irradiation, it was thought that the use of monochromatic light would be enlightening for this work. With this aim, we represented the UV-spectra of both isomers of **7** in the same graph to analyze which wavelength should be used to irradiate preferably one isomer over the other one. For this

purpose, a 5.36E-5 M solution in $CHCl_3$ of ***E*-7** and its photoisomer were prepared to study their UV spectra independently (Figure 4.14). This compound was chosen because the *Z*-isomer could be obtained in pure form from the irradiation.

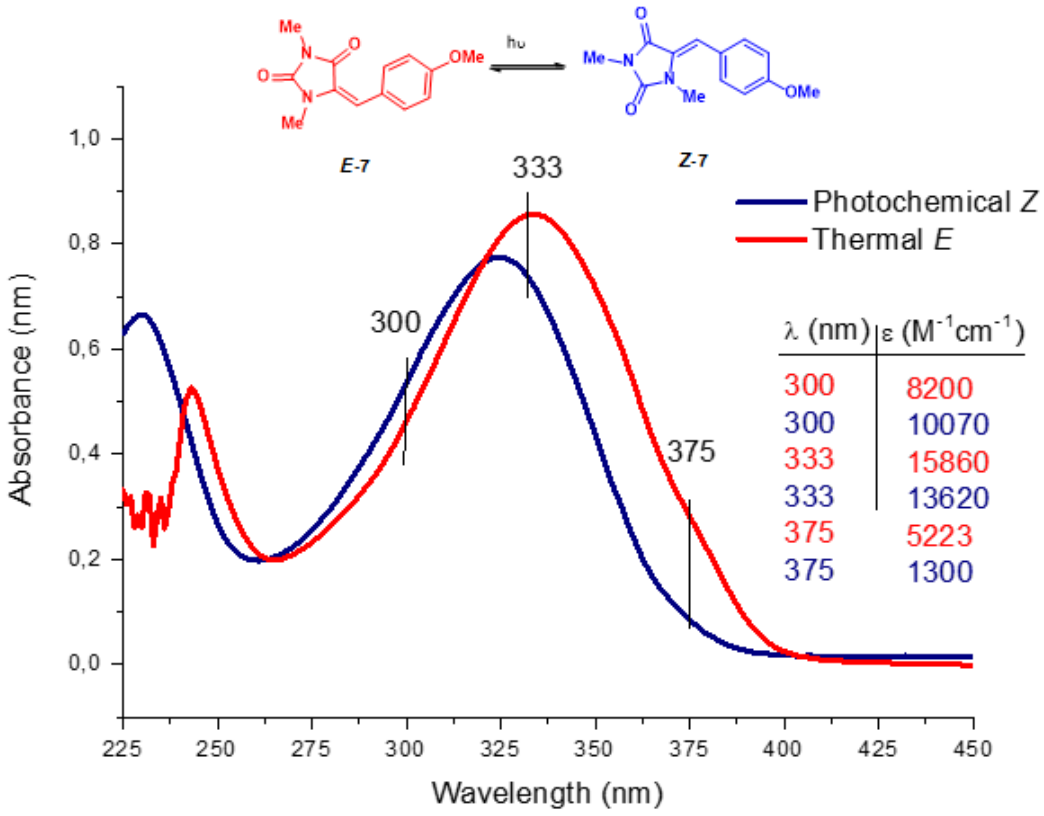

Figure 4.14. UV-Vis spectra of ***E*-7** and ***Z*-7**.

In the figure above, a slight displacement between the absorption bands of both isomers can be observed. Therefore, depending on the region of the spectrum we are evaluating, the *E*-isomer features a higher or lower absorption than the photoisomer. Indeed, this could be relevant as it could be possible to irradiate preferably one isomer over the other one. Consequently, in this experiment the photoswitching direction could be able to be controlled. It is expected when the irradiation will be centered at 333 or 375 nm the forward reaction *(E→Z)* should take place. In contrast, the use of 300 nm as excitation wavelength should lead to the back reaction photochemically.

To this end, a 5.36E-5 M solution in $CHCl_3$ of ***E*-7** was prepared and subsequently three wavelengths were chosen to evaluate their effect on the PSS of **7** (Figure 4.14). The irradiation was carried out using a monochromator, which provided a narrow band for the light emission. The sample was irradiated in a quartz cuvette. Moreover, to determine the isomers ratio in the mixture, a GC-MS was used due to the low concentration used for the experiments. The amount of each isomer was taken from the integration of each peak.

Firstly, it was irradiated at the absorption maximum of ***E*-7** (333 nm), where the *E*-isomer was preferably irradiated (Figure 4.14). It should be noted that at this irradiation wavelength the *Z*-isomer also presented a high absorbance and the difference between the absorption of both isomers was not large. Consequently, throughout the irradiation, the concentration of *Z*-isomer in the mixture was increasing and the back photochemical reaction could take place. This was the reason that the PSS obtained after two hours of irradiation (Table 4.6) was not very enriched in the *Z*-isomer.

To produce the reverse reaction photochemically, we used the same sample and the irradiation was carried out at 300 nm (Figure 4.14). The PSS obtained was 78% *E* / 22% *Z*; in this case it was producing the back reaction photochemically *(Z→E)* as we expected, since we were irradiating the *Z* isomer over the thermal one.

Finally, when the sample was irradiated at 375 nm (Figure 4.14), the PSS was enriched in the *Z*-isomer (Table 4.6). This was due to the fact that the *Z*-isomer features low absorbance at 375 nm, so the reverse photochemical reaction is not favored. Thus, the equilibrium is very displaced to the *Z*-isomer formation.

λ (nm)	PSS	
	E-isomer (%)	*Z*-isomer (%)
300	75	22
333	55	45
375	25	75

Table 4.6

In the design of these experiments, the same sample was used because the PSS is not dependent on the mixture ratio present at the beginning of the experiment.

In Table 4.6, it has been demonstrated that using monochromatic light was a really good tool to control the direction of photoswitching. When irradiating the sample at the short wavelength or in the maximum of the absorption band (300 and 333 nm), we obtained mixtures enriched in the *E*-isomer. In contrast, when irradiating the tail of the band (375 nm), the ratio changed obtaining mainly the *Z*-isomer.

A similar study was performed with **5** as isomerization of this compound is quantitative using a 125-W medium pressure Hg lamp. Therefore, solutions of 5E-5 M of each isomer were prepared. Then, the UV-spectra of each isomer were measured separately (Figure 4.15).

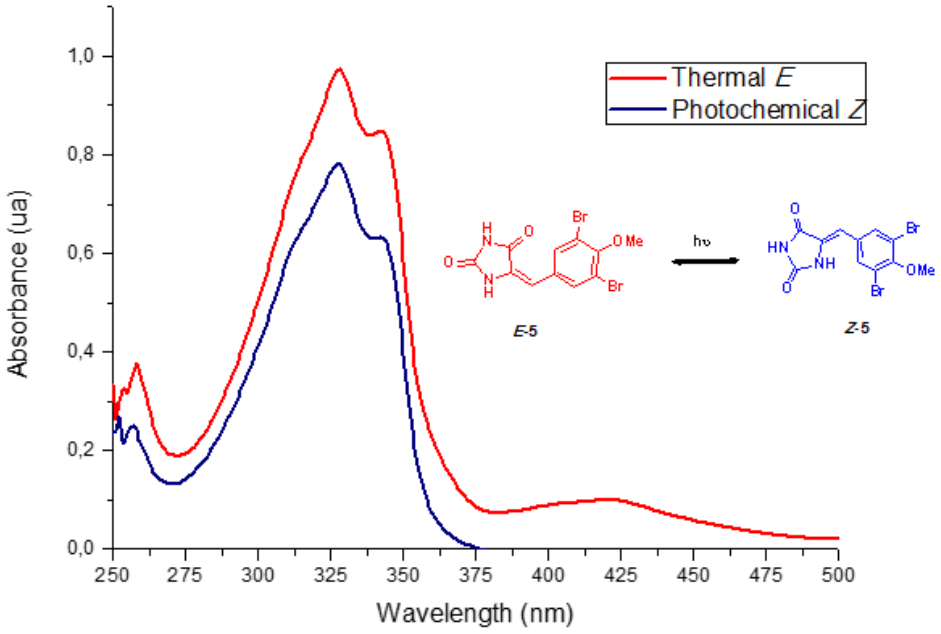

Figure 4.15. UV-Vis spectra of ***E*-5** and ***Z*-5.**

In this case, as is seen in the figure above, it was not possible to irradiate the *Z*-isomer preferentially, so the irradiation was not carried out since in each irradiation a different PSS would be obtained, but the reverse reaction would not be able to be controlled photochemically at any wavelength.

This study has demonstrated that the PSS is very dependent on the relative absorbance of both isomers, which in turn can be modified by the light source used for the irradiation. Besides, other properties are dependent on the difference absorption of both isomers such as the kinetics.

To explore this point in hydantoin-based molecular switches, the use of monochromatic light was used to irradiate a freshly made 5E-5 M solution of ***E*-7** each time. Several factors affect to the kinetics of a photoswitch:

- The concentration of the solution; the more molecules in the solution, the slower reaction.
- The energy of the lamp; if the source of light is very powerful, the photoreaction will be faster.

Those were the reasons why three solutions of the same concentration were prepared, and the irradiation was carried out using the same lamp, this way the intensity of the lamp did not vary. The monochromatic wavelengths used to isomerize the compound **7** were the same used before (300, 333 and 375 nm) (Figure 4.16).

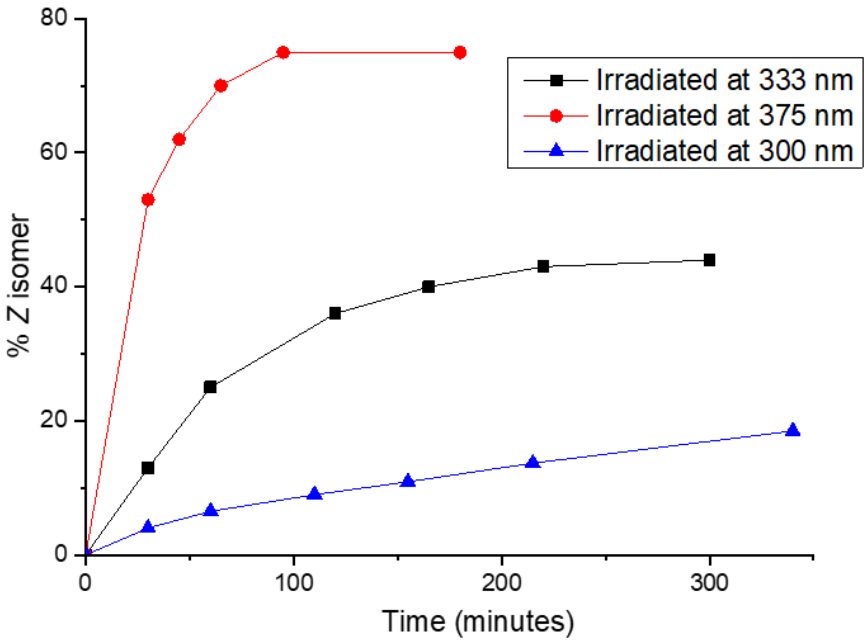

Figure 4.16. Irradiation of **7** at different wavelengths.

In Figure 4.16, it is plotted the isomerization of three solutions of ***E*-7** (5.5E-5 M) using three different monochromatic lights. The ratio mixture was determined by GC-MS at different periods of time until the PSS was reached.

In the first experiment, the sample was irradiated at 375 nm during 175 minutes until the PSS was reached. Using this wavelength, the process was very fast due to the big difference in absorption for both isomers as it is shown in Figure 4.14. Besides, at this wavelength the *Z* isomer had almost no absorption, so the *Z* → *E* isomerization is less relevant and the PSS, as we mentioned before, is very displaced to the formation of the *Z*-isomer.

Sequentially, another sample of the same concentration of ***E*-7** was irradiated at the absorption maximum. Using 333 nm for irradiating the sample, the irradiation was quite fast because the absorption of the *E*-isomer was notably greater than the *Z*-isomer (Figure 4.14).

Finally, when the irradiation was carried out at 300 nm, the process was very slow as it is shown in Figure 4.16, this was due to the absorption of both isomers being very similar (Figure 4.14), so both isomers were absorbing light in equal measures and forward and back photochemical reaction was occurring with similar rates.

To conclude, it can be assured with all the experimental data showed during this section that the PSS could be controlled by means of external factors.

2.4. Isomerization quantum yield.

A very relevant feature to define the behavior of a photoswitch is to study its isomerization quantum yield. This feature measures how many photons absorbed by the molecular switch are used to effectively rotate the C=C double bond resulting in the photoisomer. So, it gives the overall efficiency of the process. This is a key feature in the study of any molecular switch, and it can be calculated mathematically using the equation below (Equation 4.1).

$$\Phi = \frac{number\ of\ molecules\ formed\ of\ the\ photoisomer}{number\ of\ photons\ absorbed\ by\ the\ molecular\ switch}$$

Equation 4.1

This value was calculated following the procedure described in the literature, using *trans*-azobenzene as actinometer.[21] It gave the number of photons emitted by the light source. Moreover, the number of photons absorbed by the sample was calculated by using the following equation:

$$E_p \text{ (mol of photons x cm}^{-2}\text{x s}^{-1}) = F(\lambda) \text{ x } \Delta A \text{ (358nm) / t(s)}$$

Equation 4.2

where ΔA(358nm) is the change in the absorbance at 358 nm of the *trans*-azobenzene solution when irradiating at 334 nm, and t(s) is the irradiation time responsible for that change. The F factor, which depends on the wavelength, it is tabulated for five specific wavelengths on the literature. It has a value of 3.6E-6 einstein x cm^{-2} at 334 nm. Thus, the number of photons absorbed corresponds to E_p multiplied by the irradiation time (in seconds).

Firstly, a solution of *trans*-azobenzene in acetonitrile was prepared as actinometer. The absorbance of this solution at 358 nm was set to 1. Then, it was irradiated in a quartz cuvette at 334 nm using the monochromator. After a short period of time, the change in absorbance at 358 nm was *ca.* 0.02.

The isomerization quantum yields of **3** and **7** were measured as their maximum absorbance wavelengths were close to 334 nm; this wavelength was fixed by the actinometer used as aforementioned. Therefore, solutions of **7** in acetonitrile or CH_2Cl_2:MeOH (1:1) in the case of **3** were prepared. The absorbance at 334 nm was adjusted to match the absorbance of the actinometer. This solution was irradiated at 334 nm to a conversion of 20%. This is an important point, because if mixtures with a high ratio

[21] Kuhn, H. J.; Braslavsky, S. E.; Schmidt, R., Chemical actinometry *Pure Appl. Chem.* **2004,** *76*, 2105-2146.

of the photoisomer are used the result obtained for the isomerization quantum yield would be inaccurate since the *Z*-isomer would also be absorbing light. The isomerization process is followed by GC/MS, because low concentration solutions were used, as in previous experiments.

An isomerization quantum yield of 15±1% was obtained for irradiation at 334 for **3** and 16±1% for **7**. These values obtained are not as high as other reported before,[22, 23] but they confirm that this family of photoswitches is quite efficient and very promising.

2.5. Thermal and photochemical stability

As it is shown in Figure 4.17, the *E*-isomer could be achieved starting from the *Z*-isomer by just heating the sample. If the energy applied is enough to overcome the barrier in each specific case, the reverse reaction will occur obtaining the most stable isomer. The energy barrier to carry out the thermal-back reaction is specific for each photoswitch, since it is very dependent on the electronic influence of the substituents on the aryl moiety that affects the transition structure of the isomerization.

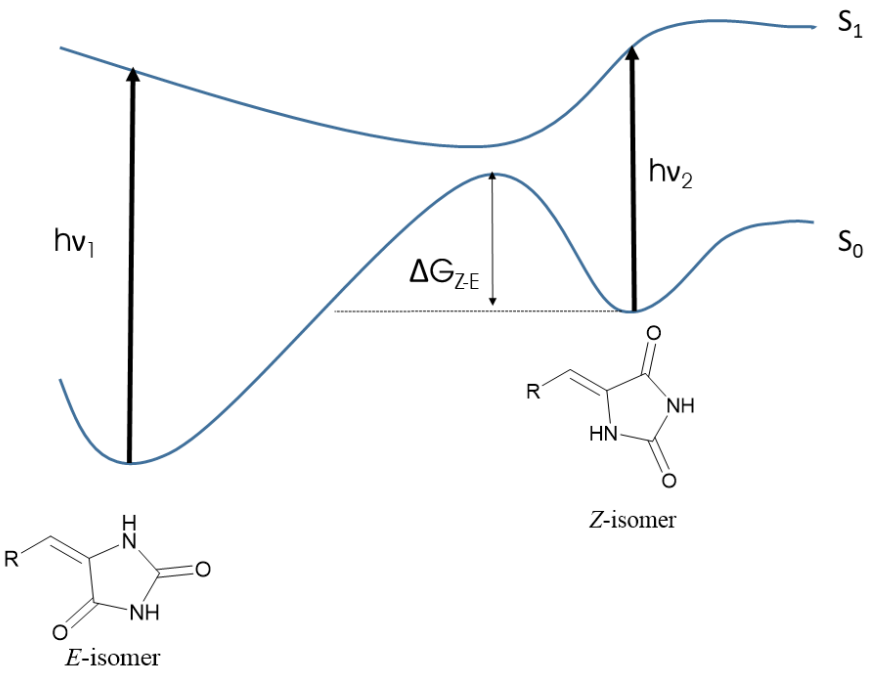

Figure 4.17. Reaction diagram of a photoswitch.

[22] Siewertsen, R.; Neumann, H.; Buchheim-Stehn, B.; Herges, R.; Näther, C.; Renth, F.; Temps, F., Highly Efficient Reversible Z−E Photoisomerization of a Bridged Azobenzene with Visible Light through Resolved S1(nπ*) Absorption Bands *J. Am. Chem. Soc.* **2009,** *131*, 15594-15595.

[23] Abbandonato, G.; Signore, G.; Nifosì, R.; Voliani, V.; Bizzarri, R.; Beltram, F., Cis–trans photoisomerization properties of GFP chromophore analogs *Eur. Biophys. J.* **2011,** *40*, 1205-1214.

Thus, with the goal of studying the thermal reverse reaction from *Z* to *E*-isomer, several compounds were tested. Specifically, these features were measured for compounds **4**, **5** and **7** since after irradiation, the mixtures were enriched in its photoisomer. To carry out these experiments, we used three different Pyrex NMR tubes; in each tube we put mixtures of *E* and *Z* isomers of the photoswitch. Finally, 0.1 M solutions of these mixtures in DMSO-d^6 were prepared. This solvent was used due to its high boiling point and the solubility of these compounds was very good in such solvent. All the experiments were followed at different times using ^{1}H NMR to evaluate the isomers ratio. The three samples were heated at 70ºC for 7 days in darkness, at this temperature a slow back reaction was found for **4**, but this process did not happen in the case of **5** and **7**. Increasing the temperature up to 100 ºC led to faster isomerization of **4** and some degree of isomerization of **7**; this temperature was maintained during 22 days, whereas no back-reaction was found for **5**. When the temperature was increased up to 120ºC, slow degradation of **5** was observed without isomerizing. Thus, it was concluded that the energy barrier to achieve ***E*-5** from ***Z*-5** was too high and this process was thermally unavailable.

In general, these compounds proved to be quite stable to the thermal-back reaction. Furthermore, thermal stability of the photoisomer is desirable in some applications, for instance in renewable energy field when the light energy should be released as heat in a controlled way.[24] Moreover, sometimes it is useful to produce large fractions of the photoisomer to control molecular targets.[25]

Apart from this issue, it is very important to prove the photostability of a molecular switch. For this purpose, there are several methods which can be used to test this feature.

Firstly, all compounds were tested dissolving them in a deuterated solvent, since the process was followed easily by ^{1}H NMR as in previous experiments. The samples were irradiated in Pyrex NMR tubes, and the light source used to study their photostability was a 125-W medium-pressure Hg lamp. Under these conditions, all photoswitches **1-11** were irradiated during 4 hours without giving any sign of decomposition. As it has been shown in previous sections, the PSSs for all compounds were achieved irradiating for 1 hour. However, this fact does not mean that both isomers were not absorbing light for longer irradiation times. In contrast, the compounds are involved in a dynamic equilibrium between the forward and back photoreactions without changing the isomers ratio.

[24] Dong, L.; Feng, Y.; Wang, L.; Feng, W., Azobenzene-based solar thermal fuels: design, properties, and applications *Chem. Soc. Rev.* **2018,** *47*, 7339-7368.

[25] Passlick, S.; Richers, M. T.; Ellis-Davies, G. C. R., Thermodynamically Stable, Photoreversible Pharmacology in Neurons with One- and Two-Photon Excitation *Angew. Chem. Int. Ed.* **2018,** *57*, 12554-12557.

The high photostability of these photoswitches has been demonstrated with this experiment. However, there is another possible way to check this feature. This method is based on the fatigue resistance; it consists of the irradiation of a mixture *(E /Z)* for a specific time to produce the *Z*-isomer, then irradiating the same sample for the same amount of time at another wavelength to carry out the photochemical back reaction. Thus, the starting isomers ratio should be achieved if the photoswich is photostable.

For this purpose, the fatigue resistance of **1** was checked using a solution 0.1 M in DMSO-d^6. This solution was placed in a quartz NMR tube and, as discussed in section 2.3.1, the forward and back reaction could be controlled using a Pyrex/quartz filter and a 125-W medium-pressure Hg lamp. Thus, firstly the sample containing just ***E*-1** was irradiated for 30 minutes using a quartz filter, then, the same sample was irradiated for the same amount of time using a Pyrex filter to produce the photoreversion. These steps were repeated several times as it can be seen below (Figure 4.18).

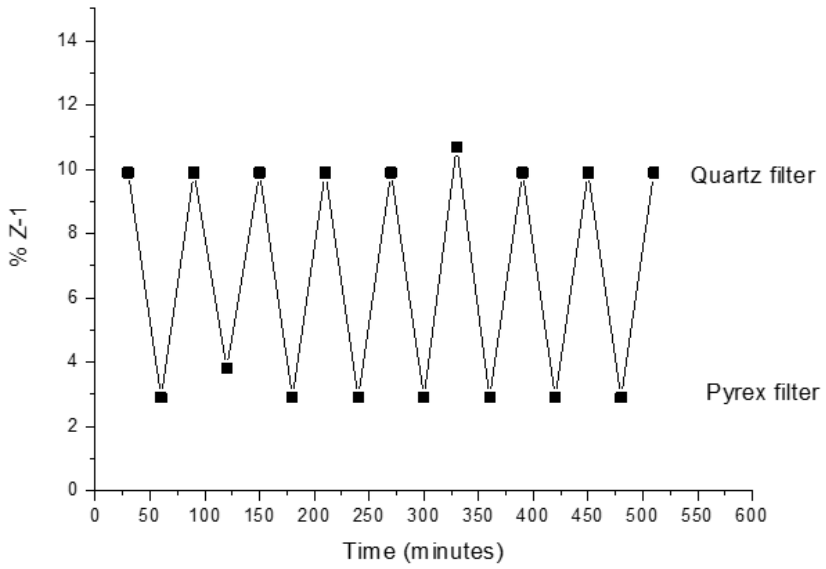

Figure 4.18. Fatigue resistance of **1**.

In the figure above, the percentage of *Z*-isomer of **1** irradiated using different types of filters is represented. As Figure 4.18 shows, the fatigue resistance of this photoswitch was very high, because it was exposed to different types of radiation successfully changing its photoswitching direction for several cycles.

To generalize this feature in hydantoin-based molecular switches, the same experiment was performed for compounds **2** and **7**. Solutions of 5E-5 M of ***E*-2** and ***E*-7** were prepared, in this case monochromatic light was used to photocontrol the isomerization. Firstly, the sample of ***E*-2** was irradiated alternatively using 360 and 270 nm

during several cycles (Figure 4.19). The PSS was followed by monitoring the absorbance at 305 nm. Then, the irradiation of ***E*-7** was performed using the same procedure, but the irradiation wavelengths were 375 and 300 nm and the PSS was followed checking the absorbance at 333 nm each cycle (Figure 4.20).

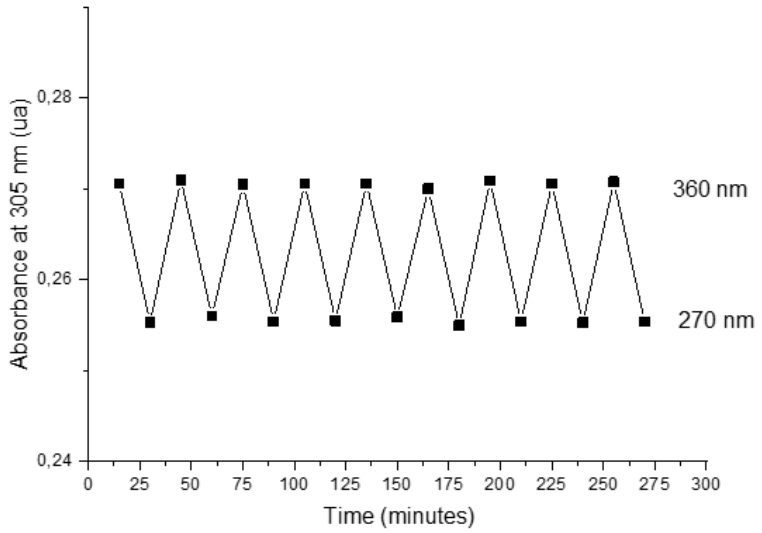

Figure 4.19. Fatigue resistance of **2**.

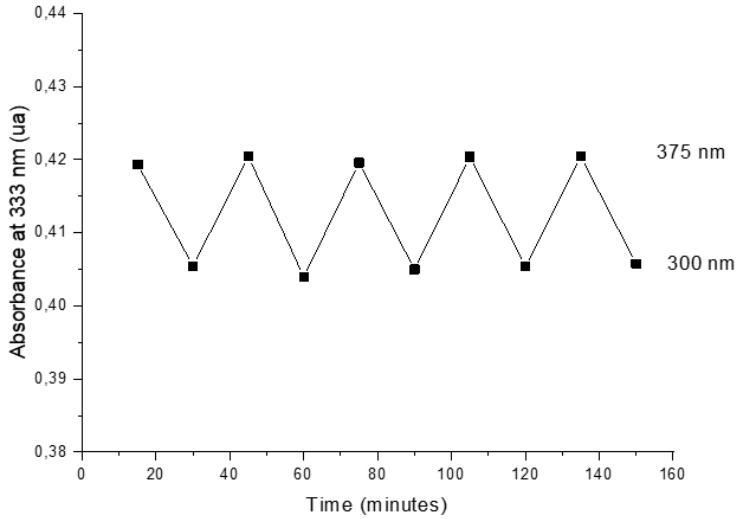

Figure 4.20. Fatigue resistance of **7**.

As is shown in the Figures above, the high fatigue resistance of these derivatives was checked, providing really good results since no signs of decomposition could be detected in Figures 4.18, 4.19 and 4.20.

3. Computational study.

To get a better understanding of the photochemical and photophysical behavior of this family of molecular switches, some theoretical calculations were done.

To perform this study, MP2 and CASPT2//CASSCF[26] calculations were carried out to calculate all the properties under study (UV-Vis spectra, MEP…). In detail, CASSCF was used to optimize the structures, while CASPT2 was used as an energy correction to improve the energy values obtained.

Due to the good experimental properties observed in the large study made of **7** in section 2, this compound was chosen to compute its properties as a representative example of this family of molecular switches. It should be noted that, although each compound showed different properties, they all share the same chromophore. Firstly, ***E*-7** and ***Z*-7** were optimized in the ground state (S_0) at the MP2/6-31G* level of theory (Figure 4.21).

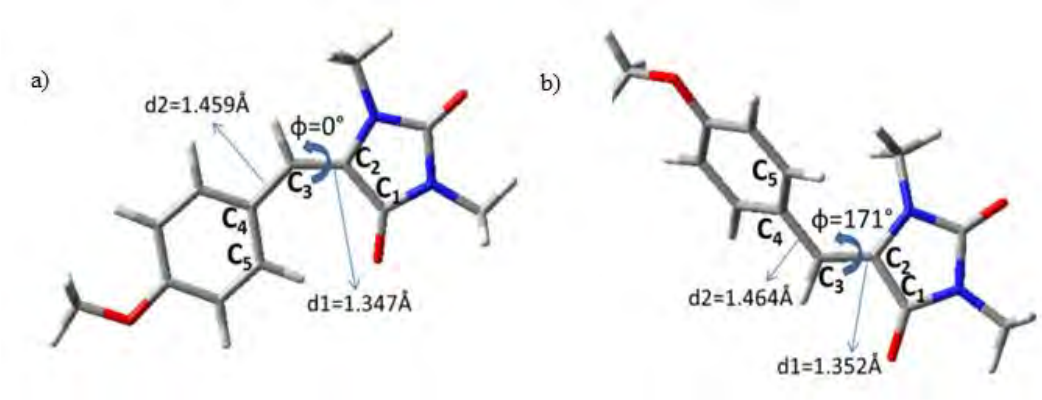

Figure 4.21. Structure of the ground state minima for the *E* (a) and the *Z* (b) isomers of compound **7**. (C1 C2 C3 C4 dihedral is defined as ϕ).

As is shown above, the ***E*-7** optimized structure is totally planar and ***Z*-7** is slightly twisted due to the steric hindrance between the methyl and phenyl groups. This is the main reason for the slightly blue-shift experimented by the absorption band of the *Z*-isomer seen in Figure 4.14

Secondly, the absorption of ***E*-7** was evaluated using the methodology MS-CASPT2//SA-CASSCF using a 6-31G* basis set. To perform this study, the active space should be chosen. Therefore, it was evaluated the effect of the active space by computing vertical transitions with several active spaces to compare their results with the ones obtained experimentally. Firstly, the vertical transitions were computed using a large

[26] Olivucci, M., *Computational Photochemistry*. Elsevier: Amsterdam, 2005; Vol. 16.

active space (16, 14); this means that 16 electrons in 14 orbitals were evaluated. Hence, six π orbitals (the complete π backbone), the corresponding π^* orbitals, and two n orbitals which correspond to the nitrogen atom and to the carbonyl moiety closer to the chromophore were evaluated. Then, the active space was reduced to (14, 13) removing the n orbital of the nitrogen atom since it was found not to be relevant (orbital occupation: 2.0). Finally, we performed the calculation with a (12,11) active space excluding the bonding π and anti-bonding π^* orbitals describing the whole phenyl ring, for the same reason. All these results are shown below (Table 4.7). It should be noted that the bigger active space, the higher the computational cost. Thus, the lowest active space compatible with a good agreement with the experimental data should be used.

Active space	State	E_{CASPT2} /eV (nm)	f
(16, 14)	S_1 ($\pi\rightarrow\pi^*$)	3.72 (333)	0.4982
	S_2 ($\pi\rightarrow\pi^*$)	4.64 (267)	0.0094
	S_3 (n$\rightarrow\pi^*$)	4.78 (259)	0.0057
	S_4 ($\pi\rightarrow\pi^*)^2$, ($\pi\rightarrow\pi^*$)	5.81 (213)	0.3885
(14, 13)	S_1 ($\pi\rightarrow\pi^*$)	3.88 (319)	0.5597
	S_2 ($\pi\rightarrow\pi^*$)	4.70 (264)	0.0068
	S_3 (n$\rightarrow\pi^*$)	4.82 (257)	0.0058
	S_4 ($\pi\rightarrow\pi^*)^2$, ($\pi\rightarrow\pi^*$)	5.98 (207)	0.2607
(12, 11)	S_1 ($\pi\rightarrow\pi^*$)	3.58 (346)	0.5091
	S_2 ($\pi\rightarrow\pi^*$)	4.37 (284)	0.0060
	S_3 (n$\rightarrow\pi^*$)	4.59 (270)	0.0057
	S_4 ($\pi\rightarrow\pi^*)^2$, ($\pi\rightarrow\pi^*$)	5.86 (212)	0.2327

Table 4.7

Keeping in mind that photoswitch **7** showed an absorption band centered at 333 nm experimentally, the theoretical calculations predicted this value correctly as it is shown in Table 4.7. By using the large active space, the value obtained was very accurate. However, the use of (12, 11) active space predicted the absorption spectra of **7** relatively agreeably with the experimental data, at a much lower computational cost. Therefore, in

order to perform other theoretical calculations such as the minimum energy path or single point energy corrections at the CASPT2 level, this active space was used.

Once the methodology appropriate for each experiment has been discussed, the absorption spectrum of ***E*-7** was computed in gas phase and chloroform. The effect of the solvent on the absorption wavelength was modeled by applying the polarizable continuum model (PCM) (Table 4.8).[27]

Isomer	Band eV (nm)	State	E^{Vacuum}_{CASPT2} eV (nm)	E^{PCM}_{CASPT2} eV (nm)	Transition	f	Relative f
***E*-7**	3.72 (333)	S_1	3.72 (333)	3.69 (336)	$^1(\pi,\pi^*)$	0.4982	0.5609
		S_2	4.64 (267)	4.65 (266)	$^1(\pi,\pi^*)$	0.0009	0.0010
		S_3	4.78 (259)	4.86 (255)	$^1(n,\pi^*)$	0.0006	0.0007

Table 4.8

From Table 4.8, it is observed that the effect of the solvent was negligible since similar results were found for the simulation of its photophysical properties in gas phase and by applying the PCM ($CHCl_3$). These results coincide with the data obtained in the experiments.

The first excited state (S_1) of ***E*-7** was optically the bright state since the oscillator strength is quite large. In contrast the second (S_2) and the third (S_3) excited states were dark states due to their low values for the oscillator strength. There was another transition that could be populated easily (S_4) but it was located at higher energies, therefore it was not useful for our study. The electronic transition nature of the bright state was described by the excitation of one electron from the bonding π to the anti-bonding π^* orbital of the central C=C double bond (Figure 4.22).

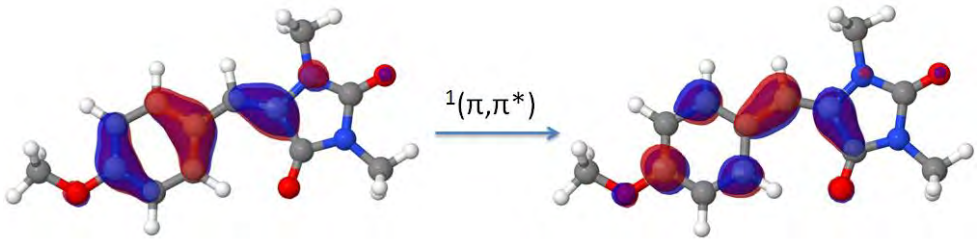

Figure 4.22. CASSCF molecular orbitals describing the electronic nature of the optically bright state.

[27] Tomasi, J.; Mennucci, B.; Cammi, R., Quantum Mechanical Continuum Solvation Models *Chem. Rev.* **2005,** *105*, 2999-3094.

It is shown above that after excitation of ***E*-7** to the bright state, the electronic density is displaced from the central C=C double bond to the rest of the molecule, allowing the photoisomerization.

Following with the theoretical study of ***E*-7**, the minimum energy path (MEP) was evaluated (Figure 4.23). After excitation of ***E*-7** to the bright state (S_1), the system minimized its energy rotating along the formal double bond 90 degrees. When this point was achieved, the energy gap between S_1 and S_0 was 20 kcal/mol at the CASPT2 level of theory and the coupling between both states is large.

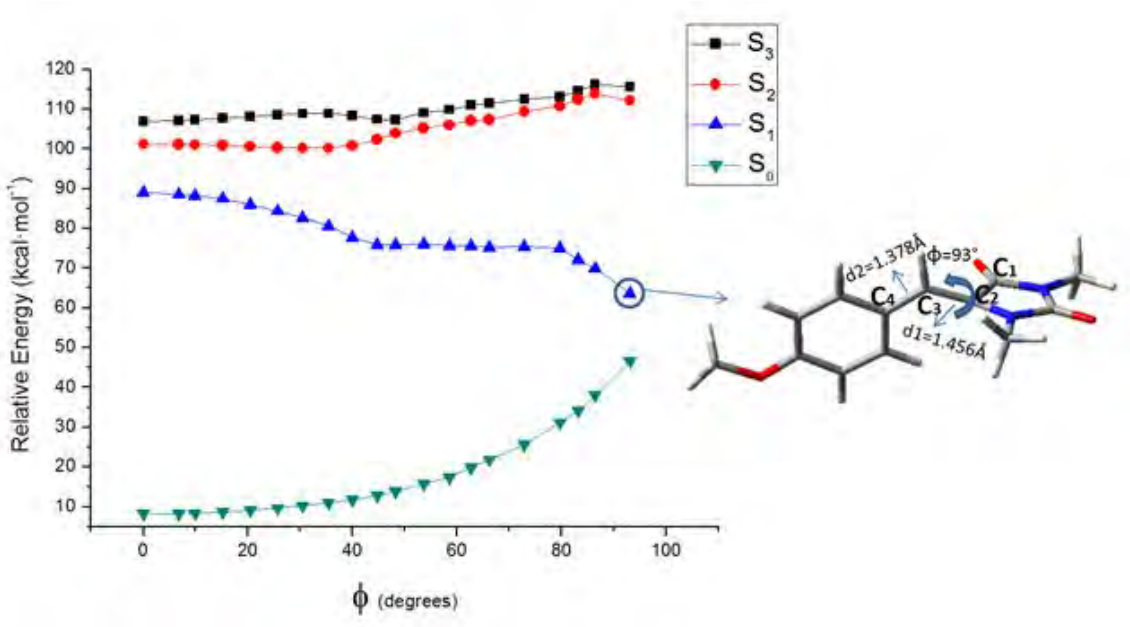

Figure 4.23. MS-CASPT2 single point energy corrections along the relaxation path on S_1 computed at the CASSCF level of theory, as a function of the central double bond torsion coordinate (φ) for **7**. The structure of the final point is depicted.

From this point, the system could return to the ground state through a radiative decay, recovering the *E* isomer or completing the photoisomerization reaching the *Z*-isomer. The emission aforementioned should be around 1430 nm, and it could not be detected experimentally due to its low energy. Thus, deactivation of the photoisomerization due to crossings with other excited states were avoided.

To evaluate the thermal reversion of ***E*-7**, from the minimum structure in S_1 the energy correction was computed along the minimum energy path of S_0 (Figure 4.24).

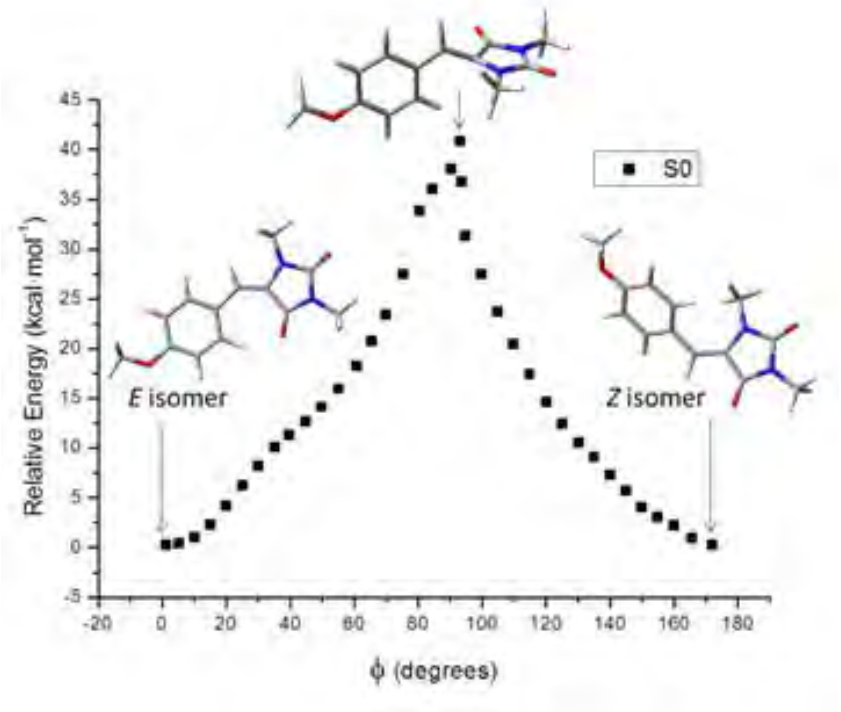

Figure 4.24. MS-CASPT2 single-point energy corrections along the minimum energy path on S_0 from S_1 minimum energy structure for **7** computed at the CASSCF level of theory.

We can conclude that all predictions carried out by the theoretical study were agreeable with the experimental data. So, the methods used to perform the calculations were correct to perform the photochemical study of this kind of photoswitches.

4. Experimental data.

4.1. General synthesis of photoswitches.

Method 1:

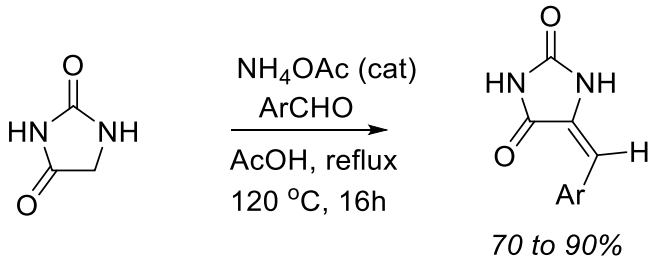

Scheme 4.2. Condensation of hydantoin in acidic conditions.

Step 1: A solution of imidazolidine-2,4-dione (2.16 g, 20 mmol) and ammonium acetate (276 mg, 3.6 mmol) in acetic acid (5 mL) was added to an aldehyde (20 mmol) and the resulting mixture was stirred at 120 °C for 16 hours. After cooling, the reaction mixture was concentrated in vacuum and purified by washing the crude with an organic solvent or by column chromatography on silica gel with different mixtures of hexane / ethyl acetate to afford the 5-arylideneimidazolidine-2,4-diones (with yields ranging from 70 to 90%).

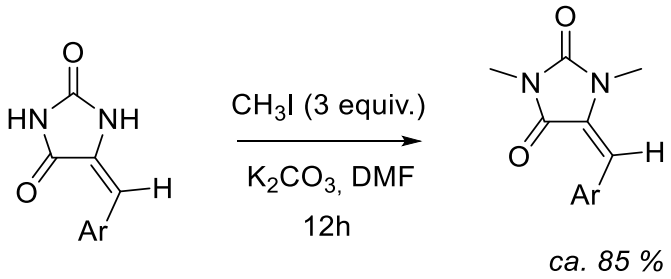

Scheme 4.3. Methylation of hydantoin based molecular switches.

Step 2: To a solution of 5-arylideneimidazolidine-2,4-dione (2 mmol) in dry DMF (50 mL) was added K_2CO_3 (0.83 g, 6 mmol) and methyl iodide (0.85 g, 6 mmol, 3 equiv.). The resulting mixture was stirred overnight at room temperature. The reaction was quenched by the addition of water. The resulting mixture was diluted with ethyl acetate (25 mL), and washed with water (15 ml x 3) and brine (50 ml). The organic layer was dried over anhydrous Na_2SO_4, filtered and concentrated. The resulting crude residue was purified by column chromatography on silica gel to give 5-arylidine 1,3-dimethylimidazolidine-2,4-diones with a yield of *ca.* 85% depending on the aryl moiety.

Method 2:

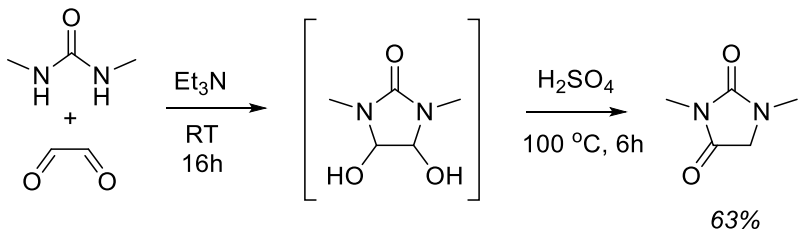

Scheme 4.4. Synthesis of methylated hydantoin.

Step 1: A 100 ml glass round-bottom flask equipped with a stirrer, thermometer and addition funnel was charged with 2.90 g (0.2 mol) of 40 wt % aqueous glyoxal solution and triethylamine (pH of the reaction mixture 9). Then, a solution of 1,3-dimethylurea (1.76 g (0.2 mol in 18 ml of water) was gradually added to the mixture at room temperature. After addition was completed, the mixture was allowed to stir at the same temperature for 3 hours. After the completion of the reaction as monitored by TLC, the solvent was removed under reduced pressure to obtain 2.97 g of crude 4,5-dihydroxy-1,3-dimethyl-2-imidazolidinone as a colorless oil which was taken further for step 2 without further purification.

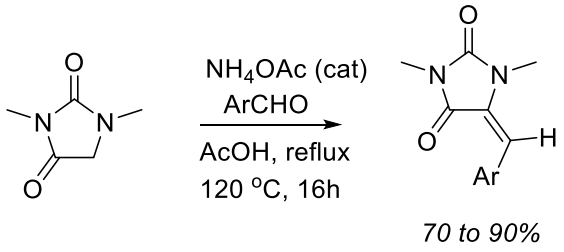

Scheme 4.5. Condensation of methylated hydantoin in acidic conditions.

Step 2: A 100 ml glass round-bottom flask equipped with a stirrer, thermometer and a reflux condenser was loaded with 2.97 g of crude 4,5-dihydroxy-1,3-dimethyl-2-imidazolidinone prepared from the previous step, H_2O (3 ml) and 98% sulfuric acid (0.54 g. 5.4 mmol) and the resulting mixture was stirred for 6 hours at 95°C to 100 °C. After completion of the reaction, the reaction mixture was cooled with an ice bath, and 0.90 g of sodium bicarbonate was added slowly. The crude residue was diluted with EtOAc/H_2O (50 ml/20 ml). The aqueous layer was separated and extracted with EtOAc (50 ml x 3). The organic layers were combined and washed with brine (50 ml), dried over anhydrous Na_2SO_4, filtered and concentrated. The crude residue was purified by column chromatography on silica gel with EtOAc-hexane (20/80 to 35/65) to obtain 1,3-dimethylimidazolidin-2,4-dione as a colorless oil (1.61 g, 40-50% yield for two steps).

4.2. Characterization data.

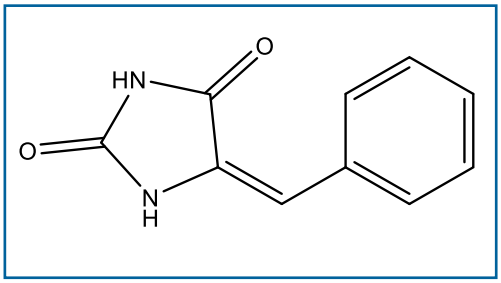

(*E*)-5-(benzylidene)imidazolidine-2,4-dione (*E*-1)

Yield = 70 %

Molecular weight: 188.19

Empiric formula: $C_{10}H_8N_2O_2$

^{1}H-NMR (300 MHz, DMSO-d^6) δ 7.61 (d, *J* = 7.5 Hz, 2H), 7.40 (t, *J* = 7.4 Hz, 2H), 7.35 – 7.29 (m, 1H), 6.41 (s, 1H).

^{13}C-NMR (75 MHz, DMSO) δ 165.6, 155.7, 133.0, 129.4, 128.8, 128.4, 128.0, 108.3.

UV-Vis (CH_2Cl_2 : MeOH): λ (nm) = 316 (ε=20471 $M^{-1}cm^{-1}$), 331 (ε= 16123 $M^{-1}cm^{-1}$).

EM-ES (+): calcd for $C_{10}H_9N_2O_2$ $[M+H]^+$ 189.0664, found 189.0671.

Observations: White solid.

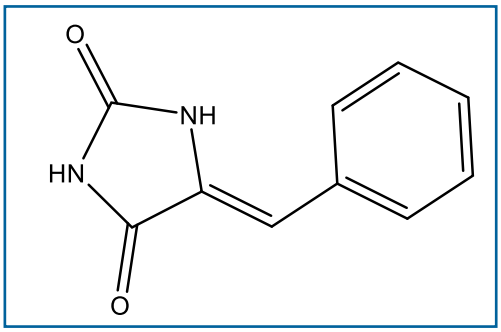

(*Z*)-5-(benzylidene)imidazolidine-2,4-dione (*Z*-1)

Molecular weight: 188.19

Empiric formula: $C_{10}H_8N_2O_2$

^{1}H-NMR (300 MHz, DMSO-d^6)) δ ppm 7.89 (d, *J* = 7.3 Hz, 2H), 7.38 – 7.28 (m, 3H), 6.32 (s, 1H).

^{13}C-NMR (75 MHz, $CDCl_3$) δ 163.6, 153.9, 133.1, 129.9, 128.1, 115.6.

UV-Vis (CH_2Cl_2 : MeOH): λ (nm) = 330 (ε=13309 $M^{-1}cm^{-1}$).

EM-ES (+): calcd for $C_{10}H_9N_2O_2$ $[M+H]^+$ 189.0664, found 189.0671.

Observations: White solid.

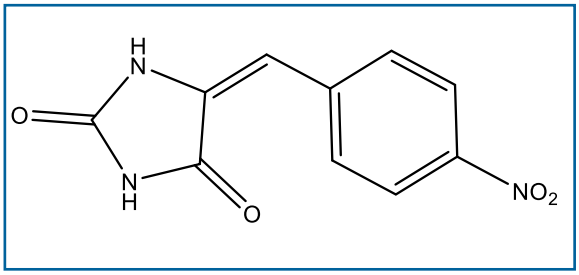

(E)-5-(4-nitrobenzylidene)imidazolidine-2,4-dione **(*E*-2)**

Molecular weight: 233.18

Empiric formula: $C_{10}H_7N_3O_4$

Yield = 78 %

^{1}H-NMR: (400 MHz, DMSO-d^6) δ ppm 8.19 (d, *J* = 8.4 Hz, 2H), 7.84 (d, *J* = 8.6 Hz, 2H), 6.49 (s, 1H).

^{13}C-NMR: (100 MHz, DMSO-d^6) δ ppm 165.3, 155.8, 146.2, 140.0, 130.9, 130.1, 123.7, 105.1.

UV-Vis (CH_2Cl_2 : MeOH (1:1)): λ (nm) = 236 (ε=8188 $M^{-1}cm^{-1}$), 353 (ε= 15854 $M^{-1}cm^{-1}$)

EM-ES (+)**:** calcd for $C_{10}H_8N_3O_4$ $[M+H]^+$ 234.0515, found 234.0515.

Observations: Brown solid.

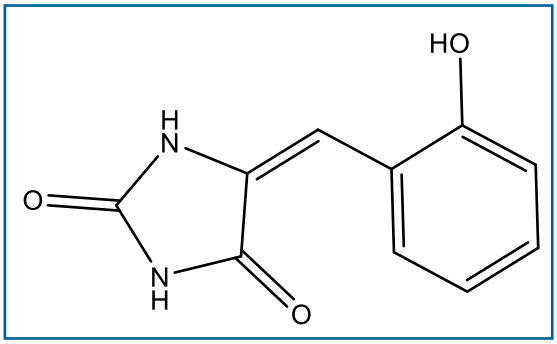

(E)-5-(2-hydroxybenzylidene)imidazolidine-2,4-dione **(*E*-3)**

Molecular weight: 204.19

Empiric formula: $C_{10}H_8N_2O_3$

Yield = 75 %

^{1}H-NMR: (400 MHz, DMSO-d^6) δ ppm 7.53 (d, *J* = 7.7 Hz, 1H), 7.15 (t, *J* = 7.9 Hz, 1H), 6.90 – 6.77 (m, 2H), 6.67 (s, 1H).

^{13}C-NMR: (100 MHz, DMSO-d^6) δ ppm 165.7, 156.0, 155.5, 130.0, 129.5, 127.2, 120.1, 119.4, 115.6, 104.0.

UV-Vis (CH_2Cl_2 : MeOH (1:1)): λ (nm) = 235 (ε=9800 $M^{-1}cm^{-1}$), 312 (ε= 13200 $M^{-1}cm^{-1}$), 340 (ε = 15200 $M^{-1}cm^{-1}$).

EM-ES (+): calcd for $C_{10}H_9N_2O_3$ $[M+H]^+$ 205.0613, found 205.0615.

Observations: White solid.

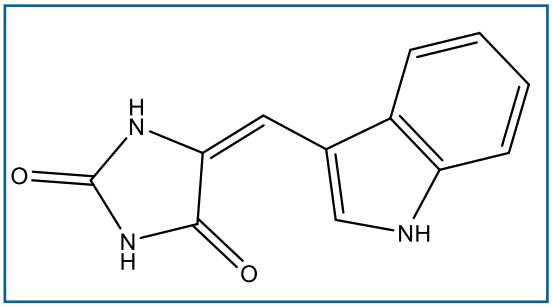

(*E*)-5-((1*H*-indol-3-yl)methylene)imidazolidine-2,4-dione (***E*-4**)

Molecular weight: 227.22

Empiric formula: $C_{12}H_9N_3O_2$

Yield = 74 % ;

^{1}H-NMR: (400 MHz, DMSO-d^6) δ ppm 8.13 (s, 1H), 7.75 (d, *J* = 7.7 Hz, 1H), 7.42 (d, *J* = 7.7 Hz, 1H), 7.21-7.09 (m, 2H), 6.75 (s, 1H).

^{13}C-NMR: (100 MHz, DMSO) δ ppm 165.7, 155.7, 136.0, 127.0, 126.8, 123.8, 122.6, 120.42, 118.2, 112.1, 108.6, 102.1.

UV-Vis (CH_2Cl_2 : MeOH (1:1)): λ (nm) =275 (ε=3602 $M^{-1}cm^{-1}$), 367 (ε=11835 $M^{-1}cm^{-1}$)

EM-ES (+): calcd for $C_{12}H_{10}N_3O_2$ [M+ H]$^+$ 228. 0773, found 228.0779.

Observations: Orange solid.

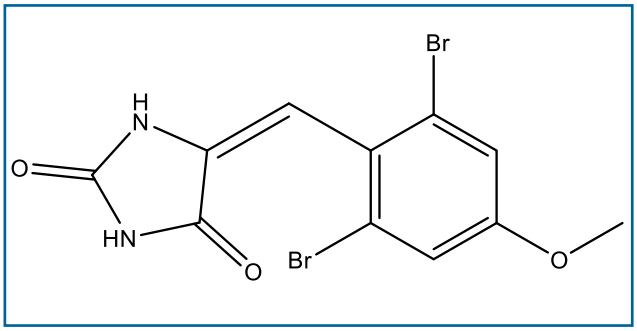

(*E*)-5-(3,5-dibromo-4-methoxybenzylidene)imidazolidine-2,4-dione (***E*-5)**

Molecular weight: 376.00

Empiric formula: $C_{11}H_8Br_2N_2O_3$

Yield = 77 %

^{1}H-NMR: (300 MHz, DMSO-d^6) δ ppm 8.09 (s, 2H), 5.59 (s, 1H), 3.76 (s, 3H).

^{13}C-NMR: (100 MHz, DMSO-d^6) δ ppm 165.4, 155.9, 152.9, 133.0, 132.4, 129.3, 117.9, 104.6, 60.5.

UV-Vis (CH_2Cl_2 : MeOH (1:1)): λ (nm) =321 (ε= 22605 $M^{-1}cm^{-1}$).

EM-ES (+): calcd for $C_{11}H_9Br_2N_2O_3$ [M+ H]$^+$ 374.8980, found 374.8974.

Observations: Brown solid.

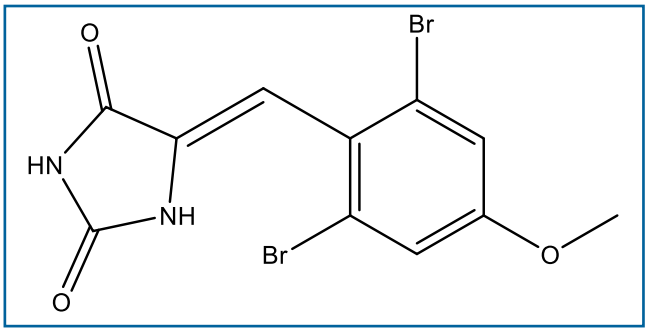

(*Z*)-5-(3,5-dibromo-4-methoxybenzylidene)imidazolidine-2,4-dione **(*Z*-5)**

Molecular weight: 376.00

Empiric formula: $C_{11}H_8Br_2N_2O_3$

^{1}H-NMR: (400 MHz, DMSO-d^6) δ ppm 7.91 (s, 2H), 6.33 (s, 1H), 3.81 (s, 3H).

^{13}C-NMR: (100 MHz, DMSO-d^6) δ ppm 165.2, 155.7, 153.0, 133.0, 132.1, 129.1, 117.9, 104.5, 60.5.

UV-Vis (CH_2Cl_2 : MeOH (1:1)): λ (nm) =328 (ε= 14942 $M^{-1}cm^{-1}$), 342 (ε= 5747 $M^{-1}cm^{-1}$).

EM-ES (+): calcd for $C_{11}H_9Br_2N_2O_3$ $[M+H]^+$ 374.8980, found 374.8974.

Observations: Brown solid.

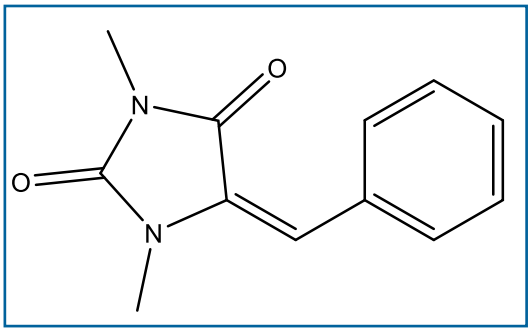

(*E*)-5-(benzylidene)-1,3-dimethylimidazolidine-2,4-dione **(*E*-6):**

Molecular weight: 216.24

Empiric formula: $C_{12}H_{12}N_2O_2$

Yield = 81 %

^{1}H NMR (300 MHz, $CDCl_3$) δ ppm 7.41-7.28 (m, 5H), 6.95 (s, 1H), 3.14 (s, 3H), 2.95 (s, 3H).

^{13}C NMR (75 MHz, $CDCl_3$) δ 163.7, 155.8, 132.6, 129.6, 129.4, 128.3, 128.7, 112.2, 30.5, 24,9.

UV-Vis ($CHCl_3$): λ (nm) =240 (ε= 7904 $M^{-1}cm^{-1}$), 309 (ε= 12316 $M^{-1}cm^{-1}$).

EM-ES (+): calcd for $C_{12}H_{13}N_2O_2$ $[M+H]^+$ 217.0977, found 217.0972 g/mol.

Observations: Yellow oil.

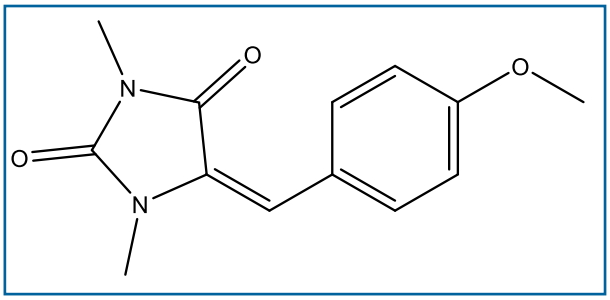

(*E*)-5-(4-methoxybenzylidene)-1,3-dimethylimidazolidine-2,4-dione **(*E*-7):**

Molecular weight: 246.27

Empiric formula: $C_{13}H_{14}N_2O_3$

Yield = 80 %

^{1}H-NMR: (400 MHz, CD_3CN) δ 7.96 (d, *J* = 8.9 Hz, 2H), 6.92 (d, *J* = 8.9 Hz, 2H), 6.28 (s, 1H), 3.81 (s, 3H), 3.12 (s, 3H), 2.98 (s, 3H).

^{13}C-NMR: (100 MHz, CD_3CN) δ (ppm) 163.1, 161.0, 154.6, 133.0, 129.1, 126.8, 117.4, 114.50, 56.0, 26.8, 24.9.

UV-Vis ($CHCl_3$): λ (nm) =333 (ε= 16346 $M^{-1}cm^{-1}$), 243 (ε= 10115 $M^{-1}cm^{-1}$).

ES-MS (+): calcd for $C_{13}H_{15}N_2O_3$ $[M+H]^+$ 247.1083, found 247.1065 g/mol.

Observations: Yellow solid.

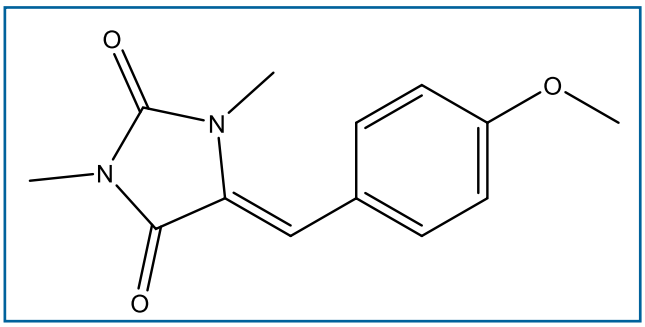

(*Z*)-5-(4-methoxybenzylidene)-1,3-dimethylimidazolidine-2,4-dione **(*Z*-7)**

Molecular weight: 246.27

Empiric formula: $C_{13}H_{14}N_2O_3$

^{1}H-NMR: (400 MHz, $CDCl_3$) δ ppm 7.24 (d, *J* = 8.7 Hz, 2H), 6.93 (s, 1H), 6.90 (d, *J* = 3.8 Hz, 2H), 3.84 (s, 3H), 3.13 (s, 3H), 3.00 (s, 3H).

^{13}C-NMR: (100 MHz, $CDCl_3$) δ ppm 164.0, 159. 9, 156.2, 131.1, 129.0, 124.9, 113.9, 112.7, 55.4, 30.6, 25.1.

UV-Vis ($CHCl_3$): λ (nm) =325 (ε= 14808 $M^{-1}cm^{-1}$).

ES-MS (+): calcd for $C_{13}H_{15}N_2O_3$ $[M+H]^+$ 247.1083, found 247.1065 g/mol.

Observations: Yellow solid.

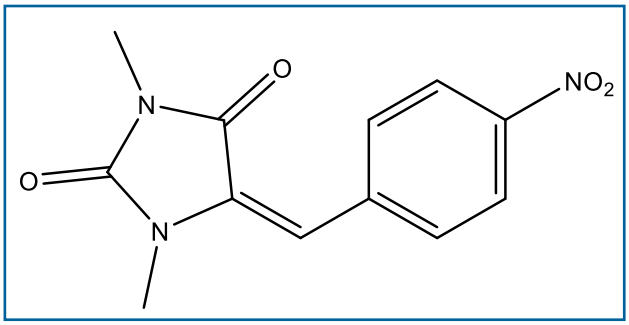

(*E*)-5-(4-nitrobenzylidene)-1,3-dimethylimidazolidine-2,4-dione (***E*-8**)

Molecular weight: 261.24

Empiric formula: $C_{12}H_{11}N_3O_4$

Yield = 90 %

^{1}H-NMR (300 MHz, $CDCl_3$) δ ppm 8.27 (d, *J* = 8.4 Hz, 2H), 7.47 (d, *J* = 8.5 Hz, 2H), 6.89 (s, 1H), 3.17 (s, 3H), 2.96 (s, 3H).

^{13}C NMR (100 MHz, $CDCl_3$) δ 163.3, 155.7, 147.5, 139.8, 131.7, 130.4, 123.6, 108.7, 30.7, 25.4.

UV-Vis ($CHCl_3$): λ (nm) =339 (ε= 11816 $M^{-1}cm^{-1}$).

EM-ES (+): calcd for $C_{12}H_{12}N_3O_4$ $[M+H]^+$ 262.0828, found 262.0822.

Observations: Orange solid.

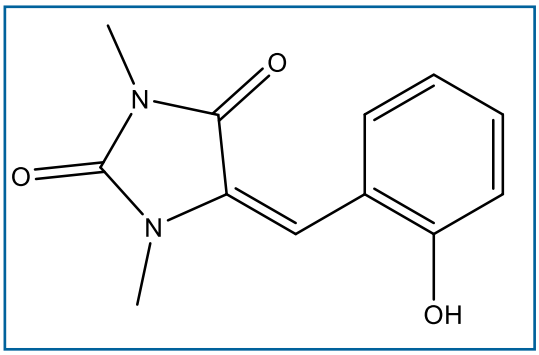

(*E*)-5-(2-methoxybenzylidene)-1,3-dimethylimidazolidine-2,4-dione (***E*-9**)

Molecular weight: 232.24

Empiric formula: $C_{12}H_{12}N_2O_3$

Yield = 79%

^{1}H NMR (300 MHz, $CDCl_3$) δ ppm 7.34 (t, *J* = 7.4 Hz, 1H), 7.16 (d, *J* = 7.4 Hz, 1H), 7.02 – 6.88 (m, 3H), 3.85 (s, 3H), 3.13 (s, 3H), 2.94 (s, 3H).

^{13}C NMR (100 MHz, $CDCl_3$) δ 163.6, 157.6, 155.8, 130.7, 130.0, 129.9, 121.5, 119.9, 110.4, 108.8, 55.4, 29.8.

UV-Vis ($CHCl_3$): λ (nm) = 242 (ε=10870 $M^{-1}cm^{-1}$), 326 (ε= 12077 $M^{-1}cm^{-1}$).

EM-ES (+): calcd for $C_{12}H_{13}N_2O_3$ $[M+H]^+$ 232.0848, found 232.0852 g/mol .

Observations: Brown solid.

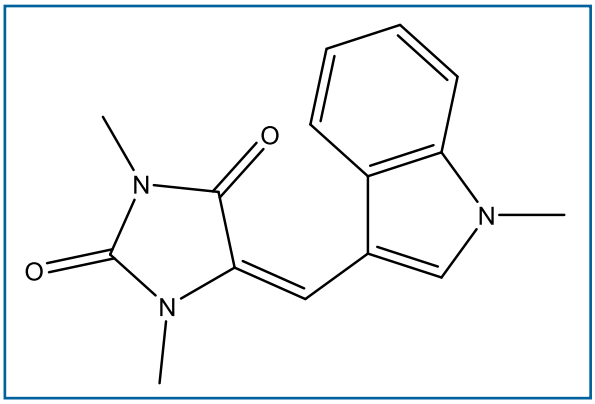

(*E*)-5-((1methyl-indol-3-yl)methylene))-1,3-dimethylimidazolidine-2,4-dione (***E*-10)**

Molecular weight: 269.30

Empiric formula: $C_{15}H_{15}N_3O_2$

Yield = 82%;

^{1}H NMR (300 MHz, $CDCl_3$) δ ppm 7.68 (d, *J* = 8.0 Hz, 1H), 7.34 (t, *J* = 8.3 Hz, 2H), 7.24-7.19 (m, 1H), 7.15 (s, 1H), 7.10 (s, 1H), 3.85 (s, 3H), 3.17 (s, 3H), 3.15 (s, 3H).

^{13}C NMR (100 MHz, $CDCl_3$) δ 164.2, 156.4, 136.8, 129.8, 128.4, 127.5, 123.0, 120.8, 119.7, 109.9, 107.7, 106.0, 33.3, 30.15, 25.09.

UV-Vis ($CHCl_3$): λ (nm) =373 (ε=13610 $M^{-1}cm^{-1}$).

EM-ES (+): calcd for $C_{15}H_{16}N_3O_2$ $[M+H]^+$ 270.1243, found 270.1242.

Observations: Brown solid.

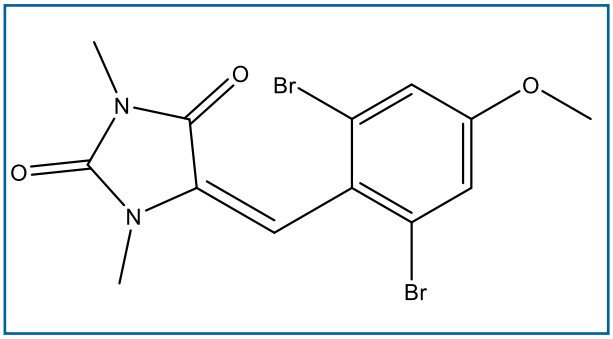

(*E*)-5-(3,5-dibromo-4-methoxybenzylidene)-1,3-dimethylimidazolidine-2,4-dione (***E*-11)**

Molecular weight: 404.06

Empiric formula: $C_{13}H_{12}Br_2N_2O_3$

Yield = 84%;

^{1}H NMR (400 MHz, $CDCl_3$) δ ppm 7.44 (s, 2H), 6.72 (s, 1H), 3.92 (s, 3H), 3.14 (s, 3H), 3.00 (s, 3H).

^{13}C NMR (75 MHz, $CDCl_3$) δ 163.4, 155.8, 154.3, 133.5, 131.4, 131.0, 118.2, 108.2, 61.0, 30.8, 25.3.

UV-Vis ($CHCl_3$): λ (nm) =316 (ε=8710 $M^{-1}cm^{-1}$).

EM-ES (+): calcd for $C_{13}H_{13}Br_2N_2O_3$ $[M+H]^+$ 402.9293, found 402.9282 g/mol.

Observations: Yellow solid.

5. Rhodopsin-based molecular switches.

Many kinds of molecular switches are responsible for controlling different biologic processes in nature. These molecular switches can be controlled electrochemically, chemically or using light as it was discussed in the background.[1] These molecules have served us to explore new possible molecular switches based on natural compounds with the aim of improving their highly effective properties in biological systems,[2] such as GFP protein or phytochrome protein. For instance, in the previous chapter it was described a new and efficient family of photoactive molecular switches based on hydantoin.

As was detailed in the background, one of the most important photoswitching processes in our lives is the responsible of vision.[3] The chromophore of the rhodopsin protein suffers a fast isomerization from 11-*cis*-retinal to all-*trans*-retinal.[4] For this reason, several structures based on PSB-retinal were reported by Sampedro such as NAIPs and NAFPs (see Background for further details).

This chromophore has inspired us to design new derivatives (Figure 5.1C).[5,6] It is tried that these derivatives will keep the good properties shown in the natural chromophore since *in vivo* the chromophore shows an ultra-fast and efficient isomerization obtaining a value of 0.67[7] for its quantum yield of isomerization (Figure 5.1).

[1] Harris, J. D.; Moran, M. J.; Aprahamian, I., New molecular switch architectures *PNAS* **2018,** *115*, 9414-9422.
[2] Pianowski, Z. L., Recent Implementations of Molecular Photoswitches into Smart Materials and Biological Systems *Chem. Eur. J.* **2019,** *25*, 5128-5144.
[3] Kim, J. E.; Tauber, M. J.; Mathies, R. A., Wavelength Dependent Cis-Trans Isomerization in Vision *Biochemistry* **2001,** *40*, 13774-13778.
[4] Kandori, H.; Shichida, Y.; Yoshizawa, T., Photoisomerization in Rhodopsin *Biochemistry* **2001,** *66*, 1197-209.
[5] Blanco-Lomas, M.; Campos, P. J.; Sampedro, D., Synthesis and Photoisomerization of Rhodopsin-Based Molecular Switches *Eur. J. Org. Chem.* **2012,** *2012*, 6328-6334.
[6] Lumento, F.; Zanirato, V.; Fusi, S.; Busi, E.; Latterini, L.; Elisei, F.; Sinicropi, A.; Andruniów, T.; Ferré, N.; Basosi, R.; Olivucci, M., Quantum Chemical Modeling and Preparation of a Biomimetic Photochemical Switch *Angew. Chem. Int. Ed.* **2007,** *46*, 414-420.
[7] Dartnall, H. J. A., The photosensitivities of visual pigments in the presence of hydroxylamine *Vision Res.* **1968,** *8*, 339-358.

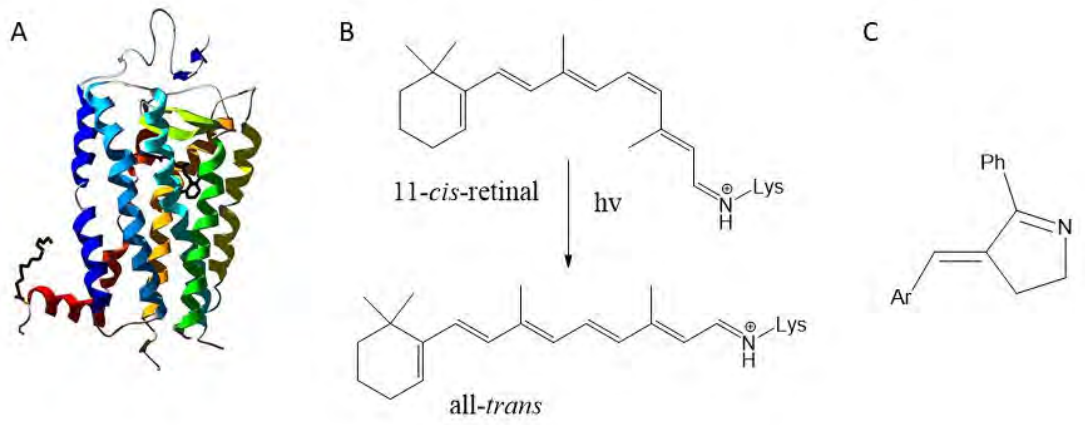

Figure 5.1. A) Rhodopsin protein structure. B) Isomerization process in rhodopsin chromophore. C) Photoswitch based on PSB-retinal.

The main goal of the present chapter is to study a molecular switch based on the PSB-retinal. For this reason, it was chosen to investigate new derivatives based on this biomolecule. Once these derivatives are explored, new modifications will be applied to improve their properties and to study their photophysical/photochemical behavior, as well as different approaches to use non-damaging light. Moreover, some possible applications will be described. Finally, some computational calculations performed to get a better understanding of the behavior of these new derivatives will be presented.

1. Design of new photoswitches based on the PSB-retinal.

The design of new photoswitches, based on biomolecules, has attracted the attention of many researchers for some time. Herein, new derivatives based on the PSB-retinal with improved properties are the subject of study. The main target to be fulfilled by these new analogues is the displacement of the absorption wavelength to lower energies, this way they could be applied with regard to biological purposes, which are not compatible with UV-light.

These new derivatives are analogues of the rhodopsin chromophore, the photoactive part being responsible for its photochemical properties. In all the target compounds, there is an imine bond which is part of an extended conjugation. In the iminic bond in the prototype, there is an extra phenyl ring that will have a clear impact on the absorption wavelength compared with the chromophore *in vivo*, red-shifting it.

Therefore, different benzylidene-pyrrolines have been proposed (Figure 5.2). Photoswitches **12** and **13** have been chosen since the effect of increasing the conjugation in the chromophore will be explored, consequently the phenyl ring (**12**) was substituted by a naphthyl group (**13**). By this approach, it was expected to produce a bathochromic shift of the absorption wavelength.

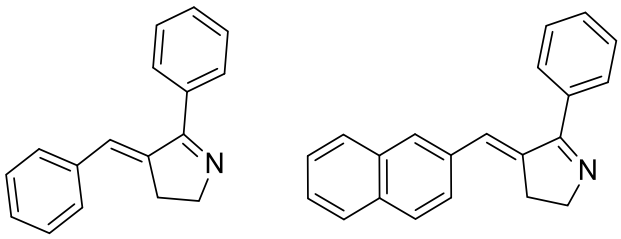

12 **13**

Figure 5.2. Structure of different compounds based on PSB-retinal.

Furthermore, using these compounds as a template to be modified, the quaternization of the nitrogen atom in the iminic bond was proposed.[8] This variation will alter the charge distribution in the chromophore, and also could change its photochemistry (isomers ratio in the PSS) and photophysical properties (absorption wavelength). Moreover, the quaternization of the iminic bond could enhance the solubility in water, making them more suitable for biological applications.

[8] Mathies, R. A.; Lugtenburg, J., Chapter 2 The primary photoreaction of rhodopsin. In *Handbook of Biological Physics*, Stavenga, D. G.; DeGrip, W. J.; Pugh, E. N., Eds. North-Holland: 2000; Vol. 3, pp 55-90.

For this purpose, the protonation or methylation of **12** and **13** could be accomplished to result in several compounds (**12-Prot**, **12-Met**, **13-Prot** and **13-Met**) (Figure 5.3).

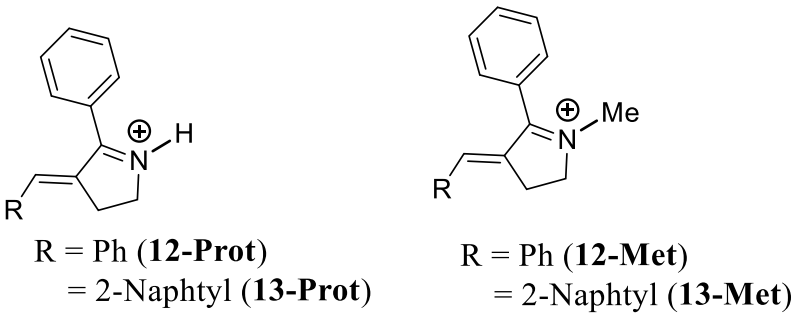

Figure 5.3. Structure of quaternized photoswitches based on PSB-retinal.

A computational study was performed to get a prediction of the photophysical properties of these molecular switches. Some TD-DFT calculations were carried out to understand the changes made in the chromophore upon quaternization. Therefore, all photoswitches under study were computed using B3LYP[9] with the standard basis set 6-31G*;[10] it was also needed to evaluate the effect of the charge stabilization by the solvent through the Polarizable Continuum Model (PCM),[11] especially for the cationic species (Table 5.1). The solvent included in the calculations was acetonitrile since this solvent will be used for measuring the UV-Vis spectra.

[9] Becke, A. D., Density-functional thermochemistry. III. The role of exact exchange *J. Chem. Phys.* **1993,** *98*, 5648-5652.
[10] Hariharan, P. C.; Pople, J. A., The influence of polarization functions on molecular orbital hydrogenation energies *Theor. Chem. Acc.* **1973,** *28*, 213-222.
[11] Tomasi, J.; Mennucci, B.; Cammi, R., Quantum Mechanical Continuum Solvation Models *Chem. Rev.* **2005,** *105*, 2999-3094.

Compound	Wavelength computed (nm)
12	305
12-Prot	360
12-Met	359
13	318, 340
13-Prot	370, 438
13-Met	370, 439

Table 5.1. Comparison of the absorption wavelength between neutral and quaternized derivatives.[12]

As is shown in Table 5.1, when changing the phenyl ring by a naphthyl group, a slight red-shift of the absorption wavelength was observed. However, a larger red-shift was predicted when the chromophore was quaternized, either by protonation or methylation. Therefore, through these calculations, it is clear that our strategy of carrying out these derivatives was on target to achieve a longer absorption wavelength.

Apart from designing new derivatives with improved properties, another different photoswitch (**14**) was also synthesized because in its structure it presents two possible anchorage points to be attached into more complex systems (Figure 5.4). In this way, the secondary structure of a peptide could be photocontrolled depending on the switch's C=C configuration of **14**.[13]

[12] Only *E*-isomer was found in the reaction mixture.

[13] Blanco-Lomas, M.; Samanta, S.; Campos, P. J.; Woolley, G. A.; Sampedro, D., Reversible Photocontrol of Peptide Conformation with a Rhodopsin-like Photoswitch *J. Am. Chem. Soc.* **2012,** *134*, 6960-6963.

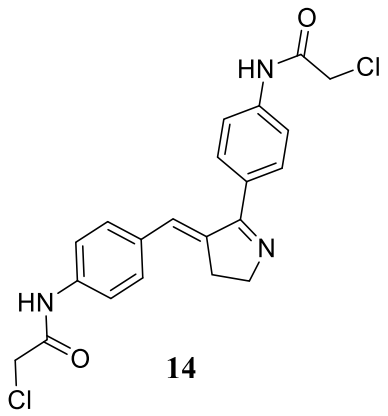

14

Figure 5.4. Structure of a photoswitch based on the PSB-retinal able to be attached into a peptide.

2. Synthesis of molecular switches based on the PSB-retinal

As it has been discussed previously, due to the red-shift of the absorption band predicted by computational calculations for the quaternized analogues (**12-Prot**, **12-Met**, **13-Prot** and **13-Met**) and **14** have been synthesized. It should be noted that **14** and its intermediates (**15**, **16B** and **17C**) were prepared in previous works of our research group.[14]

Many synthetic routes have been reported before to afford similar compounds.[15,16] Our procedure was based on the retrosynthesis described in the following Scheme 5.1.[17]

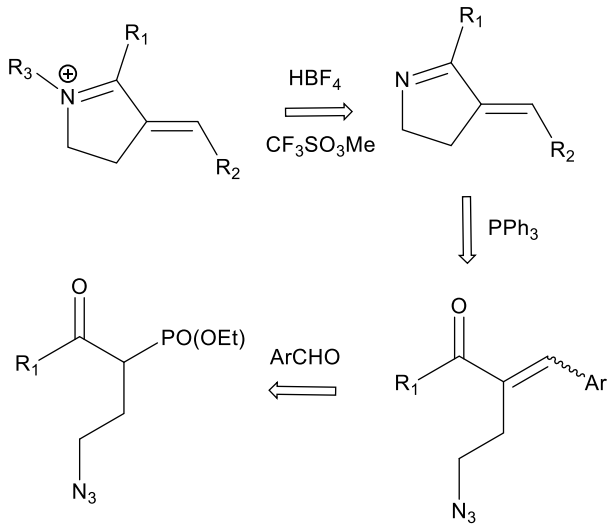

Scheme 5.1. Retrosynthetic route to afford photoswitches based on the PSB-retinal.

For this purpose, the starting reagent was the corresponding phosphonate to afford the desired compound. In photoswitches **12** and **13**, the corresponding phosphonate was commercially available, therefore there was no need to synthesize it previously. On the contrary, in the case of photoswitch **14**, the suitable phosphonate was not commercially available. So, the first step of this synthetic route was to synthesize the phosphonate which could lead us to **14** (Scheme 5.2).

[14] See ref. 13.

[15] Mandal, S.; Mahato, S.; Jana, C. K., Direct β-C(sp3)–H Functionalization of Aliphatic Amines to α,β-Unsaturated Imines, Aldehydes, and Chromenes *Org. Lett.* **2015,** *17*, 3762-3765.

[16] Rivado-Casas, L.; Sampedro, D.; Campos, P. J.; Fusi, S.; Zanirato, V.; Olivucci, M., Fluorenylidene−Pyrroline Biomimetic Light-Driven Molecular Switches *J. Org. Chem.* **2009,** *74*, 4666-4674.

[17] Snider, B. B.; Zhou, J., Synthesis of Lanopylin B1 *J. Org. Chem.* **2005,** *70*, 1087-1088.

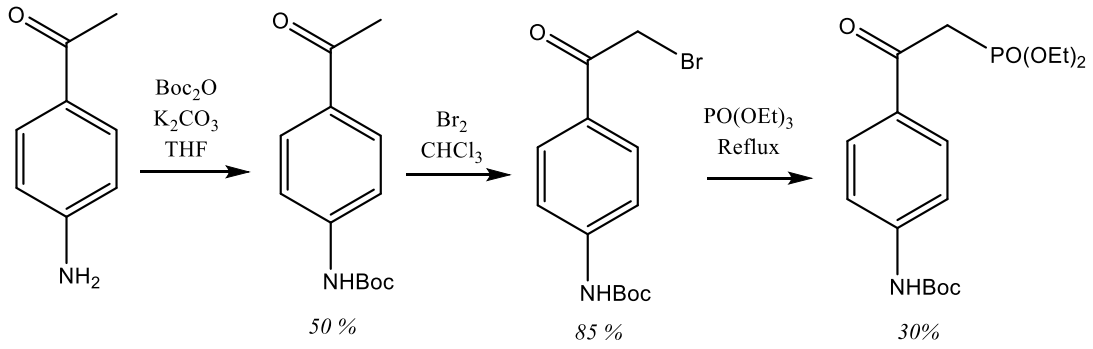

Scheme 5.2. Synthetic route to afford **intermediate 15**

In Scheme 5.2, it is shown how the target phosphonate (**intermediate 15**) was synthesized according to the literature.[18] The next step was to add 2-iodoethylazide to the corresponding phosphonate, necessary to form the pyrrolidine moiety later (Scheme 5.3).

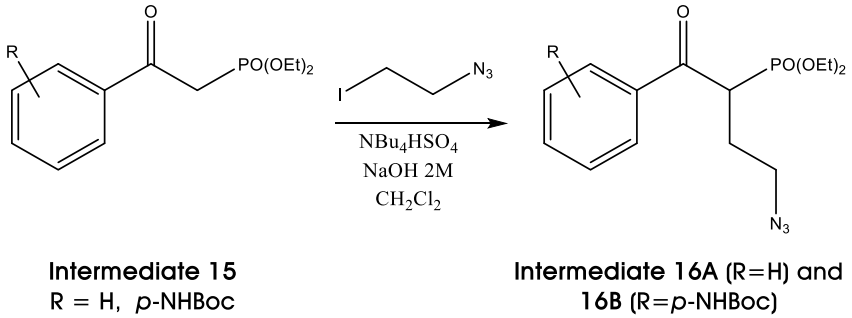

Scheme 5.3. Synthetic route to afford **intermediates 16A and 16B.**

It is observed in Scheme 5.3 that using both phosphonates, the extra phenyl ring in the pyrrolidine moiety was added to red-shift the absorption wavelength. Once the synthesis of the desired phosphonates was afforded through a phase-transfer procedure, the corresponding products were purified by column chromatography in silica gel, using as eluent a mixture of hexane/ethyl acetate.

Then, the central C=C double bond was formed through a Wittig-Horner reaction between an aldehyde and the phosphonate previously synthesized (Scheme 5.4).[19]

[18] Blanco-Lomas, M. Design, Synthesis and Computational Study of Photoactive Molecular Devices. PhD. Thesis, University of La Rioja, Logroño, 2012.

[19] Pascariu, A.; Ilia, G.; Bora, A.; Bora, A.; Iliescu, S.; Popa, A.; Dehelean, G.; Pacureanu, L., Wittig and Wittig-Horner reactions under phase transfer catalysis conditions *Cent. Eur. J. Chem.* **2003,** *1*, 491-534.

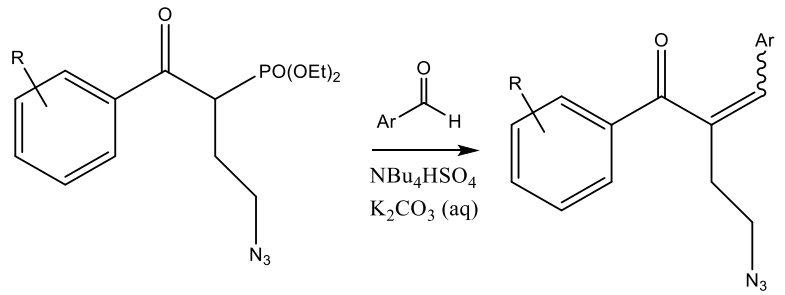

Intermediate 16A and 16B

Intermediate 17A (R=H, Ar=Ph), 17B (R=H, Ar=2-naphtyl) and 17C (R, Ar=*p*-NHBoc)

Scheme 5.4. Synthetic route to afford the **intermediates 17A, 17B and 17C.**

The compounds were purified by column chromatography using as eluent a mixture of hexane/ethyl acetate. **Intermediates 17A, 17B** and **17C** were afforded as a mixture of both isomers (*E* and *Z*). Then, the mixture of isomers was used to afford the final **12**, **13** and **14**, since both isomers resulted in the same product after carrying out the cyclization forming the pyrrolidine ring (see experimental data for further details) (Scheme 5.5). The only isomer found in the reaction mixture was the isomer in which the central C=C double bond was in *E*-configuration, checked by NMR experiments.

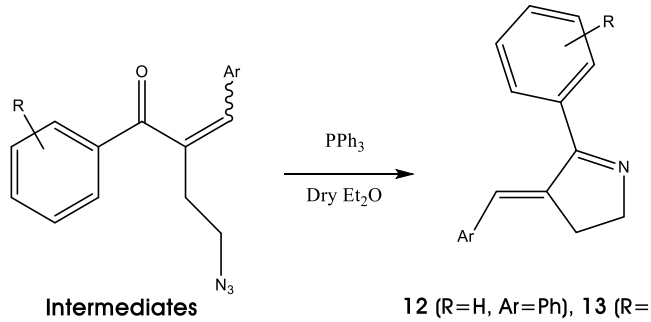

Intermediates 17A, 17B and 17C

12 (R=H, Ar=Ph), 13 (R=H, Ar=2-naphtyl) and 14 (R, Ar=*p*-NHBoc)

Scheme 5.5. Synthesis of **12**, **13** and **14**.

Other strategies such as using different electron donating/withdrawing groups in the aromatic ring were used previously for the synthesis of these derivatives.[20] It was found by changing the electronic properties of the aromatic ring, the absorption wavelength was tuned, as well as the isomers ratio in the PSS.[21]

Once the synthesis of **12** and **13** was accomplished, the protonation or methylation of them was afforded. The protonation was carried out by the addition of 1 equivalent of HBF_4 in ether to a 0.1 M solution of **12** or **13** in CD_3CN. The reaction was

[20] See ref. 5.

[21] Beharry, A. A.; Sadovski, O.; Woolley, G. A., Azobenzene Photoswitching without Ultraviolet Light *J. Am. Chem. Soc.* **2011,** *133*, 19684-19687.

carried out in a Pyrex NMR tube (Scheme 5.6) and the product did not need further purification, as it was determined by ^{1}H NMR.

For the methylated derivatives, methyl triflate was used to afford their synthesis in dry toluene. These derivatives could be easily isolated since the iminium salt formed was not soluble in toluene, therefore compounds **12-Met** and **13-Met** were achieved by filtration (Scheme 5.6).

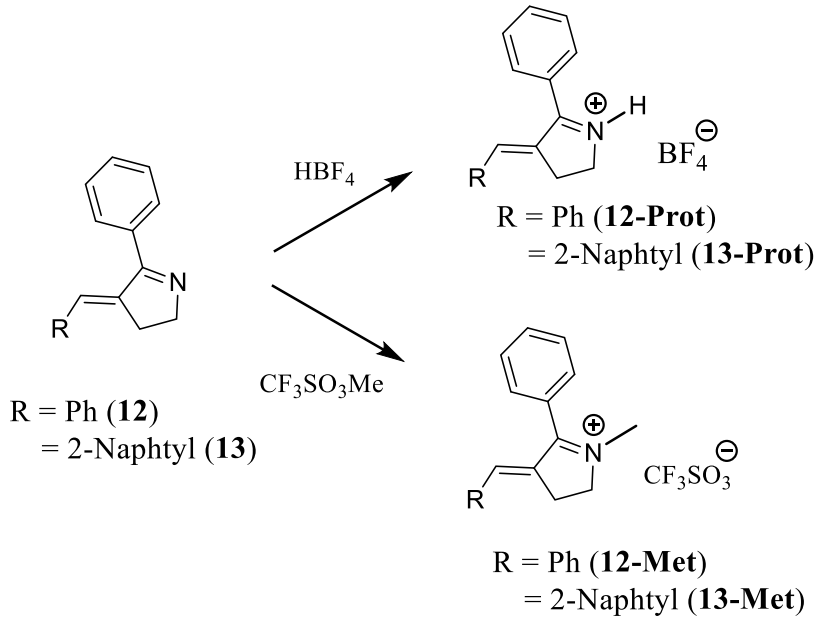

Scheme 5.6. General procedure to methylate or protonate the chromophore.

Once **12**, **13** and their derivatives were synthesized, a photochemical study of them was performed. This will be described in the following section. As it was demonstrated in the design section by some computational calculations, it is expected to get at least a different absorption band between the new derivatives and their neutral analogues. Depending on their properties, they could be used in new applications as will be discussed later (see section 4).

3. Photochemical study.

3.1. Photophysical properties of novel quaternized molecular switches based on the PSB-retinal.

Prior to the irradiation of the photoswitches based on the PSB-retinal, their UV-Vis spectra were recorded. The neutral compounds (**12** and **13**) and their related derivatives (**12-Prot**, **12-Met**, **13-Prot** and **13-Met**) were dissolved in acetonitrile to prepare solutions with a concentration around 5E-5 M for each photoswitch. All the solutions were placed in a quartz cuvette to perform the measurements.

Firstly, the effect of increasing the conjugation in the neutral chromophore replacing the phenyl ring (**12**) by a naphthyl ring which led to **13** was evaluated. (Figure 5.5)

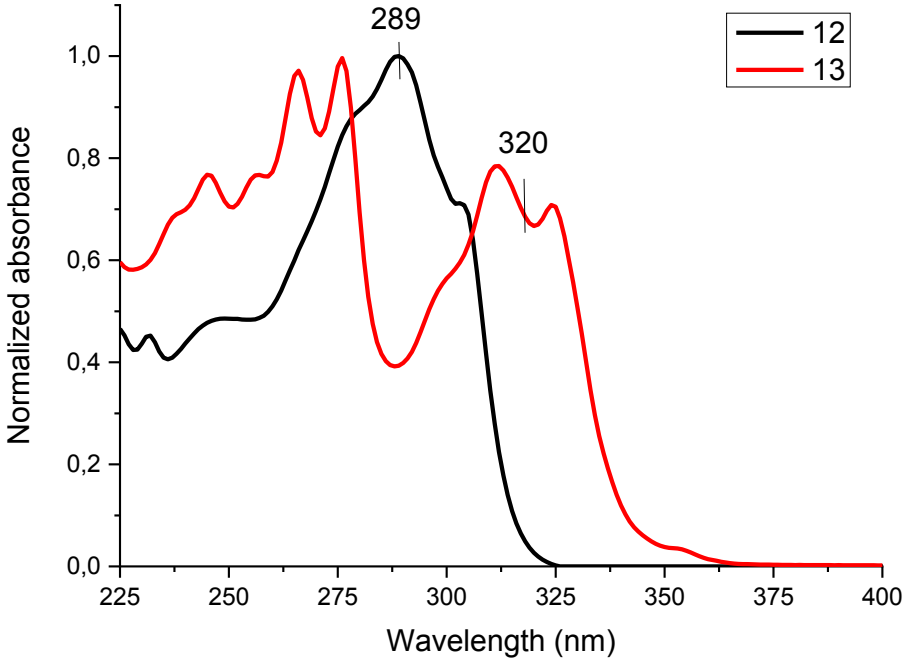

Figure 5.5. UV-Vis spectra of **12** and **13** in acetonitrile.

As was expected, Figure 5.5 demonstrates the displacement in the absorption band which is experimented by a molecule when its conjugation is increased. This bathochromic shift confirmed that the planarity of the molecule was totally or partially maintained, because if the naphthyl group was arranged perpendicularly, the conjugation would be broken, consequently no displacement of the absorption wavelength due to this effect would be observed.

It has been demonstrated that the absorption wavelength was red-shifted by increasing the conjugation of the system. Then, the effect of the quaternization of the chromophore on the photophysical properties was evaluated. For this purpose, different solutions of **12-Prot** and **12-Met** were prepared in acetonitrile to achieve a concentration of 5E-5 M. Firstly, the UV-Vis spectrum of the neutral photoswitch (**12**) was compared with its corresponding derivative (**12-Met**) (Figure 5.6).

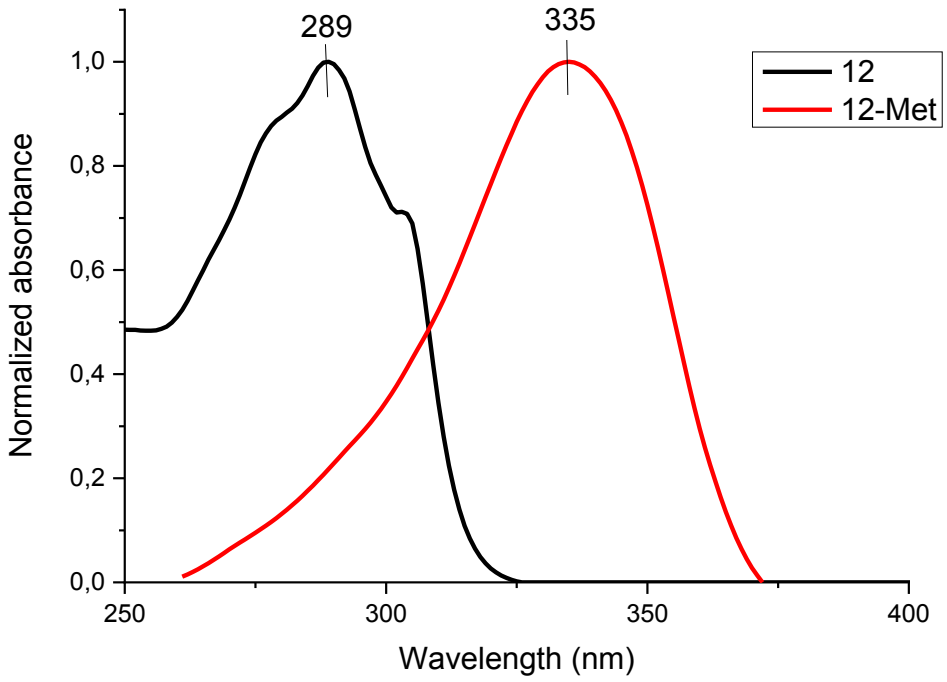

Figure 5.6. UV-Vis spectra of **12** and **12-Met** in acetonitrile.

As is shown in Figure 5.6, the quaternization of the nitrogen atom presented in the iminic bond was a really good tool to modify its absorption band, since it was responsible for producing a big red-shift (*ca.* 50 nm) on the absorption wavelength. Interestingly, it should be remarked that **12-Prot** shares the same UV-Vis spectrum with its methylated analogue (**12-Met**).

With all this data, two successful methods to red-shift the absorption wavelength of this kind of photoswitches have been revealed. With the aim of getting a greater bathochromic shift, both effects described before (the increase of the conjugation and the quaternization of the iminic bond) were combined to result in an improved effect. Therefore, the UV-Vis spectra of **13** and **13-Met** measuring both solutions of 5E-5 M in acetonitrile was carried out (Figure 5.7).

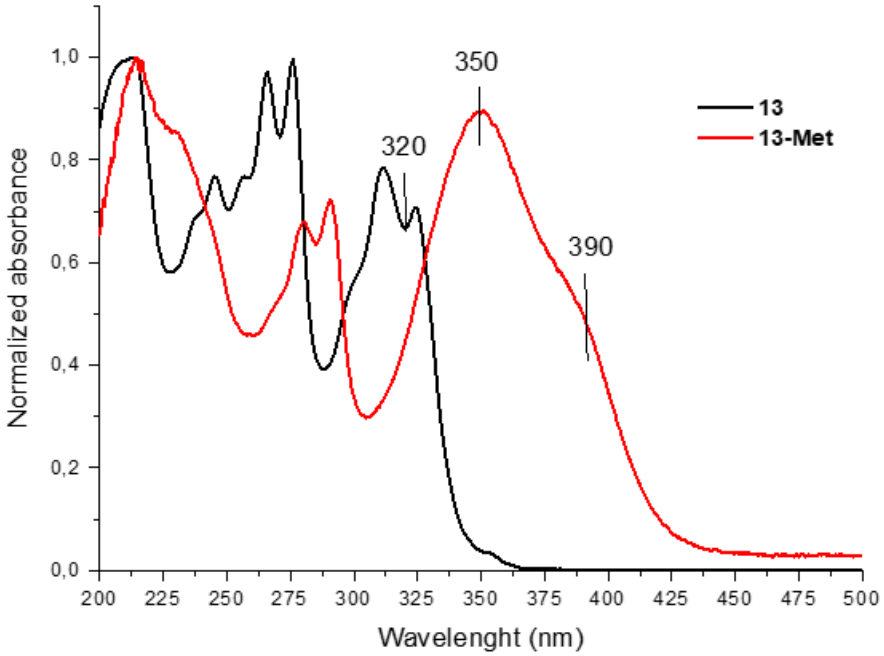

Figure 5.7. UV-Vis spectra of **13** and **13-Met**.

As is shown above, a large improvement was achieved, since joining both effects **13-Met** and **13-Prot** absorbed in the visible region. This kind of light is more compatible with biological media than UV-light due to its lower-energy. As was found in the previous case, **13-Prot** and **13-Met** feature the same UV-vis spectra; this implies that the quaternization of the switches yielded different compounds, under different reaction conditions but with the same absorption. In turn, this could be of practical importance for the use of these photoswitches in biological applications.

Moreover, the experimental data of these derivatives is compared with the absorption wavelength computed previously in Table 5.2.

Compound	Wavelength computed (nm)	Experimental (nm)
12	305	289
12-Prot	360	334
12-Met	359	334
13	318. 340	311, 324
13-Prot	370, 438	350, 415
13-Met	370, 439	350, 415

Table 5.2

As it can be seen, no differences were found in the absorption wavelength computed between the protonated and methylated analogues, as it was experimentally found. It should be noted that a qualitative agreement between the experimental data and the computed absorption bands was found. It is observed that the theoretical bands for all photoswitches were red-shifted by 20-30 nm with respect to the experimental bands.

Furthermore, the orbital contributions of **12** and **12-Prot** were studied. In the case of the neutral form (**12**), as it can seen in Figure 5.8 the main orbital contribution corresponded to a $\pi - \pi^*$ transition that was located mainly in the central C=C double bond.

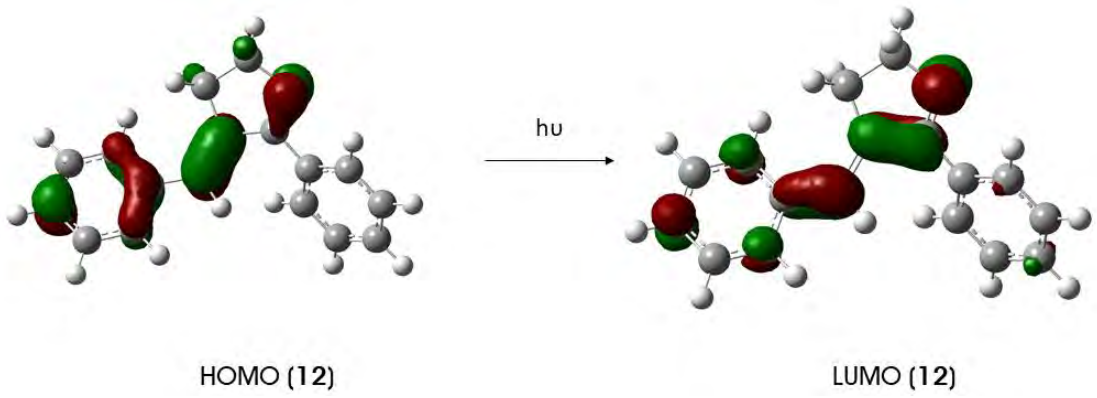

Figure 5.8. Molecular orbitals calculated describing the electronic nature of the bright state of **12**.

The orbital contributions for compound **12-Prot** were also computed, the same transition nature was found for this derivative, therefore a $\pi - \pi^*$ transition was found (Figure 5.9).

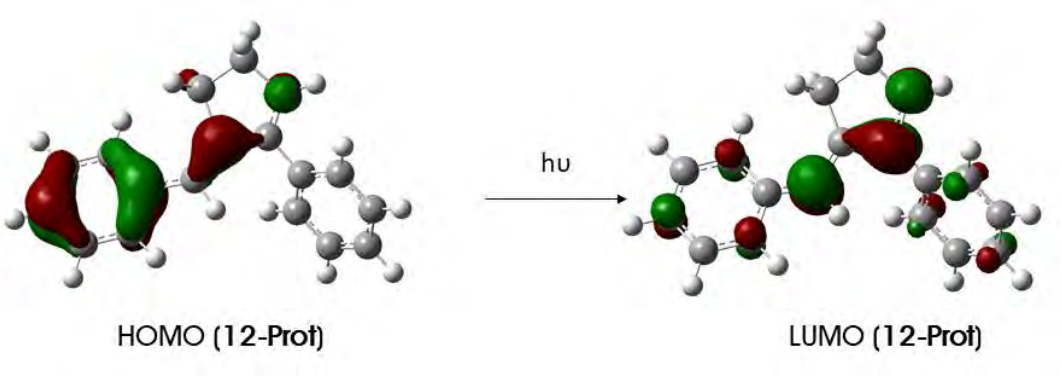

Figure 5.9. Molecular orbitals calculated describing the electronic nature of the bright state of **12-Prot**.

After studying the absorption wavelength of these photoswitches, it has been concluded that the absorption band is very dependent on their structure.

The emission of these derivatives was also evaluated. For that purpose, 5E-5 M solutions of **12-Met** and **13-Met** were prepared, but no significant emission bands were found in their spectra. Therefore, it was concluded that the radiative decay was not a probable path to deactivate the excited state in these photoswitches, due to their low value for its emission quantum yield (Φ_{em}<1%). This value was fixed as the experimental threshold value.

For this reason, these photoswitches could be very efficient since they do not waste light energy in radiative processes.

3.2. Irradiation of photoswitches.

It is well known that the rhodopsin features an efficient chromophore switching *in vivo* raising a value of 0.67 for its isomerization (*Z:E*) quantum yield.[22] Due to this fact, it was expected that molecular switches based on PSB-retinal will show a fast and efficient photoswitching. This assumption was proved in previous works since the isomerization of neutral retinal switches has been widely studied, as well as the multiplicity of the excited state involved in the photoreaction (see background for further details).

In section 2.2 of Chapter 4, the importance of the multiplicity of the excited state was discussed, since depending on the nature of the electronic state involved in the photoreaction, it could lead to different reaction products.

[22] See ref. 7.

3.2.1. Photoswitching by direct irradiation.

The irradiation of molecular switches based on PSB-retinal as **12**, **13** and their related derivatives **12-Met**, **12-Prot**, **13-Met** and **13-Prot** were performed. For that purpose, 0.1 M solutions in CD_3CN of each photoswitch were prepared in different NMR tubes. The irradiation procedure was followed by ^1H NMR as in the hydantoin-based molecular switches. In this kind of photoswitches, the ^1H NMR signals corresponding to two -CH_2- groups which form the pyrrolidine moiety were distinctive. Therefore, these signals were suitable to follow the photoswitching process by ^1H NMR. In the same way as in other cases, the isomers mixture was determined integrating the signals for each isomer (*E*/*Z*).

Once the UV-Vis spectra of the photoswitches under study were analyzed (Figure 5.5, 5.6 and 5.7), the source of light should be chosen. In these cases, all the photoswitches present neat absorptions in the ultraviolet and visible region. Therefore, a 125-W medium-pressure Hg lamp was chosen due to its wide emission from high-energetic ultraviolet light to far-visible light and a Pyrex filter was used during the irradiation to avoid all the wavelengths below 290 nm; this emission was filtered because it could produce undesired side reactions due to its high-energy.

All photoswitches were irradiated in different NMR tubes at once. The irradiation took about 30 minutes in all cases to reach the corresponding PSS. In case of ***E*-12**, the ^1H NMR showed two signals centered at 4.12 and 3.05 ppm (red spectrum in Figure 5.10), but when it was irradiated, a new pair of signals appeared at 4.03 and 2.93 ppm corresponding to the *Z*-isomer (green spectrum in Figure 2.9)

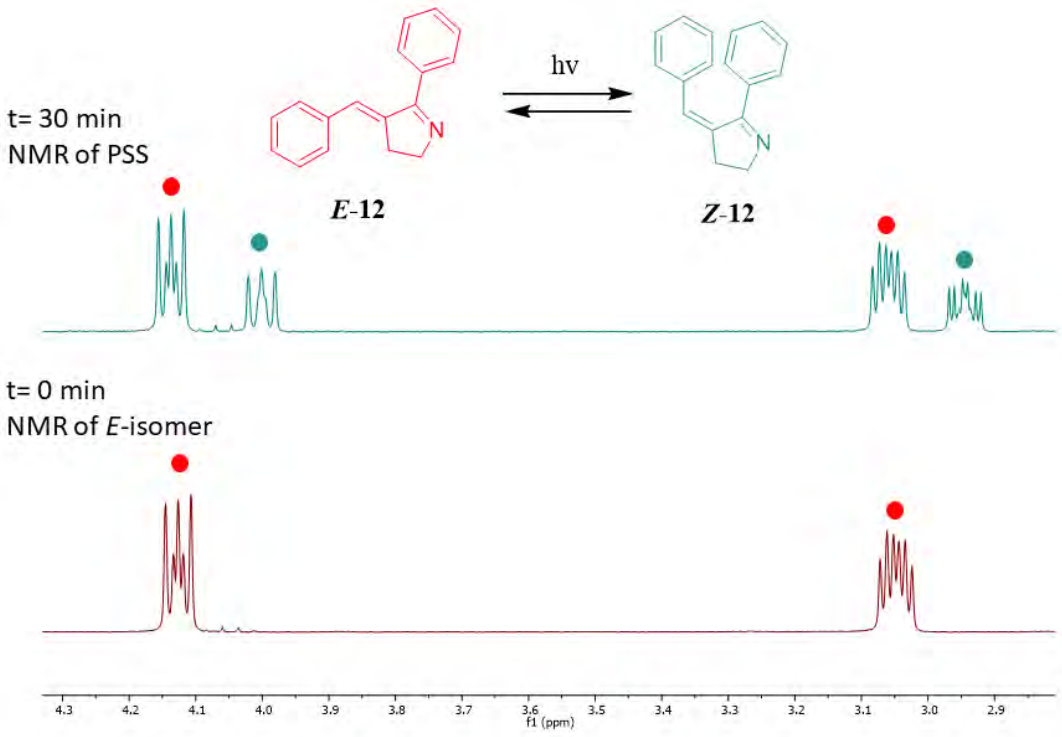

Figure 5.10. Irradiation procedure followed by ^{1}H NMR.

Following the irradiation procedure detailed above, the isomers mixture reached in the PSS for all photoswitches as shown in Table 5.3.

Compound	*E*-isomer (%)	*Z*-isomer (%)
12	70	30
12-Prot	90	10
12-Met	90	10
13	48	52
13-Prot	75	25
13-Met	75	25

Table 5.3. Isomers ratio in the PSS.

As observed in Table 5.3, the PSSs reached by the neutral photoswitches (**12** and **13**) and its corresponding analogues were compared. It was observed that different mixtures were found in the equilibrium between them. Analyzing the results given for the PSS of **12-Met** *vs* **12-Prot** and **13-Met** *vs* **13-Prot**, it should be remarked that they shared the same photochemical properties as occurred with the absorption wavelength.

From these results, it could be deduced that in all cases the percentage of *Z*-isomer at the PSS was higher when the compounds were in their neutral form than when they were quaternized. But, as was demonstrated in the previous chapter, PSS is highly dependent on the source of light used and the relative absorption of both isomers.

Using the irradiation conditions detailed above, when the irradiation took place, a vertical allowed transition from the ground state (S_0) to a singlet (S_1) was found, without varying the multiplicity of the system.[23, 24] Just that state was populated by direct irradiation because no intersystem crossing was found to populate the triplet state. Then, an efficient mechanism to deactivate the excited state (S_1) was the switching from *E*-isomer to obtain the corresponding *Z*-isomer. As was explained before, radiative processes were not effective in these photoswitches.

3.2.2. Sensitization processes.

In organic photochemistry, sensitized processes are well-known due to their important role in organic synthesis (see introduction, section 2.3.2).[25]

As has been said, the use of photosensitization involved many advantages for organic chemists, since using this methodology different products impossible to achieve by direct irradiation could be produced. Likewise, the use of photosensitizers allows us to irradiate in another spectral region in which the organic molecule does not absorb. By using this methodology, visible light could be employed instead of high-energetic ultraviolet light. Also, as has been discussed before, the use of non-damaging light is essential for many applications.

3.2.2.1. Photoswitching through triplet state.

In this part of my thesis, the study of the triplet state of a neutral photoswitch (**12**) and its protonated analogue (**12-Prot**) is presented.

Before carrying out the sensitized irradiation of **12**, several issues must be considered. Firstly, it should be evaluated how it would be possible to avoid the absorption of light by the photoswitch under study. Then, a sensitizer must be selected regarding its triplet energy level and its UV-Vis absorption band.

---

[23] See ref. 5.

[24] Seyed Hosseini, S. M.; Agha Mohammadi, M.; Mousavi, M., Study of Photoisomerization in Cis-Retinal as a Natural Photo Switch in Vision Using Density Functional Theory *Int. J. Adv. Biol. Biomed. Res.* **2013,** *1*, 1505-1511.

[25] Zhou, Q.-Q.; Zou, Y.-Q.; Lu, L.-Q.; Xiao, W.-J., Visible-Light-Induced Organic Photochemical Reactions through Energy-Transfer Pathways *Angew. Chem. Int. Ed.* **2019,** *58*, 1586-1604.

Considering that the absorption of **12** goes up to 325 nm (Figure 5.5), a filter must be used to avoid the absorption of the photoswitch (**12**). To this end, a 0.4 M sodium metavanadate ($NaVO_3$) solution in 5% NaOH was prepared, since it cuts all radiation of wavelength below 375 nm (Figure 5.11).

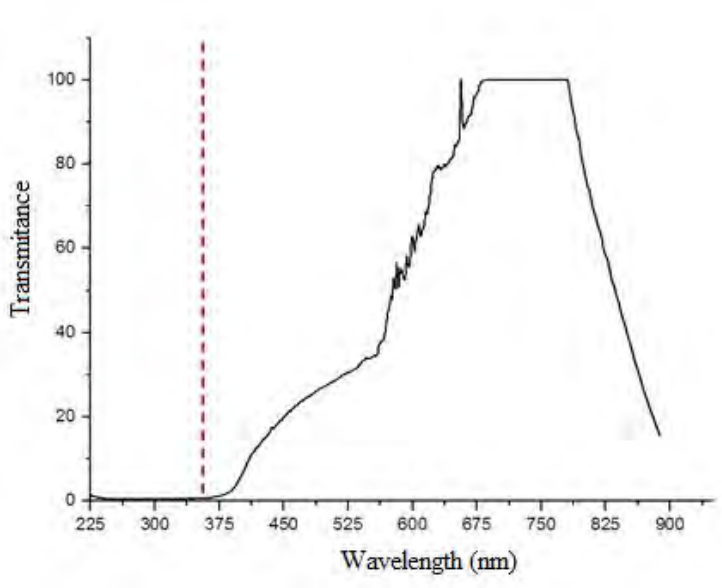

Figure 5.11. Transmittance spectrum of the filter solution made by 0.4 M sodium metavanadate ($NaVO_3$) solution in 5% NaOH

As is observed in Figure 5.11, the filter solution made by sodium metavanadate absorbs the whole spectral region up to 375 nm. Therefore, it fits perfectly to avoid the absorption of light by **12**.

Then, under these irradiation conditions, the sensitizer must absorb light to form its triplet state. In this case thioxanthone was chosen due to its high energy triplet (E_T = 63.2 kcal/mol) and its well-suited absorption band (Figure 5.12).

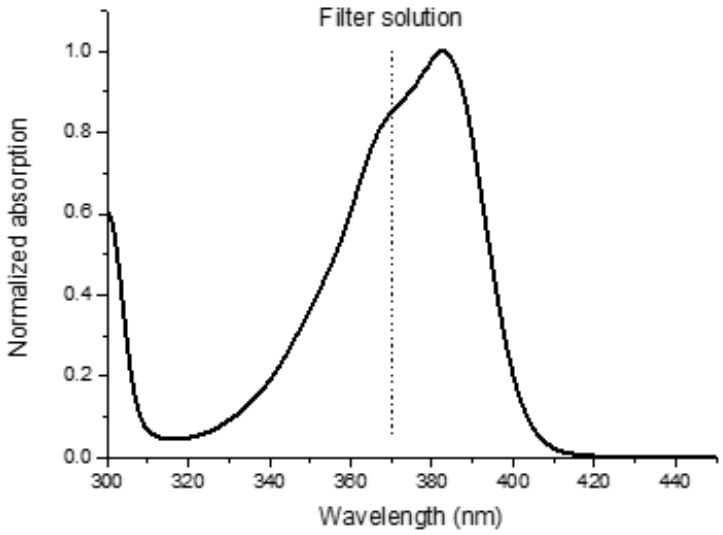

Figure 5.12. UV-Vis spectrum of thioxanthone.

Once the perfect conditions to carry out the sensitized irradiation of **12** had been found, a 0.1 M solution of it in CD_3CN was prepared. The irradiation was carried out in a NMR tube using a 125-W medium-pressure Hg lamp, putting the filter solution between the lamp and the sample. To this solution, 1 equivalent of thioxanthone was added.

The resulting solution was deoxygenated by bubbling argon throughout the mixture since if forming the triplet of **12**, the oxygen could quench it (see Chapter 4, section 2.2).

Thus, the activation of the switch must come from an energy transfer from the sensitizer. The sensitized irradiation of **12** was followed by ^{1}H NMR measuring several NMR spectra until the PSS was reached. Interestingly, using these sensitized irradiation conditions a mixture of isomers 80:20 (*E*:*Z*) was found in the PSS. This result was very similar to the PSS achieved by direct irradiation (76 *E*: 24 *Z*). Therefore, a similar situation could be achieved by using both direct irradiation of **12** (maximum absorbance at 289 nm) and sensitized irradiation (maximum absorbance at 380 nm). Through the use of this methodology, these photoswitches would be able to be used in applications which require the use of less energetic light, since under sensitized conditions, a lower energy irradiation was enough to activate the switch, in fact, the wavelength of effective irradiation was shifted *ca.* 100 nm.

In the light of the results of this study, similar experiments were performed with other related sensitizers which present lower triplet energies (E_T)[26] than thioxanthone. By these experiments, it will be possible to delimit experimentally the energy of the triplet state of **12.** These results are shown in Table 5.4.

Sensitizer	λ_{max}	E_T (kcal/mol)	PSS (*E:Z*)
thioxanthone	380	63.2	80:20
acridone	390	58.3	56:44
4-nitroaniline	380	55.2	66:34
acridine	370	45.4	100:0

Table 5.4. Sensitized irradiation of **12** using several sensitizers.

In Table 5.4, various sensitizers with the corresponding absorption maxima are shown. As can be seen, the absorption wavelength of all selected sensitizers goes beyond 375 nm, therefore the same solution filter could be used to activate **12**. On analyzing the composition mixture of both isomers in the PSS, it is observed that the PSS is highly dependent on the sensitizer used. Interestingly, using acridone as sensitizer, the ratio of *Z*-isomer was notably increased.

It is deduced that the energy of the triplet state of photoswitch **12** must be between 55.2 and 45.4 kcal/mol, because 4-nitroaniline allowed the isomerization process, while by the use of acridine, no photoreaction was observed.

Even though using these sensitizers, it still implied the use of relatively high-energy light (370-390 nm).

So, to improve these results, the possibility of using a common visible sensitizer such as $[Ru(bpy)_3]^{2+}$ was explored, this way we could activate the switch red-shifting the effective absorption wavelength further. This sensitizer shows a strong metal-ligand charge transfer (MLCT) absorption at 452 nm (Figure 5.13) and it has an E_T value of 48.0 kcal/mol.

[26] L Murov, S.; Carmichael, I.; Hug, L., *Handbook of photochemistry*. CRC Press: Bosa Roca, United States, 1973.

Then, its triplet energy value is placed in our range. Moreover, $[Ru(bpy)_3]^{2+}$ has been used as an absorber-sensitizer in a variety of arrays.[27,28]

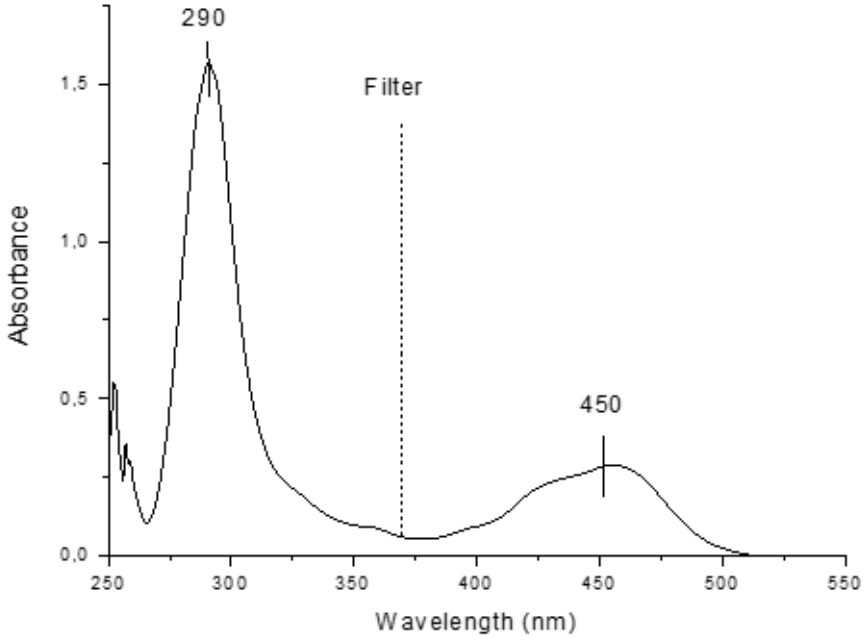

Figure 5.13. UV-Vis spectrum of $[Ru(bpy)_3]^{2+}$.

Therefore, if the isomerization of **12** takes place, this complex could be used to further delimit the triplet energy state of **12** and, even more important, the use of visible light to promote the isomerization of **12.** When performing a similar experiment as those described before using $[Ru(bpy)_3]^{2+}$ as sensitizer, a PSS of 42:58 (*E*:*Z*) was reached. Thus, using this sensitizer the triplet-triplet energy transfer took place and several relevant conclusions could be pointed out:

- The E_T of **12** was delimited between 48.0 and 45.4 kcal/mol. So, the triplet energy value was determined experimentally to be within an interval of 2.6 kcal/mol only.
- The activation of **12** could take place using visible light. While the absorption band of **12** was centered at 289 nm, the effective absorption in the sensitized process was 450 nm. Therefore through this methodology, the light used to activate **12** was red-shifted *ca.* 160 nm.

[27] Zhao, J.; Wu, W.; Sun, J.; Guo, S., Triplet photosensitizers: from molecular design to applications *Chem. Soc. Rev.* **2013,** *42*, 5323-5351.
[28] Wu, W.; Ji, S.; Wu, W.; Shao, J.; Guo, H.; James, T. D.; Zhao, J., Ruthenium(II)–Polyimine–Coumarin Light-Harvesting Molecular Arrays: Design Rationale and Application for Triplet–Triplet-Annihilation-Based Upconversion *Chem. Eur. J.* **2012,** *18*, 4953-4964.

- A PSS with a higher ratio for the photochemical *Z*-isomer was obtained under these conditions.

To sum up, after the use of sensitized conditions, the use of less-energetic light in rhodopsin-based molecular switches was not limited to those which presented neat absorptions in the visible region in acidic conditions, such as **12-Prot** or **13-Prot**.

In addition, if the photoswitching process of **12-Prot** and **13-Prot** could also take place under sensitized conditions, the use of visible light could be applied in different reaction conditions without using acidic solutions. This fact could make them more suitable for different applications, so the use of these switches could be widely increased.

To check this fact, a similar study for **12-Prot** was also performed. Regarding the transmittance spectrum of the filter corresponding to the sodium metavanadate solution (Figure 5.11) and the absorption spectrum of **12-Prot** (Figure 5.6), it is observed that they fitted perfectly to perform the same experiment without varying the irradiation conditions as previously used for **12**.

Therefore, several 0.1 M solutions of **12-Prot** were prepared in CD_3CN, the irradiation took place in each NMR tube after deoxygenating the solution bubbling argon through it for 10 minutes. To each solution, 1 equivalent of different sensitizers was added. Finally, to carry out the irradiations, a 125-W medium-pressure Hg lamp and the solution filter were used, as was discussed previously.

The sensitized irradiation of **12-Prot** was performed using the same sensitizers as for **12**. Surprisingly, no photoreaction was found in any case. This fact could be due to different reasons. For example, the triplet-triplet energy transfer did not occur since **12-Prot** could have a higher triplet energy than **12**, and it could not be populated under these sensitized conditions. Another possible reason is that the triplet state of **12-Prot** did not lead to the photoisomerization, and another deactivation pathway was followed by its triplet state.

To get a better understanding of the behavior of the triplet state of **12** and **12-Prot**, both were studied by laser flash photolysis.

3.2.2.2. Laser flash photolysis studies.

The study of short-lived species was revolutionized by Norris and Porter when, in 1949, they employed the technique of flash photolysis.[29] This technique consists of the observation of an excited state which has been generated by a short and intense pulse of light. Once the pulse is over, this technique study how the system changes with time.

The use of a laser produces a large electronically excited state population. Then, the time evolution of these excited states can be monitored by absorption or emission spectroscopy. Thanks to this technique, species with a lifetime shorter than a few milliseconds can be studied.[30, 31]

In Figure 5.14, it is shown schematically how equipment for laser flash photolysis works. In our case, the laser used for the population of the excited state is an excimer laser XeF, which generates intense pulses of 351 nm. Another important part of the apparatus is the detection system, in our case it is formed by a monochromator, which splits the different wavelengths, and a photomultiplier which detects the signal at the wavelength selected. Finally, the oscilloscope allows us to plot the voltage signal coming from the photomultiplier as a time dependent function. It is connected to a computer to save and study the results obtained.

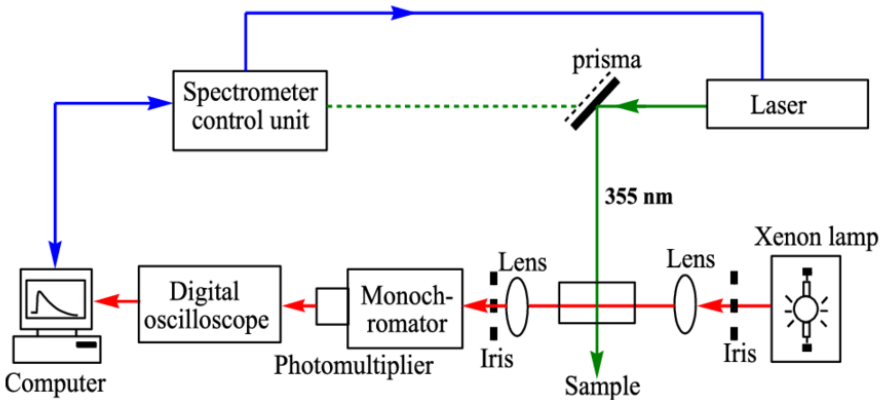

Figure 5.14. Representation of a laser flash photolysis equipment.[32]

This system is a single beam spectrofluorometer, but it behaves as double one, but with the reference and the sample separated in time instead of in space. The reference

[29] Porter, G.-N.; Norrish, R. G. W., Flash photolysis and spectroscopy. A new method for the study of free radical reactions *Proc. R. Soc. Lond. A.* **1950,** *200*, 284-300.
[30] Scaiano, J. C., *CRC handbook of organic photochemistry* CRC Press: Boca Raton, Fla. :, 1989.
[31] Wardle, B., *Principles and applications of photochemistry*. Wiley: Hoboken, N.J., 2009.
[32] Ma, J.; Zhu, C.; Lu, J.; Lei, Y.; Wang, J.; Chen, T., *Photochemical reaction between triclosan and nitrous acid in the atmospheric aqueous environment*. 2017; Vol. 157.

measured is the absorption before the irradiation and the sample is recorded immediately after the laser pulse was concluded. Therefore, the difference of the absorption (Δ(OD)) is evaluated at different times (Equation 5.1).

$$\Delta(\mathrm{OD}) = -log(I_0 / I)$$

Equation 5.1

The value of Δ(OD) as a time dependent function results in an exponential decay (first order). This is the simplest situation, when there is just one transient species experimenting a simple deactivation (colliding with the solvent or through non-radiative processes), following the Equation 5.2.

$$\Delta(\mathrm{OD}) = Ae(-k_D t)$$

Equation 5.2

Where Δ(OD) is the absorption change suffered by the sample, A is the pre-exponential factor, t is the time and k_D is the first order rate constant for transient decay. This constant can also be represented as Equation 5.3 where τ is the lifetime of the transient species.

$$k_D = 1/\tau$$

Equation 5.3

The triplet state of **12** was studied as a quencher of the triplet state of xanthone by laser flash photolysis. Therefore, an acetonitrile solution containing xanthone (3mL of 4.03E-4 M, absorbance = 0.4 a. u. at 351 nm) in a quartz cuvette was purged with argon for about 10 min. The sample was exposed to the laser pulse (351 nm, 1 Hz, 25 mJ/pulse) and the decay of xanthone triplet at 620 nm was observed. Small amounts (12 μL) of the quencher (**12**) were added to the solution, and after each addition the decay was measured. All graphs were fitted with exponential functions in order to find the xanthone lifetime, τ, for each experiment. (Figure 5.15)

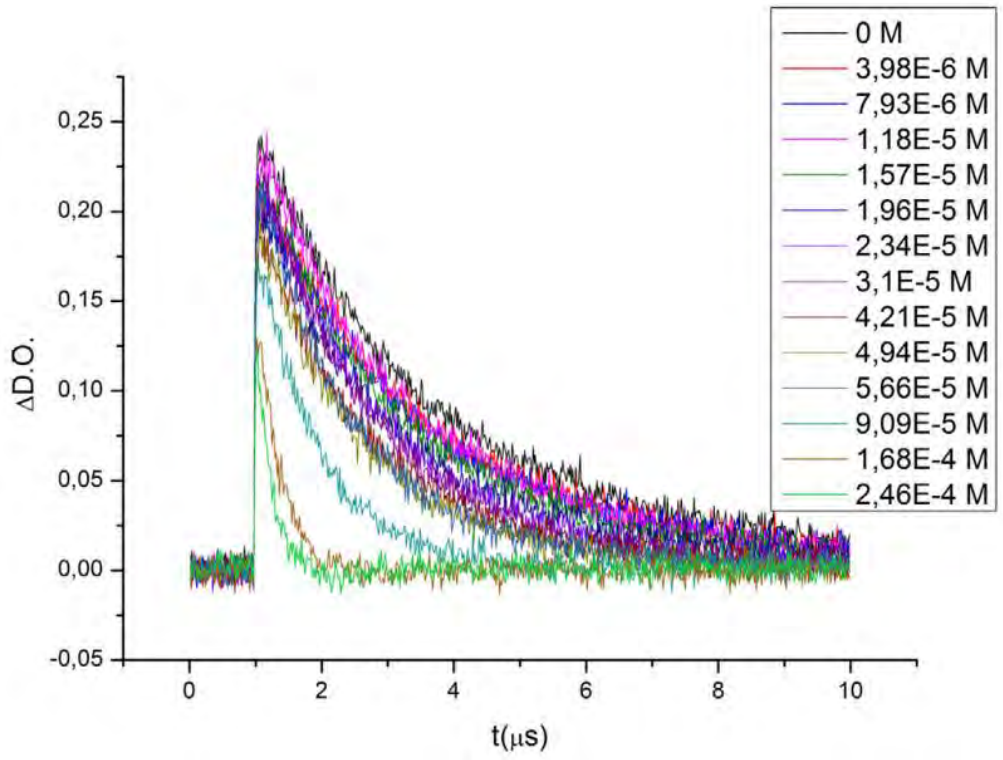

Figure 5.15. Triplet stay decay of a 4.03E-4 M solution of xanthone in acetonitrile in the presence of **12**.

As is shown in Figure 5.15, when the amount of **12** was increased, the lifetime of the triplet state of xanthone decreased. So, the triplet-triplet energy transfer occurred, populating the triplet state of **12**. Therefore, we can conclude that when the triplet state of xanthone was generated, photoswitch **12** deactivated it. Then, the quenching rate (k_d) was obtained from a plot of the measured decay rates (k_D, τ inverses) *vs* the amount of photoswitch added according to the Equation 5.4 (Figure 5.16) (Table 5.5).

$$k_D = k_d\,[\text{switch}] + k_0$$

Equation 5.4

Concentration (M)	τ (μs)	$k_D = 1/\tau$ (10^3 s^{-1})
7.93E-6	2.43	410
1.18E-5	2.27	439
1.57E-5	2.15	464
1.96E-5	2.02	495
2.34E-5	1.89	529
3.1E-5	1.74	575

Table 5.5

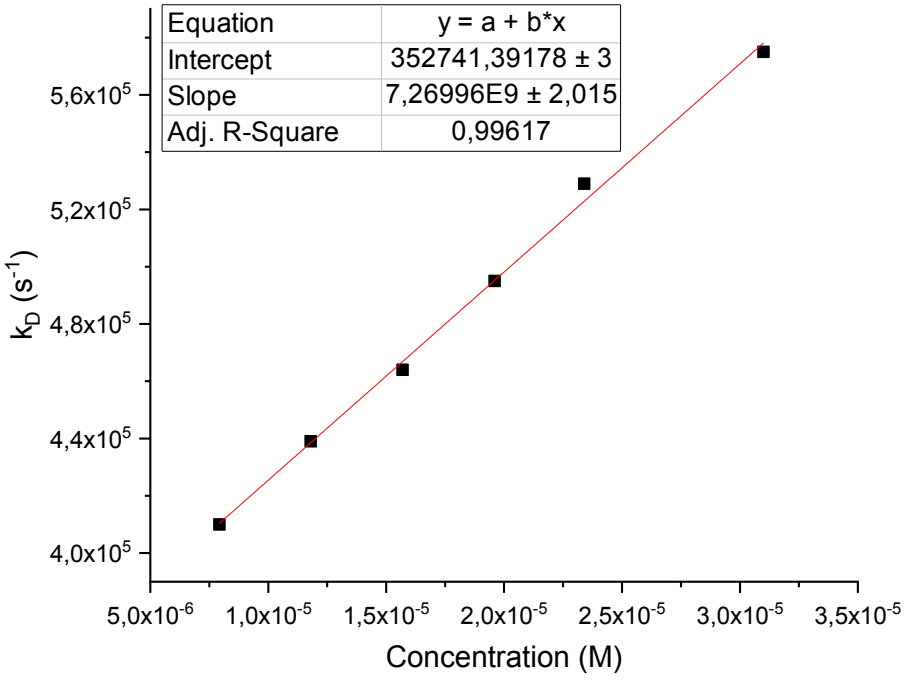

Figure 5.16

The quenching rate (k_d) was measured to be 7.27E9 $M^{-1}s^{-1}$ from the linear fit slope. This value indicates that **12** is a triplet quencher of the triplet state of xanthone. Moreover, it is a typical value for a diffusion deactivation; this means that the deactivation came from the collision between an excited xanthone molecule against **12** in its ground state inside the fluid.

Following the same experimental conditions, a similar study was performed for the protonated version **12-Prot.** The decay of the emission of the triplet state by **12-Prot** is shown in Figure 5.17.

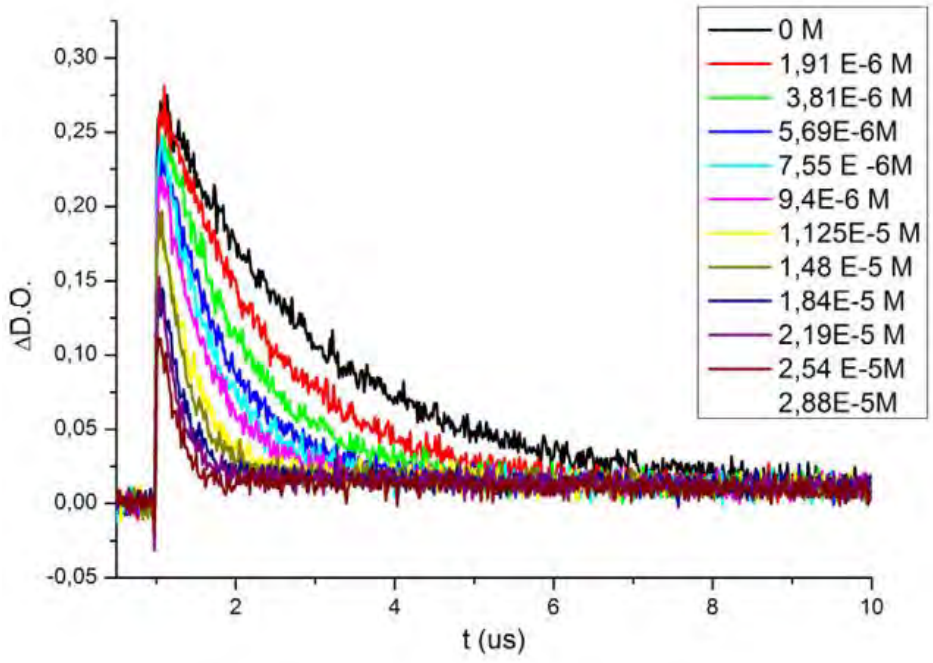

Figure 5.17. Triplet stay decay of a 4.03E-4 M solution of xanthone in acetonitrile in the presence of **12-Prot**.

It is observed in Figure 5.17 that **12-Prot** is also capable of inducing the triplet state decay of xanthone, therefore the triplet state of **12-Prot** was also populated. Moreover, the quenching rate was measured in the same way as before, using data in Table 5.6, it was represented the inverse values of τ *vs* the concentration of photoswitch added (Figure 5.18).

Concentration (M)	τ (μs)	$k_D = 1/\tau$ (10^3 s^{-1})
1.91E-6	1.99	501
3.81E-6	1.39	717
5.69E-6	1.08	919
7.55E-6	0.87	1146
9.4E-6	0.72	1393
1.125E-5	0.65	1533

Table 5.6

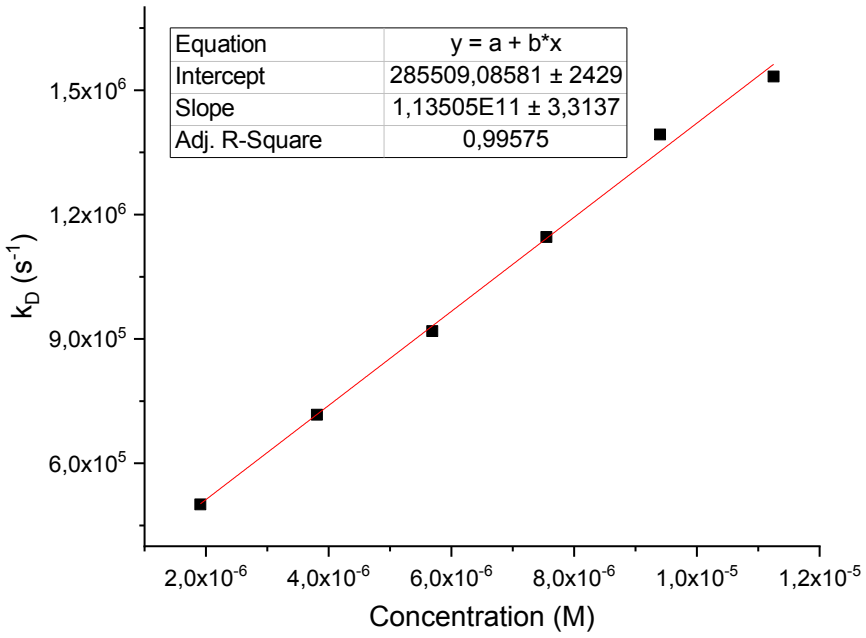

Figure 5.18

From the linear fit slope, it was obtained the quenching rate for **12-Prot**, k_d was measured to be 1.14E11 $M^{-1}s^{-1}$. In spite of the lack of photoisomerization when **12-Prot** was irradiated under sensitized conditions, its triplet state was populated by a triplet-triplet energy transfer. This implies that the triplet state was deactivated by other effective pathways, which was not the isomerization of its C=C double bond.

To get a better understanding of the triplet state behavior of **12-Prot**, a computational study was performed to explore the lack of triplet state photoisomerization.

Using the density functional theory (DFT) methodology, the B3LYP functional together with the standard 6-31G* basis set, the triplet state energies of **12** and **12-Prot** were computed. The value found for the neutral derivative (**12**) was 43.0 kcal/mol; this value was agreed with the experimental range which was fixed between 45.4 and 48.0 kcal/mol. When the protonated analogue (**12-Prot**) was computed, the value of the triplet state was found to be in 46.1 kcal/mol.

Analyzing these results, we concluded that both triplet states were populated under the sensitized conditions experimentally tested. Besides, as it was demonstrated by laser flash photolysis, that in both compounds the triplet-triplet energy transfer occurred. But, the triplet state of **12-Prot** did not react leading to the *Z*-isomer.

Therefore, to further explore this point, a detailed computational study including a multiconfigurational method should be performed. However, the use of DFT methods should be enough for a qualitative understanding of the different behavior of both photoswitches. So the triplet potential energy surfaces of **12** and **12-Prot** were computed. Firstly, an optimization along the T_1 surfaces starting from the ground state geometries led to two different minima for **12** and **12-Prot** with different features (Figure 5.19).

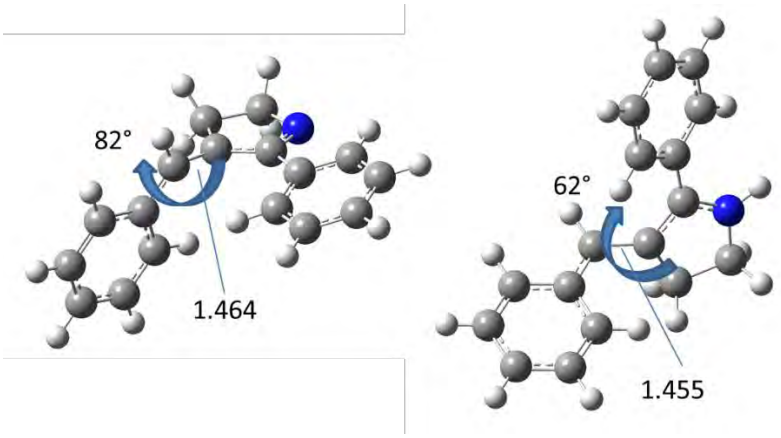

Figure 5.19. Minima in the triplet state energy surface for **12** (left) and **12-Prot** (right).

As Figure 5.19 shows, the neutral switch (**12**) was completely twisted (dihedral angle 82º) and the C=C double bond was elongated (1.464 Å). So, the isomerization of **12** was favored and it yielded different isomers ratio in the PSS under sensitized irradiation conditions. In contrast, **12-Prot** showed its C=C double bond in a more planar disposition since the dihedral angle was 62º. Besides the C=C distance was shorter (1.455 Å). Therefore, due to the features of the triplet state of **12-Prot**, it did not lead to an efficient photoswitching and other deactivation processes took place.

3.3. Thermal back reversion.

Once the photoisomerization of neutral and quaternized derivatives from *E* to *Z*-isomer had been deeply studied in both the singlet and triplet states, the next step was to study the thermal-back reversion from *Z* to *E*-isomer of **12**, **12-Prot**, **12-Met, 13**, **13-Prot and 13-Met**.

Different solutions 0.1 M in CD_3CN of **12**, **13** and its quaternized analogues in its PSS were prepared. These solutions were placed in different NMR tubes and they were kept at room temperature in darkness; the thermal-back reaction was followed by ^1H NMR.

In the case of **12**, **12-Prot** and **12-Met** the thermal reversion took place within hours in the conditions detailed above. This feature would be a drawback in applications which would require an energy liberation at room temperature, for instance. But it could be an asset for controlling the pharmacological action of a photodrug into our body, deactivating the medical effect by itself.

On the other hand, no back reaction was found in 6 days by ^1H NMR at room temperature in darkness for compounds **13**, **13-Prot** and **13-Met**. When increasing the temperature up to 60ºC the *E*-isomer recovery was easily performed for all of them.

Different behavior was found in the thermal conversion depending on the substituent conjugated with the C=C double bond. Some theoretical calculations were performed to clarify the experimental observations. For that purpose, the transition structures in the ground state (TS´s) for the thermal-back reaction were computed by DFT calculations with B3LYP functional and the standard 6-31G* basis.

Looking at the transition structures (Figure 5.20) for **12** and **13**, similar features could be noticed, and only small differences could be found. These differences should be responsible for different experimental results obtained.

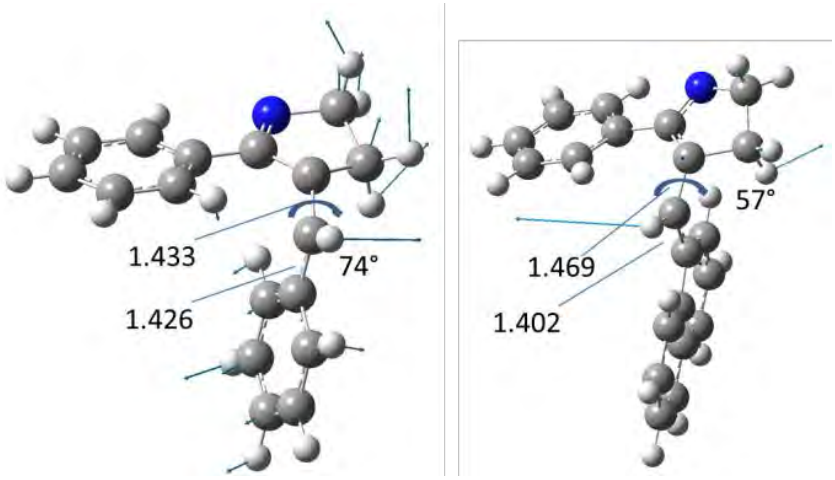

Figure 5.20. Computed transition structures (TS) and displacement vector for the thermal reversion for **12**(left) and **13** (right).

As can be seen in Figure 5.20, the TS found for **12** is more twisted than the one computed for **13**, with the molecule divided into two halves in both molecular switches. The second aromatic ring in **13** causes an extended conjugation in the naphtyl moiety that leads to an increase C=C distance, and thus a TS higher in energy (57.6 kcal/mol for **12**, 71.8 kcal/mol for **13**). Taking into account that the computed energy values were qualitatively too high due to the level of theory used, only the energy difference between both TS´s should be considered, allowing us to assure that the thermal back reaction was more hampered when the substituent was a naphthyl group (**13**).

Performing the same calculation for methylated derivatives, similar results were found with barriers of 53.4 kcal/mol for **12-Met** and 69.6 kcal/mol for **13-Met** regarding protonated analogues. So, the conclusion was the same as in the case of neutral species.

4. Applications.

The use of molecular switches has been applied in a lot of fields of research, reporting amazing applications of the photocontrol of many processes from polymers[33] to peptide conformations.[34] As has been discussed in the background, photoswitches based on the azobenzene core have been used to control a lot of biologic processes by using light.[35] Despite the huge implementation of photoswitches based on *E*/*Z* isomerism, there are some applications that have been almost unexplored, as for example, how these kind of molecular switches can store the light energy.

4.1. Molecular Solar thermal system (MOST).

The goal of these compounds is to store the energy which comes from the sun in chemical energy. This is a key aspect for our society since in the future the fossil fuels available to produce energy will be eventually exhausted. For this purpose, molecules based on norbornadienes are the most studied systems in this field.[36, 37]

Therefore, the development of new molecules which could behave as a molecular solar thermal system (MOST) device is of great importance. Here under, it will describe the features needed for a molecular switch based on *E*/*Z* isomerization to be turned into an efficient MOST.

Firstly, every molecule´s evaluated capacity, to behave as a MOST system, must absorb light and use this energy to interconvert the system between two different states. Sometimes, when the photoisomer is produced after absorbing light, the thermal-back reaction could occur at different temperatures. Both isomers should not be isoenergetic because if the difference between both states is large, more energy will be stored in the photoisomer form (Figure 5.21).

[33] Asadirad, A. M.; Boutault, S.; Erno, Z.; Branda, N. R., Controlling a Polymer Adhesive Using Light and a Molecular Switch *J. Am. Chem. Soc.* **2014,** *136*, 3024-3027.
[34] See ref. 13.
[35] Mart, R. J.; Allemann, R. K., Azobenzene photocontrol of peptides and proteins *Chem. Commun.* **2016,** *52*, 12262-12277.
[36] Dreos, A.; Wang, Z.; Udmark, J.; Ström, A.; Erhart, P.; Börjesson, K.; Nielsen, M. B.; Moth-Poulsen, K., Liquid Norbornadiene Photoswitches for Solar Energy Storage *Adv. Energy Mater.* **2018,** *8*, 1703401.
[37] Jorner, K.; Dreos, A.; Emanuelsson, R.; El Bakouri, O.; Fdez. Galván, I.; Börjesson, K.; Feixas, F.; Lindh, R.; Zietz, B.; Moth-Poulsen, K.; Ottosson, H., Unraveling factors leading to efficient norbornadiene–quadricyclane molecular solar-thermal energy storage systems *J. Mater. Chem. A* **2017,** *5*, 12369-12378.

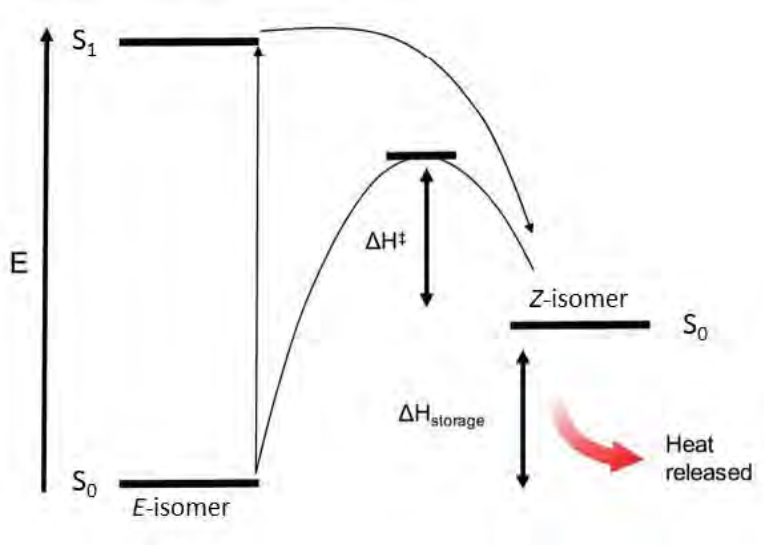

Figure 5.21. Energy diagram of a MOST device.

In Figure 5.21, it is described schematically how a MOST device based on *E*/*Z* isomerism should work. As it is represented in the figure above, the thermal-back reaction should be hampered under certain conditions. In the case of all these features being accomplished, the system could be evaluated as an efficient energy storage device.

In these kind of switches, the energy of a photon is transferred to the system and the difference in energy between the two isomers could be released once the energy barrier is overcome.

Looking into our described compounds, **13-Met** accomplished all the requirements to be a MOST device, since both isomers were not isoenergetic, the thermal-back reversion was hampered, and it could be activated by visible light. Although a deeper study would be needed to evaluate these photoswitches as a template to afford efficient MOST systems.

But it has been shown how small modifications in the general structure of rhodopsin-based molecular switches could modify its properties, to match the requirements of MOST systems.

4.2. Modification of a peptide conformation.

In previous works **14** was attached to a model peptide, to photocontrol its secondary structure irradiating the system. This peptide did not have any specific function. It was selected as a model example, as the distance between the two anchorage points had to match with the end to end distance of the photoswitchable cross-linker (***E*-14**).[38] To

[38] See ref. 13.

attach our molecular switch **14** to a peptide, two cysteines were necessary, then through a reaction between the thiol group of each cysteine and the chloroacetamides of **14**, the cross-linked peptide was prepared.

In this part of my thesis, it was envisioned to go one step further. For that purpose, we planned to attach **14** to a peptide responsible for some biological functions.

The complex system to photocontrol was based on the proadrenomedullin NH_2-Terminal 20 peptide (PAMP) (Figure 5.22). It has been reported that this peptide is responsible for many biological functions:

- It is described as an important angiogenic factor, this means that it controls the formation of new blood vessels, which for example are responsible for a tumor growth, resulting in metastasis.[39]
- It also increases the kinesin´s velocity which is important in the intracellular transport over the microtubules.[40]
- This peptide controls the polymerization of the tubulin, which is responsible for the formation of the microtubules, crucial for the formation of the cytoskeleton and the cellular division.[41]

Once the main features of this peptide have been shown, the importance of controlling the structure of this peptide to alter its properties by light should be remarked upon, since it is a clean source of energy and it shows a high temporal and spatial resolution.

Thus, a new peptide based on PAMP should be designed, taking into account that there are no cysteines in PAMP to link our photoswitch **14** (Figure 5.22). The peptide nomenclature used is described in the literature.[42]

ARLDVASEFRKKWNKWALSR-NH_2

PAMP

[39] Martínez, A.; Zudaire, E.; Portal-Núñez, S.; Guédez, L.; Libutti, S. K.; Stetler-Stevenson, W. G.; Cuttitta, F., Proadrenomedullin NH_2-Terminal 20 Peptide Is a Potent Angiogenic Factor, and Its Inhibition Results in Reduction of Tumor Growth **2004,** *64*, 6489-6494.
[40] Larráyoz, I. M.; Martínez, A., Proadrenomedullin N-Terminal 20 Peptide Increases Kinesin's Velocity Both in Vitro and in Vivo *Endocrinology* **2012,** *153*, 1734-1742.
[41] Chirgwin, J. M.; Cuttitta, F.; Martínez, A.; Ozbun, L.; Sackett, D. L.; Wessner, L.; Zudaire, E., Intracellular proadrenomedullin-derived peptides decorate the microtubules and contribute to cytoskeleton function *Endocrinology* **2008,** *2898*, 2888-2898.
[42] IUPAC-IUB Joint Commission on Biochemical Nomenclature (JCBN). Nomenclature and symbolism for amino acids and peptides. Recommendations 1983 **1984,** *219*, 345-373.

Figure 5.22. proadrenomedullin NH_2-Terminal 20 peptide sequence.

Regarding previous works, the S-S distance (length between the two anchorage points) in the peptide should be around 17 Å; this means that there should be 11 aminoacids between the two cysteins. For that purpose, two cysteines were introduced in the active part of the PAMP (Figure 5.23).

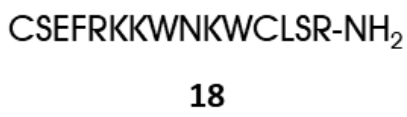

18

Figure 5.23. Sequence of peptide **18**.

It has been reported that small fragments of PAMP kept their biological activity, moreover the three amino acids peptide LSR-NH_2 exhibited some activity increasing the tubulin polymerization as the complete PAMP.[43] It should be noted that for the biological activity of the PAMP, the carboxyl end has to be capped by an amide group.

The structure of the PAMP has been determined by NMR and it consists of an α-helix along the whole molecule.[44] Moreover, the length of **18** is adequate to be photocontrolled through the linkage of a molecular switch (**14**). Therefore, the cross-linked peptide **19** was synthesized (Figure 5.24).

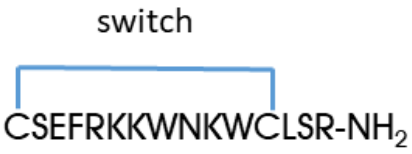

19

Figure 5.24. Schematic representation of cross-linked peptide **19**.

It is shown in Figure 5.24 is shown that the active part was not modified in the new proposed design, so it is expected that the biological properties would be mainly unaltered.

Firstly, the synthesis of the peptide designed (**18**) was accomplished using solid phase synthesis. This means that the reaction was not performed in solution; a solid surface was used to carry out the reaction, such as a resin. Once the peptide was synthesized, the purification was performed by high performance liquid chromatography (HPLC) using

[43] See ref. 40.

[44] Lucyk, S.; Taha, H.; Yamamoto, H.; Miskolzie, M.; Kotovych, G., NMR conformational analysis of proadrenomedullin N-terminal 20 peptide, a proangiogenic factor involved in tumor growth *Biopolymers* **2006,** *81*, 295-308.

as eluent a gradient mixture of water and acetonitrile. When the peptide was pure, the linkage between the peptide and **14** was carried out according to the method developed by Prof. Andrew Woolley in the University of Toronto. Then, another purification was performed with different eluent conditions, for further details, see experimental data.

4.2.1. Photochemical study of the cross-linked peptide.

Once the synthesis of the system was accomplished, a photochemical study of **19** was carried out. Firstly, the UV-Vis spectra were recorded at different pH (Figure 5.25). For that purpose, a 5E-5 M solution of **19** in water was prepared.

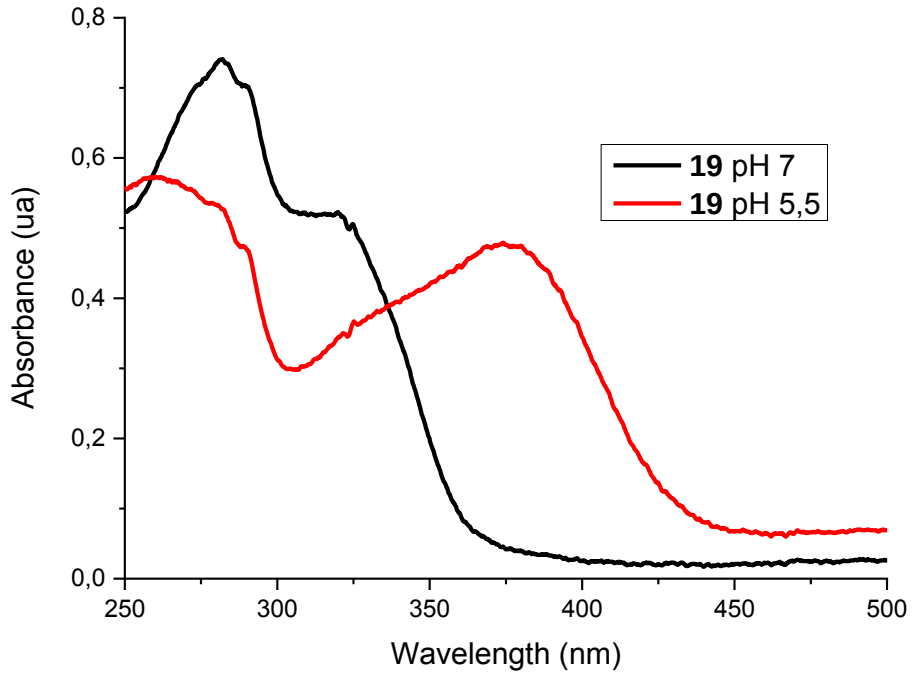

Figure 5.25. UV-Vis spectra of **19** at different pH.

As we can see in Figure 5.25, when the medium was slightly acidic, the photoswitch **14** based on rhodopsin molecular switches was protonated, inducing a bathochromic shift of its absorption wavelength, as has been discussed before.

Once the UV-Vis spectrum was described, the appropriate source of light could be selected to induce the photoswitching process represented in Figure 5.26. For this purpose, a photoreactor whose emission was centered at 350 nm was chosen.

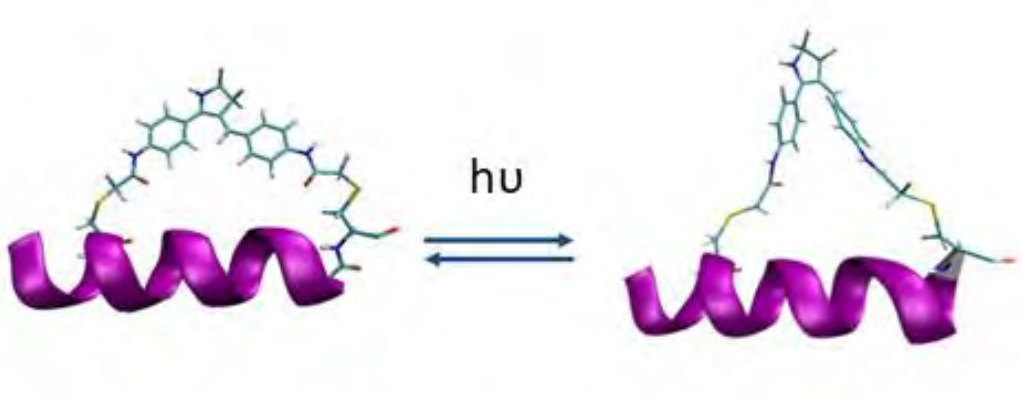

Figure 5.26. Photoswitching of the cross-linked peptide.

It should be noted, that two possible forms of **19** would be possible, since the photoswitch (**14**) used is not symmetric. And so when it was attached to a peptide, two regioisomers were found (***E*$_1$-19**, ***E*$_2$-19**). The photoisomerization process was followed by analytical HPLC using a C18 column. Both *E*-regioisomers of **19** were separated using a different linear gradient 75-70% water (containing 0.1% TFA) / acetonitrile over a period of 30 minutes (Figure 5.27).

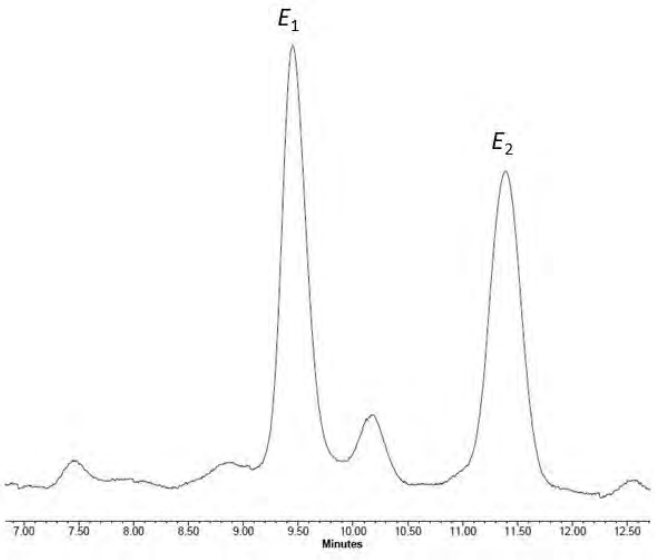

Figure 5.27. Chromatogram of two *E*-isomers.

In the chromatogram showed above, two major peaks corresponding to the two possible *E*-forms (E_1 and E_2) can be seen; the other small peaks correspond to impurities. As a preliminary test, a solution of 5E-5 M of **19** in cytoskeleton buffer solution (pH 6.1) was prepared to irradiate it using a photoreactor which emission was centered at 350 nm.

The solution was irradiated for 45 minutes and then, a HPLC experiment was run to observe if any change occurred (Figure 5.28).

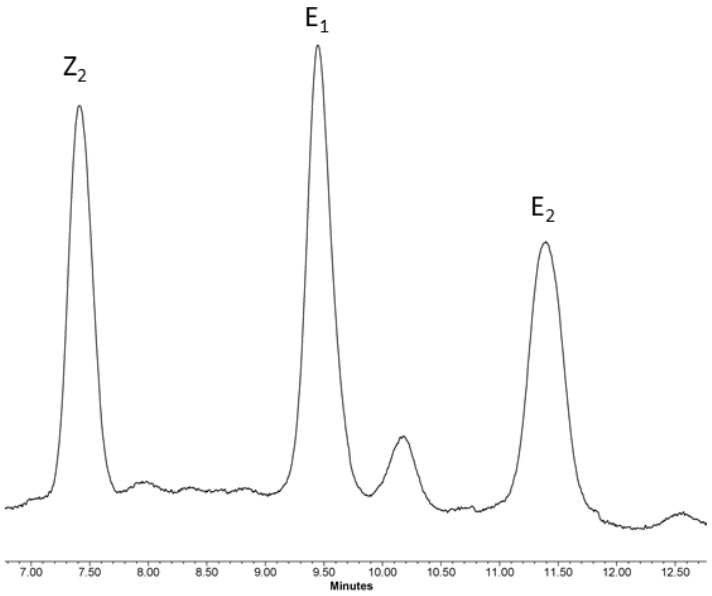

Figure 5.28. Chromatogram after the irradiation of ***E*-19** isomers.

As is shown in Figure 5.28, the appearance of a new peak was observed; it could be related to one *Z* isomer of the two possible. In this case, we hypothesize that this new peak comes from the E_2-regioisomer because its size decreased compared to the data prior to the irradiation. Therefore, the photoisomerization under the irradiation conditions took place easily.

In order to find out which peak was corresponding to each form, E_1 and E_2 were separated by HPLC using the same conditions as in the previous case. Then, the chromatograms were recorded of both regioisomers.

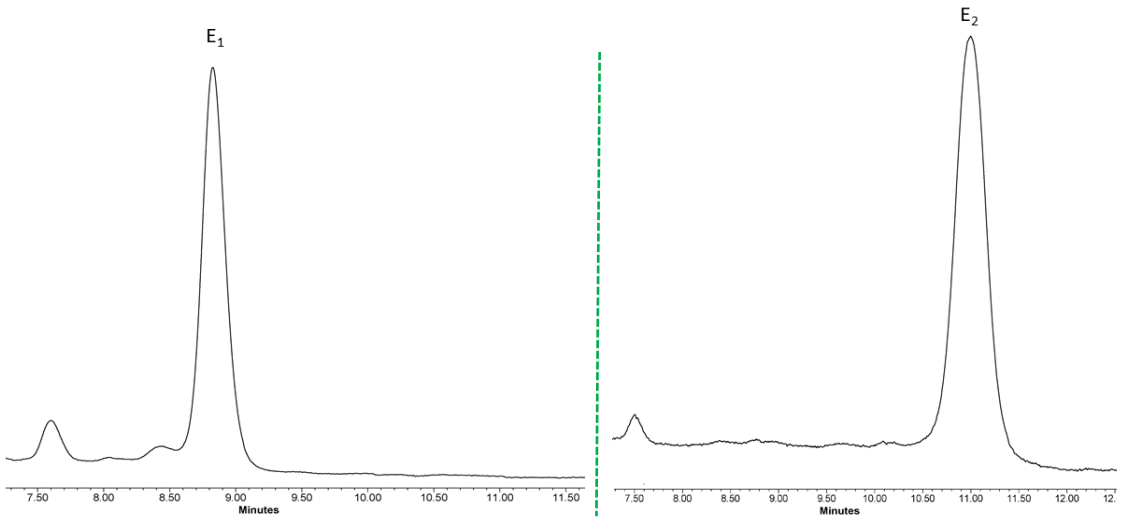

Figure 5.29. Chromatograms of both regioisomers.

In Figure 5.29, it is demonstrated that the separation of both cross linked regioisomers was achieved successfully. So, their irradiations were studied separately.

For that purpose, a 5E-5 M solution of each regioisomer in cytoskeleton buffer solution (pH 6.1) were irradiated. Then, HPLC analysis of both peaks was recorded (Figure 5.30).

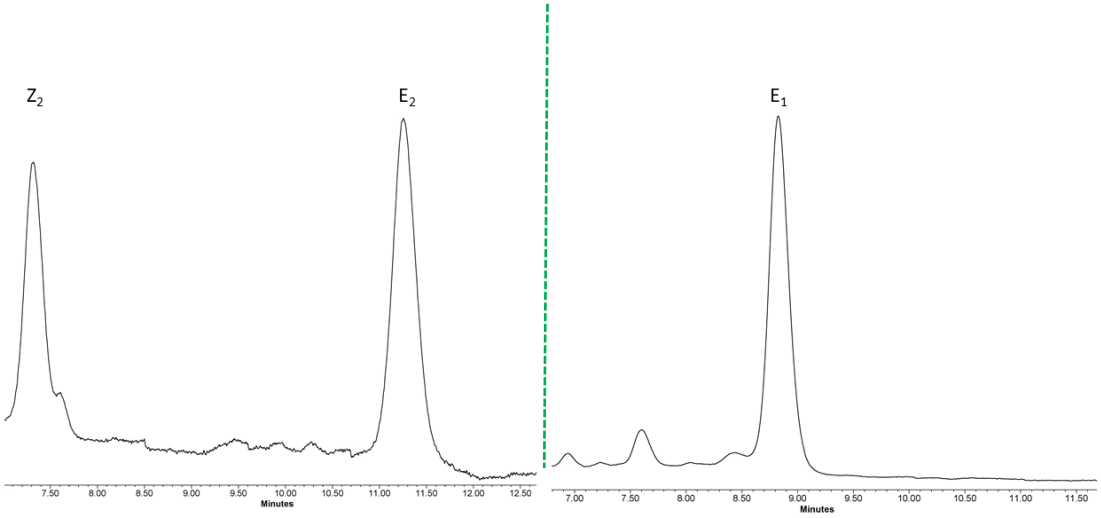

Figure 5.30. Irradiation each regioisomer separately.

In Figure above, when E_2 was irradiated the photoisomerization of the double bond took place leading to Z_2-isomer. In contrast, when E_1 was irradiated no new peaks appeared in the chromatogram; this may be due to the Z_1-isomer appearing at the same retention time as E_1, so no new chromatographic peaks were found after running out the HPLC experiment.

Therefore, we could control the isomerization of a photoswitch attached to a more complex system as a peptide, and were able to photocontrol the secondary structure of a peptide with a defined biological function.

The relevance of controlling the *Z*-*E* isomerization by heating or light has been mentioned before. This system experimented the thermal-back reversion in a few hours at 50ºC, recovering the *E*-isomer.

Moreover, it was very interesting to note that the mixture of *Z* and *E*-isomers could be irradiated in buffer solution which was slightly acidic. This allowed us to use a white LED as a source of light. Under these conditions, the photoreversion (*Z*-*E*) took place. Therefore, the back reaction could be controlled by heating or using light, recovering the initial regioisomers.

4.2.2. Biological study.

Once the photoswitching of the peptide was studied and controlled by light, it could be analyzed if it could also control their biological properties by activating the switch using light.

The control of the tubulin polymerization by PAMP derivatives has been reported. So, it was decided to test **18** and the system formed by the cross-linked peptide in their two possible forms (***E*-19** and ***Z*-19**).

For that purpose, tubulin polymerization assays were performed. The methodology used was the usual to perform these experiments.[45] For doing the assay, to a solution of 400 μg of bovine brain tubulin was added 10 μM of each compound. In this case, the activity of the peptide **18** and both isomers ***E*-19** and ***Z*-19**. The process could be monitored by the change in the absorbance value at 340 nm of the sample at different intervals of time for one hour. When tubulin polymerization was increasing over time, the absorbance at 340 nm also raised up. Therefore, using this methodology provided us with a very precise and easy way to follow this biological assay.

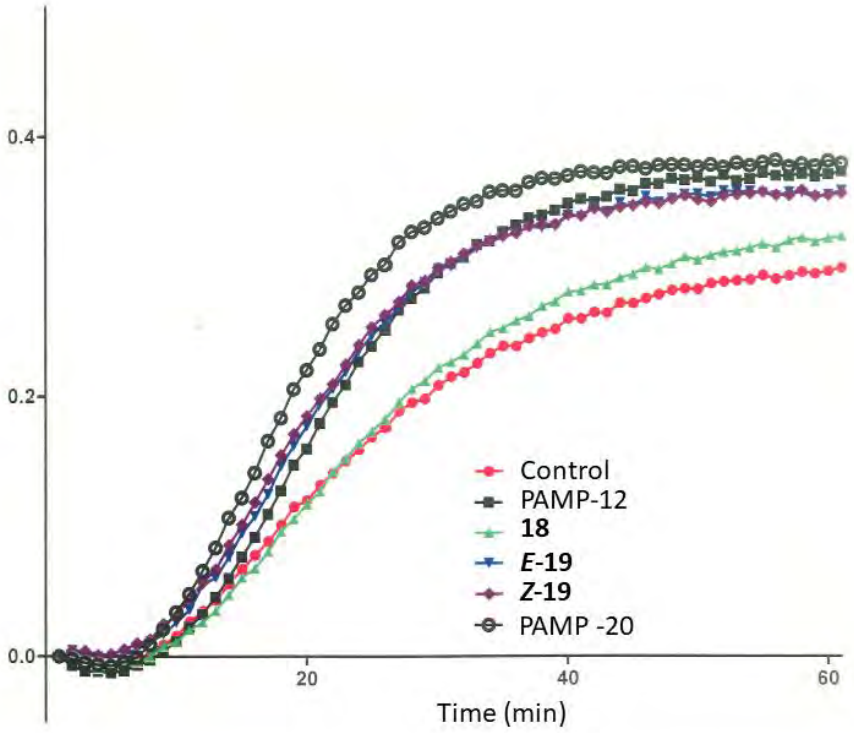

Figure 5.31. Evaluation of the biological activity of **18**, ***E*-19** and ***Z*-19.**

In Figure 5.31, several assays are represented; the red circles (control) had no peptide to influence the tubulin polymerization. Two different PAMP fragments (PAMP-12 and PAMP-20) were the natural peptides without any modification. These fragments showed almost the same effect on the tubulin polymerization. Interestingly, it is shown that when the two cysteines were introduced in the peptide chain (**18**), it lost the whole activity.

[45] See ref 40.

But, when evaluating the cross-linked peptide **19**, the activity was recovered showing the same effect as PAMP-12. This effect might be due to the structure fixation made by the switch, losing its flexibility. In many pharmacologic processes, the importance of the stapled peptides is well known; this kind of peptides are those in which its secondary structure is fixed by a synthetic brace to enhance their target affinity.[46] Unfortunately, no differences were found between ***E*-19** and ***Z*-19** isomer, so this process could not be controlled by light, but this is a good starting point to design new photoswitchable peptides.

[46] Iegre, J.; Ahmed, N. S.; Gaynord, J. S.; Wu, Y.; Herlihy, K. M.; Tan, Y. S.; Lopes-Pires, M. E.; Jha, R.; Lau, Y. H.; Sore, H. F.; Verma, C.; O' Donovan, D. H.; Pugh, N.; Spring, D. R., Stapled peptides as a new technology to investigate protein–protein interactions in human platelets *Chem. Sci.* **2018,** *9*, 4638-4643.

5. Experimental data.

- **Synthesis of intermediate 15.**

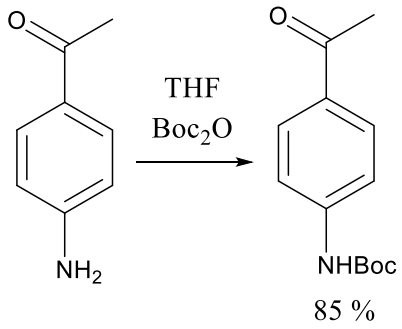

Scheme 5.7.

The first step of the synthesis was the protection of 4-aminoacetophenone. The aniline (5 mmol, 675 mg) was dissolved in THF using Boc_2O (5.5 mmol, 1.26 g) and K_2CO_3 (10 mmol, 1.38 g). The reaction was carried out overnight at room temperature. When the reaction was completed, the solvent was evaporated under reduced pressure and the resulting crude was washed with hexane to afford *tert*-butyl (4-acetylphenyl)carbamate pure as a white solid.

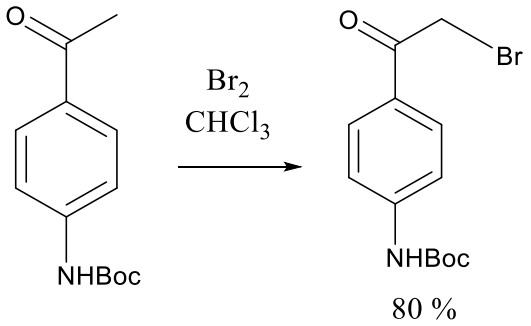

Scheme 5.8.

Once the aniline was protected with Boc, the bromination of the acetyl group was afforded. For that purpose, *tert*-butyl (4-acetylphenyl)carbamate (1 mmol, 235 mg) was dissolved in $CHCl_3$, to this solution 1,2 mmol. of bromine (Br_2) was added dropwise at 0ºC. The mixture was stirred at 0ºC for 20 minutes. Then, the reaction was stirred for 2 hours at room temperature. The solvent was reduced until 20 ml left and the mixture was kept at -20 ºC overnight. Finally, the precipitate was filtered to afford *tert*-butyl (4-(2-bromoacetyl)phenyl)carbamate pure as a yellow solid.

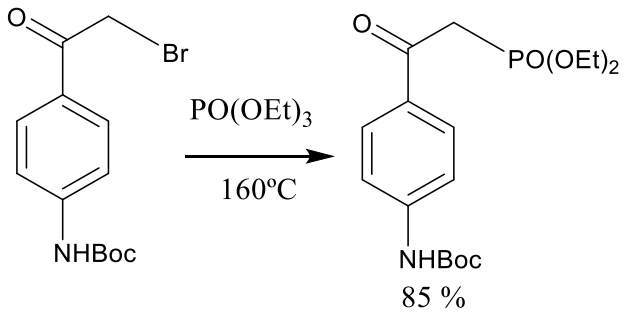

Intermediate 15

Scheme 5.9.

Finally, *tert*-butyl (4-(2-bromoacetyl)phenyl)carbamate (1 mmol, 313 mg) was dissolved in triethyl phosphite (3 ml). The mixture was heated at 160ºC for 3 hours. The solvent was evaporated under reduced pressure. **Intermediate 15** was purified by column chromatographic using as eluent a mixture of hexane/ethyl acetate (3:1).

- **Synthesis of intermediates 16A and 16B.**

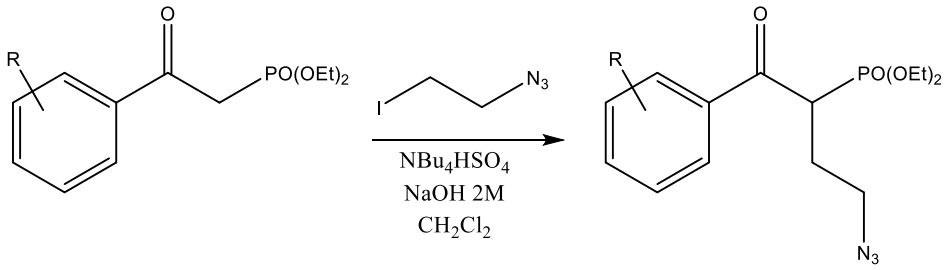

R = H, *p*-NHBoc

Intermediate 16A (H), 16B (*p*-NHBoc)
30%

Scheme 5.10

The phosphonate which led to **intermediate 16A** was commercially available. The corresponding phosphonate (1mmol) was dissolved in CH_2Cl_2, to this mixture was added 1.5 mmol. of tetrabutylammonium bisulfate, 2 mmol of sodium hydroxide (2 M) and 1.5 mmol of iodoethylazide. The reaction was stirred at room temperature for 36 hours. When the reaction was completed, 20 ml of water was added, and the mixture was extracted three times with 25 mL of CH_2Cl_2 each time. The organic phases were evaporated under reduced pressure. Then, the residual oil was purified by column chromatographic using different mixtures of hexane/ethyl acetate as eluent to afford the two phosphonates. The yields were around 30% in the synthesis of **intermediates 16A, 16B.**

- **Synthesis of intermediates 17A, 17B and 17C.**

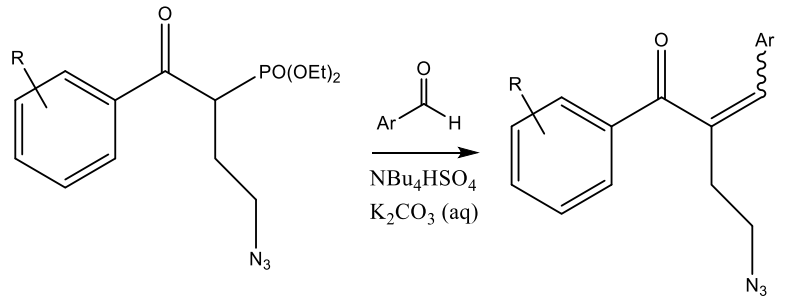

Intermediate 16A and 16B

Intermediate 17A (R=H, Ar=Ph), 17B (R=H, Ar=2-naphtyl) and 17C (R, Ar=*p*-NHBoc)

ca. 30%

Scheme 5.11.

Both **intermediates 16A** and **16B** were dissolved in THF (1 mmol) separately. To each solution, tetrabutylammonium bisulfate (0.2 mmol) and potassium carbonate (2 mmol) dissolved in water were added. Different reaction times were found depending on the intermediate involved in the reaction, so the procedures were followed by TLC. When the reactions were completed, the mixture was extracted three times with 25 ml of CH_2Cl_2 each time. The organic phases were evaporated under reduced pressure. Then, the residual oil was purified by column chromatographic using different mixtures of hexane/ethyl acetate as eluent to afford the pure compounds.

- **Synthesis of 12, 13 and 14.**

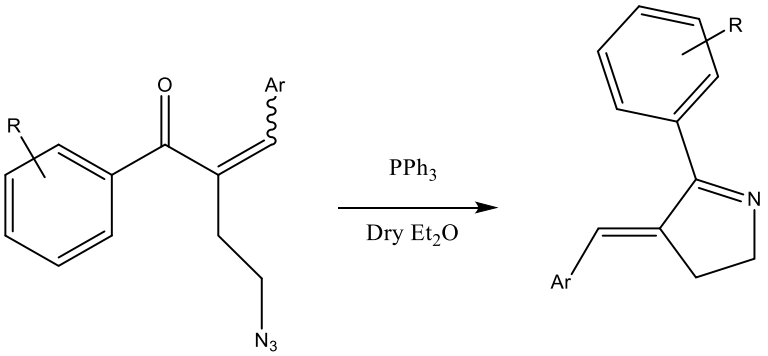

R = H (**12** and **13**), *p*-NHBoc (**14**)

Ar = Ph (**12**), 2-naphtyl (**13**), *p*-NHBoc (**14**)

12, 13 and 14

ca. 60%

Scheme 5.12.

To synthesize **12** and **13**, **intermediate 17A** and **17B** (1 mmol) were dissolved in diethyl ether separately, respectively. To each solution, 3 mmol of triphenyl phosphine was added. The resulting mixtures were stirred at room temperature for 24 h. Then, the

solvent was evaporated and the purification was afforded by column chromatography in silica gel using as eluent different mixtures of hexane/ethyl acetate.

To get compound **14**, following the same procedure as **12** and **13**, two additional steps were necessary. Then, the Boc deprotection was achieved using TFA in CH_2Cl_2 (1:1) for 15 minutes. Without further purification, 2 equiv. of chloroacetyl chloride was added to the mixture, the reaction was carried out during 30 minutes until compound **14** precipitated and it was isolated pure by filtration.

- **Synthesis of 12-Met and 13-Met**

The methylated photoswitches were achieved starting from each neutral form (0.5 mmol); it was dissolved in dry toluene (2 ml) under nitrogen atmosphere and was added methyl triflate (0.5 mmol). The reaction was stirred for 10 minutes at room temperature. It was observed that the *N*-methylated compounds precipitated and they were separated by filtration. No further purification was needed.

- **Synthesis of 12-Prot and 13-Prot.**

To a solution of the neutral photoswitch (0.2 mmol) in CD_3CN was added a drop of a HBF_4 in ether solution. The compound was quantitatively formed.

- **Synthesis of 18 by solid phase synthesis.**

The preparation of **18** was performed through an automatic synthesizer. It was used the solid phase peptide synthesis (SPPS) assisted with microwaves to accelerate all the reactions that were carried out. The strategy used was Fmoc/^{t}Bu to synthesize **18**. Moreover, the Rink-amide MBHA resin was used to get the amide instead of the terminal carboxylate, this fact was very important to maintain the biological properties of PAMP mutants.

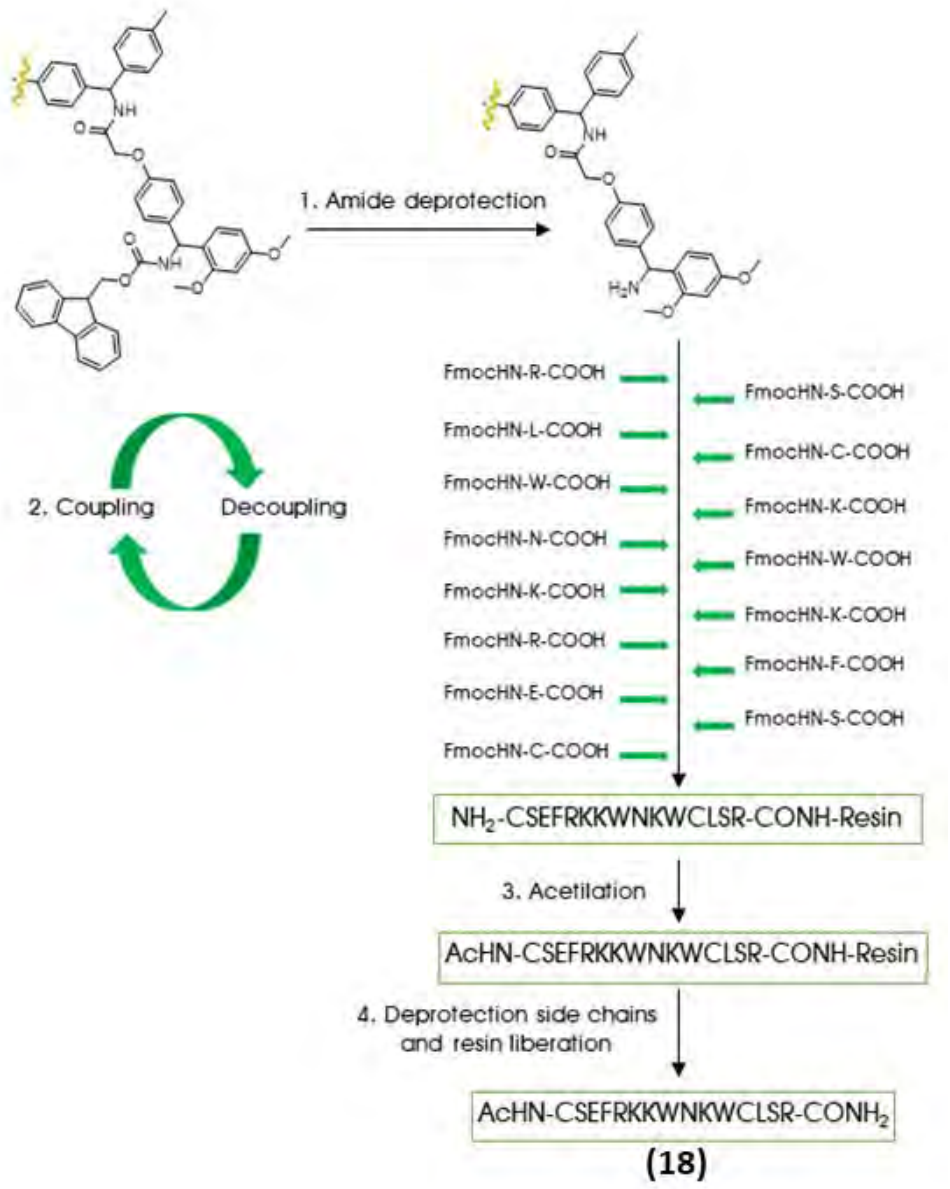

Figure 5.32. Schematic synthesis of **18** by SPPS.

In Figure 5.32, it is well described how the automatic synthesizer works. The first step of this process was to deprotect the resin (0.1 mmol scale, 235 mg); it reacted with 1 ml of piperidine in DMF (3 ml) for 10 minutes. Then, the first aminoacid was dissolved in 3 ml of DMF and it was added to this solution DIEA (1 ml) and HBTU (3.4 mg in DMF). The mixture was allowed to react for 10 minutes. Following this reaction, the mixture was washed with 3 x 2 ml of DMF prior the next step, when the deprotection of Fmoc group was performed adding piperidine (1 ml) dissolved in 3 ml of DMF. The mixture was washed with 3 x 2 ml of DMF. These two steps have to be repeated for each aminoacid.

Once all the couplings/deprotections were done, the resin was put out of the synthesizer to carry out the acetylation of the amine group. For this purpose, the resin was treated with 2 ml of pyridine and 1 ml of acetic anhydride for 2 hours.

Finally, the resin was released and the side chains of the amino acids deprotected using a mixture which contained 1.9 ml of TFA, 50 μL of TIS, 50 μL of EDT and 50 μL of H_2O. The resulting mixture was stirred for two hours. When the reaction was completed, diethyl ether at 0ºC was added. As a consequence the peptide precipitated, and it was isolated by filtration. The solid was purified by HPLC using a linear gradient from 5% to 30% of acetonitrile afford **18**.

The peptide **18** was characterized by MALDI (+): Calc. for $C_{90}H_{139}N_{28}O_{21}S_2$ $[M+H]^+$ 2012.011, found 2012.023.

- **Synthesis of 19.**

The cross-linking reaction to afford **19** was based on the method developed by Prof. Andrew Woolley in the University of Toronto to attach a molecular switch to a peptide. The reaction was carried out in 60 mM Tris Buffer at pH 8 containing 2 mM TCEP. In this case, the peptide was added to the reaction mixture to give a concentration of 0.5 mM of **18** and 2 mM of **14.** The solvent used in the reaction was composed by 20% of DMSO in 80% of water. The reaction mixture was stirred overnight at 40ºC. When the reaction was completed, **19** was purified by HPLC using a C18 column with a linear gradient of 5% to 30% of acetonitrile to afford **19**.

The cross-linking peptide **19** was characterized by ESI-MS (+): Calc. for $C_{111}H_{159}N_{31}O_{23}S_2$ $[M+H]^{4+}$ 589.5411, found 589.5433.

5.1. Characterization data.

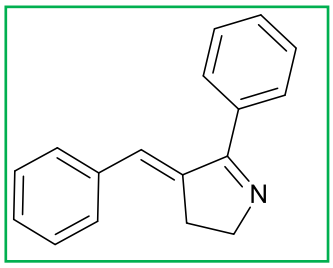

(E)-4-benzylidene-5-phenyl-3,4-dihydro-2*H*-pyrrole (**12**)

Empiric formula: $C_{17}H_{15}N$

Molecular weight: 233.1204

Yield = 60 %

^{1}H-NMR (300 MHz, DMSO-d^6) δ 7.65 (m, 2H), 7.40 (m, 2H), 7.26 (m, 1H), 6.83 (s, 1H) 4.21 (m, 2H), 3.06 (m, 2H).

^{13}C-NMR (75 MHz, DMSO-d^6) δ 174.9, 142.1, 137.0, 134.5, 129.6, 128.9, 128.8, 128.6, 128.5, 127.9, 127.8, 59.6, 31.0.

UV-Vis (CH_2Cl_2 : MeOH): λ (nm) = 289 (ε=22232 $M^{-1}cm^{-1}$), 303(ε= 15707 $M^{-1}cm^{-1}$).

EM-ES (+): calcd for $C_{17}H_{16}N$ $[M+H]^+$ 234.1277, found 234.1284.

Observations: White solid.

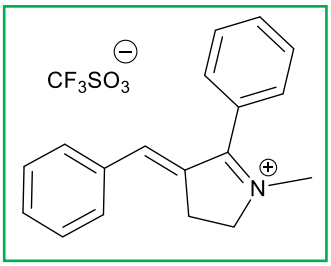

(E)-4-benzylidene-1-methyl-5-phenyl-3,4-dihydro-2*H*-pyrrolium, trifluoromethanesulfonate salt (**12-Met**)

Empiric formula: $C_{19}H_{18}NSO_3$

Molecular weight: 397.41

Yield: 95%

^{1}H NMR (300 MHz, CD_3CN): δ (ppm) 7.74 (m, 3H), 7.57 (m, 7H), 7.05 (s, 1H), 4.41 (m, 2H), 3.43 (m, 2H), 3.40 (s, 3H).

^{13}C NMR (75MHz, CD_3CN): δ (ppm) 180.5, 144.6 , 139.4, 135.1, 133.7, 132.2, 131.8, 130.4, 130.1, 129.9, 125.9, 60.5, 39.2, 27.7.

UV-VIS (CH_3CN): λ (nm) 334 (ε = 19418 $M^{-1}cm^{-1}$).

ES-MS (+) calcd for ($C_{18}H_{18}N^+$) [M^+]: calc. for 248.1434, found 248.1441.

Observations: Brown oil.

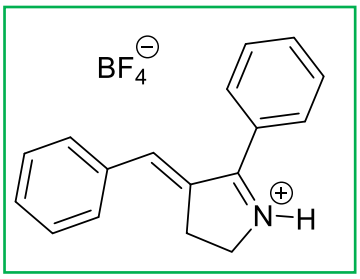

(E)-4-benzylidene-5-phenyl-3,4-dihydro-2*H*-pyrrolium, tetrafluoroborate salt (**12-Prot**)

Empiric formula: $C_{17}H_{16}NBF_4$

Molecular weight: 321.12

Yield: quantitative

^{1}H NMR (300 MHz, CD_3CN) δ 7.60 (t, J = 11.9 Hz, 2H), 7.58 – 7.46 (m, 5H), 7.41 (t, J = 6.4 Hz, 2H), 7.36 (m, 1H), 6.92 (s, 1H), 4.11 (m, 2H), 3.11 (m, 2H).

^{13}C NMR (75 MHz, CD_3CN) δ (ppm) 176.6, 142.1, 137.3, 133.7, 131.5, 131.4, 130.2, 129.8, 129.6, 129.6, 129.5, 58.5, 30.9.

UV-VIS (CH_3CN): λ (nm) 334 (ε = 19030 $M^{-1}cm^{-1}$).

ES-MS (+) calcd for ($C_{17}H_{16}N^+$): calc. for 234.1283, found 234.1283.

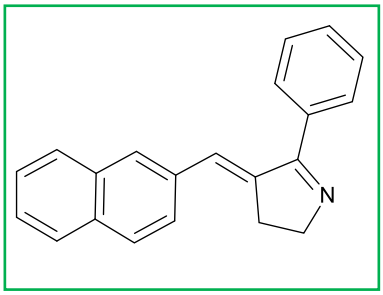

(E)-4-(naphthalen-1-ylmethylene)-5-phenyl-3,4-dihydro-2*H*-pyrrole (**13**)

Empiric formula: $C_{21}H_{17}N$

Molecular weight: 283.37

Yield: 60%

^{1}H-NMR (300 MHz, $CDCl_3$): δ (ppm) 7.89 (s, 1H), 7.83 (m, 3H), 7.70 (m, 2H), 7.57 (m, 1H), 7.51 (m, 5H), 7.01 (s, 1H), 4.28 (m, 2H), 3.20 (m, 2H).

^{13}C-NMR (75MHz, $CDCl_3$): δ (ppm) 175.2, 142.4, 134.6, 134.5, 133.5, 132.9, 129.8, 128.9, 128.6, 128.6, 128.3, 128.2, 127.8, 126.6, 126.6, 59.7, 31.2.

UV-VIS (CH_3CN): λ (nm) 245 (ε = 26342 $M^{-1}cm^{-1}$), 266 (ε = 34448 $M^{-1}cm^{-1}$), 275 (ε = 34853 $M^{-1}cm^{-1}$), 311 (ε = 28368 $M^{-1}cm^{-1}$), 324 (ε = 24316 $M^{-1}cm^{-1}$).

ES-MS (+) calcd for ($C_{21}H_{18}N$) [M^+]: calc. for 284.1434, found 284.1439.

Observations: Yellow solid.

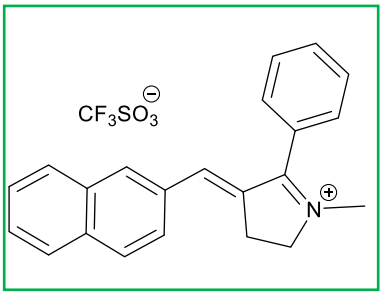

(E)-1-methyl-4-(naphthalene-2-ylmethylene)-5-phenyl-3,4-dihydro-2*H*-pyrrolium, trifluoromethanesulfonate salt **(13-Met)**

Empiric formula: $C_{23}H_{20}NF_3SO_3$

Molecular weight: 447.47

Yield: 85%

^{1}H NMR (300 MHz, CD_3CN): δ (ppm) 8.13 (m, 1H), 7.93 (m, 3H), 7.76 (m, 3H), 7.60 (m, 5H), 7.23 (s, 1H), 4.42 (m, 2H), 3.57 (m, 2H), 3.42 (s, 3H).

^{13}C NMR (75 MHz, CD_3CN): δ (ppm) 180.5, 144.9, 144.9, 139.5, 135.1, 134.0, 133.8, 133.3, 132.7, 130.5, 129.9, 129.8, 129.4, 128.7, 128.1, 127.6, 126.0, 60.5, 39.3, 27.9.

UV-VIS (CH_3CN): λ (nm) 214 (ε = 18250 $M^{-1}cm^{-1}$), 280 (ε = 12500 $M^{-1}cm^{-1}$), 290 (ε = 13250 $M^{-1}cm^{-1}$), 350 (ε = 16500 $M^{-1}cm^{-1}$).

ES-MS (+) calcd for ($C_{22}H_{20}N^+$) [M^+]: calc. 298.1583, found 298.1583.

Observations: Orange solid

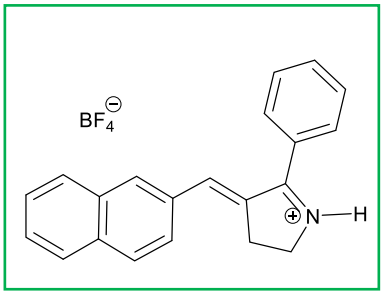

(E)-4-(naphthalene-2-ylmethylene)-5-phenyl-3,4-dihydro-2*H*-pyrrolium, tetrafluoroborate salt **(13-Prot)**

Empiric formula: $C_{21}H_{18}NBF_4$

Molecular weight: 371.19

Yield: quantitative

^{1}H NMR (300 MHz, CD_3CN) δ 8.99 (s, 1H), 8.18 (s, 1H), 7.99 (t, J = 8.0 Hz, 3H), 7.74 (m 6H), 7.63 (d, J = 7.7 Hz, 3H), 4.30 (m, 2H), 3.57 (m, 2H).

^{13}C NMR (75 MHz, CD_3CN) δ (ppm) 181.9, 146.2, 137.1, 135.4, 135.2, 134.0, 133.4, 132.8, 130.9, 130.6, 130.0, 129.8, 129.5, 128.7, 128.2, 127.7, 126.6, 52.1, 29.2.

UV-VIS (CH_3CN): λ (nm) 214 (ε = 18250 $M^{-1}cm^{-1}$), 350 (ε = 16200 $M^{-1}cm^{-1}$).

ES-MS (+) calcd for ($C_{21}H_{18}N^+$) [M^+]: calc: 284.1434, found 284.1434.

6. Metronidazole-based molecular switches.

Photopharmacology, as the use of light to control the bioactivity of drugs, has become an important topic of research in the last few years (see background for further details).[1] Due to this relevance, the biological activity has been photocontrolled.[2] For this purpose, it is very usual to add a photoswitchable moiety into a bioactive structure. This way, it would be possible to control the bioactive molecule isomerizing the photoswitchable unit by light.

For instance, the importance of controlling the antibacterial properties of a molecule is well known, since the overuse and misuse of antibiotic treatments is very usual in our society, causing problems in human health and in the environment.[3,4] Hence, the research into the photocontrol of these kind of bioactive molecules is emerging rapidly.[5] These studies are focused on the inspection of photoswitchable moieties based on antibiotics as quinolones (Figure 6.1) (see background section 4.2.2.1).[6]

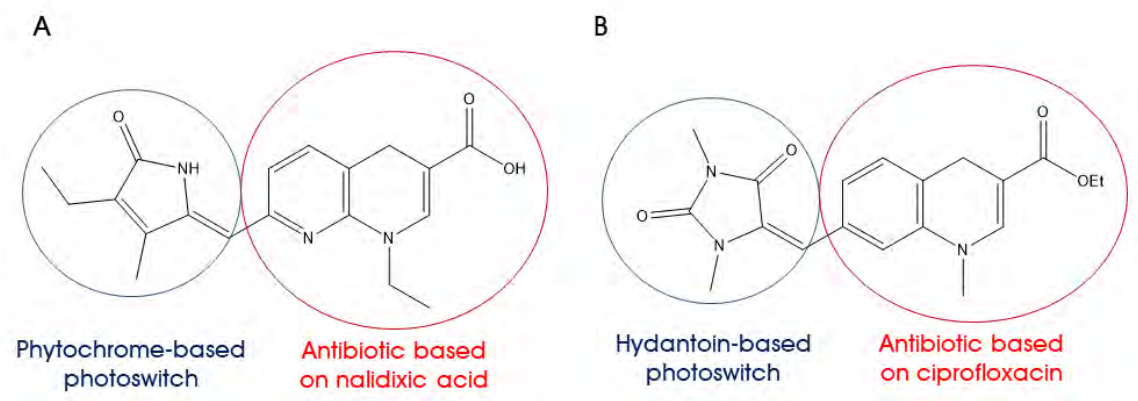

Figure 6.1. Photoswitches reported with antibacterial properties.

In Figure 6.1, different antibacterial molecules based on different molecular switches are described. Other functions have been controlled using the same strategy of attaching a photoswitchable moiety to a target molecule, as it was detailed in the background. Most of the recent studies in this field are focused on the use of azobenzene

[1] Velema, W. A.; Szymanski, W.; Feringa, B. L., Photopharmacology: Beyond Proof of Principle *J. Am. Chem. Soc.* **2014,** *136*, 2178-2191.
[2] Szymański, W.; Beierle, J. M.; Kistemaker, H. A. V.; Velema, W. A.; Feringa, B. L., Reversible Photocontrol of Biological Systems by the Incorporation of Molecular Photoswitches *Chem. Rev.* **2013,** *113*, 6114-6178.
[3] Llor, C.; Bjerrum, L., Antimicrobial resistance: risk associated with antibiotic overuse and initiatives to reduce the problem *Ther. Adv. Drug Saf.* **2014,** *5*, 229-241.
[4] Kümmerer, K., Resistance in the environment *J. Antimicrob. Chemother.* **2004,** *54*, 311-320.
[5] Velema, W. A.; van der Berg, J. P.; Hansen, M. J.; Szymanski, W.; Driessen, A. J. M.; Feringa, B. L., Optical control of antibacterial activity *Nature Chem.* **2013,** *5*, 924.
[6] Contreras-García, E.; Martínez-López, D.; Alonso, C. A.; Lozano, C.; Torres, C.; Rodríguez, M. A.; Campos, P. J.; Sampedro, D., Optical Control of Antimicrobial Activity in Quinolone Derivatives *Eur. J. Org. Chem.* **2017,** *2017*, 4719-4725.

as the photoswitchable moiety to photocontrol a specific biological activity.[7] For instance, several successful studies to photocontrol ion channels have been performed.[8] Ion channels are essential in neuron transmission, consequently, they play an important role on the nervous system. Among all ion channels, the voltage-gated ion channels are the most studied ones since 2004, when a photoswitch was reported with the ability of controlling potassium channels (see background).[9, 10]

Moreover, many efforts have been devoted to the discovery of different photodrugs to treat cancer disease.[11] As is well known, cancer is one of the most important mortal diseases in our daily lives. One approach to treat this severe disease was mainly based on applying light to destroy cancer cells in tissues by generating an active form of oxygen (PDT), which lead to the cellular death (see background for further details). This active form is based on the photosensitization of molecular oxygen to form singlet oxygen. The main drawback of this approach is the low concentration of oxygen in solid tumours.[12] Therefore, the production of singlet oxygen was not effective enough for the treatment of these kind of tumours.[13]

Photopharmacology could be a smart answer to solve the selectivity of the usual treatments used in chemotherapy. Therefore, the selectivity that might be achieved with photoactive drugs, together with the high spatiotemporal resolution offered by light, could turn these processes into promising tools for the clinical treatment of several diseases, including cancer.

There are already some promising studies to address the fight against cancer from this point of view. It is well known that *cis*-diamminedichloroplatinum (II) (*cis*-platin) is effective against many sorts of cancer but simultaneously, it is responsible for many side

[7] Hüll, K.; Morstein, J.; Trauner, D., In Vivo Photopharmacology *Chem. Rev.* **2018,** *118*, 10710-10747.
[8] Mourot, A.; Fehrentz, T.; Le Feuvre, Y.; Smith, C. M.; Herold, C.; Dalkara, D.; Nagy, F.; Trauner, D.; Kramer, R. H., Rapid optical control of nociception with an ion-channel photoswitch *Nat. Methods* **2012,** *9*, 396.
[9] Banghart, M.; Borges, K.; Isacoff, E.; Trauner, D.; Kramer, R. H., Light-activated ion channels for remote control of neuronal firing *Nat. Neurosci.* **2004,** *7*, 1381.
[10] Bregestovski, P. D.; Maleeva, G. V., Photopharmacology: A Brief Review Using the Control of Potassium Channels as an Example *Neurosci Behav Physi* **2019**.
[11] Nilsson, J. R.; Li, S.; Önfelt, B.; Andréasson, J., Light-induced cytotoxicity of a photochromic spiropyran *Chem. Commun.* **2011,** *47*, 11020-11022.
[12] Höckel, M.; Vaupel, P., Tumor Hypoxia: Definitions and Current Clinical, Biologic, and Molecular Aspects *J. Natl. Cancer Inst.* **2001,** *93*, 266-276.
[13] Henderson, B. W.; Busch, T. M.; Vaughan, L. A.; Frawley, N. P.; Babich, D.; Sosa, T. A.; Zollo, J. D.; Dee, A. S.; Cooper, M. T.; Bellnier, D. A.; Greco, W. R.; Oseroff, A. R., Photofrin Photodynamic Therapy Can Significantly Deplete or Preserve Oxygenation in Human Basal Cell Carcinomas during Treatment, Depending on Fluence Rate *Cancer Res.* **2000,** *60*, 525-529.

effects due to their low selectivity.[14] In Figure 6.2, its mechanism of action is represented, which is bound covalently to the DNA leading to apoptosis of healthy and cancer cells.[15]

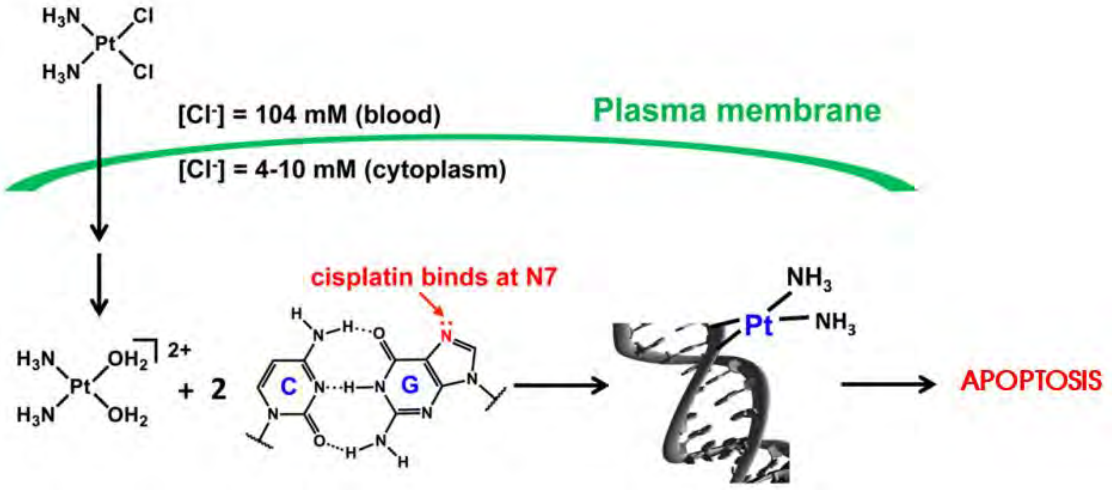

Figure 6.2. Mechanism of action of *cis*-platin.[16]

To afford the problem of selectivity in chemotherapeutical drugs, photoactive derivatives have been reported in which the therapeutic activity is controlled by the isomerization of a molecular switch based on diarylethenes (open/closed form).[17]

Also, metal nanoparticles have been used to (photo)release drugs with high precision. This way, the use of nanoparticles as vehicles to deliver therapeutic drugs in a specific tissue enhance the therapeutic effect. Moreover, by this method the side effects are profoundly minimized.[18]

Another strategy is based on turning conventional drugs into photoactive derivatives that can be controlled by light. For instance, combretastatin A-4 (CA-4) that is presented in Figure 6.3, is a stilbene derivative used in clinical trials for cancer therapy as an inhibitor of tubulin polymerization. In Chapter 5, it was said that tubulin is a protein which is essential in the microtubule formation during the cellular division, so the control of tubulin polymerization would allow us to control the cellular division, and therein lies the

[14] Rosenberg, B., Platinum coordination complexes in cancer chemotherapy *Naturwissenschaften* **1973,** *60*, 399-406.
[15] Reedijk, J.; Lohman, P. H. M., Cisplatin: Synthesis, antitumour activity and mechanism of action *Pharm. Weekbl. Sci.* **1985,** *7*, 173-180.
[16] Wang, D.; Lippard, S. J., Cellular processing of platinum anticancer drugs *Nat. Rev. Drug Discov.* **2005,** *4*, 307.
[17] Presa, A.; Brissos, R. F.; Caballero, A. B.; Borilovic, I.; Korrodi-Gregório, L.; Pérez-Tomás, R.; Roubeau, O.; Gamez, P., Photoswitching the Cytotoxic Properties of Platinum(II) Compounds *Angew. Chem. Int. Ed.* **2015,** *54*, 4561-4565.

[18] Rwei, A. Y.; Wang, W.; Kohane, D. S., Photoresponsive nanoparticles for drug delivery *Nano Today* **2015,** *10*, 451-467.

importance of its photocontrol. In detail, the bioactive form is the *cis*-isomer, which is not stable over time recovering the most stable form (*trans*-isomer) (Figure 6.3).

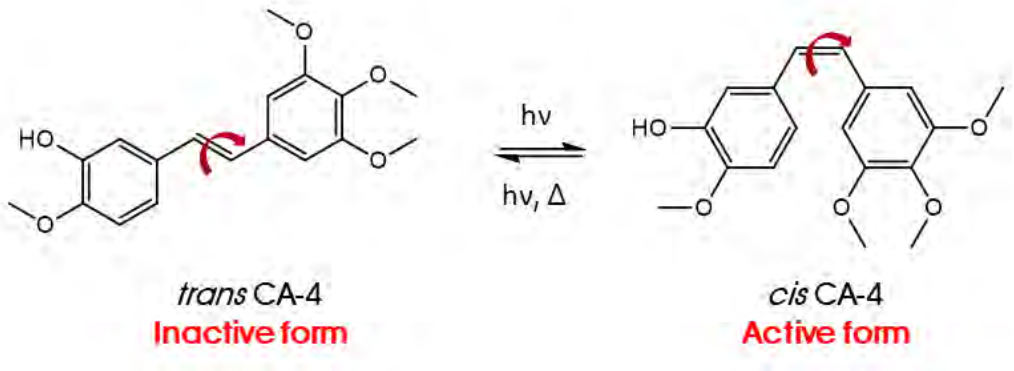

Figure 6.3. Photoisomerization of CA-4.

For this reason, many *cis*-restricted CA-4 analogues have been prepared and their effectiveness evaluated.[19,20] Other attempts of photogenerating the active isomer, which over time must be as stable as much as possible, have been done (see background for further details). For that purpose, the C=C double bond of CA-4 was changed by an *azo*-bond (N=N). In this way, the half-life of the *cis*-isomer was extended from 6.2 min to 85 min.[21]

As has been demonstrated, the exploration of new photoactive molecules is a trendy field of research. Hence, the design and study of new molecular switches with different photochemical properties (absorption wavelength, photostationary state or photochemical stability) or different photochemical properties (solubility, stability) are crucial for each specific application.

For this reason, the goal of this chapter is to design new photoswitches focused on the photocontrol of a biological target activating or deactivating the switch. Herein, the synthesis, photochemical study and cytotoxic evaluation of new candidates for the photocontrol of anticancer properties are presented.

[19] Głowacka, A.; Gensicka, M.; Cholewinski, G.; Dzierzbicka, K., Synthesis of Combretastatin A-4 Analogs and their Biological Activities *Anticancer Agents Med. Chem.* **2016,** *16*.

[20] Wang, L.; Woods, K. W.; Li, Q.; Barr, K. J.; McCroskey, R. W.; Hannick, S. M.; Gherke, L.; Credo, R. B.; Hui, Y.-H.; Marsh, K.; Warner, R.; Lee, J. Y.; Zielinski-Mozng, N.; Frost, D.; Rosenberg, S. H.; Sham, H. L., Potent, Orally Active Heterocycle-Based Combretastatin A-4 Analogues: Synthesis, Structure−Activity Relationship, Pharmacokinetics, and In Vivo Antitumor Activity Evaluation *J. Med. Chem.* **2002,** *45*, 1697-1711.

[21] Sheldon, J. E.; Dcona, M. M.; Lyons, C. E.; Hackett, J. C.; Hartman, M. C. T., Photoswitchable anticancer activity via trans–cis isomerization of a combretastatin A-4 analog *Org. Biomol. Chem.* **2016,** *14*, 40-49.

The new photoswitchable prototypes are based on metronidazole (Figure 6.4), which is a well-known antibiotic to treat bacterial vaginosis and endocarditis among others,[22] but it has also been reported that 5-nitroimidazole derivatives may be potent cytotoxic drugs. For this reason, our goal is to make them efficient molecular switches in order to control their cytotoxicity by light.

[22] Ingham, H. R.; Selkon, J. B.; Hale, J. H., The antibacterial activity of metronidazole *J. Antimicrob. Chemother.* **1975,** *1*, 355-361.

1. Design of new photoswitches based on metronidazole moiety.

With the aim of preparing new and efficient candidates to photocontrol their structure and activity based on the metronidazole ring, the inclusion of a photoisomerizable C=C double bond in its structure should be performed. It was selected as responsible for the photoisomerization process due to its good properties shown in other molecular switches.[23, 24] So, the essential part of our novel design is the addition of a C=C double bond into the chromophore (Figure 6.4).

Moreover, in Figure 6.4 it is shown that the most convenient part of the molecule to include the C=C double bond capable of photoisomerizing is the methyl group (Figure 6.4). This approach would provide a facile and versatile synthesis to afford a series of different metronidazole-based molecular switches. It would give us a whole range of possibilities to modify the structure, since different groups with different electronic properties could be conjugated with the central C=C double bond. In this way, depending on the group introduced in the structure, the photochemical and photophysical properties could be totally different. This would allow the absorption wavelength to be tuned, which is very relevant because these derivatives must absorb in the visible region to be applied in biological applications.[25]

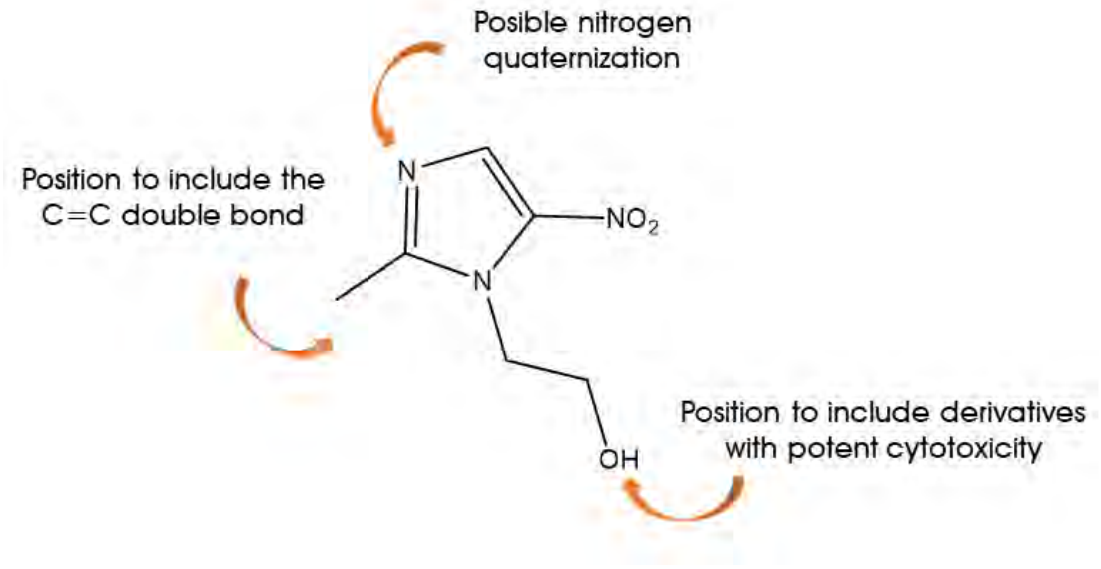

Figure 6.4. Design of new molecular switches signalling its possible modification points.

[23] Martínez-López, D.; Yu, M.-L.; García-Iriepa, C.; Campos, P. J.; Frutos, L. M.; Golen, J. A.; Rasapalli, S.; Sampedro, D., Hydantoin-Based Molecular Photoswitches *J. Org. Chem.* **2015,** *80*, 3929-3939.
[24] Gozem, S.; Luk, H.; Schapiro, I.; Olivucci, M., Theory and Simulation of the Ultrafast Double-Bond Isomerization of Biological Chromophores *Chem. Rev.* **2017,** *117*.
[25] Dong, M.; Babalhavaeji, A.; Samanta, S.; Beharry, A. A.; Woolley, G. A., Red-Shifting Azobenzene Photoswitches for in Vivo Use *Acc. Chem. Res.* **2015,** *48*, 2662-2670.

In the Figure above, it is shown that an iminic nitrogen could be quaternized to change the chromophore features; this strategy was followed in Chapter 5 in PSB-retinal like photoswitches. Beyond the control of the possible photochemical properties, after quaternization, the resulting derivatives would be more water soluble. This is a compulsory requirement in biological applications.[26] Both neutral and quaternized derivatives were synthesized and their photochemical properties will be compared and discussed in the following sections.

In Figure 6.4, it is also shown where these derivatives can be derivatized. In detail, the hydroxyl group could be derivatized easily to get a compound with higher cytotoxic properties. 1,4-benzodioxane was chosen to be included in that position due to its reported influence in the cytotoxic activity in related derivatives described previously.[27]

In short, the design includes two different parts in the structure for the proposed compounds. On the one hand, the conjugated moiety (blue box in Figure 6.5) is responsible for the photochemical properties and structural photocontrol. On the other hand, the cytotoxic activity is mainly located in the imidazole ring and its substituents (red box in Figure 6.5). Ideally, these two parts should be orthogonal, thus, the photochemical properties and the cytotoxicity should be tuned independently. However, as the imidazole ring affects both types of properties, some influence between the two parts is expected.

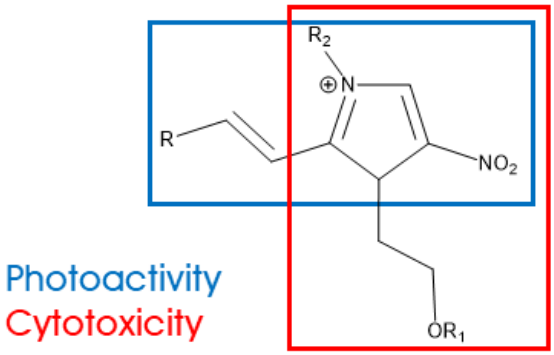

Figure 6.5. General structure of metronidazole-based photoswitches.

[26] Beharry, A. A.; Woolley, G. A., Azobenzene photoswitches for biomolecules *Chem. Soc. Rev.* **2011,** *40*, 4422-4437.

[27] Sang, Y.-L.; Duan, Y.-T.; Qiu, H.-Y.; Wang, P.-F.; Makawana, J. A.; Wang, Z.-C.; Zhu, H.-L.; He, Z.-X., Design, synthesis, biological evaluation and molecular docking of novel metronidazole derivatives as selective and potent JAK3 inhibitors *RSC Advances* **2014,** *4*, 16694-16704.

2. Synthesis of metronidazole-like photoswitches.

The preparation of new photoswitches based on metronidazole was afforded by condensation of metronidazole and different aldehydes (Scheme 6.1). Several aldehydes with different electronic properties were chosen to study their photochemical behaviour depending on the aldehyde used, as in other cases. This one-step synthesis allowed the preparation of neutral derivatives **20-23** in high yields (80 - 90%).[28] Furthermore, the purification of these derivatives was extremely easy, since after 4 hours of stirring at room temperature, 20 ml of water was added to the reaction mixture precipitating the pure compound (**20-23**). Therefore, all neutral compounds were isolated by filtration.

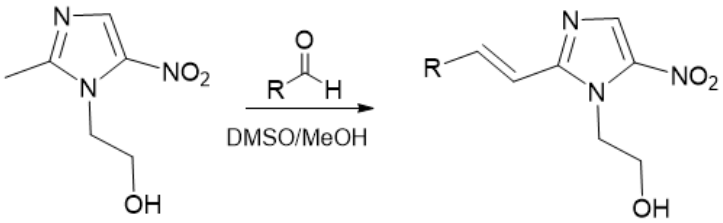

20 - 23

R= Ph (**20**), 2-naphtyl (**21**), *p*-NO_2Ph (**22**), *p*-MeOPh (**23**).

Scheme 6.1. General synthesis of neutral derivatives.

As aforementioned, the synthesis of different aldehydes was afforded to tune the absorption wavelength among other photochemical properties. For instance, **21** was synthesized to analyse the effect of increasing the conjugation adding an extra phenyl ring. Moreover, **22** and **23** were prepared to analyse the effect on the absorption wavelength and PSS of the introduction of an electron-withdrawing or electron-donating group in this new family of molecular switches, respectively.

It is confirmed that in an easy and rapid way these derivatives could be achieved. Once **20-23** were synthesized, preliminary experiments on their solubility in water were carried out. These experiments revealed that all neutral compounds (**20-23**) showed poor solubility in such solvent.

To resolve this hindrance and to allow the use of these derivatives in a biological application, quaternization of the nitrogen atom present in the iminic bond was addressed. In this way, in case of **20** three different compounds were achieved (*i.e.* protonation, methylation and acetylation) to afford **20a**, **20b** and **20c** (Scheme 6.2).

[28] Duan, Y.-T.; Sang, Y.-L.; Makawana, J. A.; Teraiya, S. B.; Yao, Y.-F.; Tang, D.-J.; Tao, X.-X.; Zhu, H.-L., Discovery and molecular modeling of novel 1-indolyl acetate – 5-Nitroimidazole targeting tubulin polymerization as antiproliferative agents *Eur. J. Med. Chem.* **2014,** *85*, 341-351.

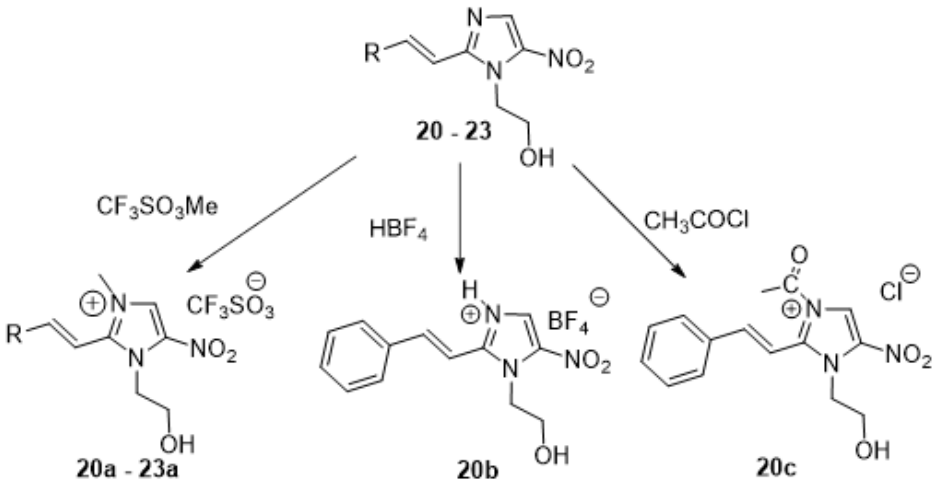

Scheme 6.2. General synthesis to afford *N*-quaternized derivatives.

As can be observed in Scheme 6.2, a simple quaternization of the nitrogen atom in the iminic moiety, either by using methyl triflate (**20a-23a**), tetrafluoroboric acid (**20b**) or acetyl chloride (**20c**) was carried out. Finally, the resulting compounds after quaternization were quite soluble in water, so the first goal was achieved.

The preparation of all compounds contributes to show a relevant generalization in the chemical structure, but in the case of protonated and methylated derivatives, their photochemical properties remained almost unaltered, as will be shown in the following sections.

Considering the photochemical properties (see section 3) and their use in biological media, the methylated analogues were chosen for further cytotoxic evaluation since protonation would be affected by the pH of the medium.

Therefore, the synthesis of a new derivative with a supposed improved cytotoxic activity was afforded. For that purpose, **22** was chosen as a pattern to introduce the 1,4-benzodioxane in the hydroxyl position (Scheme 6.3).[29, 30]

[29] Hou, Y.-P.; Sun, J.; Pang, Z.-H.; Lv, P.-C.; Li, D.-D.; Yan, L.; Zhang, H.-J.; Zheng, E. X.; Zhao, J.; Zhu, H.-L., Synthesis and antitumor activity of 1,2,4-triazoles having 1,4-benzodioxan fragment as a novel class of potent methionine aminopeptidase type II inhibitors *Bioorg. Med. Chem.* **2011,** *19*, 5948-5954.
[30] See ref. 27.

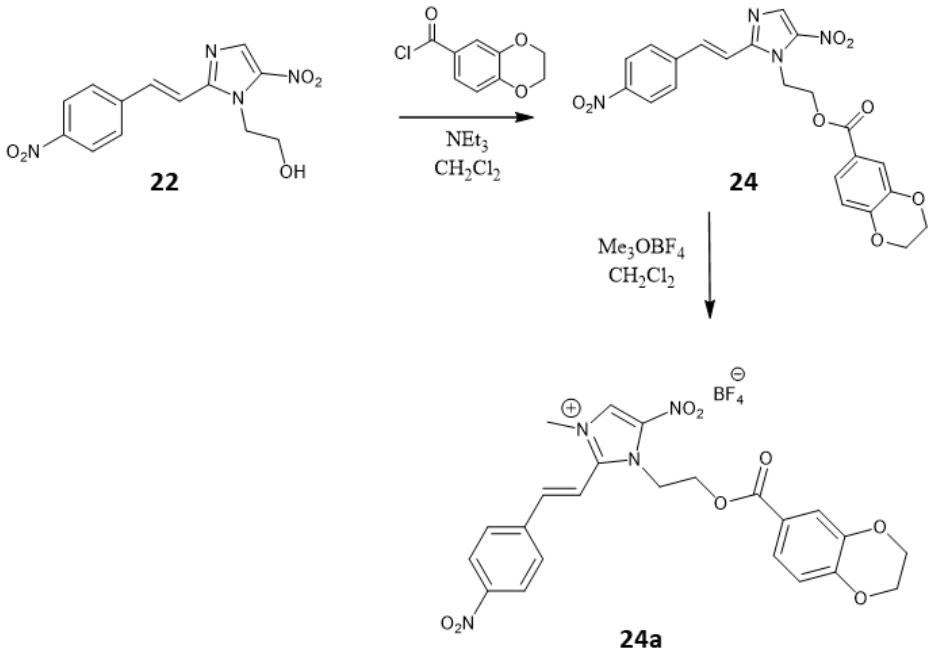

Scheme 6.3. Synthetic route of **24a**.

As can be observed in Scheme 6.3, to afford **24a**, a different methylating agent was used instead of methyl triflate, since using this reagent the reaction did not occur and some decomposition was observed by TLC. This way, **24a** was synthesized easily with 1.2 equivalents of trimethyloxonium tetrafluoroborate. The reaction was carried out overnight at room temperature.

It should be noted that only the *E*-isomer was found in the reaction mixture. This fact was confirmed by X-ray data (Figure 6.6).

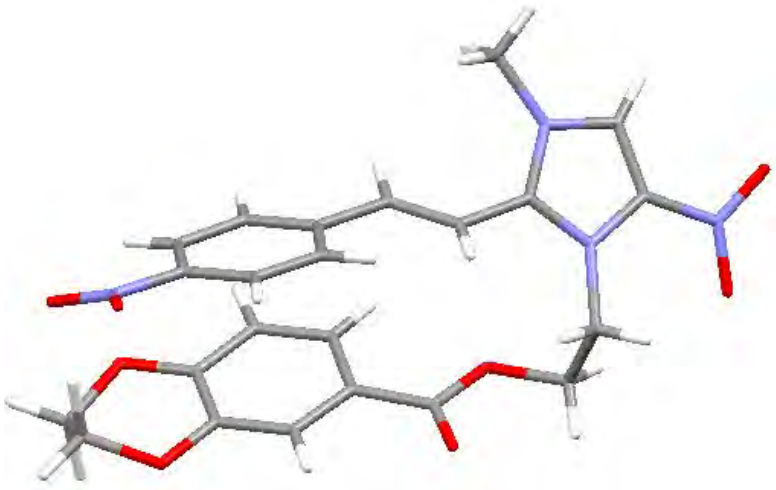

Figure 6.6. X-Ray structure of ***E*-24a**.

3. Photochemical and photophysical studies.

In these sections, efforts will be mainly focused on the study of the absorption wavelength and PSS, depending on the modifications carried out in the molecule. Moreover, their behaviour will be rationalized by some computational studies.

3.1 Absorption wavelength.

Firstly, the effect of the quaternization of the nitrogen atom in the iminic bond was evaluated. For that purpose the neutral derivative **20** was compared with its analogues **20a**, **20b** and **20c**. Therefore, 5E-5 M solutions of each compound were prepared in methanol. All solutions were measured in a quartz cuvette with a path length of 1 cm (Figure 6.7 and Table 6.1).

Compound	R	R_1	R_2	UV max (nm)	ε ($M^{-1}cm^{-1}$)
20	Ph	OH	-	375	21400
20a	Ph	OH	Me	320	13700
20b	Ph	OH	H	320	22300
20c	Ph	OH	COMe	375	20840
21	2-Naphtyl	OH	-	380	22600
21a	2-Naphtyl	OH	Me	330	7700
22	*p*-NO_2Ph	OH	-	380	22600
22a	*p*-NO_2Ph	OH	Me	320	17800
23	*p*-MeOPh	OH	-	390	31500
23a	*p*-MeOPh	OH	Me	360	11900
24	*p*-NO_2Ph	BzDO	-	375	17200
24a	*p*-NO_2Ph	BzDO	Me	330	18100

Table 6.1. Photophysical properties of **20 - 24** in MeOH.

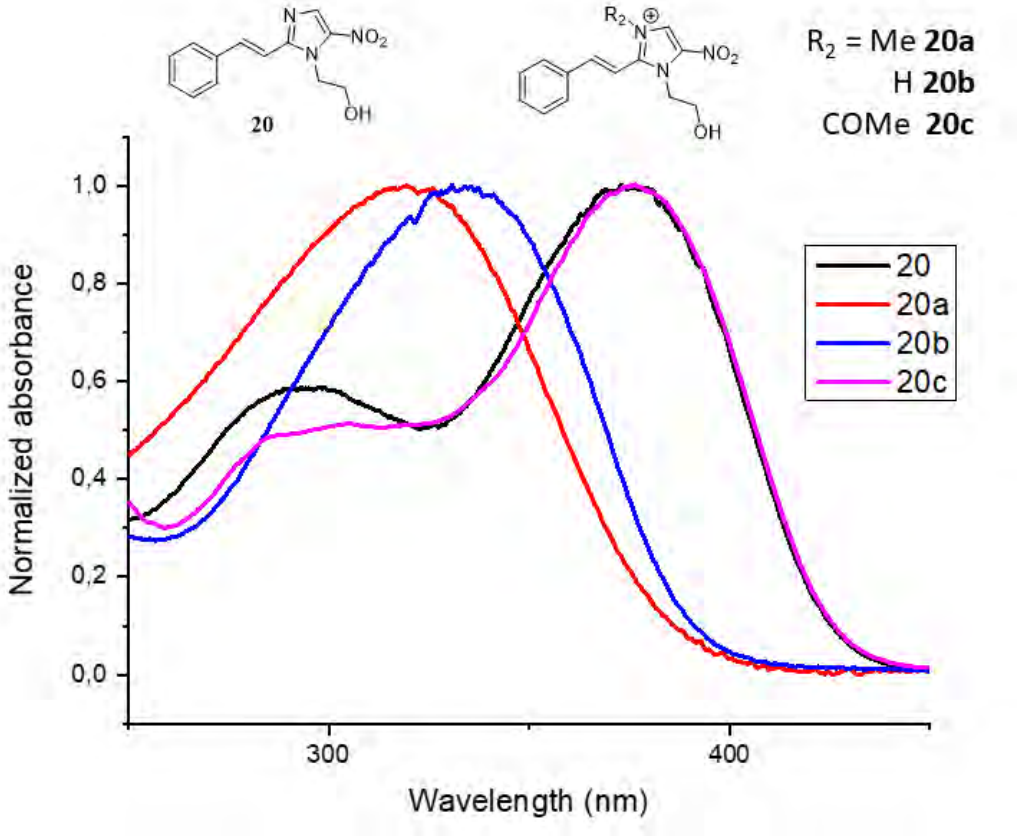

Figure 6.7. UV-Vis spectra of *N*-quaternized analogues of **20**.

As can be seen above, it was possible to tune the absorption spectrum by changing the group leading to *N*-quaternized derivatives based on metronidazole. It should be noted that methylated (**20a**) and protonated (**20b**) analogues showed a blue-shift absorption wavelength comparing them with the neutral one (**20**). Interestingly, when the chromophore was acetylated (**20c**), its UV-Vis spectrum remained unaltered. Hence, it has been demonstrated that the absorption spectrum could be tuned easily just quaternizating the chromophore with different groups. This effect will be rationalised by a computational study in the next section to get a better understanding of this phenomena.

The effect of *N*-quaternization on the photophysical properties was compared. The introduction of different substituents with different electronic properties in the chromophore will be evaluated maintaining the nitrogen of the iminic bond methylated. Therefore, electron withdrawing (**22a**) or electron donating groups (**23a**) were included in the aromatic ring to red-shift the absorption wavelength (Figure 6.8 and Table 6.1). This bathochromic shift could also be achieved by increasing the aromaticity of the system, and for that purpose a naphthyl moiety (**21a**) was introduced instead of the phenyl ring (Figure 6.8 and Table 6.1).

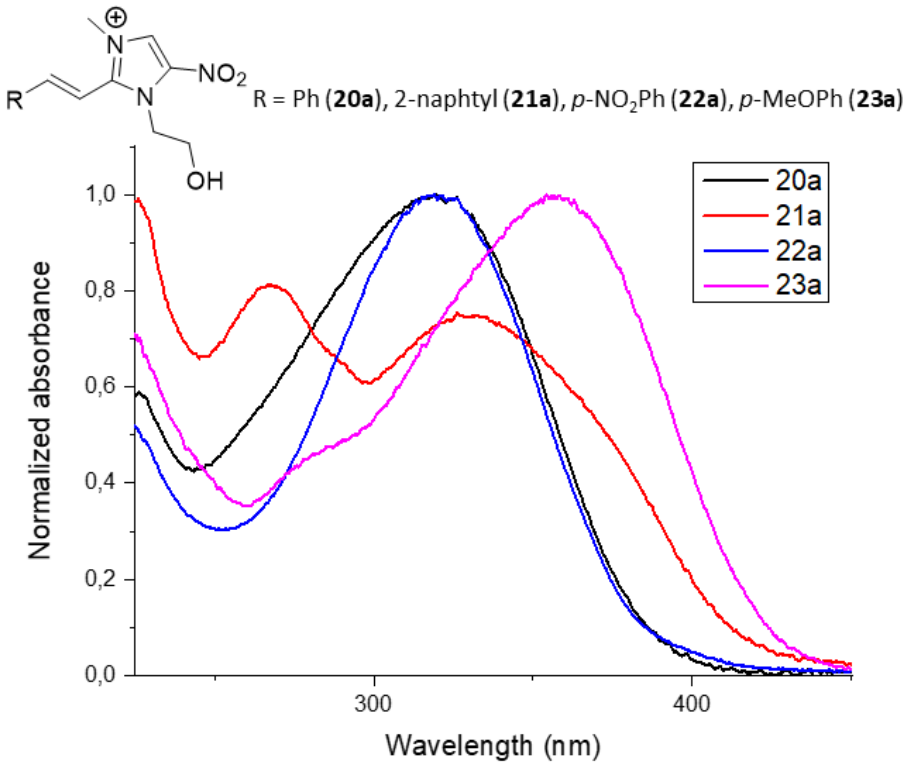

Figure 6.8. UV-Vis spectra of **20a**, **21a**, **22a** and **23a**.

It is shown in Figure 6.8 that a clear effect on the UV-Vis spectrum occurred when introducing releasing groups (**23a**). A slight red-shift *ca.* 10 nm was observed when a naphthyl ring was introduced in the chromophore (**21a**). It should be remarked that although the absorption maxima of **21a** and **22a** were in the UV region, they could also be activated by visible light due to the presence of a tail extended into this spectral range.

Regarding data shown in Table 6.1, all methylated analogues suffered a blue-shift of *ca.* 40 nm of its absorption wavelength. Finally, the UV-Vis spectrum of **24a** will be analysed and compared with its related analogue **22a**. In this case, they should share the absorption band since the chromophore is the same (Figure 6.9).

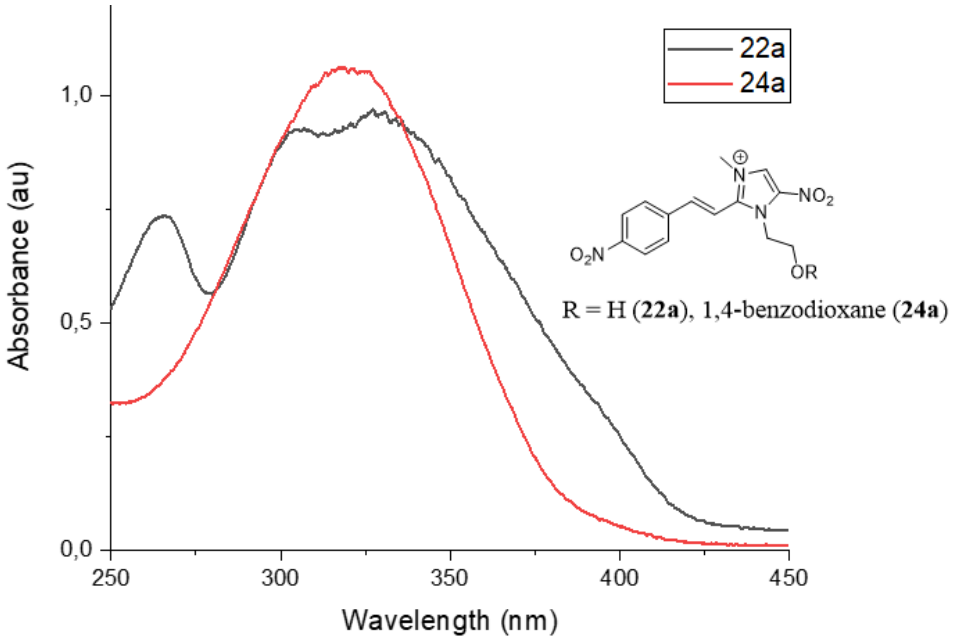

Figure 6.9. UV-Vis spectra of **22a** and **24a**.

As was expected, Figure 6.9 shows that both compounds share the same absorption band as aforementioned.

3.1.1. Computational calculations.

To get a better understanding of the behaviour seen in the photophysical properties of these derivatives, some theoretical calculations were carried out.

For this purpose, the photophysical properties of **24** and **24a** were computed to analyse the hypsochromic shift observed in their UV-Vis spectra when the nitrogen atom in the iminic bond was methylated (this shift was seen in all derivatives). It should be considered that **24** and its analogue **24a** could present several conformers due to the position of the benzodioxane substituent of the five-membered ring. Therefore, a conformational study at the DFT level was performed considering three sets of conformers depending on the benzodioxane-6-carboxilate orientation (Figure 6.10A), those formed by rotation of the carboxyl group (Figure 6.10B) or of the benzodioxane group (Figure 6.10C).

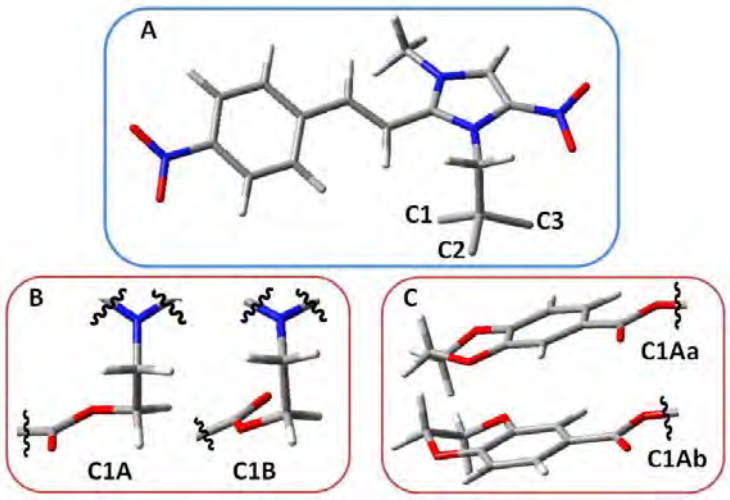

Figure 6.10. Schematic-representation of the possible conformers for **24a**.

All conformers were optimized at CAM-B3LYP/6-31+g(d,p) level of theory[31] and their population at 298K calculated by performing a Boltzmann distribution. It should be noted in all calculations carried out in this chapter that the solvent (methanol) was considered by means of PCM because the solvent could stabilize the charge of the chromophore.[32] The calculations were carried out for the *E*-isomer of **24** and **24a**.

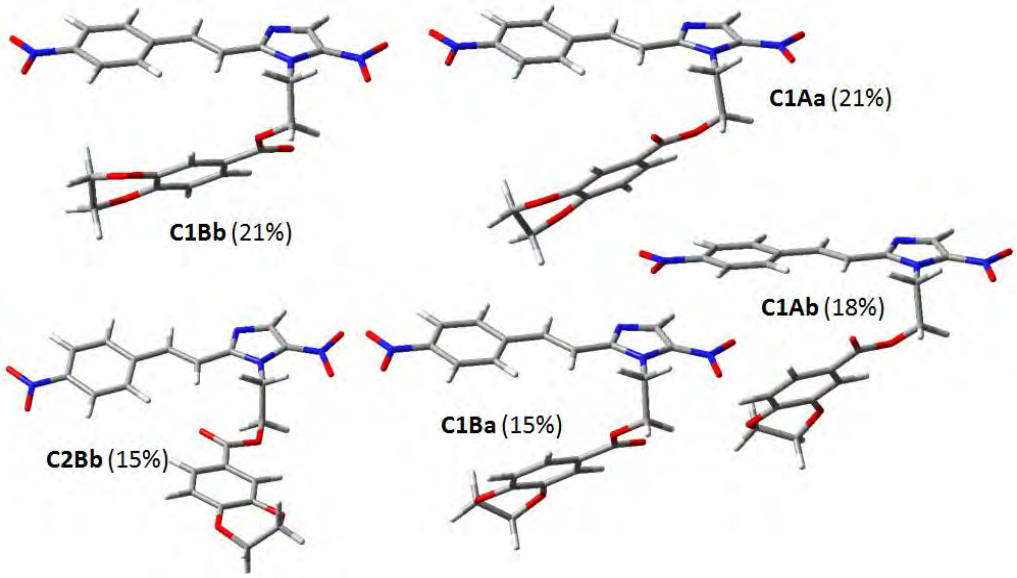

Figure 6.11. Structure and population of the most thermally stable conformers of ***E*-24** at 298K.

[31] Yanai, T.; Tew, D. P.; Handy, N. C., A new hybrid exchange–correlation functional using the Coulomb-attenuating method (CAM-B3LYP) *Chem. Phys. Lett.* **2004,** *393*, 51-57.
[32] Tomasi, J.; Mennucci, B.; Cammi, R., Quantum Mechanical Continuum Solvation Models *Chem. Rev.* **2005,** *105*, 2999-3094.

In Figure 6.11, it is shown that five conformers of ***E*-24** represented 90% of the population at 298K.

The same calculation was performed for compound ***E*-24a** maintaining the level of theory (Figure 6.12). Then, the most stable conformers of the neutral derivative (***E*-24**) and its *N*-methylated analogue were compared.

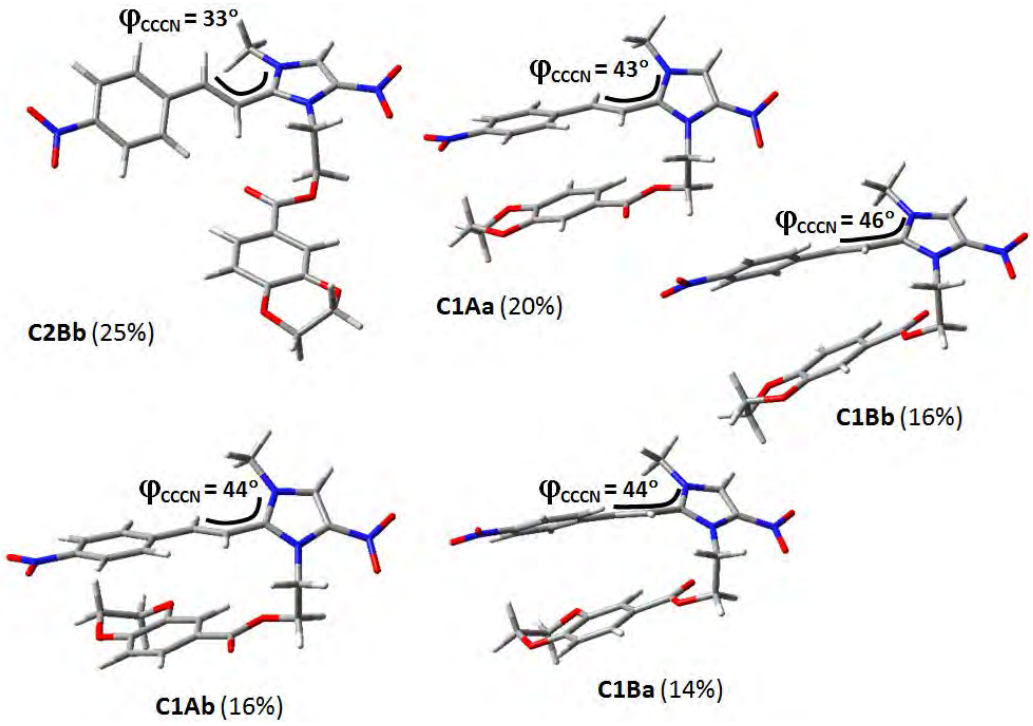

Figure 6.12. Structure and population of the most thermally stable conformers of ***E*-24a** at 298K.

In Figure 6.12, as in the previous case, it can be concluded that for **24a** five conformers represent 90% of the population at 298K. In fact, four conformers of ***E*-24** and ***E*-24a** were C1 type probably due to a π-π stacking between the benzodioxane moiety and the phenyl ring. Comparing these findings with the X-Ray structure obtained for **24a** (Figure 6.6), it can be seen that it corresponds to the second most stable conformer in solution for ***E*-24a**. This is reasonable since in solid state ***E*-24a** could crystalize in its more packed structure.

Regarding the most stable conformers for ***E*-24** and ***E*-24a** and comparing their structures (Figure 6.13), the reason why the absorption spectrum was blue shifted when ***E*-24** was methylated can be analysed.

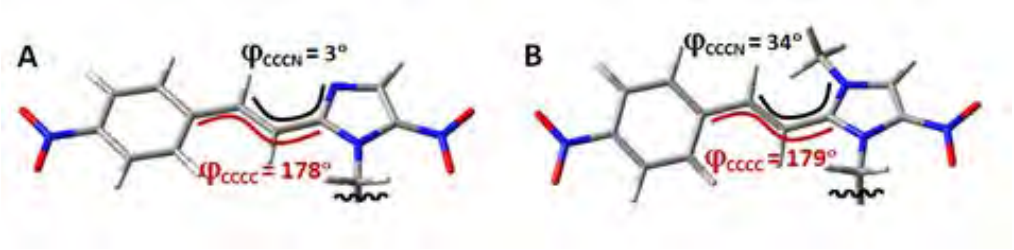

Figure 6.13. Geometries of the most thermally stable conformers of ***E*-24** (A) and ***E*-24a** (B).

As can be seen in Figure 6.13, the most stable conformer of ***E*-24** and ***E*-24a** present different structures, indeed also different energies. Whereas the metronidazole moiety of compound ***E*-24** was almost totally coplanar with the central C=C double bond and the phenyl ring maintaining the whole conjugation, in ***E*-24a** the conjugation was partially broken due to the rotation of the imidazole ring to release the steric hindrance between the methyl group and the vinylic hydrogen. This fact directly affected the absorption wavelength, blue-shifting it.

Moreover, the computed vertical transitions were calculated finding that in both cases the first-singlet state (S_1) was optically the bright state which corresponds to a π-π^* transition with the electron density mainly located in the photoisomerizable double bond.

The simulated spectra of ***E*-24** and ***E*-24a** were compared with the experimental spectra to analyse their relation (Figure 6.14). As can be seen the computed and the experimental data in each case agreed.

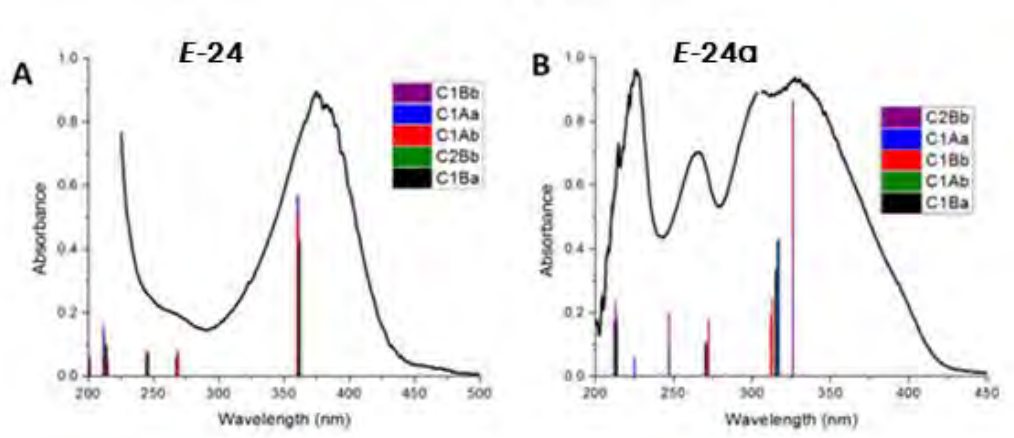

Figure 6.14. Computed vertical electronic transitions of the most stable conformers of ***E*-24** and ***E*-24a.**

As seen in Figure 6.14, the UV-Vis spectra of both compounds were computed agreeably with the experimental data, since the absorption maximum was well reproduced, as well as the hypsochromic shift experimented by ***E*-24a**.

Furthermore, the different effect on the absorption wavelength of the acetilated analogues was computed. To this end, geometries of **20a** and **20c** were optimized in their ground state at the DFT level of theory (CAM-B3LYP/6-31+g(d,p)). Then, the vertical transitions were computed at TD-DFT level using the same functional and basis set as before. The electronic nature of the excited states of **20a** and **20c** were analysed and they were compared (Figure 6.15).

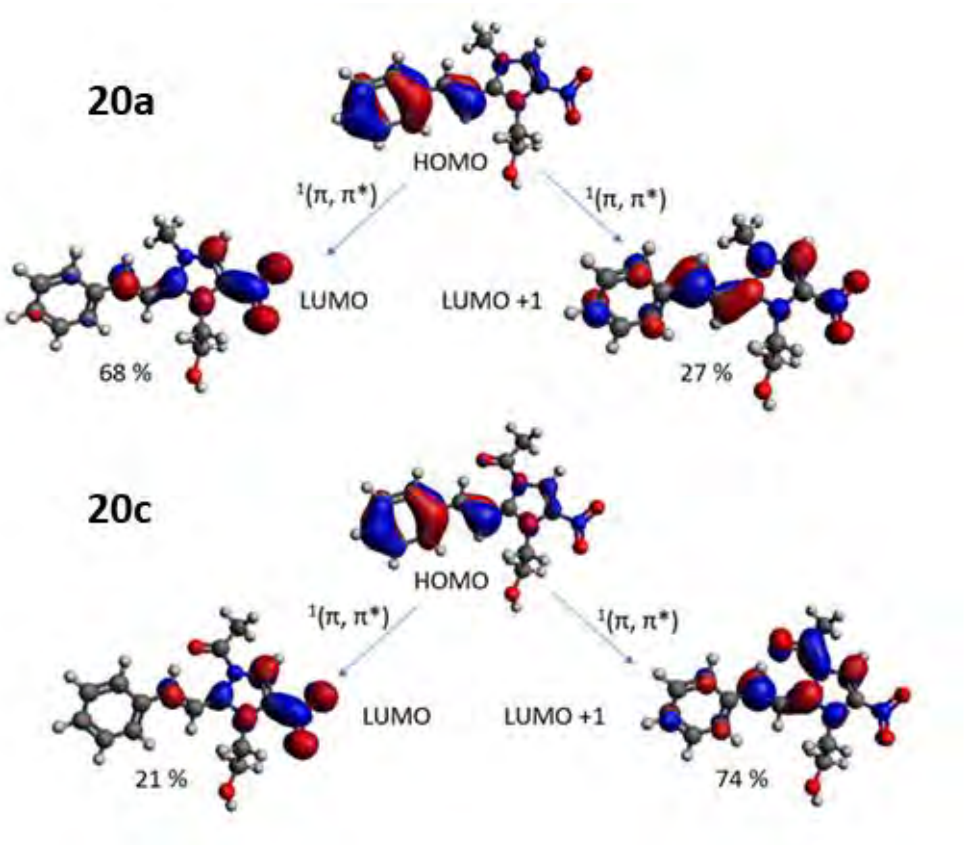

Figure 6.15. Electronic nature of the absorption transition for **20a** and **20c**.

The optically bright state for **20a** is described in Figure 6.15, it is formed by a mixture of two monoelectronic π-π* transitions corresponding to a 68% HOMO $\rightarrow$ LUMO and 27% HOMO $\rightarrow$ LUMO +1. In its place, for **20c** the weights of these transitions were interconverted (21% HOMO $\rightarrow$ LUMO and 74% HOMO $\rightarrow$ LUMO+1). In addition, it was observed that the molecular orbitals involved in these transitions were very similar. Nevertheless, the LUMO+1 was slightly different since in **20a** the electron density was focused on the backbone, whereas in compound **20c** it was located in the acceptor acetyl group. This could explain the red-shift observed in **20c** since the acetyl group

stabilized the electron density in the excited state thanks to its acceptor ability, which allowed delocalizing the electron density into this part of the molecule.

3.2. Irradiation of molecular switches based on metronidazole.

Once a deep photophysical study of all compounds has been performed, it is known which kind of electromagnetic radiation interacts with the derivatives synthesized. Then, the adequate irradiation can be proposed for each compound using the appropriate source of light.

Firstly, the behaviour of neutral derivatives (**20-23**) towards irradiation was evaluated. To this end, 0.1 M solutions of each compound were dissolved in MeOD. These solutions were irradiated using a 125-W medium-pressure Hg lamp since it emits radiation from the high energetic UV to far-visible light. As in irradiations of other photoswitches in previous chapters, a Pyrex filter was used to avoid high energetic light of wavelength below 290 nm. The irradiation process was followed by ^{1}H NMR as in other cases. The results obtained are shown in Table 6.2.

Compound	R	R_1	R_2	PSS	
				E-isomer	Z-isomer
20	Ph	OH	-	-	-
20a	Ph	OH	Me	12	88
20b	Ph	OH	H	20	80
20c	Ph	OH	COMe	63	37
21	2-Naphtyl	OH	-	-	-
21a	2-Naphtyl	OH	Me	37	63
22	*p*-NO_2Ph	OH	-	-	-
22a	*p*-NO_2Ph	OH	Me	12	88
23	*p*-OMePh	OH	-	-	-
23a	*p*-OMePh	OH	Me	87	13
24	*p*-NO_2Ph	BzDO	-	-	-
24a	*p*-NO_2Ph	BzDO	Me	12	88

Table 6.2. Photochemical properties in MeOD of **20-24**.

As is observed in Table 6.2, no photoisomerization was found in any neutral compound (**20-24**). Furthermore, after 15 minutes of irradiation the solution completely changed its colour and the ^{1}H NMR spectrum revealed that all neutral derivatives were totally decomposed under the irradiation conditions detailed above.

It has been reported before that metronidazole is not stable under exposure to light,[33] this might be the reason why the neutral metronidazole derivatives were not stable, and photodecomposition occurred. This finding will be studied in the next section by some computational calculations.

On the contrary, when the same irradiation conditions were used to perform the irradiation of *N*-quaternized derivatives, the photoisomerization took place easily. These switches were irradiated for more than three hours and no decomposition was found, demonstrating its high photostability.

As can be seen in Table 6.2, after irradiation each *N*-quaternized photoswitch in MeOD for 15-20 minutes led to different isomer mixtures after reaching each PSS. It is highly dependent on the substitution made in the molecule, achieving in each case different PSS. It should be noted that in **22a** and **24a**, the same isomer mixture was found in the PSS because they share the chromophore, being responsible for the photochemical properties. Moreover, **20a** and **22a** mainly yielded the *Z*-photoisomer, but in the case of **23a** the initial isomer was the main compound after irradiation.

Especially relevant is the case of **24a**, which containing the 1,4-benzodioxane moiety which has been reported to have potential capabilities of producing anticancer activity. Hence, its properties will be studied widely. This photoswitch reached a PSS enriched in the photoisomer (Figure 6.16), which makes it convenient to test the different biological activity of each isomer. From the solution of **PSS-24a**, it was possible to isolate a monocrystal of the photoisomer, thus we obtained its X-Ray structure (Figure 6.16).

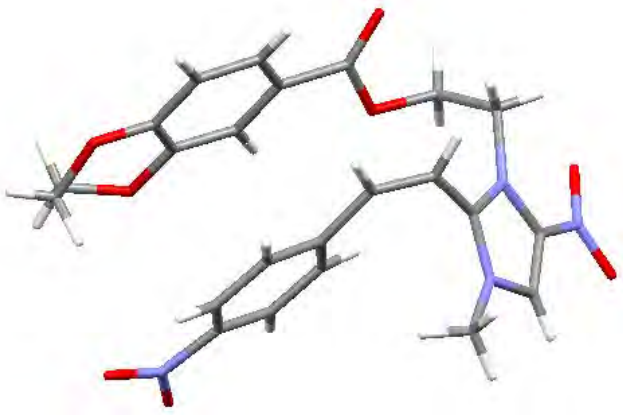

Figure 6.16. X-Ray structure of ***Z*-24a**.

To rationalize the PSS of **24a**, the UV-Vis spectrum of ***E*-24a** and its PSS was measured. For that purpose, a 5E-5 M solution of ***E*-24a** in MeOH was irradiated in a quartz

[33] A/Karim, E. I.; Ibrahim, K. E.; Adam, M. E., Studies on the photochemical decomposition of metronidazole *Int. J. Pharm.* **1991,** *76*, 261-264.

cuvette using a 125-W medium-pressure Hg lamp. In this irradiation a Pyrex filter was used to avoid harmful light. The irradiation was accomplished for 15 minutes, then the UV-Vis spectrum of the PSS mixture was measured (Figure 6.17).

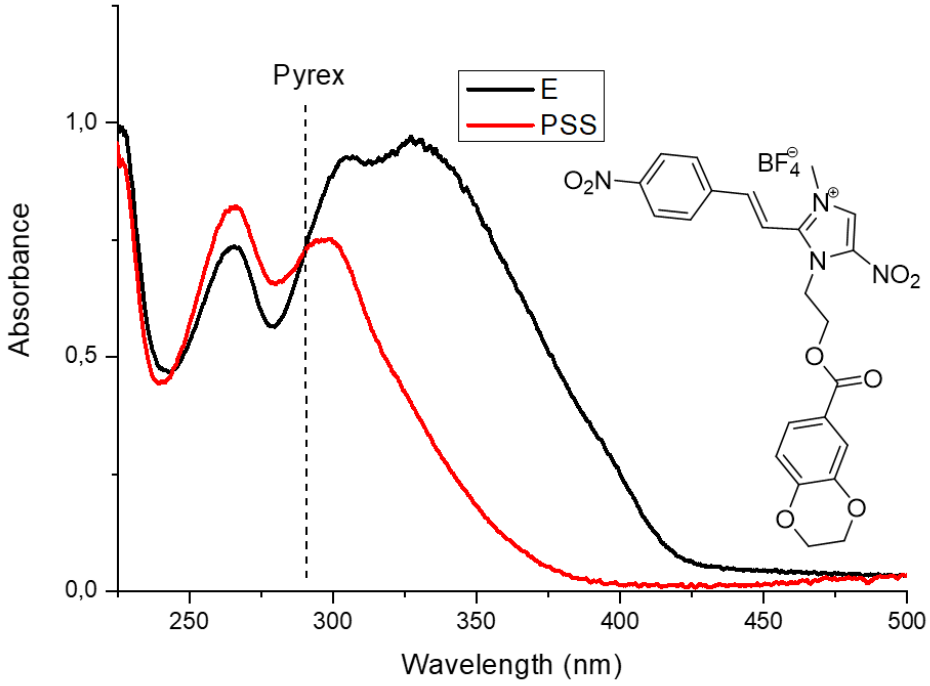

Figure 6.17. UV-Vis spectra of ***E*-24a** and its PSS.

As can be seen above, the absorption spectrum of ***Z*-24a** was clearly blue shifted. Therefore, in the irradiation conditions detailed above, the *E*-isomer absorbed preferably the emitted light, so the isomerization process favoured was from *E* to *Z*-isomer.

***E*-24a** presents absorption in the visible range due to the presence of an extended band. It is necessary to use this photoswitch in a biological application.

As ***E*-24a** absorbs visible light, the photoswitching process was studied using this kind of light. For this purpose, a 5E-5 M solution of ***E*-24a** in MeOH was irradiated using monochromatic light centered at 400 nm (Figure 6.18). The process was followed by CG-MS since the solution was very diluted and it prevented the use of ^{1}H NMR.

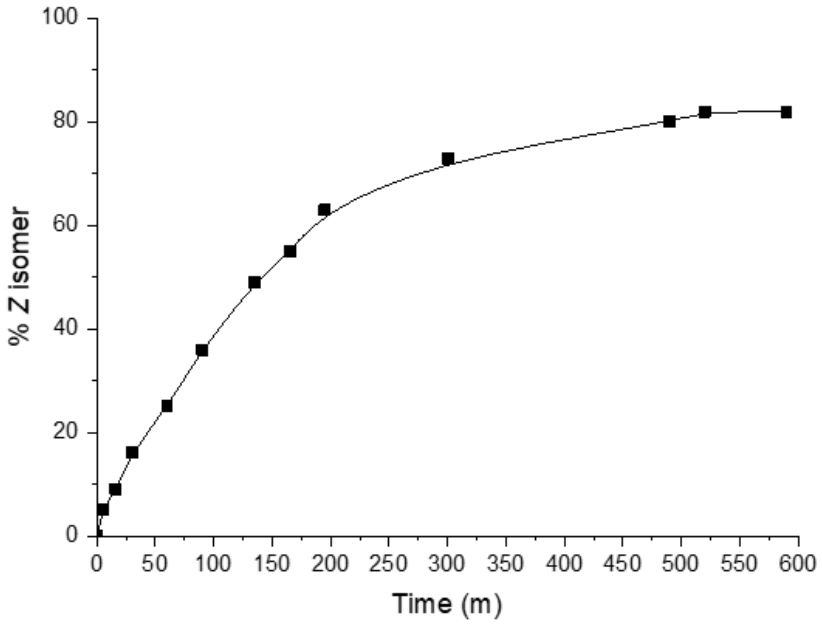

Figure 6.18. Isomerization of **24a** irradiating at 400 nm.

As seen above, the irradiation procedure took 10 hours to reach the PSS under the irradiation conditions detailed before. Moreover using 400 nm as excitation wavelength, the PSS was enriched in the photoisomer obtaining 80% of *Z*-isomer. This fact proved that it was possible to perform the isomerization of ***E*-24a** using visible light, which is compatible with biological media.

Besides, it should be remembered that the *N*-quaternized derivative was quite soluble in water, so this requirement was also fulfilled by ***E*-24a** to be applied in a biological system.

Therefore, by quaternization the nitrogen atom of the iminic bond, it was achieved a relevant generalization of this family of photoswitches, including an increase in water solubility and the modulation of the absorption wavelength allowing the use of visible light, properties that make them altogether more compatible with biological applications

3.2.1. Computational calculations.

Several aspects will be studied in this section. Firstly, it will be rationalized as to why neutral compounds were not stable under exposure to UV light and photoisomerization did not take place. In contrast, *N*-quaternized metronidazole derivatives showed an easy photoisomerization reaching different PSSs.

To get insight into this issue, it was decided to compute a neutral derivative (***E*-24**) and its analogue (***E*-24a**), since this derivative could present potent cytotoxic activity due to the presence of 1,4-benzodioxane in its structure. Therefore, the photoisomerization

path on S_1 for both compounds was computed using TD-DFT and CAM-B3LYP/6-31+g(d,p) as level of theory.[34] For both compounds, after excitation to S_1 the system minimized the energy along the stretching coordinate reaching an almost planar minimum. From this minimum, a scan along the torsion coordinate (φ_{cccc}, see Figure 6.5) was performed, finding an energy barrier along this coordinate to reach a conical intersection (CI) with the ground state from where it can either complete the isomerization (*Z*-isomer) or revert to the *E*-isomer. Nevertheless, a main difference was found between the path computed for the neutral derivative and its methylated analogue (Figure 6.19).

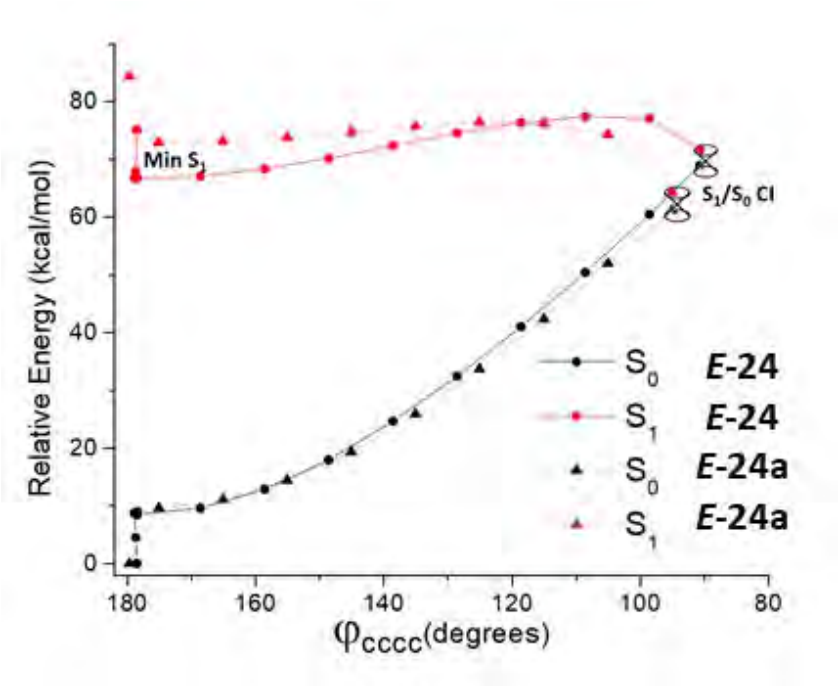

Figure 6.19. Computed photoisomerization path for **24** and ***E*-24a**.

As can be seen in the figure above, the energy barrier between the minimum and the TS in S_1 that ***E*-24** should overcome (*ca*. 10 kcal/mol) was significantly higher than the one computed for ***E*-24a** (*ca*. 3.5 kcal/mol). Besides, the energies of S_1 minimum and the CI for the neutral form are similar; consequently, isomerization will not be a favourable process. Therefore, while for ***E*-24a** the photoisomer could be reached easily, in the case of ***E*-24** this process was hampered and alternative pathways such as decomposition occurred.

Moreover, the change in the absorption spectrum of ***Z*-24a** was rationalized compared to its thermal isomer. Experimentally it was found a clear blue shift of the absorption wavelength. Performing the same calculations carried out for ***E*-24a** in section 3.1.1 a conformational analysis for ***Z*-24a** was performed (Figure 6.20).

[34] See ref. 31.

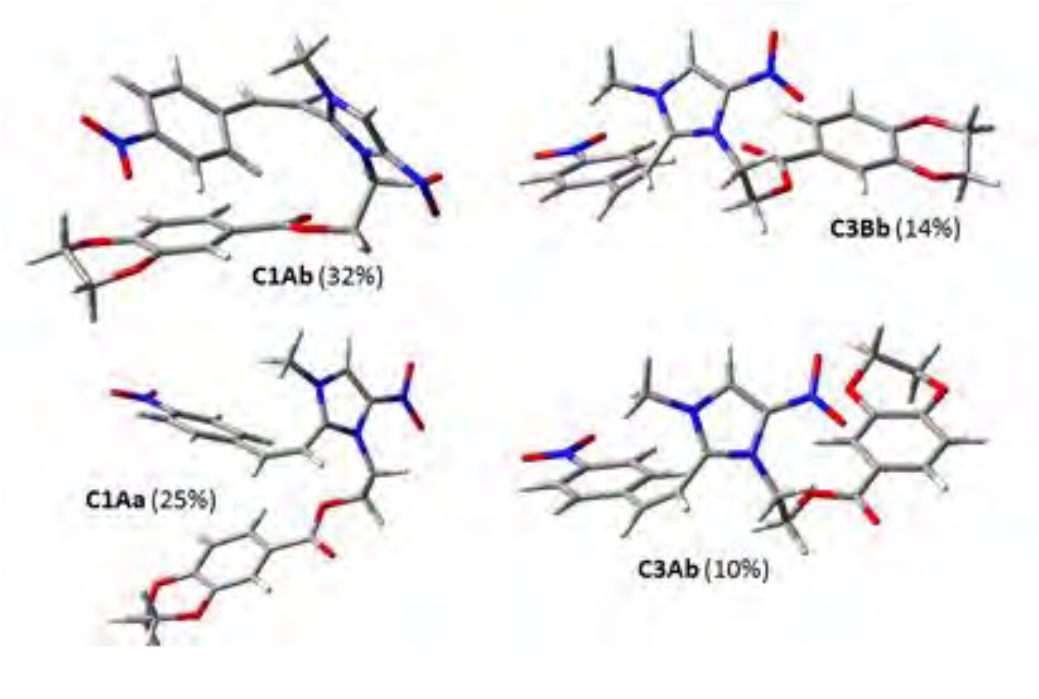

Figure 6.20. Structure and population of the most thermally stable conformers of ***Z*-24a** at 298K.

Figure 6.20 reveals that four conformers were the most stable ones by far. Specifically, the population of C1Ab is greater than the rest of conformers, due to it having the lowest energy. Interestingly, in this case the most stable conformational structure matched with the X-Ray structure showed in Figure 6.16.

Then, comparing the structures of the most thermally stable conformers of ***E*-24a** and ***Z*-24a** gives the reason for their photophysical behaviour (Figure 6.21).

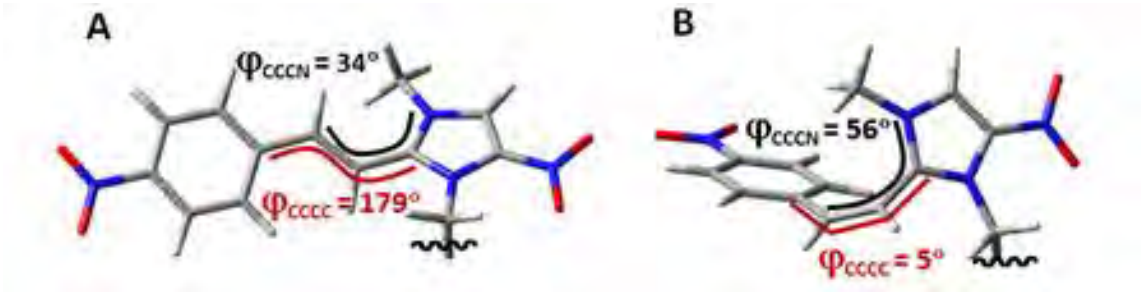

Figure 6.21. Electronic structure of the most thermally stable conformers of ***E*-24a** and ***Z*-24a**.

The structure of the *Z* isomer is more twisted: the photoisomerizable double bond pretwist is *ca.* 5 degrees and the five-membered ring is rotated 20 degrees more compared to the *E*-isomer (Figure 6.21). Thus, as it was expected the more planar geometry of the *E*-isomer presented a lower excitation energy, blue shifting the maximum absorption wavelength of the *Z* isomer.

Then, the computed spectrum of ***Z*-24a** was compared to the experimental one (Figure 6.22). As it can be observed, the UV-Vis spectrum is well predicted since the blue shift experimentally observed was found, as well as the absorbance band maxima.

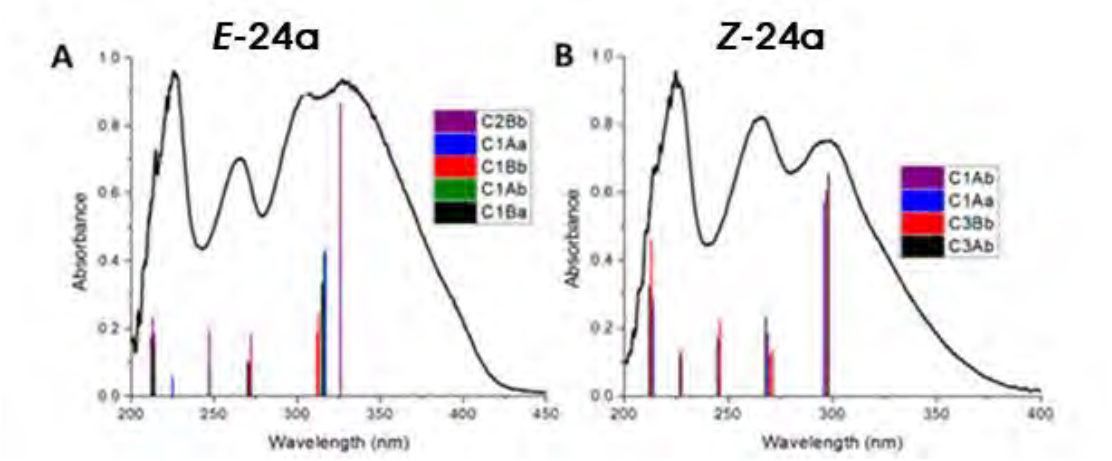

Figure 6.22. Computed vertical electronic transitions of the most stable conformers of ***E*-24a** and ***Z*-24a.**

3.2.2. Isomerization quantum yield of ***E*-24a**.

The isomerization quantum yield of ***E*-24a** was tested at 313 nm. The value obtained was 0.37 which implied a quite efficient process. It was calculated following the procedure described in the literature, using *trans*-stilbene as actinometer.[35] In order to determine the quantum yield of the compound, the *Z*-isomer percentage was plotted against the irradiation time for both, the actinometer and the sample. The slope of this function represented is proportional to the quantum yield (Equation 6.1):

$$\%\, photoproduct = \frac{\phi EpA}{MV}\, t \; ; m = \frac{\phi EpA}{MV}$$

Equation 6.1

Where Ep is the number of photons absorbed by the sample, A is the area of the cuvette, M is the concentration of the prepared solution and V is the volume of the solution placed in the cuvette.

[35] Ho, T.-I.; Su, T.-M.; Hwang, T.-C., A convenient method of measuring quantum yields of photoisomerization of trans-stilbene *J. Photochem. Photobiol. A Chem.* **1988,** *41*, 293-298.

The quantum yield could be calculated with the following equation 6.2, assuming that the area of the cuvette used for both, the actinometer and the sample experiments were the same:

$$\phi\text{sample} = \frac{msample\ Msample\ Vsample\ \phi\text{reference}}{mreference\ Mreference\ Vreference}$$

Equation 6.2

3.2.3. Thermal back reversion.

A mixture of isomers (*E* and *Z*) of each photoswitch (**20a-24a**) was prepared to check its thermal back reversion. For that purpose, each mixture of isomers was dissolved in MeOD in different NMR tubes. Each sample was heated in darkness to carry out the isomerization. Interestingly, the thermal reversion did not take place from the initial *E*-isomer at 37°C for 3 days for all the compounds; these conditions were the same as used in biological assays. This thermal stability allowed the preparation of the PSS and the evaluation of its cytotoxic activity for long periods of time without losing its activity. These results showed a clear improvement over azobenzenes reported before in which its photoisomer was not stable over time.[36]

When the temperature was increased to 60°C the thermal back reversion took place slowly for all compounds.

3.2.4. Stability of *E*-24a.

Before applying these molecular switches in a biological assay, their stability should be checked. To this end, the stability of ***E*-24a** was tested in a concentrated solution of glutathione (10 mM) which is a tripeptide present in animal cells. This peptide is able to reduce a double bond; for example, the N=N double bond in azobenzene derivatives is usually reduced efficiently. Therefore, a solution of ***E*-24a** with glutathione was prepared in water. The process was followed by UV-Vis spectroscopy (Figure 6.23).

[36] Engdahl, A. J.; Torres, E. A.; Lock, S. E.; Engdahl, T. B.; Mertz, P. S.; Streu, C. N., Synthesis, Characterization, and Bioactivity of the Photoisomerizable Tubulin Polymerization Inhibitor azo-Combretastatin A4 *Org. Lett.* **2015,** *17*, 4546-4549.

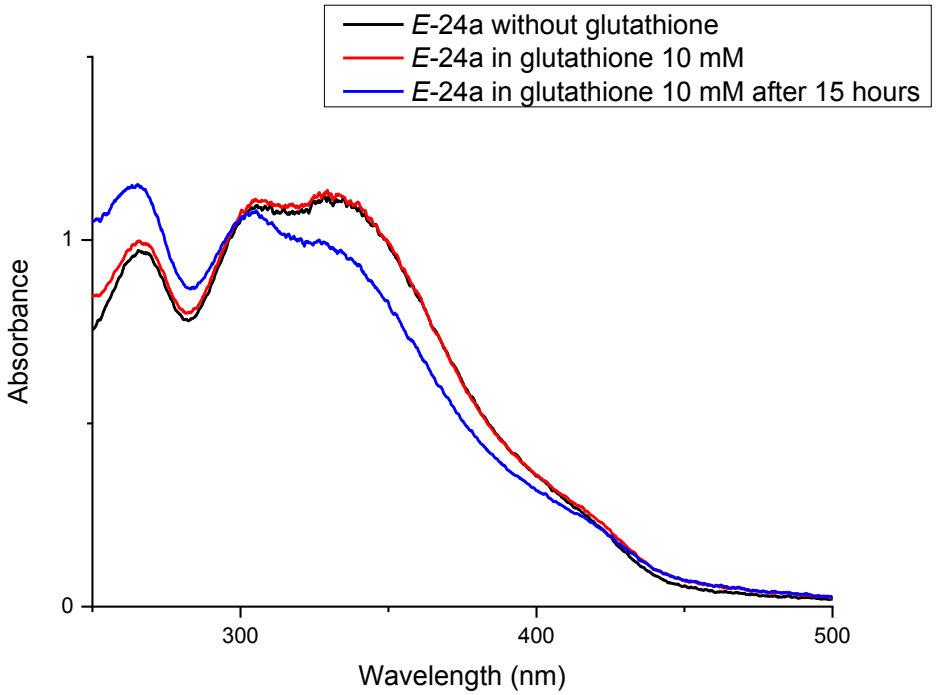

Figure 6.23. Stability of ***E*-24a** in glutathione (10 mmol).

After 15 hours in darkness, the effect of the glutathione in ***E*-24a** was checked. As can be seen in Figure 6.23, the effect that could have the degradation of ***E*-24a** by glutathione was negligible.

4. Biological study.

In view of the cytotoxic activity reported in metronidazole derivatives by He,[37] which showed cytotoxicities in the micromolar range, the anticancer activity of the photoswitches **20a**, **22a** and **24a** was tested. These photoswitches were chosen due to the almost quantitative photoconversion to the *Z*-isomer in the PSS; this way the different activity of *E* and *Z* isomers of each compound, measuring its PSS will be more noticeable.

The cytotoxic activity of these derivatives was tested by using a colorimetric assay called *MTS* (3-(4,5-dimethylthiazol-2-yl)-5-(3-carboxymethoxyphenyl)-2-(4-sulfophenyl)-2*H*-tetrazolium). The MTS assay is based on the transformation of tetrazolium salt into a coloured species by mitochondrial activity of living cells at 37ºC for 1 hour.[38] Finally, measuring the absorbance at 490 nm, it is known which cell viability it is after the exposure upon a chemical. By using this methodology, the half maximal inhibitory concentration (IC_{50}) of each compound will be obtained. This value points out the concentration needed to inhibit a specific biological process, in this case the cell viability.

Then in vitro anticancer activities of **20a**, **22a** and **24a** were checked towards human cancer cell lines A549 (adenocarcinomic alveolar basal ephitelial cells) and HeLa (epithelioid cervix carcinoma cells), by means of a cell viability assay (Table 6.3).

[37] See ref. 27.

[38] Malich, G.; Markovic, B.; Winder, C., The sensitivity and specificity of the MTS tetrazolium assay for detecting the in vitro cytotoxicity of 20 chemicals using human cell lines *Toxicology* **1997,** *124*, 179-192.

Compound	IC_{50} (μM)	
	A549	HeLa
***E*-20a**	149.70 ± 7.86	196.40 ± 12.75
PSS-20a	Non-toxic	Non-toxic
***E*-22a**	108.01 ± 8.76	144.00 ± 11.01
PSS-22a	222.30 ± 15.72	318.45 ± 13.85
***E*-24a**	Non-toxic	Non-toxic
PSS-24a	44.06 ± 2.52	45.82 ± 2.60
Cisplatin	6.45 ± 0.47[39]	13.60 ± 0.99

Table 6.3. Cytotoxic IC_{50} values (μM) of the *E* isomer and the PSS of **20a**, **22a**, **24a** and *cis*-platin.[40]

It is shown in the case of **20a** and **22a**, both isomers displayed a relatively low cytotoxicity towards the cell lines under study (Table 6.3 and Figure 6.24). It should be noted that the PSS is less cytotoxic than the *E*-isomer in both cases. In these cases, the photocontrol induced by the photoswitching implied an *on/off* process of drug photodeactivation, which is less relevant for the clinical use because it is more useful to activate the drug exactly in one part of the body through the use of light, than deactivate it in all healthy cells.

[39] Berenguer, J. R.; Pichel, J. G.; Giménez, N.; Lalinde, E.; Moreno, M. T.; Piñeiro-Hermida, S., Luminescent pentafluorophenyl-cycloplatinated complexes: synthesis, characterization, photophysics, cytotoxicity and cellular imaging *Dalton Trans.* **2015,** *44*, 18839-18855.

[40] IC_{50} > 300 µM is appointed as non-toxic.

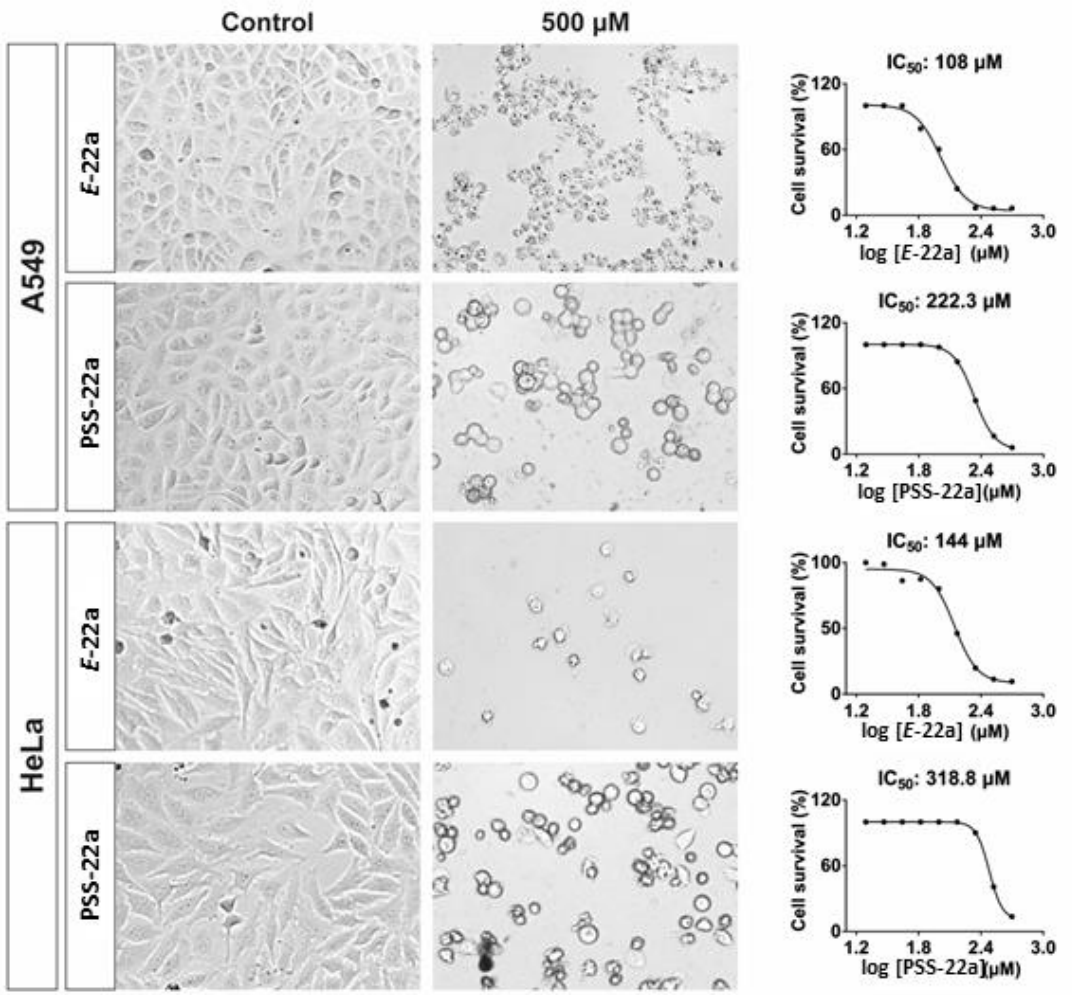

Figure 6.24. Cytotoxicity of **22a** isomers for A549 and HeLa cell lines.

In Figure above, the shape of the cells can be observed when they were non-treated with any compound. When these cells were treated with ***E*-22a** or **PSS-22a** the cells died after 72 hours of exposure towards the cytotoxic agent. It can be observed that different concentrations were needed to kill all of them. Similar behaviour was found for compound **20a**, except that it needed an increased concentration of the drug to kill all cells. Therefore, in Table 6.3, **20a** displayed a lower IC_{50} than **22a**.

The IC_{50} achieved for **20a** and **22a** were surprisingly high, because the neutral derivatives showed a potent anticancer activity towards these cell lines.[41] But, it should be noted that several differences were addressed between the neutral derivatives and the *N*-quaternized analogues; for example the planarity of the molecule was lost and there is a positive charge in the molecule. These factors could be responsible for losing part of their bioactivity.

[41] See ref. 27.

On the other hand, **24a** showed a completely different behaviour to the other photoswitches studied up to now. **24a** showed a considerable level of cytotoxicity displaying similar values of IC_{50} for both cell lines. These values proved that the strategy was on target when it was decided to add a cytotoxic ligand to potent its antitumor activity (Table 6.3 and Figure 6.25).

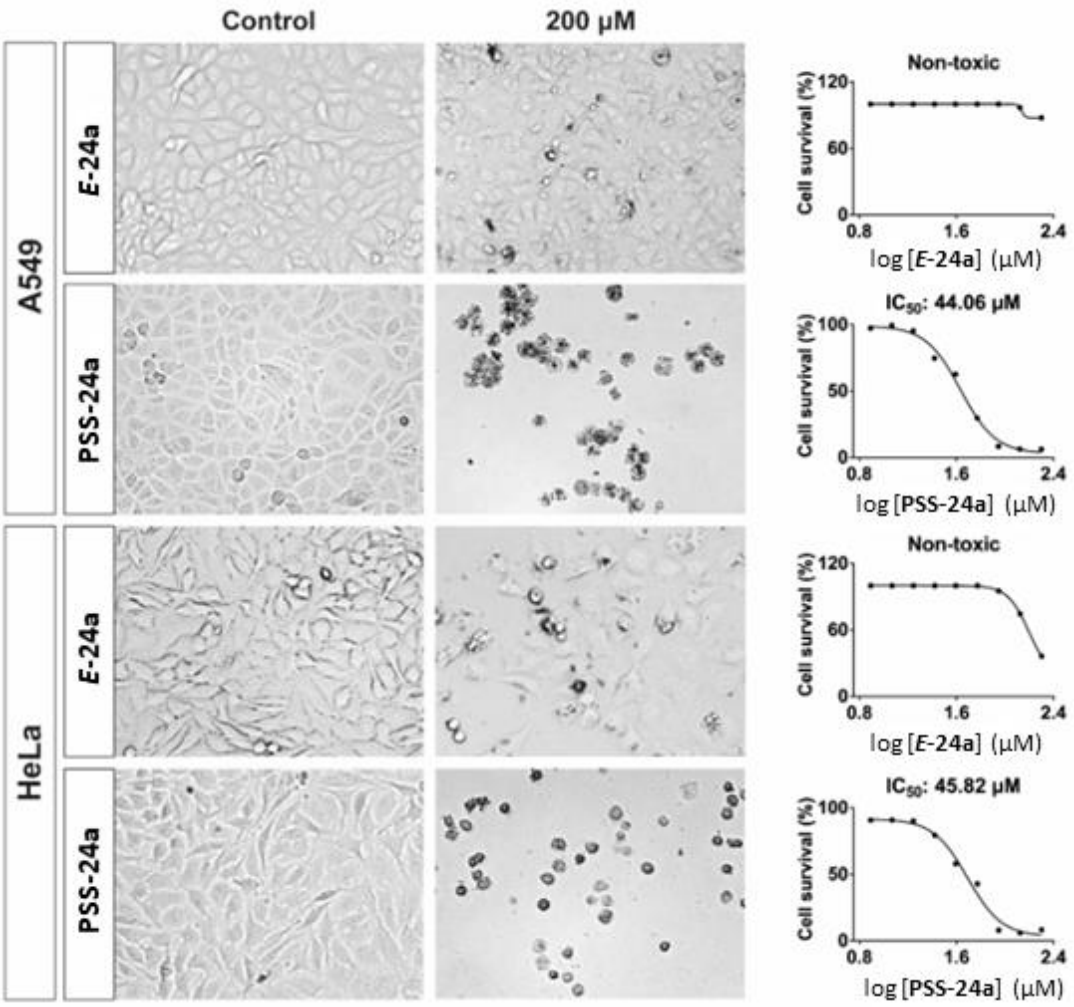

Figure 6.25. Cytotoxicity of **24a** isomers for A549 and HeLa cell lines.

As is represented in Figure 6.25, the use of this photoswitch provided good values of IC_{50} when the PSS was evaluated. Moreover, the thermal isomer was not toxic at all for the cell lines tested. In addition, in this case the *off/on* photoactivation of its antitumor activity could be very helpful to be applied in clinical trials, because it could be possible to localize the cytotoxic action in a specific part of the body, minimizing the side effects of the chemotherapeutic agent.

Trying to go beyond this point, the mechanism of the action of ***E*-24a** and **PSS-24a** was explored. The neutral derivatives based on metronidazole displayed antitumor

activity because they are capable of destabilizing the microtubule polimerization, producing apoptosis of cancer cells.[42]

Therefore, ***E*-24a** and its PSS were tested as microtubule destabilizers. For that purpose, A549 cells were prepared and ***E*-24a, PSS-24a** or nocodazole was added in order to achieve either 2E-4 M of ***E*-24a** and **PSS-5a**, or 10^{-5} M of nocodazole (see experimental data for further details) resulting in different samples (Figure 6.26). Nocodazole is well known as an antineoplastic agent with the capacity of interfering in the polymerization of microtubules; in this experiment it will be studied as a control. In this way, the shape of the cells treated with nocodazole with those which were treated with ***E*-24a** and its PSS will be able to be compared (Figure 6.26).

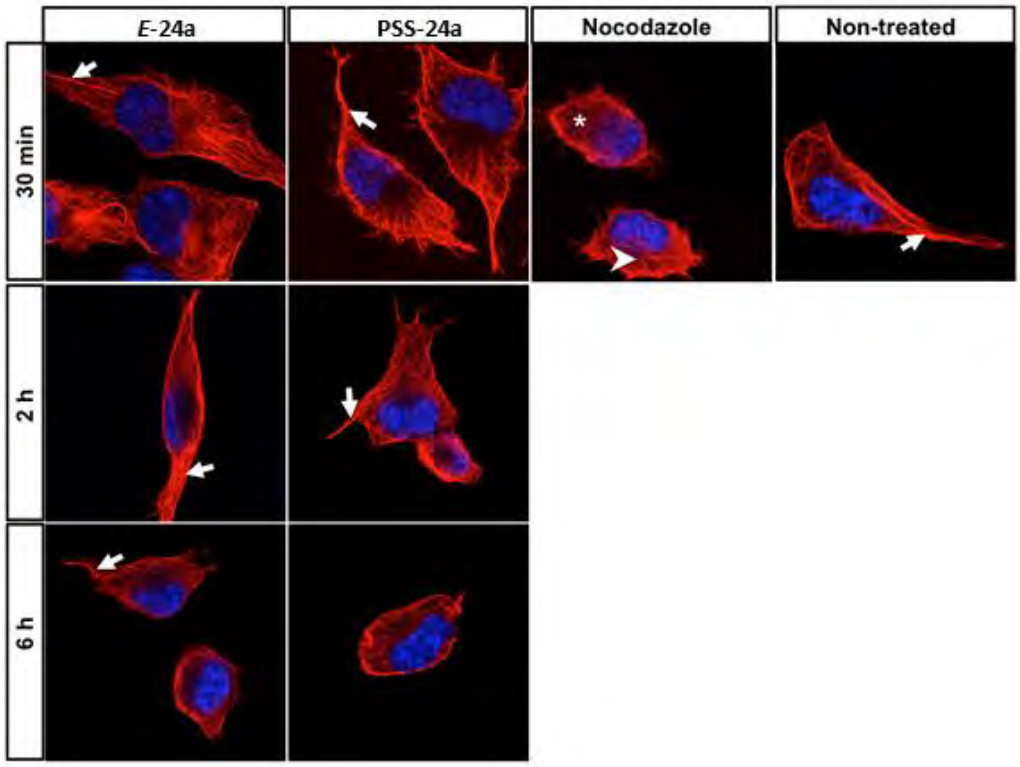

Figure 6.26. Representative images of double colour confocal microscopy images of A549 cells untreated or treated with ***E*-24a** and its PSS or nocodazole.

As can be seen in Figure 6.26, when the A549 cells were treated with nocodazole, their shape changed after 30 minutes of incubation generating rounded cells. This effect was not observed in cells treated with ***E*-24a** or its PSS, since they kept their fusiform shape after 30 minutes and 2 hours of incubation.

[42] See ref. 28.

Therefore, it was concluded that this mechanism of action was not responsible for the cytotoxic activity of **PSS-24a**. Indeed, further studies should be carried out to determine the correct mechanism of action in cells and how to control the biological properties of **24a**.

5. Experimental data.

- **General procedure to synthesized neutral derivatives (20-23).**

Firstly, metronidazole (1 mmol) was dissolved in the minimum volume of DMSO needed. Then, an aldehyde (1 mmol) was added to the solution. The mixture was treated dropwise with 0.89 mmol of sodium methylate in 1ml of methanol (Scheme 6.4). The reaction was carried out for ten hours at room temperature. The reaction was checked by TLC until the metronidazole was consumed. Then, 20 mL of water was added to the mixture, consequently the product was precipitated immediately. The crude products were recristalyzed using a mixture of ethanol/hexane (2:5) and the solid obtained was dried under high vacuum pump.

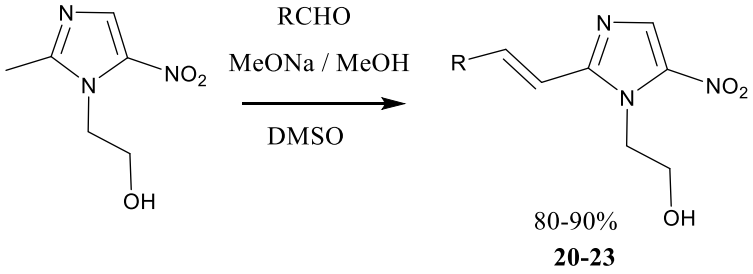

R = Ph (**20**), 2-naphthyl (**21**), *p*-NO_2 (**22**), *p*-OMe (**23**)

Scheme 6.4. Reaction conditions to afford the neutral compounds.

- **General procedure to quaternized metronidazole derivatives.**

All quaternized compounds were synthesized from the neutral forms. These compounds (1 mmol) were dissolved in dry dichloromethane and methyl triflate (3 mmol) was added dropwise to afford the methylated analogue (**20a-23a**). All reactions were carried out at room temperature for 10 hours. The reactions were followed by TLC. Then, the solvent was removed under vacuum and the resulting oil was dissolved in dichloromethane (1 mL) and precipitated adding diethyl ether (15 mL) using an ice bath. The same procedure was used to afford **20c** using acetyl chloride (1 mmol) instead of methyl triflate.

For the synthesis of **24a**, a modification of the method described in the literature was used. 1,4-benzodioxane-6-carboxylic acid (3 mmol) was dissolved in refluxing thionyl chloride (6 mmol) for 4 hours giving the corresponding acid chloride. Then, the prepared 1,4-benzodioxane-6-carboxylic chloride (1 mmol) was added drop by drop to a solution

of compound **22** (1 mmol) and triethylamine (3 mmol) in dichloromethane and the reaction was maintained for 12 hours (Scheme 6.5).

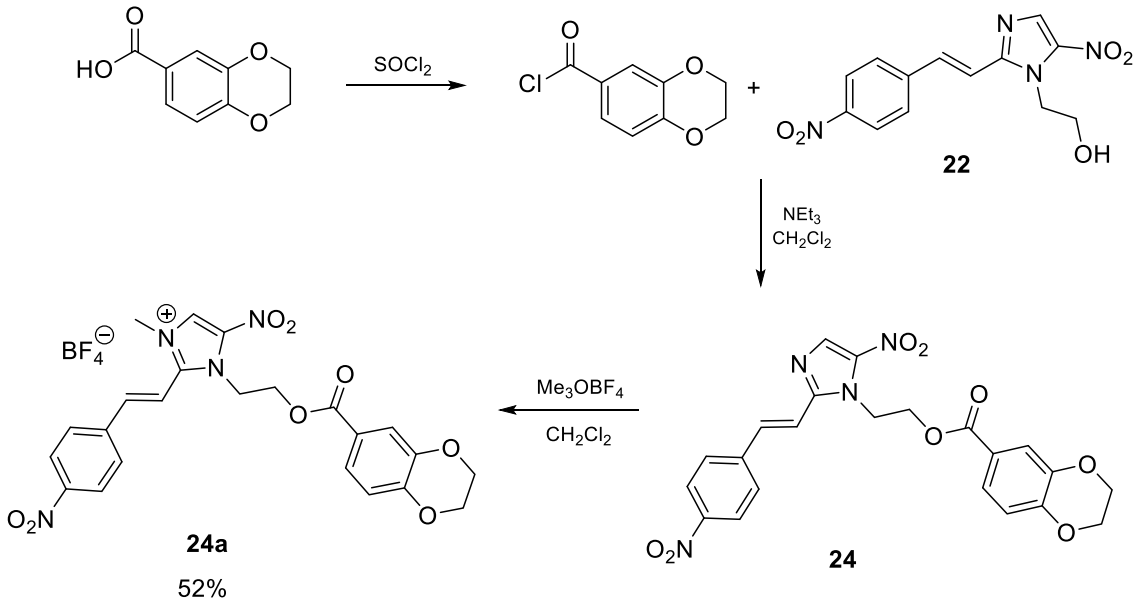

Scheme 6.5. Reaction conditions to afford **24a**.

Then, the product was purified by column chromatography using as eluent hexane and ethyl acetate (1:1) to give the final compound **24**. In this case, tetrafluoroborate trimethyloxonium was used as a methylating agent instead of methyl triflate to give **24a**.

In order to synthesize the protonated derivatives as **20b**, the neutral compound (1 mmol) was dissolved in acetonitrile and 1 mmol of tetrafluoroboric acid was then added. The reaction was carried out quantitatively.

- **Cell lines and culture conditions.**

A549 (adenocarcinomic alveolar basal epithelial) and HeLa (epitheloid cervix carcinoma) human cell lines were cultured following the American Type Culture Collection (www.atcc.org) recommendations and standard methods. Cells were maintained in RPMI 1640 medium supplemented with 10% fetal bovine serum (FBS), 2.0 mM penicillin (100 U/mL) and streptomycin (100 μg/mL). Cultures were maintained under a humidified atmosphere of 85% air and 5% CO2 at 37°C, and were sub-cultured before they get confluent using a 0.25% trypsin-EDTA solution.

- **Cytotoxicity assay.**

The MTS (3-(4,5-dimethylthiazol-2-yl)-5-(3-carboxymethoxyphenyl)-2-(4-sulfophenyl)-2*H*-tetrazolium) hydrolysis method (MTS-based CellTiter 96® AQueous One Solution Cell Proliferation Assay; Promega Corp., Madison, WI) was used to determine the cell viability as an indicator for A549 and HeLa cells sensitivity to the complexes as previously reported. Briefly, 50 μL of exponentially growing cells were seeded at a density of 1.5 x 10^3 cells per well in a 96-well flat-bottomed microplate in growing media, with reduced concentrations of FBS (5%) in the case of A549. 24 h later, cells were incubated for 72 h with the compounds. ***E*-20a** and ***E*-22a** were dissolved at 20 mM in saline solution (0.15 M NaCl), **PSS-20a** and **PSS-22a** at 2 mM in growing media and ***E*-24a** and **PSS-24a** at their maximal solubility in DMSO (16 mM). As a reference, cisplatin (Alfa Aesar; Karlsruhe, Germany) was dissolved at 6.4 mM in saline solution.[43] These stock solutions were kept frozen until they were dissolved in test medium as nine serial dilutions (1:1.5). 50 μL of each compound dilution or medium alone was added to growing cells in the 96-well plate designed as previously recommended.[44] Final concentrations in sextuplicates ranged from: 19.5 to 500 μM (***E*-20a**, **PSS-20a**, ***E*-22a** and **PSS-22a**) and 7.8 to 200 μM (***E*-24a** and **PSS-24a**) for both cell lines. In case of cisplatin, serial dilutions were 1:1.5 ranging from 1.56 to 40 μM for A549 cells[45] and 1:2 ranging from 0.78 to 200 μM for HeLa cells. After 72 h at 37°C, 20 μl of MTS was added and plates were incubated for 1 h at 37°C. Finally, the optical density was measured at 490 nm using a 96-well multiscanner autoreader (POLARstar Omega, BMG Labtech; Germany). Each experiment was repeated three times with cells from different passages. Appropriate solvent controls were run along with samples to discard the cytotoxic effect of DMSO. The IC50 was calculated by plotting the

[43] Hall, M. D.; Telma, K. A.; Chang, K.-E.; Lee, T. D.; Madigan, J. P.; Lloyd, J. R.; Goldlust, I. S.; Hoeschele, J. D.; Gottesman, M. M., Say No to DMSO: Dimethylsulfoxide Inactivates Cisplatin, Carboplatin, and Other Platinum Complexes **2014,** *74*, 3913-3922.
[44] Agasti, S. S.; Chompoosor, A.; You, C.-C.; Ghosh, P.; Kim, C. K.; Rotello, V. M., Photoregulated Release of Caged Anticancer Drugs from Gold Nanoparticles *J. Am. Chem. Soc.* **2009,** *131*, 5728-5729.
[45] See ref. 39.

percentage of growing inhibition versus log of the drug concentration using the GraphPad Prism v6.0 (La Jolla, CA) software. The IC50 values correspond to the dose required to inhibit 50% cellular growth determined from the dose-dependence of surviving cells after cellular exposure to compounds for 72 h. When IC50 values could not be determined as a relevant percentage of cytotoxicity at any concentration tested, compounds were considered non-toxic. Cells were examined under an inverted microscope (DMI 4000B, Leica Microsystems, Mannheim; Germany) and documented using a 20x objective with an additional 3x digital zoom.

- **Effects on microtubule stabilization: cell treatment, immunocytochemistry and confocal microscopy.**

A549 and HeLa cells were cultured over 1 cm diameter Poly-L-Lysine coated coverslips into a 24-well plate with 0.5 mL/well of supplemented culture medium (5% in case of A549 cells) for 48 h. Then, 0.5 mL of medium containing ***E*-24a, PSS-24a** or nocodazole (Sigma-Aldrich) was added in order to achieve either 2 x 10^{-4} M of ***E*-24a** and **PSS-24a**, or 10^{-5} M nocodazole. Cells were incubated with the compounds at 37°C at different time points (30 min, 2h and 6h), medium was removed, cells were washed twice with phosphate buffer saline (PBS, pH 7.2), and fixed in 4% paraformaldehyde in PBS. Nocodazole was used to induce microtubule depolymerisation as reported.[46] For immunocytochemical fluorescent staining, cells were permeabilized with 0.5% IGEPAL (Sigma-Aldrich) and 100 mM glycine in PBS (pH 7.4), washed with PBS, blocked with 5% FBS in PBS, and exposed to a mouse monoclonal anti-β tubulin primary antibody (clone TUB 2.1; Sigma-Aldrich) (1:1000 dilution in blocking solution) overnight at 4°C to specifically label microtubules. The following day, after three washes in 0.02% Tween-20 (Sigma-Aldrich) in PBS, Cy3 goat antimouse IgGs (Jackson Immuno Research) (1:400 dilution in blocking solution) were applied to the cells for 2 h. Finally, after a final round of PBS washes, coverslips were placed on glass slides using ProLong Gold Antifade Reagent (Molecular Probes) containing 4',6-diamidino-2-phenylindole (DAPI) (Molecular Probes) as a nuclear counterstain. Slides were examined under a confocal microscope (TCS SP5, Leica Microsystems) and documented using a 63x oil immersion objective and additional 4x zoom with help of LAS AF Lite microscopy software (Leica Microsystems). Images were projected into a single layer and the resulting two-dimensional data set was merged using

[46] Chirgwin, J. M.; Cuttitta, F.; Martínez, A.; Ozbun, L.; Sackett, D. L.; Wessner, L.; Zudaire, E., Intracellular proadrenomedullin-derived peptides decorate the microtubules and contribute to cytoskeleton function *Endocrinology* **2008,** *2898*, 2888-2898.

the Fiji Open Source image processing software package. [47]

[47] Schindelin, J.; Arganda-Carreras, I.; Frise, E.; Kaynig, V.; Longair, M.; Pietzsch, T.; Preibisch, S.; Rueden, C.; Saalfeld, S.; Schmid, B.; Tinevez, J.-Y.; White, D. J.; Hartenstein, V.; Eliceiri, K.; Tomancak, P.; Cardona, A., Fiji: an open-source platform for biological-image analysis *Nat Meth* **2012,** *9*, 676-682.

5.1. Characterization data.

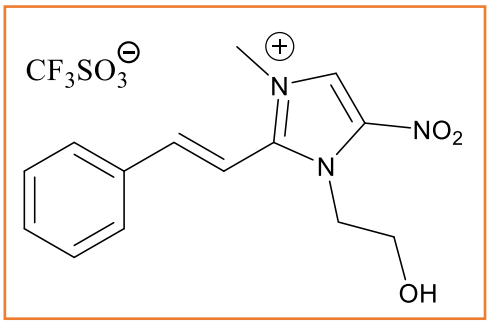

(E)-1-(2-hydroxyethyl)-3-methyl-5-nitro-2-styryl-1*H*-imidazol-3-ium trifluoromethanesulfonate **(20a).**

Empiric Formula: $C_{15}H_{16}F_3N_3O_6S$.

Molecular weight: 423.36

Yield: 65%

^{1}H NMR (300 MHz, Methanol-d_4) δ ppm 8.95 (s, 1H), 7.78 (d, J = 16.7 Hz, 3H), 7.54 (s, 3H), 7.29 (d, J = 16.8 Hz, 1H), 4.82 (s, 2H), 4.10 (s, 3H), 4.01 (s, 2H).

^{13}C NMR (75 MHz, Methanol-d_4) δ ppm 150.1, 148.2, 139.0, 135.2, 132.7, 130.3, 129.5, 127.7, 107.6, 60.9, 52.3, 38.2.

UV-Vis (MeOH): λ (nm) = 320 ε = 13700 M^{-1} cm^{-1}.

EM-ES (+): calcd for $C_{14}H_{16}N_3O_3$ $[M]^+$ 274.1186, found: 274.1188.

Observations: Yellowish solid.

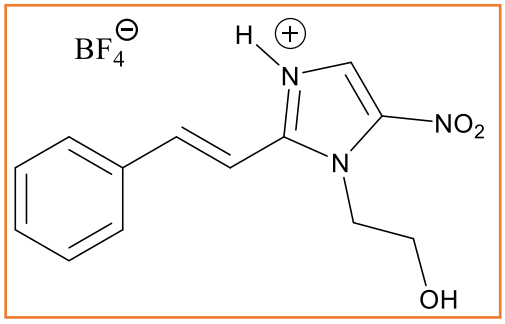

(E)-1-(2-hydroxyethyl)-5-nitro-2-styryl-1*H*-imidazol-3-ium tetrafluoroborate **(20b).**

Empiric Formula: $C_{13}H_{14}F_4N_3O_3B$.

Molecular weight: 347.08

Yield: 80%

^{1}H NMR (300 MHz, Methanol-d_4) δ ppm 8.76 (s, 1H), 7.80 (t, J = 13.2 Hz, 3H), 7.54 – 7.39 (m, 5H), 4.84 (s, 2H), 3.98 (s, 2H).

^{13}C NMR (75 MHz, Methanol-d_4) δ ppm 148.9, 145.7, 135.5, 132.5, 130.3, 129.5, 126.6, 125.5, 109.3, 61.1, 40.3.

UV-Vis (MeOH): λ (nm) = 330 (ε = 22350 M^{-1} cm^{-1}).

EM-ES (+): calcd for $C_{13}H_{14}N_3O_3$ $[M]^+$: 260.1030, found: 260.1034.

Observations: Yellowish solid.

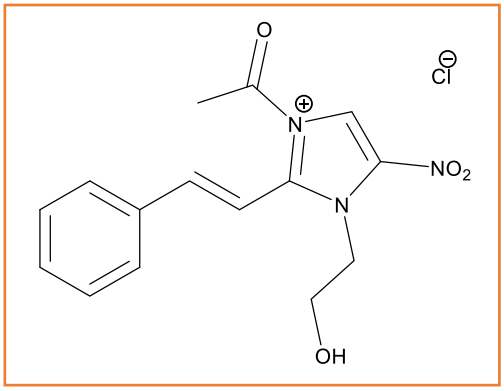

(E)-3-acetyl-1-(2-hydroxyethyl)-5-nitro-2-styryl-1*H*-imidazol-3-ium chloride **(20c).**

Empiric formula: $C_{15}H_{16}N_3O_4Cl$

Molecular weight: 337.76

Yield: 68%

^{1}H NMR (300 MHz, Methanol-d4) δ ppm 8.14 (s, 1H), 7.93 (d, J = 15.7 Hz, 2H), 7.59 (dd, J = 7.8, 2.0 Hz, 2H), 7.49 – 7.34 (m, 3H), 6.96 (d, J = 15.7 Hz, 1H), 4.78 (t, J = 5.3 Hz, 2H), 4.48 (t, J = 5.3 Hz, 2H), 1.95 (s, 3H).

^{13}C NMR (75 MHz, Chloroform-d) δ ppm 170.8, 150.7, 140.3, 135.3, 135.1, 130.1, 129.3, 127.6, 111.4, 77.4, 62.7, 44.3, 29.9.

UV-Vis (MeOH): λ (nm) = 375 (ε = 20850 M^{-1} cm^{-1}).

EM-ES (+): calcd for $C_{15}H_{16}N_3O_4$ $[M]^+$: 302,1135, found 302.1138.

Observations: Yellowish oil.

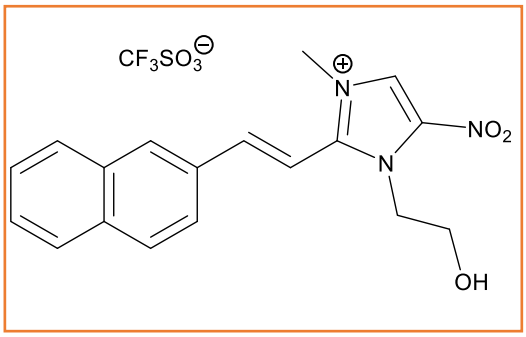

(E)-1-(2-hydroxyethyl)-3-methyl-2-(2-(naphthalen-2-yl)vinyl)-5-nitro-1*H*-imidazol-3-ium trifluoromethanesulfonate **(21a).**

Empiric Formula: $C_{19}H_{21}F_3N_4O_6S$.

Molecular weight: 473.42

Yield: 69%

^{1}H NMR (400 MHz, Methanol-d_4) δ ppm 8.96 (s, 1H), 8.23 (s, 1H), 7.95 (d, *J* = 27.4 Hz, 6H), 7.59 (s, 2H), 7.39 (d, *J* = 16.7 Hz, 1H), 4.84 (s, 2H), 4.13 (s, 3H), 4.02 (s, 2H).

^{13}C NMR (101 MHz, Methanol-d_4) δ ppm 150.1, 148.3, 136.3, 134.7, 132.7, 132.3, 130.2, 129.9, 129.2, 129.0, 128.2, 127.8, 124.0, 107.6, 60.9, 52.3, 38.3.

EM-ES (+): calcd for $C_{18}H_{18}N_3O_3$ $[M]^+$: 324.1343, found: 324.1348.

UV-Vis (MeOH): λ (nm) = 330 (ε = 7700 M^{-1} cm^{-1}).

Observations: Yellowish solid.

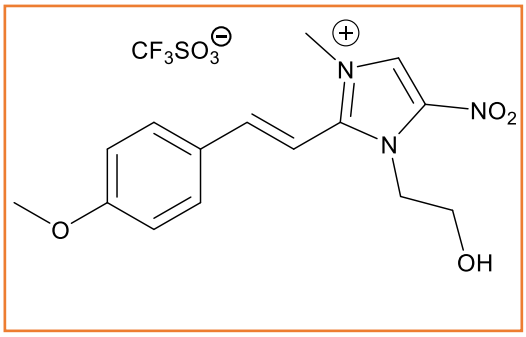

(E)-1-(2-hydroxyethyl)-3-methyl-5-nitro-2-(4-nitrostyryl)-1*H*-imidazol-3-ium trifluoromethanesulfonate **(22a).**

Empiric Formula: $C_{24}H_{21}F_3N_4O_{11}S$.

Molecular weight 453.39

Yield: 60%

^{1}H NMR (400 MHz, Methanol-d_4) δ ppm 8.96 (s, 1H), 8.35 (d, J = 8.8 Hz, 2H), 8.03 (d, J = 8.8 Hz, 2H), 7.84 (s, 1H), 7.48 (s, 1H), 4.83 (s, 2H), 4.11 (s, 3H), 4.00 (s, 2H).

^{13}C NMR (100 MHz, Methanol-d_4) δ ppm 150.5, 147.3, 147.2, 141.1, 139.1, 130.5, 128.0, 125.2, 112.1, 60.9, 52.4, 38.3.

EM-ES (+): calcd for $C_{23}H_{21}N_4O_8^+$ $[M]^+$: 319.1037, found: 319.1039.

UV-Vis (MeOH): λ (nm) = 320 (ε = 17800 M^{-1} cm^{-1}).

Observations: Yellow solid.

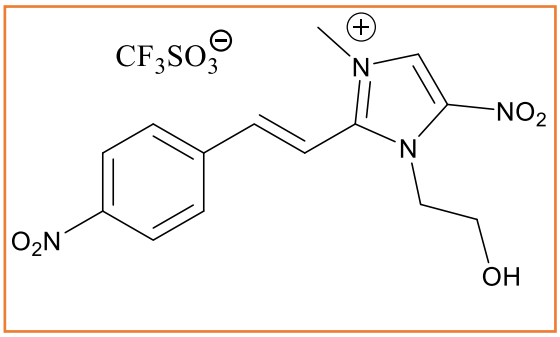

(E)-1-(2-hydroxyethyl)-2-(4-methoxystyryl)-3-methyl-5-nitro-1*H*-imidazol-3-ium trifluoromethanesulfonate **(23a)**.

Empiric Formula: $C_{16}H_{18}F_3N_3O_7S$.

Molecular weight: 468.36

Yield: 81%

^{1}H NMR (400 MHz, Methanol-d_4) δ ppm 8.90 (s, 1H), 7.81 – 7.64 (m, 3H), 7.14 – 6.99 (m, 3H), 4.78 (s, 2H), 4.07 (s, 3H), 3.98 (s, 2H), 3.88 (s, 3H).

^{13}C NMR (75 MHz, Methanol-d_4) δ ppm 164.2, 149.7, 148.7, 131.5, 131.0, 127.9, 127.7, 115.7, 104.4, 60.9, 56.1, 52.1, 38.3.

EM-ES: m/z calc'd for $C_{15}H_{18}N_3O_4^+$: 304.1292; found: 304.1289.

UV-Vis (MeOH): λ (nm) =360 (ε = 11900 M^{-1} cm^{-1}).

Observations: Orange solid.

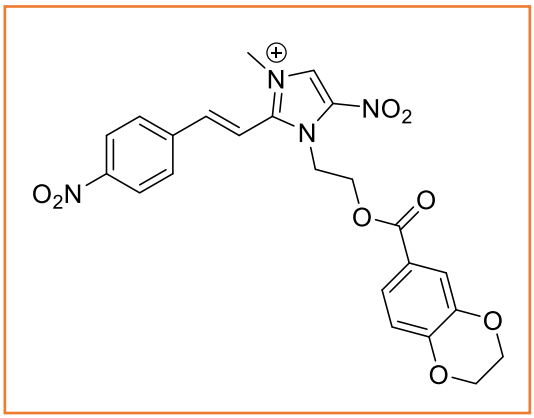

(E)-1-(2-((2,3-dihydrobenzo[b][1,4]dioxine-6-carbonyl)oxy)ethyl)-3-methyl-5-nitro-2-(4-nitrostyryl)-1*H*-imidazol-3-ium tetrafluoroborate **(*E*-24a).**

Empiric Formula: $C_{23}H_{21}BF_4N_4O_8$.

Molecular weight: 481.44

Yield: 52%

^{1}H NMR (400 MHz, Acetonitrile-d_3) δ ppm 8.52 (s, 1H), 8.25 (d, J = 8.8 Hz, 2H), 7.75 (d, J = 8.8 Hz, 2H), 7.46 (d, J = 16.8 Hz, 1H), 7.29 - 7.23 (m, 2H), 7.12 (d, J = 16.8 Hz, 1H), 6.73 (d, J = 8.5 Hz, 1H), 5.02 (s, 2H), 4.69 (s, 2H), 4.25 (s, 2H), 4.18 (s, 2H), 3.97 (s, 4H).

^{13}C NMR (101 MHz, DMSO-d_6) δ ppm 164.8, 148.3, 147.9, 145.0, 144.4, 142.8, 139.9, 137.0, 129.0, 128.0, 123.8, 122.9, 121.6, 117.9, 116.9, 111.0, 64.3, 63.7, 62.6, 47.3, 38.3.

EM-ES: m/z calc'd for $C_{14}H_{15}N_4O_5^+$: 481.1354 $[M]^+$; found: 481.1349.

UV-Vis (MeOH): λ (nm) = 320 (ε = 18100 M^{-1} cm^{-1}).

Observations: Yellow solid.

7. Donor-Acceptor Stenhouse Adducts

These new molecular switches have aroused considerable interest since 2014, when Read de Alaniz realized about their good photochromic properties.[1] Since then, as it was described in the background (Section 3.2.3), many efforts have been applied on the synthesis of new and novel derivatives based on DASAs.

Remarkably, their photophysical properties could be easily tunable changing the acceptor/donor groups in its structure (Figure 7.1).

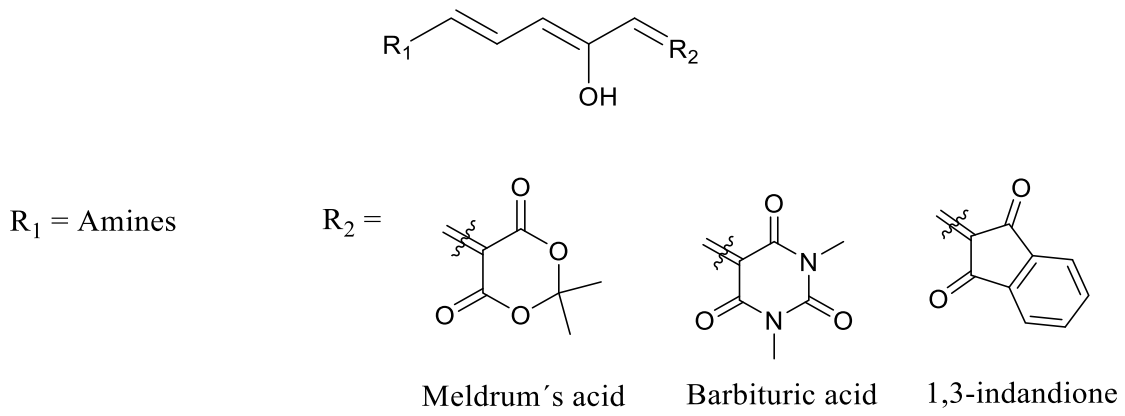

Figure 7.1. General structure of molecular switches based on DASAs already reported.

As it can be seen in Figure 7.1, many derivatives were synthesized combining the three moieties shown as acceptor group with different types of amines. The absorption band, as well as their photochemical properties were very dependent on the properties of the substituents used in the sides (R_1 and R_2). [2]

During the photochemical process, two forms can be found in the equilibrium; the triene and the cyclopentenone form. The most thermally stable isomer is the triene, whereas the cyclopentenone is formed after irradiation (Scheme 7.1).

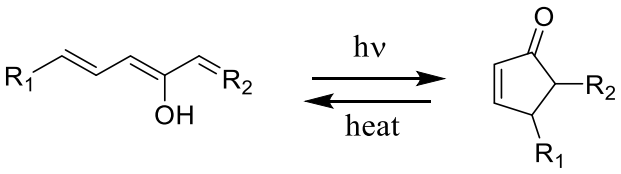

Scheme 7.1. General photocyclization process of DASAs-based molecular switches.

[1] Helmy, S.; Oh, S.; Leibfarth, F. A.; Hawker, C. J.; Read de Alaniz, J., Design and Synthesis of Donor–Acceptor Stenhouse Adducts: A Visible Light Photoswitch Derived from Furfural *J. Org. Chem.* **2014,** *79*, 11316-11329.

[2] Hemmer, J. R.; Poelma, S. O.; Treat, N.; Page, Z. A.; Dolinski, N. D.; Diaz, Y. J.; Tomlinson, W.; Clark, K. D.; Hooper, J. P.; Hawker, C.; Read de Alaniz, J., Tunable Visible and Near Infrared Photoswitches *J. Am. Chem. Soc.* **2016,** *138*, 13960-13966.

As it is shown in Scheme 7.1, the photochemical reaction involves the cyclization of the triene, leading to a molecule completely different. This system is a negative photochromic material, since upon exposure to light, it leads to the formation of the closed-ring, colorless and zwitterionic[3] isomer (in first generation of DASAs) (see Background, section 3.2.3). Some applications have been proposed for these systems, for instance, due to the huge color change between both forms, they have been developed as optical sensors.[4]

The most accepted mechanism proposed for the photoswitching of these molecular switches is shown in Figure 7.2.[5]

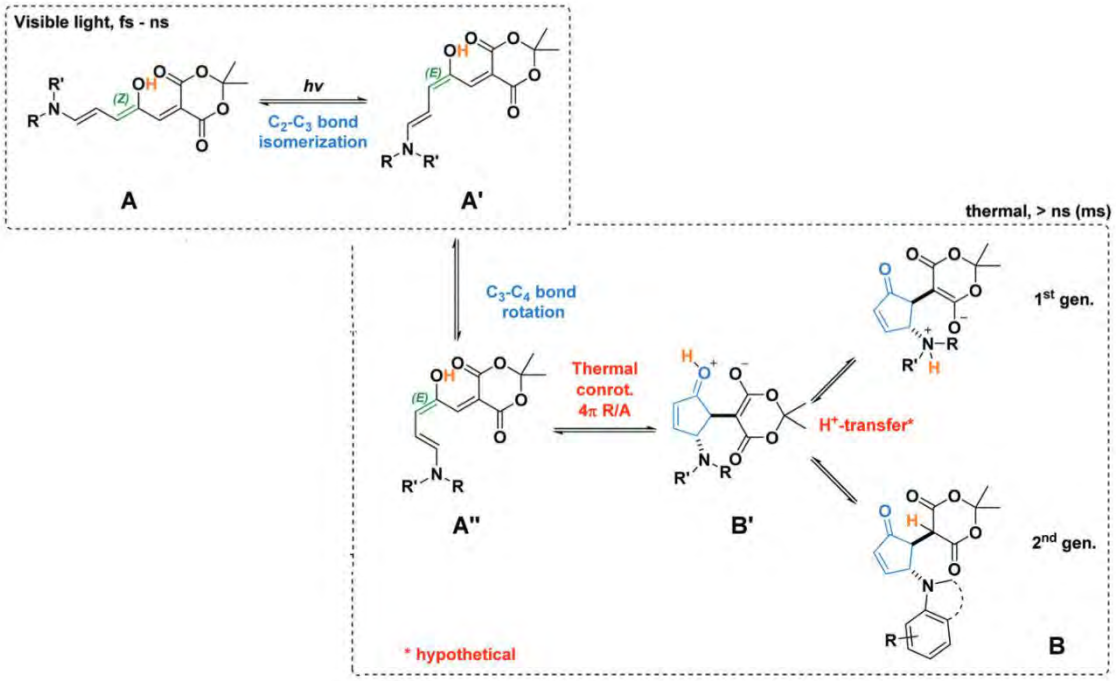

Figure 7.2. Photoswitching mechanism of DASAs-based molecular switches. [6]

It is shown that the first step is a *Z/E* isomerization of one of its C=C double bonds, the mechanism for the formation of the cyclopentenone is still being under revision.[7]

[3] Laurent, A. D.; Medveď, M.; Jacquemin , D., Using Time-Dependent Density Functional Theory to Probe the Nature of Donor–Acceptor Stenhouse Adduct Photochromes *ChemPhysChem* **2016,** *17*, 1846-1851.
[4] Balamurugan, A.; Lee, H.-i., A Visible Light Responsive On–Off Polymeric Photoswitch for the Colorimetric Detection of Nerve Agent Mimics in Solution and in the Vapor Phase *Macromolecules* **2016,** *49*, 2568-2574.
[5] Lerch, M. M.; Wezenberg, S. J.; Szymanski, W.; Feringa, B. L., Unraveling the Photoswitching Mechanism in Donor–Acceptor Stenhouse Adducts *J. Am. Chem. Soc.* **2016,** *138*, 6344-6347.
[6] Lerch, M. M.; Szymanski, W.; Feringa, B. L., The (photo)chemistry of Stenhouse photoswitches: guiding principles and system design *Chem. Soc. Rev.* **2018,** *47*, 1910-1937.
[7] Zulfikri, H.; Koenis, M. A. J.; Lerch, M. M.; Di Donato, M.; Szymański, W.; Filippi, C.; Feringa, B. L.; Buma, W. J., Taming the Complexity of Donor–Acceptor Stenhouse Adducts: Infrared Motion Pictures of the Complete Switching Pathway *J. Am. Chem. Soc.* **2019,** *141*, 7376-7384.

1. Design of new derivatives based on DASAs.

As it was said before, the modifications introduced in the chemical structure up to now were focused on the sides of the unsaturated chain. Since, many derivatives were synthesized combining different donor and acceptor groups that were joint by an unsaturated chain.[8] When the extent of the charge transfer character from the donor and acceptor group was increased, the UV-Vis spectrum was red-shifted, reaching absorption bands centered in the far-visible region (669 nm).

With the aim of going further on the red-shift of the absorption wavelength (see Background, section 2 and 4.2) of these derivatives, another new strategy was raised. Thus, the modification of the unsaturated chain was explored, adding new substituents able to produce a bathochromic shift of the absorption wavelength.

For this purpose, it should be evaluated which position/s of the chain could be modified so that these modifications will not avoid the photoswitching process (Figure 7.1).

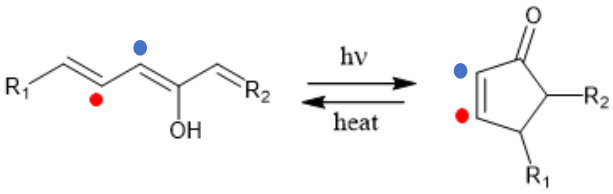

Figure 7.3. General structure of DASAs based photoswitch, showing the bridge positions that can be modified.

In the light of the mechanism proposed, the only two positions that are not occupied in the structure, allowing the photoswitching process, are shown in Figure 7.3 as red / blue circles in the triene isomer and cyclopentenone. Therefore, the target derivatives are based on the structure shown in Figure 7.4.

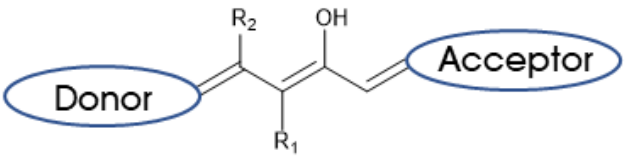

Figure 7.4. Disubstituted derivatives based on DASAs molecular switches.

[8] See ref. 1

In order to design these new derivatives based on DASAs, it must be explored by computational calculations which substituent is the best choice to include in the chain in order to red-shift the absorption wavelength. To perform this study, the excitation energies were calculated at the TD-DFT level of theory with the B3LYP[9] functional and the 6-31+G* basis set.[10] Also, the solvent (toluene in this case) was considered through the Polarizable Continuum Model (PCM).[11]

First, it was required to validate the level of theory used to calculate the excitation energies of the proposed derivatives. For this purpose, it was chosen two compounds already synthesized and characterized photochemically by Read de Alaniz (Figure 7.5).[12] This way, we would be able to compare the experimental data with our computational results (Table 7.1).

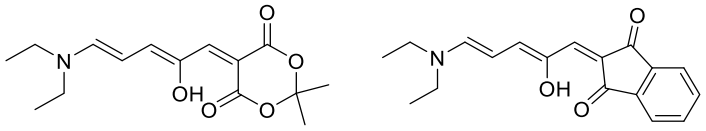

25 **26**

Figure 7.5. Structures of different DASAs based molecular switches.

Compound	Exp. Value in toluene (nm)	S_1 energy eV (nm)	Oscillator strength (f)
25	545	2.8516 (435)	1.2111
26	600	2.4558 (505)	0.3295

Table 7.1

As we can see in Table 7.1, using this level of theory, a shift of *ca.* 100 nm was obtained between the computed and the experimental value of the maximum absorption wavelength. Actually, it is known that this level of theory do not predict perfectly the excitation energies in push-pull systems such as DASAs derivatives.[13] But, this difference seemed to be consistent, so when doing the calculations to predict the absorption wavelength of our novel modified compounds, an additional shift of 100 nm must be

[9] Becke, A. D., Density-functional thermochemistry. III. The role of exact exchange *J. Chem. Phys.* **1993,** *98*, 5648-5652.
[10] Hariharan, P. C.; Pople, J. A., The influence of polarization functions on molecular orbital hydrogenation energies *Theor. Chem. Acc.* **1973,** *28*, 213-222.
[11] Tomasi, J.; Mennucci, B.; Cammi, R., Quantum Mechanical Continuum Solvation Models *Chem. Rev.* **2005,** *105*, 2999-3094.
[12] See ref. 1.
[13] Fabian, J., TDDFT-calculations of Vis/NIR absorbing compounds *Dyes Pigm.* **2010,** *84*, 36-53.

considered to get a value close to the experimental one. This way, the systematic error will be sorted out.

Then, it was evaluated the effect on the photophysical properties of placing different substituents with unlike electronic properties (methoxy, dimethylamine or bromine groups) in the positions pointed out as R_1 and R_2 (Figure 7.6). This way, it will be analyzed which group would be the responsible of causing a greater red-shift of the absorption band.

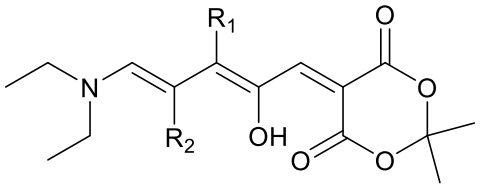

Figure 7.6. Selected DASA analogues to test the effect of the chain substituents modifications.

R_1	R_2	S_1 excitation energy eV (nm)	f S_1
H	H	2.8516 (435)	1.2111
OMe	H	2.7238 (455)	1.0407
H	OMe	2.7598 (449)	1.1578
OMe	OMe	2.6162 (474)	0.9831
NMe_2	H	2.6095 (475)	0.7562
H	NMe_2	2.7187 (456)	0.0727
NMe_2	NMe_2	2.5113 (494)	0.7030
Br	H	2.6663 (465)	1.0000
H	Br	2.7458 (452)	1.0753
Br	Br	2.4912 (498)	0.6273

Table 7.2

As it is shown in Table 7.2, the introduction of different groups in the unsaturated chain seems to be a good strategy to red-shift the absorption wavelength. It should be noted that by introducing two bromine atoms in the R_1 and R_2 positions (Figure 7.4), the absorption wavelength is red-shifted around 70 nm. Furthermore, a clear effect is also

seen when just one position is occupied by a bromine atom, although a better result was achieved when both positions were modified.

As it is observed, the same effect was produced by dimethylamine and bromine, but in order to perform the new analogs based on DASAs, the bromine derivatives were afforded instead of dimethylamine derivatives, since their synthesis were much easier. Moreover, the bromine atom can be changed straightforwardly by other substituents, providing a great versatility to the synthetic route.

Therefore, these new derivatives will present one or two bromine atoms in the unsaturated chain which connects the acceptor and the donor moieties.

Once it is clear the effect produced on the absorption wavelength by introducing different substituents into the chain, it was also evaluated if an improved effect could be achieved by modifying the chain and the sides (acceptor and donor moiety) simultaneously. This way, in case of getting a bigger red-shift of the absorption band, reaching the far-visible or infrared region, it could be concluded that both effects were additive. It should be boted that this strategy to red-shift the absorption wavelength has not been investigated up to now.

To explore this fact, the same level of theory was used to predict the absorption wavelength of the new derivatives. For this purpose, in first place the absorption energy changing the acceptor moiety was investigated (Figure 7.7), keeping the same donor group in the structure. Regarding the acceptor moieties, it was selected the barbituric acid and 1,3-indandione, this last presents a greater electron withdrawing ability than the barbituric acid.

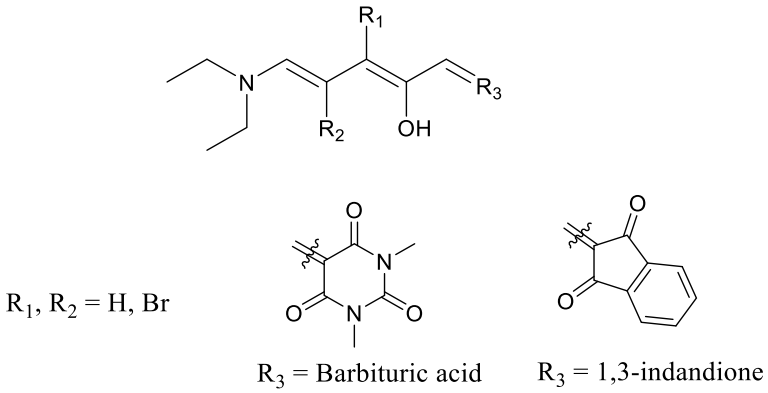

Figure 7.7. Structures based on DASAs with different acceptor moieties and groups in the unsaturated chain.

Compound	R_1	R_2	R_3	S_1 excitation energy eV (nm)
27	Br	Br	Barbituric acid	2,2385 (554)
28	Br	Br	1,3-indandione	2,1153 (586)
29	Br	H	Barbituric acid	2,3514 (527)
30	Br	H	1,3-indandione	2,2385 (554)

Table 7.3

As it can be seen in Figure 7.7 and Table 7.3, when increasing the acceptor capacity of the group from barbituric acid to 1,3-indandione placed on one side, an improved effect was observed when the unsaturated chain was substituted with bromine atoms.

By this methodology, it is predicted an absorption band centered at 586 nm for compound **28**. But, as using this level of theory the absorption energy calculated is blue-shifted around 100 nm compared to the experiment, it is expected to get experimentally an absorption band placed on the far-visible region, around 680 nm.

Then, the same experiment was carried out to explore the effect of changing the donor moiety and the substitution in the unsaturated chain, keeping the same acceptor group (Figure 7.8 and Table 7.4). Depending on the type of the amine, as it was discussed in the background, it will lead to different generations of DASAs. In this case, it will be used an aliphatic amine (first generation) or a cyclic amine (second generation). Specifically, *N,N*-diethylindolin-5-amine was selected due to its big electron donating ability, thus it is expected a huge red-shift of the absorption band using this cyclic amine.

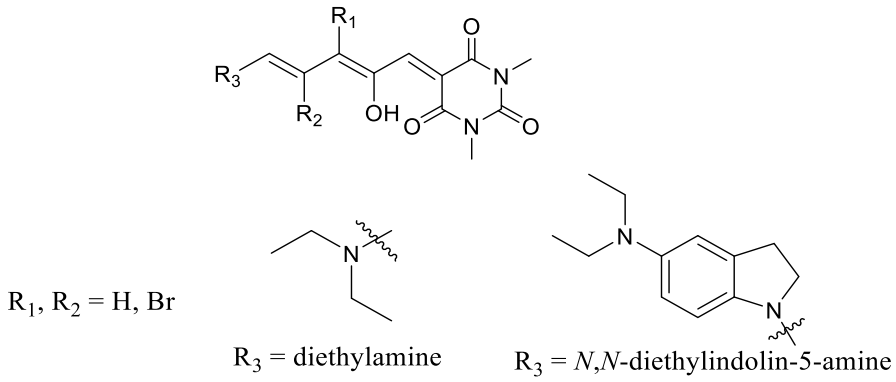

Figure 7.8. Structures based on DASAs with different acceptor moieties and groups in the unsaturated chain.

Compound	R_1	R_2	R_3	S_1 excitation energy eV (nm)
27	Br	Br	diethylamine	2,2385 (554)
31	Br	Br	*N,N*-diethylindolin-5-amine	2.0063 (618)
29	Br	H	diethylamine	2,3514 (527)
32	Br	H	*N,N*-diethylindolin-5-amine	1,7711 (700)

Table 7.4

As it was expected, a huge bathochromic shift was found when increasing the ability of the amine to donate electron density to the system, together with the presence of one or two bromine atoms in the chain.

Therefore, according to the data previously obtained, it was concluded that both effects were additive. So, it will be useful to explore where is centered the absorption band mixing the best acceptor and donor groups with one or two bromine atoms in the unsaturated chain (Figure 7.9 and Table 7.5).

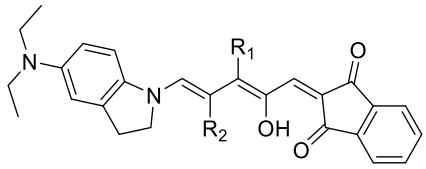

R_1, R_2 = H, Br

Figure 7.9. New structure based on DASAs with improved properties.

Compound	R_1	R_2	S_1 excitation energy eV (nm)
33	Br	H	1,9250 (644)
34	Br	Br	1,6640 (745)

Table 7.5. Compounds afforded with the highest charge transfer character from the donor and acceptor groups with the unsaturated chain substituted by bromine atoms.

As it is shown in Table 7.5, the absorption bands are very red-shifted through the strategy that has been planned. Thus, it is expected to get experimentally red-shifted spectra regarding the computed values, as it was mentioned before.

2. Synthesis of new derivatives based on DASAs.

2.1. Synthesis of dibromide derivatives.

Once it has been explored the promising properties of these novel derivatives, the synthesis detailed in the following is proposed. First, a retrosynthetic scheme is raised to afford these new derivatives (Scheme 7.2).

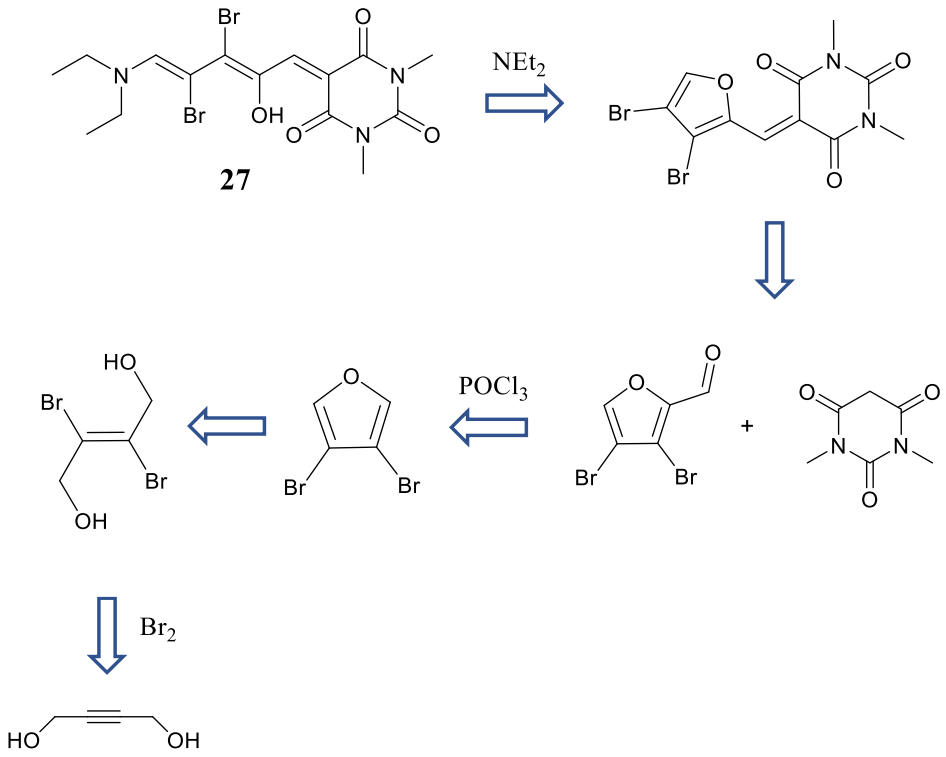

Scheme 7.2. Retrosynthetic route of dibromide analogues.

The first step in this synthetic procedure implies the addition of bromine into the alkyne, the resulting product is an alkene. By the conditions detailed in Scheme 7.3, the addition of bromine into **35** is stereospecific, leading to the final alkene in its *trans*-configuration (Scheme 7.3).[14,15]

[14] Kavala, V.; Naik, S.; Patel, B. K., A New Recyclable Ditribromide Reagent for Efficient Bromination under Solvent Free Condition *J. Org. Chem.* **2005,** *70*, 4267-4271.
[15] Karabiyikoglu, S.; Iafe, R. G.; Merlic, C. A., Ring-Closing Metathesis with Vicinal Dibromoalkenes as Protected Alkynes: A Synthetic Approach to Macrocyclic Enynes *Org. Lett.* **2015,** *17*, 5248-5251.

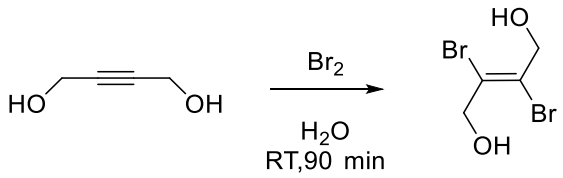

90%

35 **36**

Scheme 7.3

Once the alkene was formed, the cyclization of **36** was carried out under strong oxidation conditions using sulfuric acid as solvent, as we can see in Scheme 7.3. Under these conditions, it was possible to afford the substituted furan which was desired (Scheme 7.4).

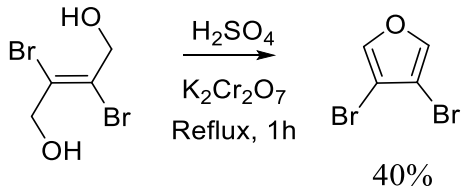

40%

37 **38**

Scheme 7.4

Then, the aldehyde **39** was afforded using the Vilsmeier-Haack reaction conditions.[16] This formylation was carried out in just one position, since by symmetry the two free positions in **38** are the same. For this reason, 1 equivalent of $POCl_3$ was used. This reaction was carried out at room temperature for 12 hours.

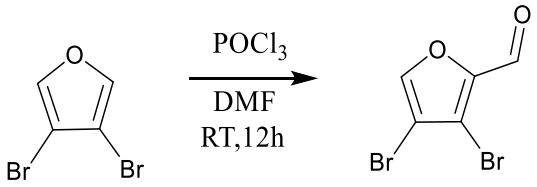

75%

38 **39**

Scheme 7.5

Once the aldehyde was afforded using the methodology just described in Scheme 7.5. A condensation between **39** and a methylene activated as barbituric acid was carried out. The reaction took place at 70°C in water for 2 hours, then the mixture was

[16] Meth-Cohn, O.; Stanforth, S. P., 3.5 - The Vilsmeier–Haack Reaction. In *Comprehensive Organic Synthesis*, Trost, B. M.; Fleming, I., Eds. Pergamon: Oxford, 1991; pp 777-794.

cooled until room temperature. Finally, the resulting solid was isolated as pure compound (**40**) by filtration.

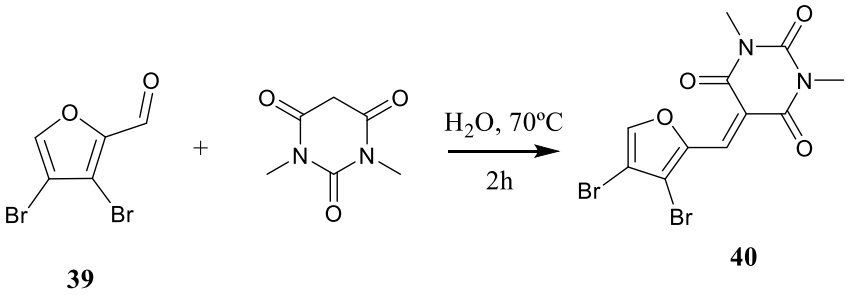

Scheme 7.6

After the adduct **40** was formed, the ring-opening of the substituted furan could be afforded using diethylamine as nucleophile. The reaction was carried out in THF at room temperature, these conditions were the same as reported by Read de Alaniz in non-substituted furans.[17] In contrast, this reaction did not take place with this kind of substrate although the temperature was increased up to 70ºC during longer times (24 hours), The reaction did not occurred maybe due to the steric hindrance made by the bromine atom in the contiguous carbon, where the nucleophilic attack should take place.

2.2. Synthesis of monobromide derivatives.

Therefore, faced the impossibility of synthesizing DASAs-based molecular switches with two bromine atoms in the unsaturated chain, it was explored the possibility of doing monosubstituted analogues, since the previous calculations also revealed good photophysical properties (Table 7.3). So, a new retrosynthetic scheme is presented (Scheme 7.7).

[17] See ref. 1.

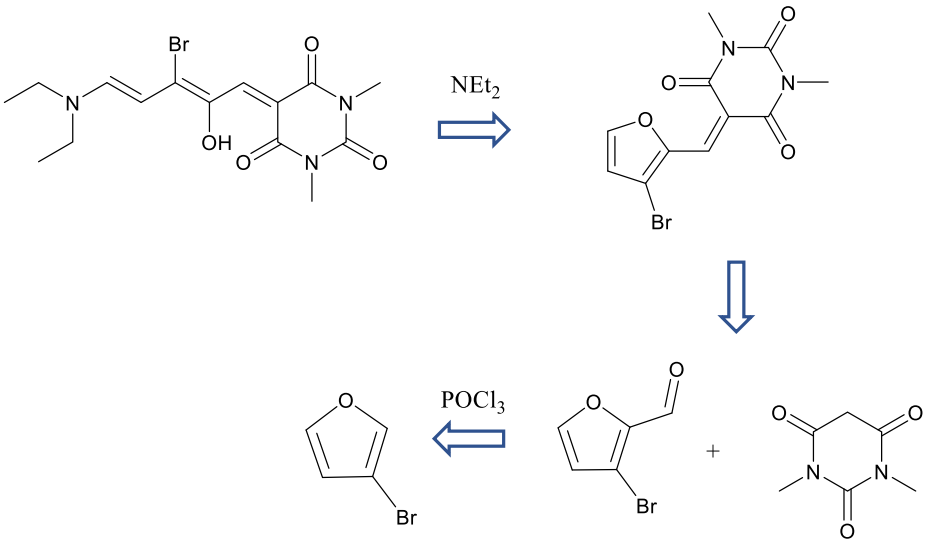

Scheme 7.7. Retrosynthetic route of monobromide analogues.

As it can be seen in Scheme 7.7, the retrosynthetic route to afford monobromide derivatives is very similar to the one shown in Scheme 7.2. First, the formylation of 3-bromofuran to result in the aldehyde **41** was achieved following the same procedure as in compound **39.**

Then, the aldehyde **41** was condensated with two substrates under the same reaction conditions as for **40** (Scheme 7.8). Once these compounds were afforded, both furans were opened with diethylamine to result in the final DASAs derivatives (**29** and **30**).

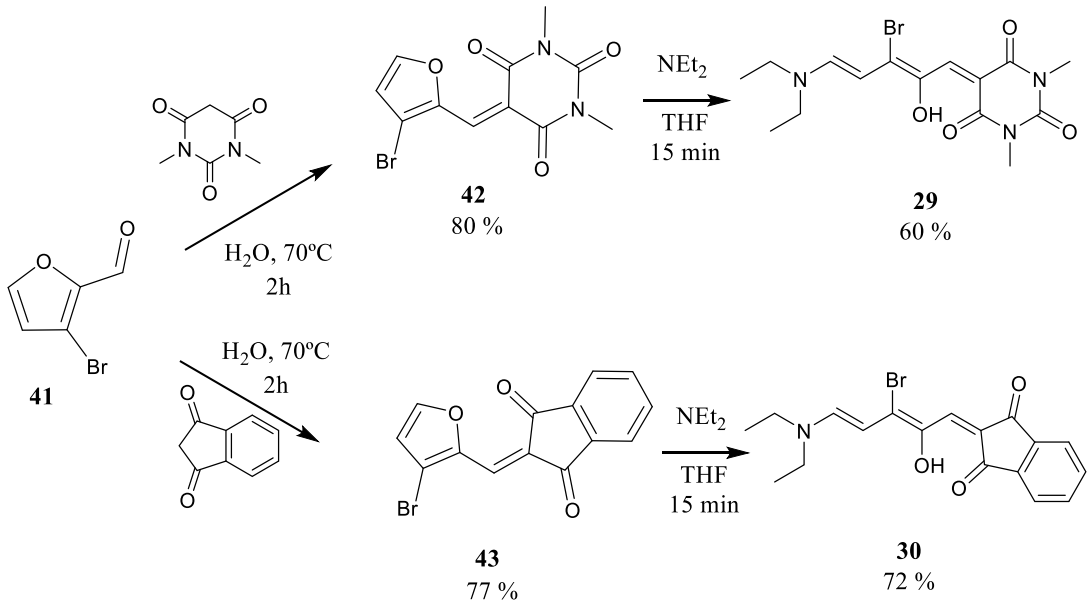

Scheme 7.8

Once **29** and **30** were synthesized, their photophysical behavior was studied. This research will be shown in the next section. Due to the good results predicted for **33** by theoretical calculations, its synthesis was also afforded successfully (Scheme 7.9).

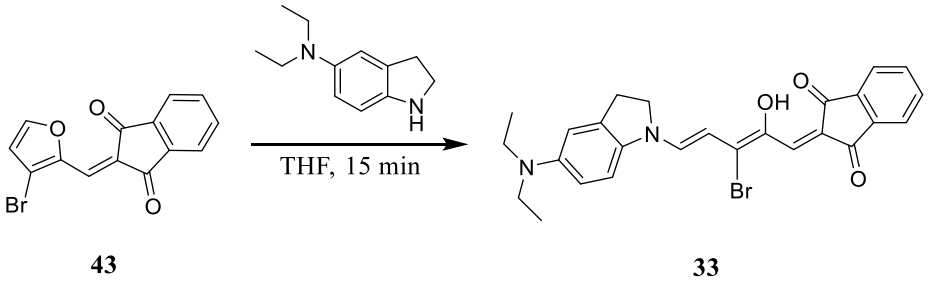

43 **33**

Scheme 7.9

2.3. Synthesis of monophenyl derivatives.

Finally, due to the importance of linking different photoswitches in more complex systems,[18] the synthesis of a new compound with one phenyl ring in the unsaturated chain was afforded. The main advantage of the design of this derivative is that it can be straightforwardly derivatized. Therefore, its photophysical properties could be tuned easily and it could be used as a linking point.

For this purpose, a new retrosynthetic route was raised trying to take advantage of the compounds already synthesized (Scheme 7.10).

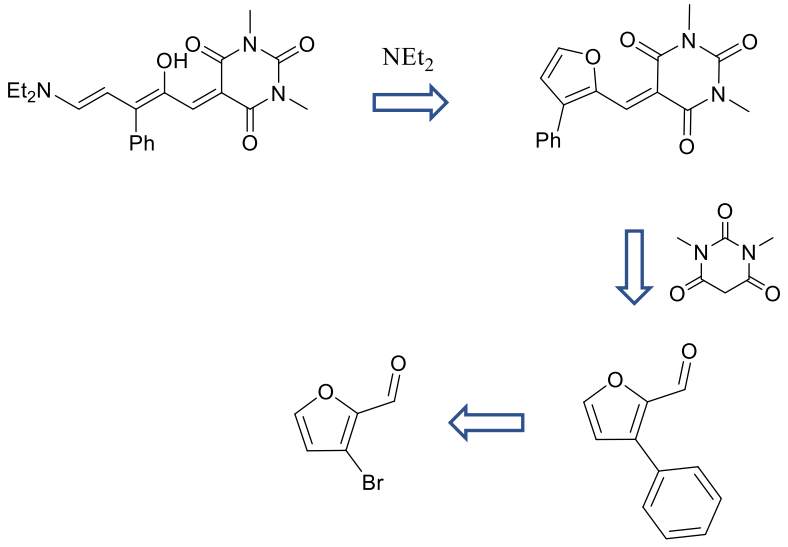

Scheme 7.10. Retrosynthetic route of phenyl derivatives.

[18] Szymański, W.; Beierle, J. M.; Kistemaker, H. A. V.; Velema, W. A.; Feringa, B. L., Reversible Photocontrol of Biological Systems by the Incorporation of Molecular Photoswitches *Chem. Rev.* **2013,** *113*, 6114-6178.

As it can be seen in the scheme above, the 3-bromofuran synthesized before was used to carry out a Suzuki reaction.[19] This method used to afford the target compound was easy and fast, so it was a proper way to exchange a bromine atom by a phenyl group. The reaction conditions are detailed in the Scheme 7.11.

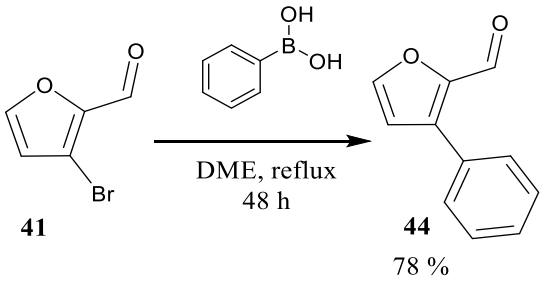

Scheme 7.11

From this point, after obtaining **44**, the condensation step with barbituric acid took place and then, the ring-opening was carried out by diethylamine (Scheme 7.12).

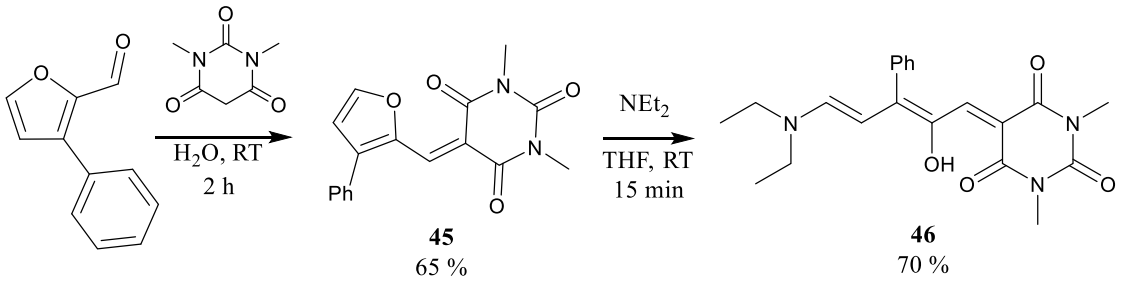

Scheme 7.12

As we can see, all the reactions described in this chapter are quite simple, because the products were obtained in good yields and the reactions were fast.

It should be noted, that it was tried to synthesize the derivative with the two positions of the bridge substituted by phenyl rings. Unfortunately, as in the case of two bromine derivatives, the reaction did not take place under different reaction conditions. So, it can be concluded that the nucleophilic attack was hampered by the size of the substituents placed in the furan ring (bromine atoms or phenyl rings).

[19] Gujral, S.; Khatri, S.; Riyal, P., Suzuki Cross Coupling Reaction-A Review *Indo glob. j. pharm. sci.* **2012,** *2*, 351-367.

Finally, another modification was made in these compounds due to the low solubility of all of them in organic solvents. This fact prevented us from measuring their NMR spectra, although it was possible to record their UV-Vis spectra.

Therefore, the aim of this modification was to increase the solubility in organic solvents, for this purpose new analogs were afforded using diheptylamine as donor moiety (**29-dihept**, **30-dihept**, **33-dihept, 46-dihept, 47-hept**) (Figure 7.10). This way the solubility of these new derivatives will be enhanced, and maybe, it would be possible to measure their NMR spectra.

It should be noted that compound **47** was already reported by Read de Alaniz (Figure 7.10),[20] but it was useful for comparison purposes to see experimentally how affects the change of the substituent on their photophysical properties. In Figure 7.10 is shown the final compounds that were ready to study their photophysical properties.

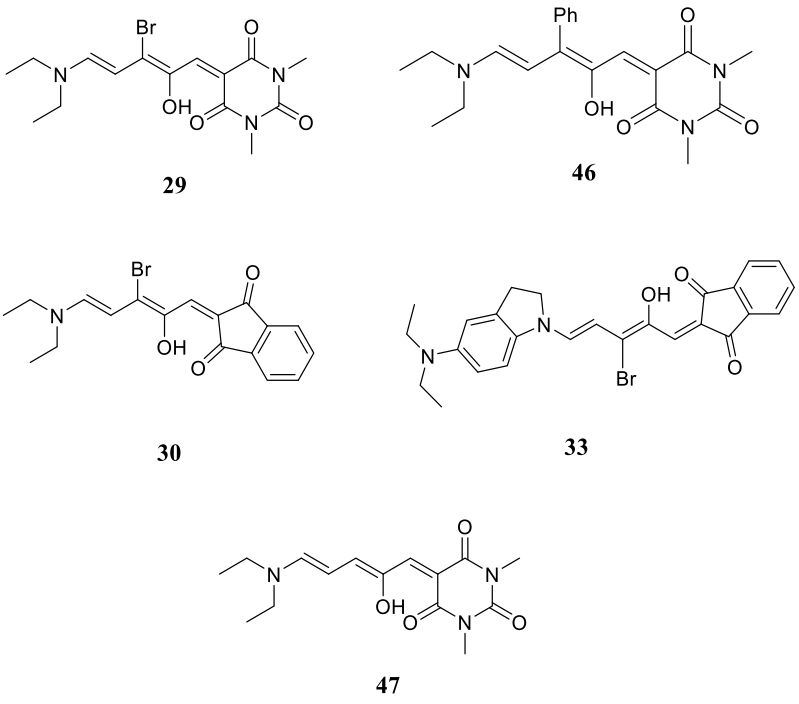

Figure 7.10. Final synthesized analogues based on DASAs.

[20] See ref. 1.

3. Photophysical study.

3.1. Absorption spectra.

First, the effect of the presence of a substituent in the unsaturated chain was evaluated. For this purpose, the sides of the chain (the acceptor and donor moieties) were kept, while it was changed the substituent in the "*π-bridge*". Therefore, different solutions of **47** (H), **46** (Ph), and **29** (Br) in CH_2Cl_2 were prepared to measure their UV-Vis spectra (Figure 7.11).

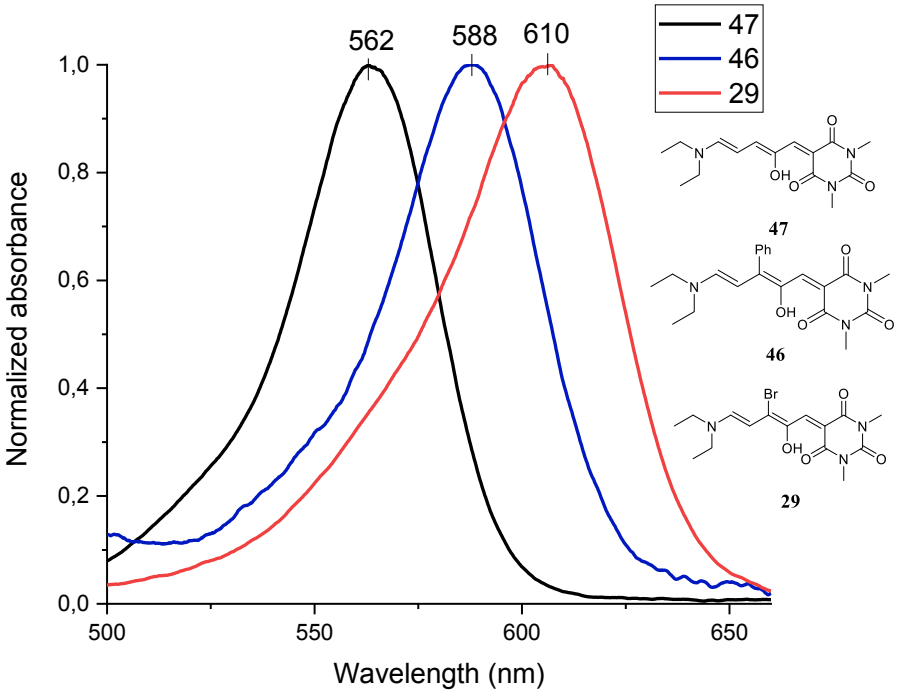

Figure 7.11. Comparison of different UV-Vis spectra depending on the substituent in the *π*-bridge.

As it is observed in Figure 7.11, a big red-shift was experimented by the absorption bands of these new photoswitches, depending on which substituent was in the chain. It can be seen that just by the fact that there was a bromine atom in the unsaturated chain, the absorption wavelength experimented a bathochromic shift of *ca.* 50 nm.

Then, the effect of changing the acceptor part in the analogues **29** and **30** with a bromine atom was explored. This way, it would be demonstrated if the red-shift produced by the presence of a better electron-withdrawing group is added to the shift attributable to the presence of a bromine atom. For this purpose, two solutions of 5E-5 M were prepared in CH_2Cl_2 to record their UV-Vis spectra (Figure 7.12)

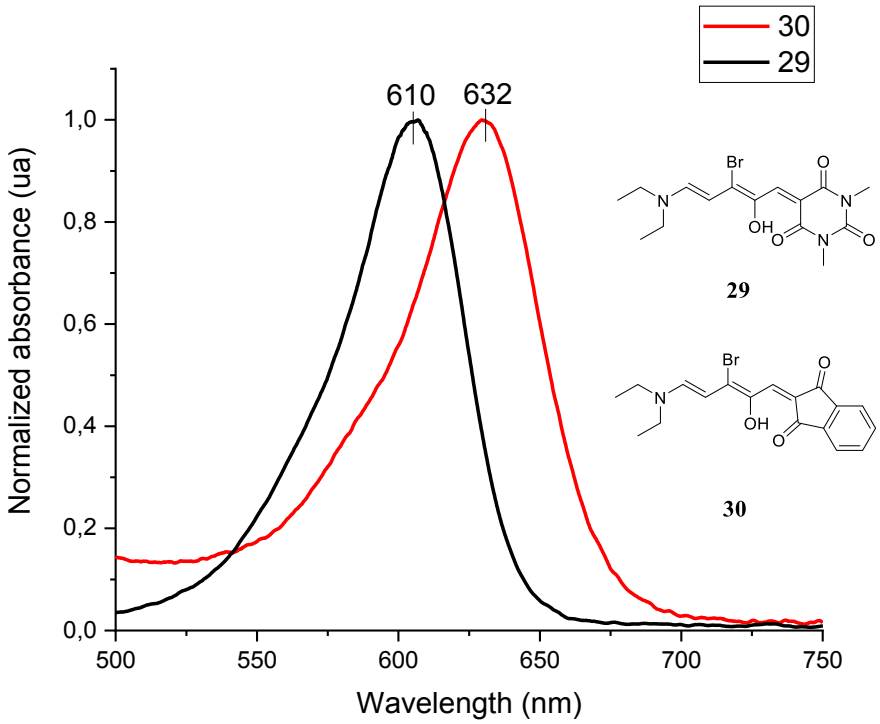

Figure 7.12. Comparison of UV-Vis spectra of **29** and **30**.

As it is shown in Figure 7.12, when increasing the charge transfer in monobromide derivatives, the absorption band is red-shifted. (Table 7.6).

Compound	Experimental wavelength (nm)	Computed wavelength (nm)
29	610	527
30	632	554

Table 7.6.

It should be noted that the absorption band of compound **30** presented an extended tail beyond 700 nm, where the infrared region starts.

The same experiment was performed maintaining fixed the acceptor moiety and changing the donor group. In this case, it is expected an improved result since it was reported that the ability of the amine to donate electron density was very decisive on the

displacement of the absorption band.[21] For this purpose, two solutions of 5E-5 M in CH_2Cl_2 of **30** and **33** were prepared to measure their UV-Vis spectra (Figure 7.13).

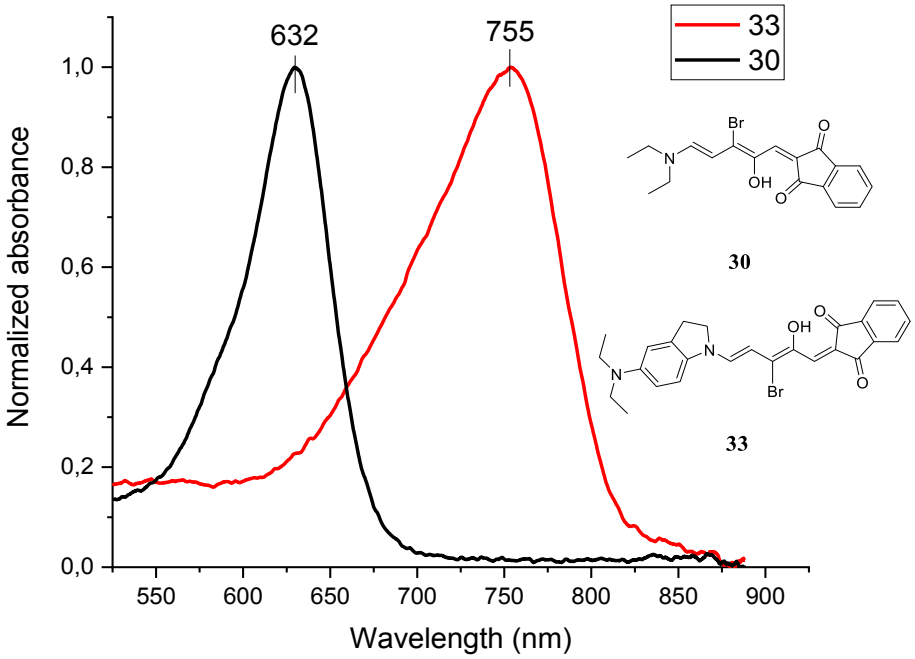

Figure 7.13. Comparison of UV-Vis spectra of **30** and **33**.

As it can be observed in Figure 7.13, by changing the amine it was found an absorption band in the therapeutic spectral window. The wavelength of maximum absorbance was centered at 755 nm and absorption tail goes up to 825 nm. These results were very good because the absorption band showed by **33** was not observed in DASAs-based molecular switches up to now.

The main disadvantage of this set of compounds was the impossibility of recording their NMR spectra, maybe due to their low solubility or their NMR relaxation time, but the study of this fact is still underway. So, we proposed the analogues exchanging the diethylamine with diheptylamine to increase the solubility in organic solvents.

In first place, it was evaluated if this slight modification involved any change in their photophysical properties. For this purpose, several solutions 5E-5 M in CH_2Cl_2 of **29**, **29-hept**, **46** and **46-hept** were prepared to compare their corresponding UV-Vis spectra (Figure 7.14).

[21] See ref. 2.

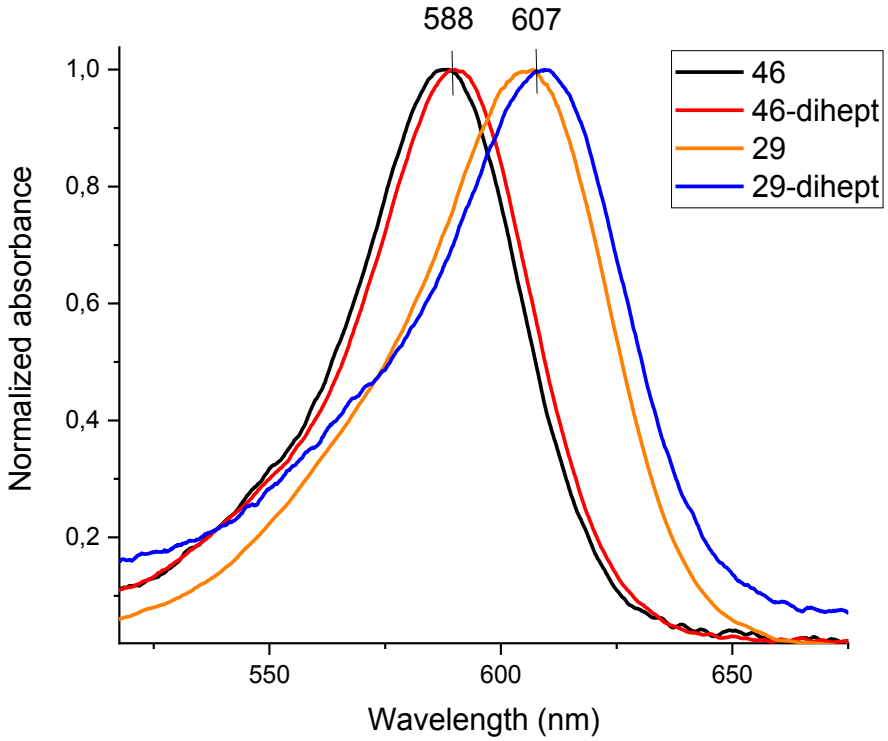

Figure 7.14. Comparison of UV-Vis spectra of **29**, **29-dihept** and **46**, **46-dihept**.

As it is shown in Figure 7.14, the structural modification detailed before does not affect the photophysical properties of the analogues, because both pairs of compounds share similar absorption bands with a slight red-shift for dihept-derivatives. Therefore, as it was expected, this modification did not alter the chromophore, so the photophysical properties remained unaltered.

4. Photochemical study.

When these molecules are irradiated, it is expected to occur the photochemical process shown in Figure 7.15. Besides, as we can see in the Figure 7.15, the photochemical process leads to two molecules which are completely different between them. Therefore, other external agents could be also the responsible of modifying the ratio of both isomers in the equilibrium. For example, through using different solvents the relative stability of both forms could change, leading to different isomers ratio in the equilibrium. Therefore, polar solvents as methanol will stabilize the zwitter-ionic form, favoring the formation of the cyclopentenone.

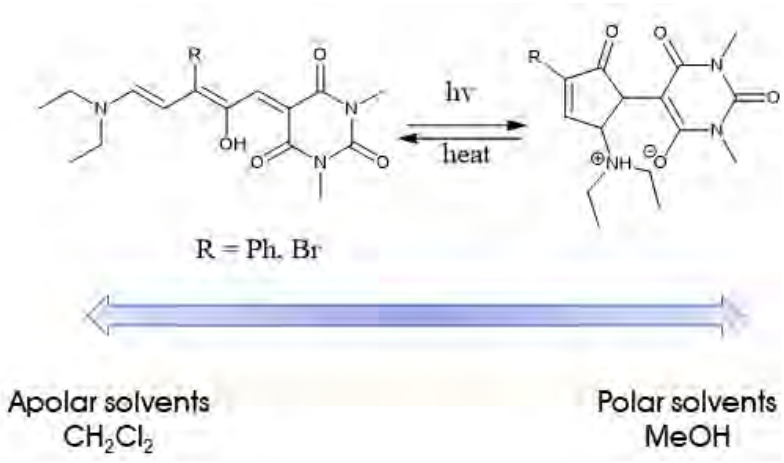

Figure 7.15. Photoswitching mechanism and solvent dependence of DASAs based molecular switches.

As we can see, the triene is a push-pull system which has an extended conjugation, due to these facts, it absorbs in the near IR-region as it was showed in the previous section. In contrast, the conjugation extent of cyclopentenone is much lower, so it is expected to present absorption in the UV-region. Therefore, this process could be monitored by UV-Vis spectroscopy, since two totally distinct bands are expected.

4.1. Irradiation of new DASAs-based molecular switches.

So, in first place a 5E-5 M solution of **5** was prepared and placed in a quartz cuvette with a magnetic stirrer. The irradiation was carried out by using a monochromator, moreover the temperature was controlled at 20ºC. The irradiation source used was centered in the wavelength of maximum absorbance of **29** (610 nm) (Figure 7.16).

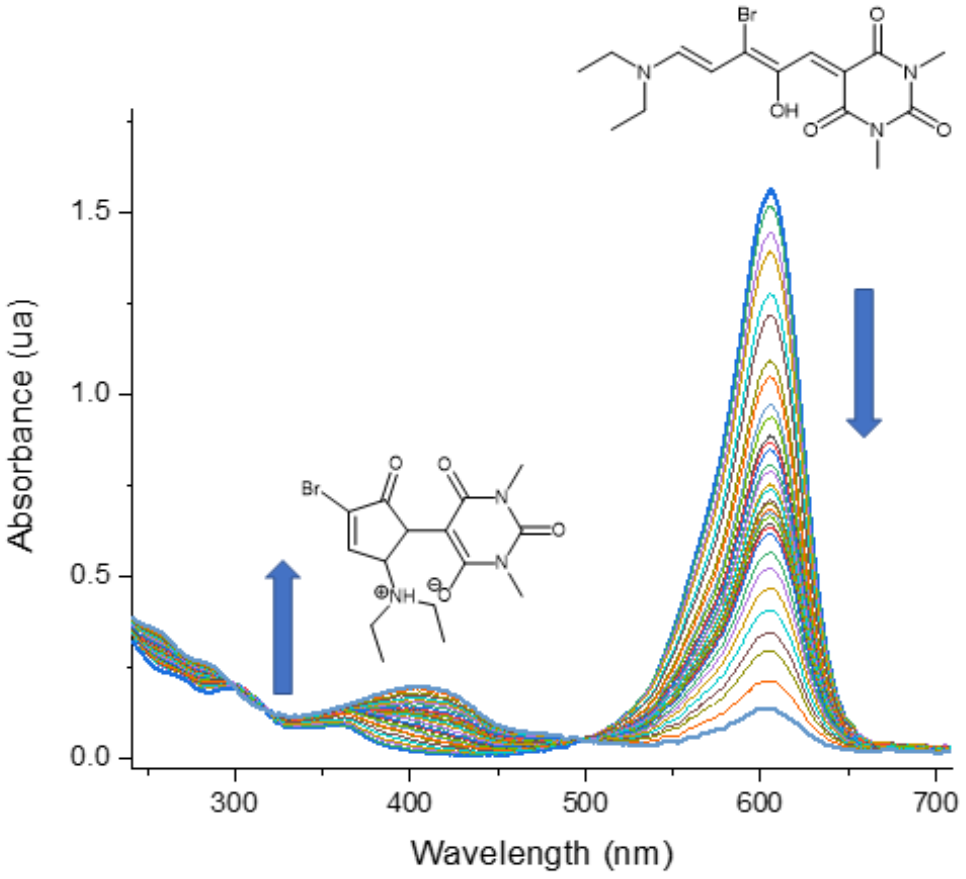

Figure 7.16. Irradiation of **29** followed by UV-Vis spectroscopy.

As it is shown in Figure 7.16, when **29** was irradiated, the UV-Vis absorption band related to the triene was decreasing throughout the irradiation. On the contrary, the absorption band of the cyclopentenone was increasing, which was placed in the range from 250 to 300 nm. Moreover, thanks to the difference between the absorption bands of both isomers, the conversion could be quantitative after 4 hours of irradiation.

As it has been demonstrated, the methodology used to monitor the photochemical process involving DASAs analogues was very convenient. This process could be reverted heating the mixture in toluene at 80°C.

Then, the same experiment was performed for other derivatives based on DASAs analogues changing the irradiation wavelength. When **33** was under the exposure of irradiation centered at 750 nm, the same photochemical process occurred, leading to the formation of the cyclopentenone (Figure 7.17).

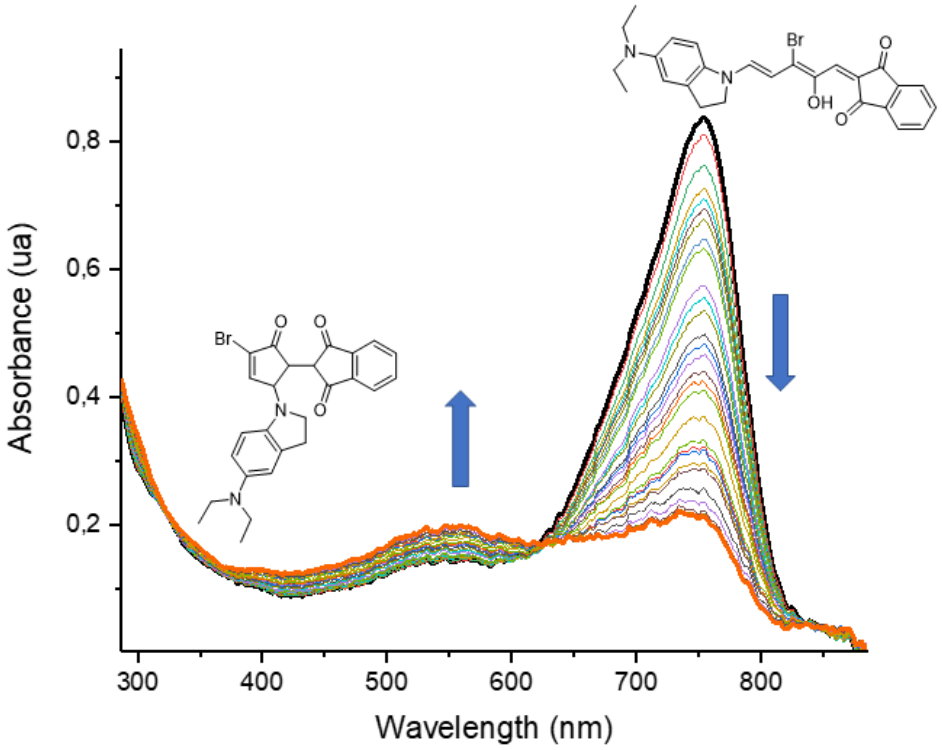

Figure 7.17. Irradiation of **33** followed by UV-Vis spectroscopy.

As it is observed, the same result was found for **33** and **29** when they were irradiated at the appropriate wavelength.

Then, it was also checked what happens in case of presenting a phenyl group in the unsaturated chain such as compound **46**. For this purpose, a solution of **46** was prepared and placed in a quartz cuvette to be irradiated by using a monochromator at 588 nm (Figure 7.18).

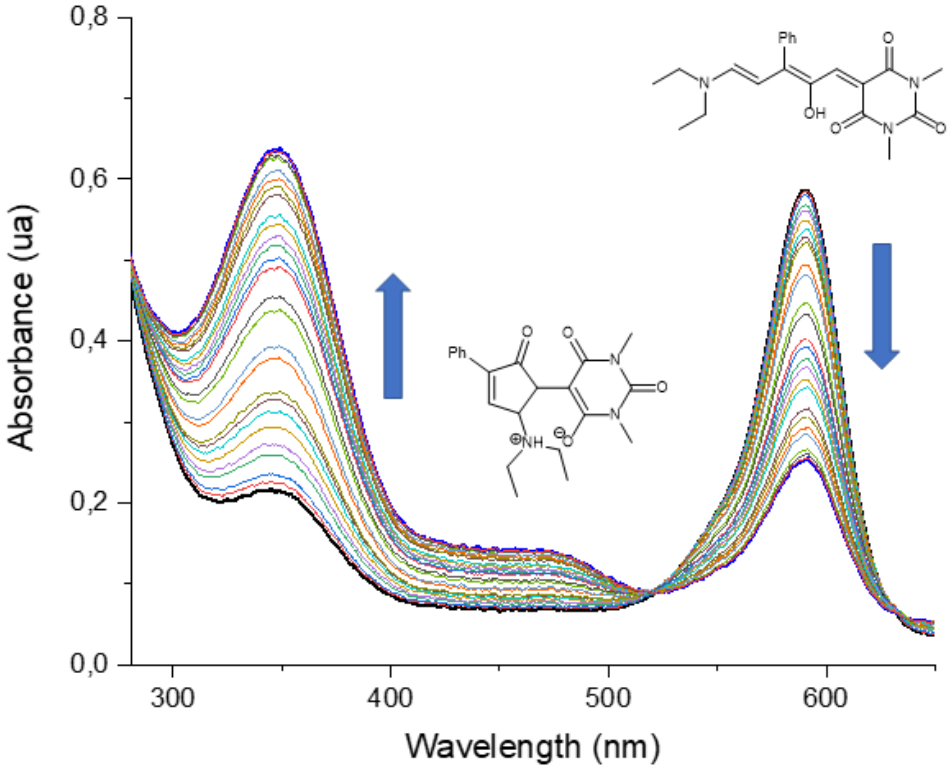

Figure 7.18. Irradiation of **46** followed by UV-Vis spectroscopy.

As it has been demonstrated, independently of which substituent is in the unsaturated chain, it does not prevent the photochemical process. Therefore, it was a good strategy to put a substituent in the chain since the same photoswitching process occurred using a longer irradiation wavelength. It was demonstrated that the same process took place using diheptylamine derivatives, as it can be observed in Figure 7.19 and 7.20.

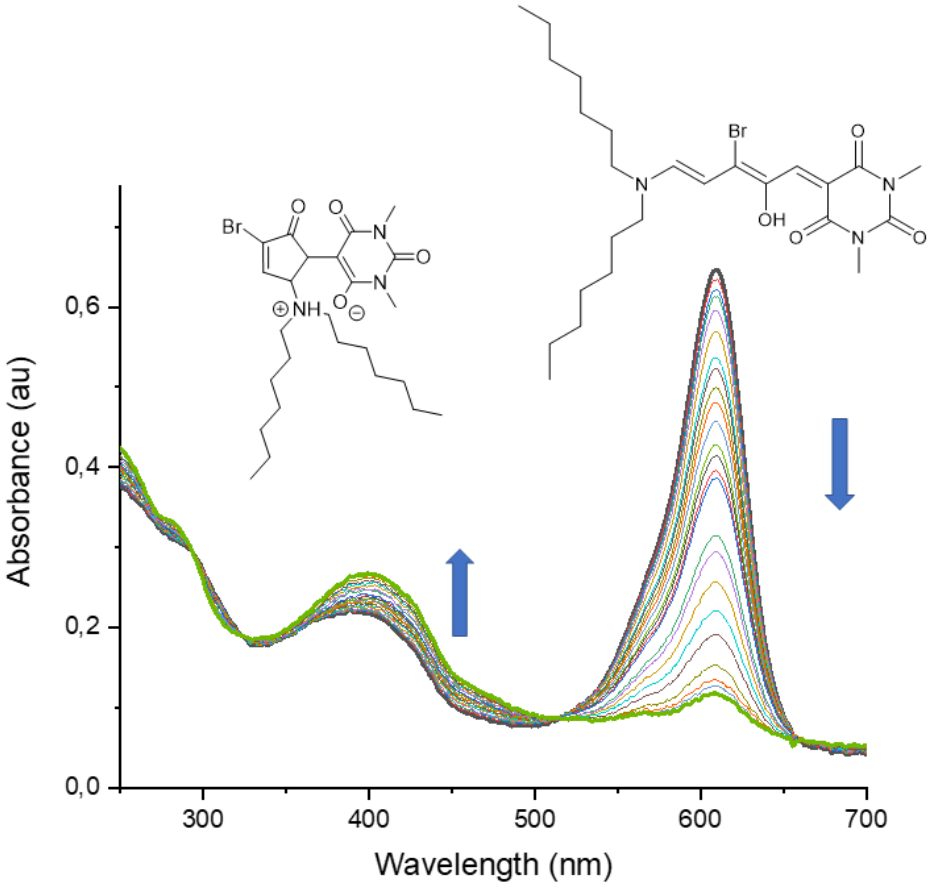

Figure 7.19. Irradiation of **29-hept** followed by UV-Vis spectroscopy.

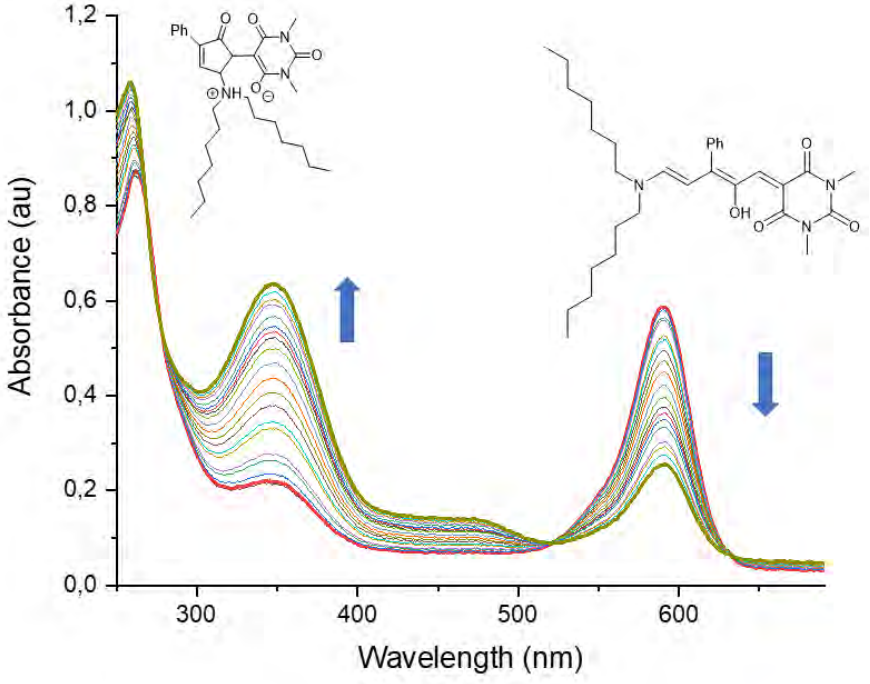

Figure 7.20. Irradiation of **46-hept** followed by UV-Vis spectroscopy.

4.2. Solvent dependence on the equilibrium.

As it was said before, due to the huge chemical difference in the structure of both isomers, the equilibrium could be easily modified by the solvent polarity. To check this effect, it was prepared a solution of **29** in CH_2Cl_2 (1.5 ml), and it was added 1.5 ml of MeOH. The experiment was carried out in darkness without irradiating the sample at 20ºC (Figure 7.21).

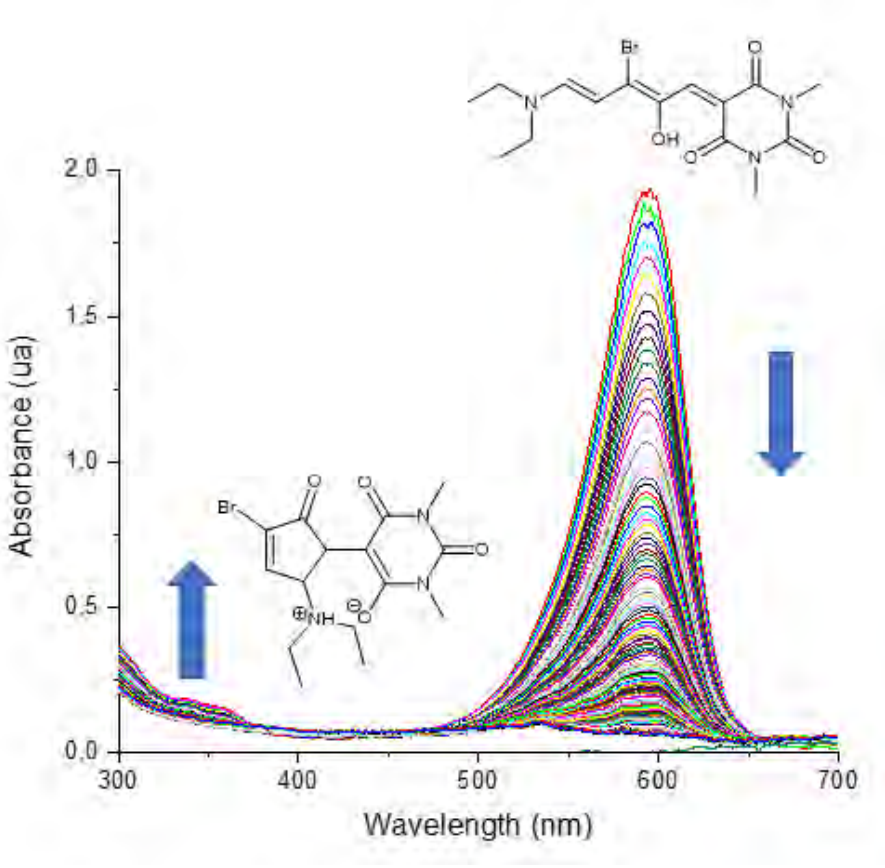

Figure 7.21. Thermal cyclization of **29** by adding MeOH.

In Figure 7.21 it is showed that the thermal switching adding MeOH was very efficient, since the triene isomer disappeared completely, displacing totally the equilibrium to the formation of the cyclopentenone. It should be noted that a main difference was addressed in UV-Vis spectra between the photoswitching process (Figure 7.16) and through the action of the solvent (Figure 7.21). When the sample was irradiated, an absorption band centered at 400 nm appeared, in contrast this band did not appear when MeOH was added. Therefore, it could be concluded that different mechanisms were responsible for the switching process in each case.

Moreover, this chemical process was very fast as it can be seen in Figure 7.22, in which it was monitored the absorption wavelength at 610 nm.

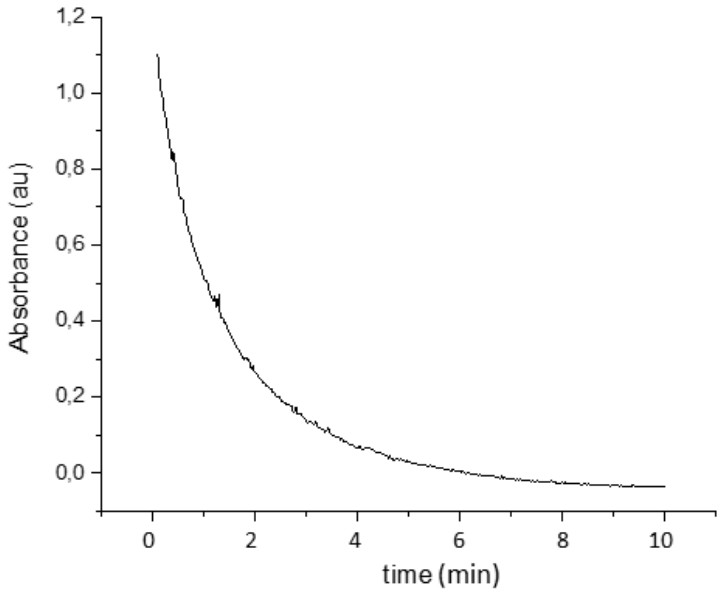

Figure 7.22. Absorbance change of **29** at 610 nm due to the addition of MeOH.

It should be noted that this work is still underway and new studies are needed to clarify the photoswitching mechanism. Moreover, new efforts are being applied to red-shift even more the absorption wavelength of these derivatives. For instance, this goal could be achieved by synthesizing new donor and acceptor moieties with improved properties or introducing new substituents in the bridge.

5. Experimental data.

5.1. General procedure to synthesize monobromide DASA-based photoswitches.

- Synthesis of 3-bromofuran-2-carbaldehyde (**41**)

3-Bromofuran (10 mmol, 0,899 ml) was dissolved in DMF, the resulting mixture was stirred in an ice-bath for 10 minutes. Then, it was added $POCl_3$ (10.5 mmol, 0,979 ml) dropwise without removing the ice-bath. The mixture was stirred at 0ºC for 1 hour. Then, the temperature was increased up to 80ºC. After this time, a solution of K_2CO_3 was added until the pH of the reaction was 9 approximately. This mixture was stirred during an additional hour. Once the reaction was finished, the solvent was removed under reduced pressure. Then, an extraction (Et_2O : H_2O) was performed and the organic fractions were collected and evaporated under reduced pressure to afford **41**, as a brown oil.

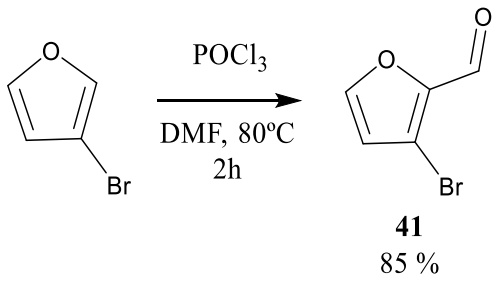

41
85 %

Scheme 7.13

- General procedure to afford the adduct by condensation.

The reaction between barbituric acid (3 mmol, 470 mg) and **41** (3.3 mmol, 580 mg) which were dissolved in water. The reaction took place at 70ºC for 2 hours. When the reaction was finished, the reaction was cooled at RT. Then, a solid appeared which was isolated by filtration. The product did not need further purification.

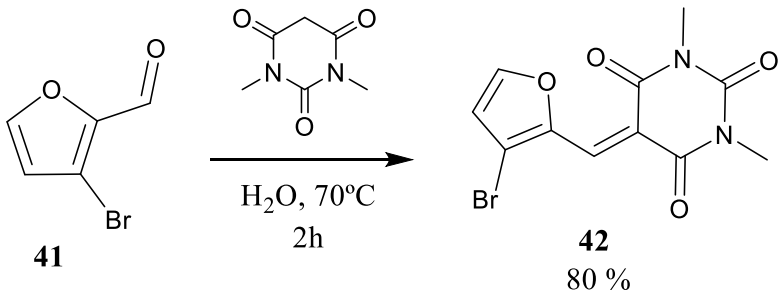

41 **42**
80 %

Scheme 7.14

Following the same steps, 1,3-indandione (1 mmol, 132 mg) was dissolved in water. To this solution, **41** (1.1 mmol, 175 mg) was added dropwise and then, the mixture was heated at 70ºC for 2 hours. The reaction was cooled at RT, and the resulting compound **43** was isolated without further purification.

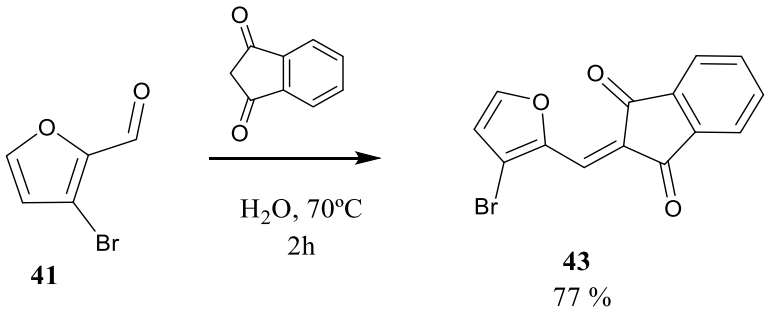

Scheme 7.15

5.2. General procedure to synthesize phenyl DASA-based molecular switches.

- Synthesis of 3-phenylfuran-2-carbaldehyde (**46**)

Compound **46** was afforded by using the previously synthesized compound (**41**) through a Suzuki reaction. For this purpose, **41** (1.91 mmol, 335 mg) was dissolved in 1,2-dimethoxyethane (DME) and, to this solution was added phenylboronic acid (7.64 mmol, 931 mg), tetrakistriphenylphosphine palladium (0) (0.382 mmol, 446 mg) and potassium carbonate (6.68 mmol, 474 mg). This mixture was under reflux for 48 hours. The reaction was monitored by TLC and when it was completed, the solvent was removed under reduced pressure. Then, the crude was extracted three times with (CH_2Cl_2:H_2O) and the organic fractions were collected. The solvent was removed and the pure compound **46** was afforded by column chromatography on silica gel using as eluent a mixture of hexane and ethyl acetate (4:1).

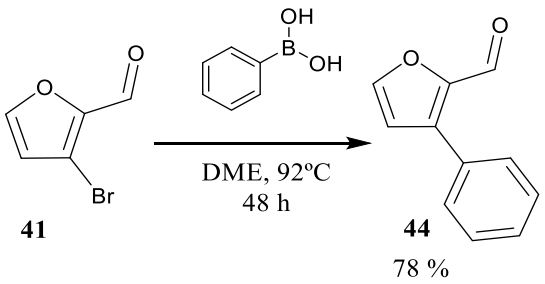

Scheme 7.16

- Condensation of the phenyl derivative (**44**) to afford the corresponding adduct (**45**).

The condensation of **44** (0.87 mmol, 150 mg) and barbituric acid (0.79 mmol, 101 mg) was performed. Both compounds were dissolved in water, and the reaction was heated at 70ºC for 2 hours. Then, the reaction was cooled at RT, and the resulting precipitate was filtrated. Compound **45** did not need further purification.

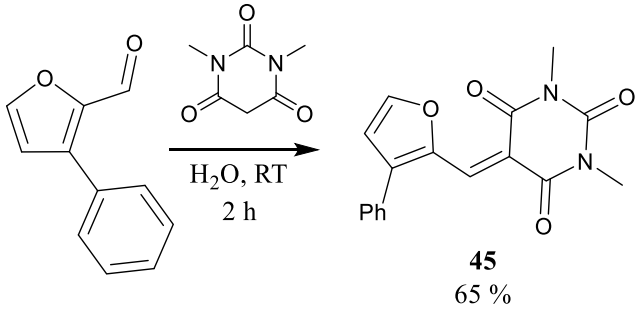

Scheme 7.17

5.3. General procedure of ring-opening of furans with an amine.

The methodology used to afford the ring-opening of the different adducts synthesized in this chapter (**42**, **43** and **45**) was done in the same way, independently of the adduct and the amine (diethylamine, diheptylamine or indoline) used. So, the adduct used (1 mmol) was dissolved in THF at 0ºC, then the corresponding amine (1.1 mmol) was added dropwise. Promptly, the solution changed its color from yellow to blue-purple. The reaction was stirred for an additional 30 minutes. This way, this reaction lead to the formation of **29**, **30**, **33**, **46**, **47** and their corresponding analogues using diheptylamine.

5.4. Characterization data.

It should be noted the problems we had to characterize by NMR these compounds. Since, it was not possible to record the NMR spectra of any derivative with diethylamine, although they were verified by mass spectroscopy and the corresponding UV-Vis spectrum featured just one absorption band. On the contrary, the compounds with diheptylamine were possible to record its NMR spectra, but just the cycled form in MeOH. It should be noted that compound **30-hept** could not be isolated pure, so their NMR spectra were not recorded.

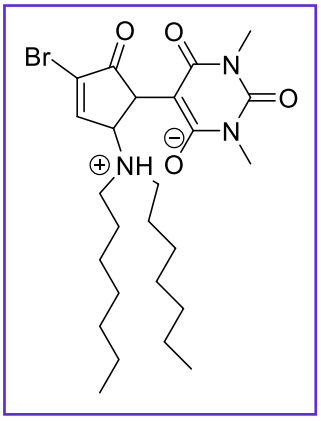

5-(3-bromo-5-(diheptylammonio)-2-oxocyclopent-3-en-1-yl)-1,3-dimethyl-2,6-dioxo-1,2,3,6-tetrahydropyrimidin-4-olate (**29-hept**)

Empiric formula: $C_{25}H_{40}N_3O_4Br$

Molecular weight: 526.51

Yield: 60%

^{1}H NMR (300 MHz, MeOD) δ 7.91 (d, J = 2.3 Hz, 1H), 4.81 (dd, J = 3.6 Hz, J = 2.3 Hz, 1H), 3.94 (d, J = 3.6 Hz, 1H), 3.23 (m, 10H), 1.66 (m, 4H), 1.29 (m, 16H), 0.90 (m, 6H).

^{13}C NMR (75 MHz, MeOD) δ (ppm) 198.64 (s), 164.88 (s), 154.62 (s), 151.32 (s), 132.75 (s), 85.30 (s), 67.83 (s), 45.34 (s), 32.71 (s), 32.67 (s), 29.89 (s), 29.80 (s), 28.08 (s), 27.53 (s), 27.42 (s), 27.33 (s), 23.56 (s), 14.38 (s).

UV-VIS (CH_2Cl_2): λ (nm) 610 (ε = 15768 $M^{-1}cm^{-1}$).

EM-ES (+): calcd for $C_{25}H_{41}N_3O_4Br$ $[M+H]^+$ 526.2275, found 526.2273.

Observations: Violet solid.

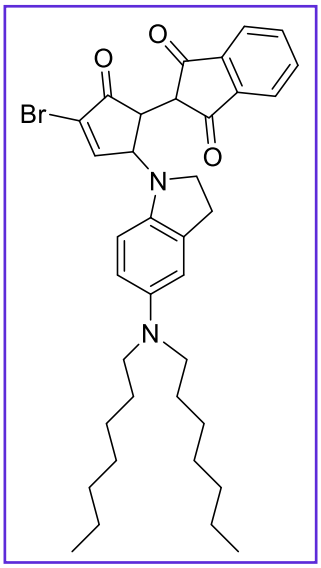

2-(3-bromo-5-(5-(diheptylamino)indolin-1-yl)-2-oxocyclopent-3-en-1-yl)-1H-indene-1,3(2H)-dione (**33-hept**)

Empiric formula: $C_{36}H_{45}BrN_2O_3$

Molecular weight: 633.67

Yield: 50%

^{1}H NMR (300 MHz, Methanol-d_4) δ 8.07 (d, *J* = 7.9 Hz, 1H), 8.01 (dd, *J* = 6.7, 1.8 Hz, 1H), 7.97 (s, 1H), 7.92 (s, 2H), 7.25 (s, 1H), 6.96 (s, 1H), 6.47 (d, *J* = 8.6 Hz, 1H), 5.30 (s, 1H), 3.75 (s, 1H), 3.70 (s, 1H), 3.51 (s, 6H), 3.14 (s, 2H), 1.51 (s, 4H), 1.29 (s, 16H), 0.90 (s, 6H).

^{13}C NMR (75 MHz, Methanol-d_4) δ 200.5, 199.2, 198.0, 162.1, 152.9, 144.0, 143.1, 137.3, 137.0, 134.5, 128.8, 126.9, 124.3, 123.9, 122.8, 119.1, 107.5, 60.3, 60.1, 47.3, 32.6, 29.8, 28.8, 27.2, 26.2, 23.5, 14.3.

UV-VIS (CH_2Cl_2): λ (nm) 750 (ε = 15033 $M^{-1}cm^{-1}$).

EM-ES (+): calcd for $C_{36}H_{46}BrN_2O_3$ $[M+H]^+$ 633.2692, found 633.2686.

Observations: Blue solid.

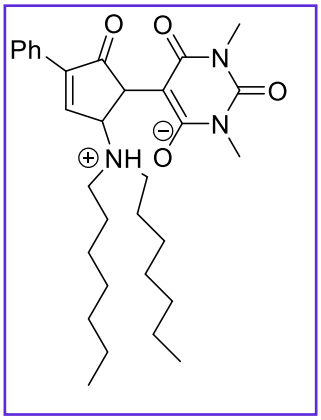

5-(5-(diheptylammonio)-2-oxo-3-phenylcyclopent-3-en-1-yl)-1,3-dimethyl-2,6-dioxo-1,2,3,6-tetrahydropyrimidin-4-olate (**46-hept**)

Empiric formula: $C_{31}H_{45}N_3O_4$

Molecular weight: 523.72

Yield: 60%

^{1}H NMR (300 MHz, Methanol-d_4) δ 7.84 (d, J = 7.7 Hz, 2H), 7.77 (s, 1H), 7.42 (d, J = 6.9 Hz, 3H), 4.93 (s, 1H), 3.99 (d, J = 3.9 Hz, 1H), 3.27 (s, 10H), 1.70 (s, 4H), 1.28 (s, 16H), 0.89 (s, 6H).

^{13}C NMR (75 MHz, Methanol-d_4) δ 204.2, 165.2, 154.7, 148.5, 146.8, 131.9, 130.6, 129.5, 128.9, 86.0, 66.7, 52.7, 49.9, 47.9, 32.7, 29.8, 28.4, 27.5, 25.8, 23.6, 14.38.

UV-VIS (CH_2Cl_2): λ (nm) 590 (ε = 18040 $M^{-1}cm^{-1}$).

EM-ES (+): calcd for $C_{31}H_{46}N_3O_4$ $[M+H]^+$ 524.3488, found 524.3482.

Observations: Blue solid.

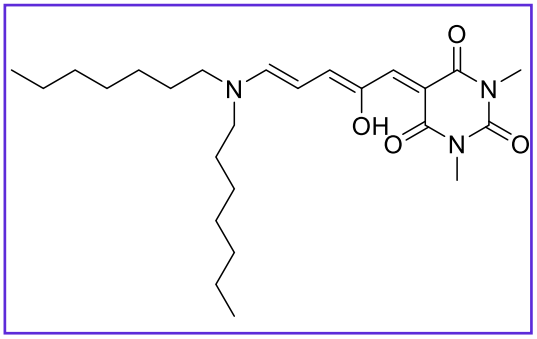

5-((2Z,4E)-5-(diheptylamino)-2-hydroxypenta-2,4-dien-1-ylidene)-1,3-dimethylpyrimidine-2,4,6(1H,3H,5H)-trione (**47-hept**)

Empiric formula: $C_{25}H_{41}N_3O_4$

Molecular weight: 447.62

Yield: 83 %

^{1}H NMR (400 MHz, Chloroform-d) δ 12.55 (s, 1H), 7.17 (d, J = 17.2 Hz, 2H), 6.75 (s, 1H), 6.06 (s, 1H), 3.35 (s, 10H), 1.67 (s, 5H), 1.30 (s, 21H), 0,90 (m, 6H).

^{13}C NMR (101 MHz, Chloroform-*d*) δ 165.3, 163.5, 157.0, 152.1, 150.9, 146.7, 139.5, 102.8, 98.7, 57.8, 49.8, 31.8, 29.2, 29.0, 28.6, 26.6, 22.7, 14.2.

UV-VIS (CH_2Cl_2): λ (nm) 570 (ε = 19000 $M^{-1}cm^{-1}$).

EM-ES (+): calcd for $C_{25}H_{42}N_3O_4$ $[M+H]^+$ 448.3175, found 448.3170.

Observations: Violet solid.

8. Conclusions / Conclusiones.

In this doctoral thesis, four new families of photoswitches based on different chromophores such as hydantoin, PSB-retinal, metronidazole and DASAs have been studied. Moreover, it has been described the rational design of new prototypes based on these chromophores, as well as their synthesis, photochemical and photophysical properties. In detail, several conclusions can be drawn, which will be outlined separately by chapters.

Firstly, in the case of hydantoin based molecular switches, some conclusions can be outlined:

- A facile synthesis to afford new 5-arylidene-hydantoins derivatives was performed.
- It has been proved that the PSS can be controlled easily by means of external factors, such as the filters or the light source used during the irradiation.
- Noticeable advantages have been described over other photoswitches, as for example they could be completely turn *on* / *off* by light. Moreover, they showed an extraordinary photostability.
- Additionally, it has been found a methodology to compute correctly its properties before synthesizing them.
- Finally, as it has been demonstrated, the main features of these photoswitches make them good candidates to be applied in different applications.

Secondly, new studies to increase the knowledge on PSB-retinal photoswitches were carried out.

- The absorption wavelength was easily modified by increasing the conjugation extent or quaternizating the nitrogen atom present in the iminic bond. Through these modifications, the absorption band was red-shifted from UV to visible region.
- Different isomer mixtures in the PSS between neutral and quaternized derivates were obtained. Moreover, it was explored the switching behavior of both forms under direct and sensitized irradiation. It was found that the quaternized analogue did not isomerize under sensitized conditions, although the triplet-triplet energy transfer took place. This finding was proved by flash photolysis and computational calculations.

- By sensitized irradiation conditions, it was possible to red-shift the absorption band of **12** from 289 to 450 nm.

- Moreover, it was completed the attachment of a photoswitch based on PSB-retinal chromophore into a PAMP peptide fragment. It was performed the photoswitching study of the cross-linked peptide, as well as the biological study of both isomers. This study concluded that the PAMP fragment lost its activity when two cysteines were introduced into the peptide backbone, although the activity was recovered due to the fixation structure done by the photoswitch. Unfortunately, the activity could not be photocontrolled by the isomerization of the C=C double bond.

It has been reported the importance of photocontrolling the activity of biomolecules. For this purpose, new molecular switches based on metronidazole have been synthesized and several conclusions can be drawn from Chapter 6:

- They have been rationally modified to achieve compounds compatible with biological media, since the preparation of water-soluble compounds absorbing in the visible region was achieved.
- New molecular switches with improved cytotoxic activity were designed. Moreover, ***E*-24a** and its PSS showed quite different antitumoral activity and the IC_{50} of the photoisomer was high enough to kill efficiently tumoral cells.
- By using **24a**, the anticancer activity could be activated in a specific point irradiating it with visible light.

Finally, it has been presented an interesting study of new derivatives based on DASAs. From this study, some useful information can be extracted:

- First, a new strategy is presented to red-shift the absorption wavelength, which is based on the substitution of the unsaturated chain.

- Then, it was concluded by computational calculations that the bromine atom produced the biggest bathochromic shift of the absorption band.

- The synthesis of different derivatives with a bromine atom in its unsaturated chain was afforded, as well as their photophysical and photochemical study.

- It was achieved a new photoswitch whose absorption band was placed in the infrared region (*ca*. 750 nm).

- Finally, the equilibrium between the two forms was found to be very dependent on the polarity of the solvent.

En esta tesis doctoral se han estudiado cuatro nuevas familias de interruptores moleculares basados en distintos cromóforos: hidantoína, la base de Schiff protonada del retinal, metronidazol y DASAs. Además, se ha descrito el diseño racional de nuevos derivados basados en estos cromóforos, así como su síntesis y el estudio de sus propiedades fotofísicas / fotoquímicas. Concretamente, se han podido extraer varias conclusiones de esta tesis doctoral, las cuales se expondrán por capítulos.

En primer lugar, tras el estudio de interruptores moleculares basados en la hidantoína, varias conclusiones pueden establecerse:

- Los derivados fueron sintetizados fácilmente siguiendo dos rutas sintéticas.
- Se comprobó que el estado fotoestacionario de estos interruptores moleculares puede ser controlado fácilmente mediante factores externos, como por ejemplo a través del uso de distintos filtros o fuentes de irradiación.
- Asimismo, se han conseguido grandes ventajas con respecto a otros interruptores, ya que se pudo obtener cuantitativamente el isómero menos estable tras la irradiación del isómero *E*. Además, todos los derivados mostraron una gran fotoestabilidad.
- Se ha descrito una metodología capaz de predecir correctamente las propiedades fotofísicas y fotoquímicas de estos derivados.
- Finalmente, como se ha demostrado, las buenas propiedades de estos interruptores moleculares permiten que sean buenos candidatos para su uso en distintas aplicaciones.

En segundo lugar, se han sintetizado nuevos interruptores moleculares basados en la PSB-retinal.

- La longitud de onda de absorción de estos derivados se modificó aumentando la conjugación del sistema, o cuaternizando el nitrógeno de la imina. A través de estas modificaciones, la longitud de onda de absorción se desplazó desde el ultravioleta al visible.
- Se alcanzaron distintas mezclas de isómeros en el estado fotoestacionario entre los derivados neutros y cuaternizados. Además, se estudió la fotoisomerización bajo distintas condiciones de irradiación (directa y sensibilizada). Se comprobó que la fotoisomerización del derivado cuaternizado no se daba bajo condiciones de irradiación sensibilizada, aunque la transferencia de energía triplete-triplete se produjese. Este hecho se comprobó mediante fotólisis de destello láser y cálculos teóricos.

- Gracias a la irradiación sensibilizada, se desplazó la longitud de onda de absorción efectiva de **12** desde 289 a 450 nm.
- Además, se realizó el anclaje de **14** en un fragmento peptídico con actividad biológica (PAMP). Se realizó el estudio fotoquímico del péptido con el interruptor anclado, así como el estudio biológico de los isómeros *E* y *Z*. Este estudio concluyó que el fragmento de la PAMP perdía su actividad al introducir dos cisteínas en la secuencia peptídica, pero que la actividad se recuperaba cuando se anclaba el interruptor al péptido al fijar su estructura. Desafortunadamente, la actividad del péptido no pudo ser fotocontrolada mediante la isomerización del doble enlace del interruptor.

En cuanto al capítulo 6, se sintetizaron nuevos interruptores moleculares basados en el metronidazol, de los cuales se han obtenido varias conclusiones tras su estudio.

- Estos derivados han sido modificados para ser compatibles con medios biológicos, ya que se logró la síntesis de derivados solubles en agua y que absorbían luz visible.
- Se diseñaron nuevos interruptores moleculares con capacidad citotóxica. Además, ***E*-24a** y su estado fotoestacionario mostraron distinta actividad antitumoral, siendo el fotoisómero capaz de matar células cancerosas eficazmente.
- La actividad antitumoral del compuesto **24a** podría ser activada en un punto específico al ser irradiado con luz visible.

Finalmente, se han estudiado otro tipo de interruptores moleculares basados en los DASAs.

- En primer lugar, se ha llevado a cabo una nueva estrategia para desplazar al rojo la banda de absorción. Esta estrategia se basó en la sustitución con distintos grupos la cadena insaturada.
- Se concluyó, mediante cálculos computacionales y experimentalmente que el átomo de bromo producía el mayor desplazamiento de la banda de absorción.
- Se realizó la síntesis de nuevos derivados con un átomo de bromo en la cadena insaturada, así como el estudio de sus propiedades fotofísicas y fotoquímicas.
- Se llevó a cabo la síntesis de un derivado cuya absorción se centró en el infrarrojo (aproximadamente a 750 nm).

- Se concluyó que el equilibrio entre las dos formas era muy dependiente de la polaridad del disolvente.

The research work showed along this PhD. Thesis has been published in different journals:

CHAPTER 4:

- Martínez-López, D.; Yu, M.-L.; García-Iriepa, C.; Campos, P. J.; Frutos, L. M.; Golen, J. A.; Rasapalli, S.; Sampedro, D., Hydantoin-Based Molecular Photoswitches *J. Org. Chem.* **2015,** *80*, 3929-3939.

CHAPTER 5:

- Blanco-Lomas, M.; Martinez-Lopez, D.; J. Campos, P.; Sampedro, D., Tuning of the properties of Rhodopsin-based molecular switches *Tetrahedron Lett.* **2014,** *55,* 3361-3394.
- Martínez-López, D.; Blanco-Lomas, M.; Campos, P. J.; Sampedro, D., Visible light sensitized isomerization of rhodopsin-based molecular switches *Tetrahedron Lett.* **2015,** *56*, 1991-1993.

CHAPTER 6:

- Martínez-López, D.; García-Iriepa, C.; Piñeiro-Hermida, S.; López, I. P.; Fernández-Martínez, D.; Alfaro-Arnedo, E.; Pichel, J. G.; Campos, P. J.; Sampedro, D., Design and Synthesis of Metronidazole-Based Photoswitches With Potential Biological Applications *ChemPhotoChem* **2019***,* 3, 1-7.

CHAPTER 7:

- Martínez-López, D.; Marazzi M.; García-Iriepa, C.; Sampedro, D., Fourth-generation DASAs: Shifting the Absorption Toward the Infrared by π-bridge Substitution. *Submitted*.

OTHER PUBLICATIONS:

- Gutiérrez, S.; Martínez-López, D.; Morón, M.; Sucunza, D.; Sampedro, D.; Domingo, A.; Salgado, A.; Vaquero, J. J., Highly Fluorescent Green Fluorescent Protein Chromophore Analogues Made by Decorating the Imidazolone Ring *Chem. Eur. J.* **2015,** *21* (51), 18758-18763.
- García-Iriepa, C.; Gueye, M.; Léonard, J.; Martínez-López, D.; Campos, P. J.; Frutos, L. M.; Sampedro, D.; Marazzi, M., A biomimetic molecular switch at work: coupling photoisomerization dynamics to peptide structural rearrangement *Phys. Chem. Chem. Phys.* **2016,** *18* (9), 6742-6753.

- Contreras-García, E.; Martínez-López, D.; Alonso, C. A.; Lozano, C.; Torres, C.; Rodríguez, M. A.; Campos, P. J.; Sampedro, D., Optical Control of Antimicrobial Activity in Quinolone Derivatives *Eur. J. Org. Chem.* **2017,** *2017* (32), 4719-4725.

9. General comments and characterization techniques

1. General comments.

Solvents.

All solvents were distilled prior to use. Furthermore, certain solvents such as dichloromethane, diethyl ether, acetonitrile and tetrahydrofuran were distilled with the solvent purification system Pure solv^{tm} 4-MD.

Chromatography.

Thin Layer chromatography (TLC) was performed using Polygram Sil G/UV254 F_{254} plates (0,2mm silica gel layer with fluorescence indicator on pre-coated plastic sheets). Column chromatography was carried out with silica gel (230-240 mesh) as stationary phase. Mixtures of hexane/ethyl acetate were used as mobile phase.

2. Characterization techniques.

- Nuclear Magnetic Resonance.

^{1}H and ^{13}C spectra were recorded on a Bruker ARX-300 and/or a Bruker Avance 400 spectrometers. $CDCl_3$ has been used as the usual deuterated solvent with TMS as internal standard. Nevertheless, other solvents have been also used to measure the NMR spectra such as dimethyl sulfoxide, methanol and acetonitrile. Chemical shifts are given in ppm and coupling constants in hertz.

- UV-Vis.

Absorption molecular spectra were recorded on two distinct equipment:

  - HP-8453A UV-VIS-NIR diode array spectrophotometer (190-1100 nm).
  - HP 8451A diode array spectrophotometer (190-820 nm).

All the experiments were carried out in quartz cuvettes (1 cm path length).

- Electrospray-Mass Spectrometry.

Electrospray mass spectra were recorded on a HP 5989B mass spectrometer with an HP59987A interface in positive-ion mode. High resolution mass spectrometry was performed in a HP Bruker Microtof-Q with an Apollo II electrospray source in positive-ion mode.

- Luminescence.

All luminescence measures were recorded at room temperature with a Jobyn-Ybon Horiba Fluorolog 3-22 Tau-3 spectrofluorimeter. Data was analyzed with different versions of Origin program.

- X-Ray diffraction.

The crystals were mounted in inert oil on glass fibers and transferred to a Nonius Kappa CCD diffractometer equipped with an Oxford Instruments low-temperature attachment. Data were collected by monochromatic Mo Kα radiation (λ = 0.71073 Å). Scan type ωw and Φ. Absorption corrections: numerical (based on multiple scans).

- Laser Flash Photolysis.

The experiments were carried out using a Luzchem miniaturized Laser Flash Photolisys mLFP (LFP-111).

3. Lamps and photochemical techniques.

- Irradiation in a medium pressure Hg lamp.

All the irradiations were carried out in photochemical reactors with a 125-W medium pressure Hg lamp (Photochemical Reactors LTD (UK)). Furthermore, a Pyrex or quartz filter was used to perform the irradiation (Figure 8.1). The sample solution was placed in an immersion well reactor or a Pyrex/quartz NMR tube.

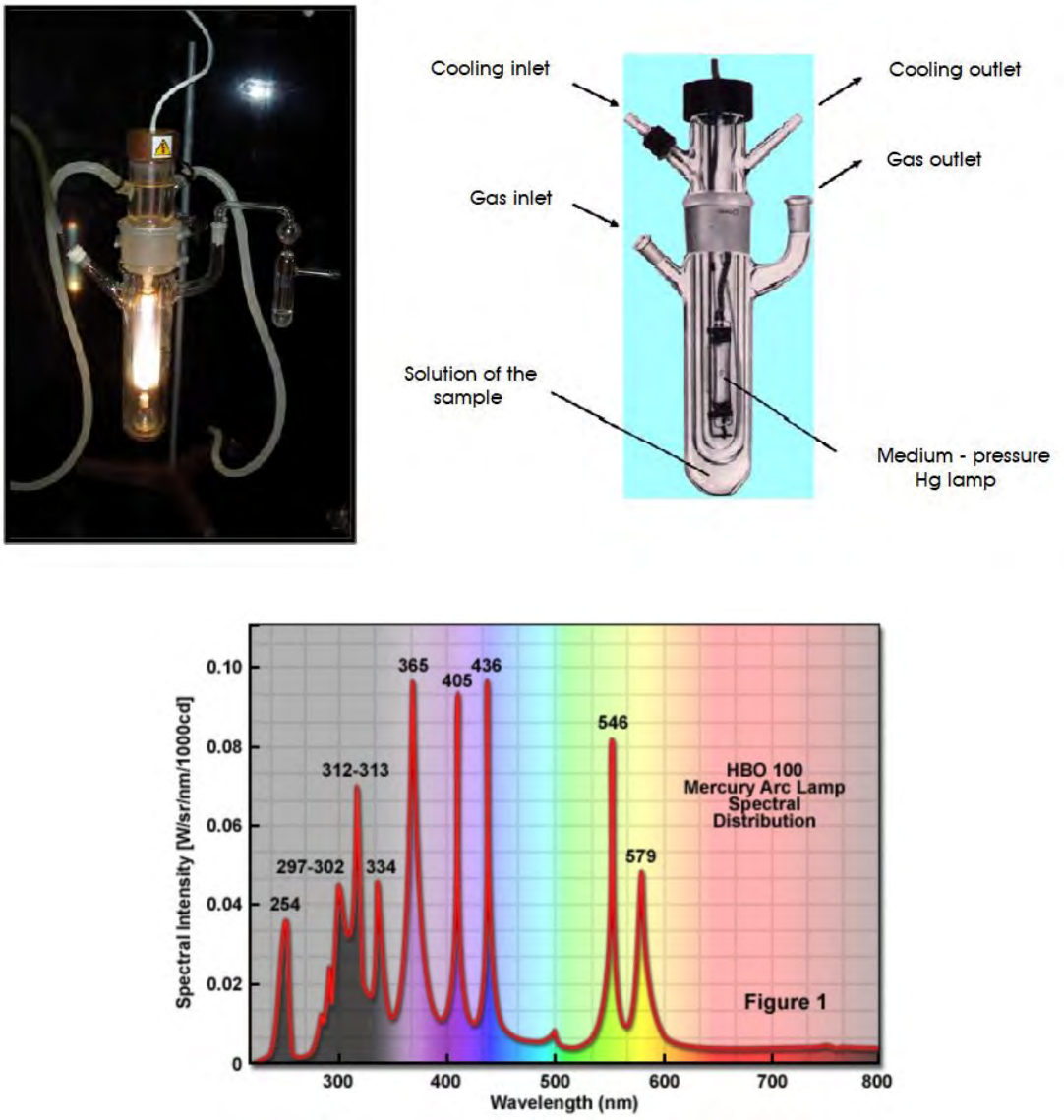

Figure 8.1. Lamps and photochemical reactors (top) and emission spectrum of a Hg lamp (bottom).[1]

- Photoreactor.

To produce the isomerization of hydantoin-based molecular switches, it was also used a Luzchem UV/Vis photoreactor (LZC-4, Figure X), provided with LZC-UVA lamps with emission wavelength centered at 350 nm (14 lamps x 8-W each lamp) (Figure 8.2).

[1] http://zeiss-campus.magnet.fsu.edu/articles/lightsources/mercuryarc.html

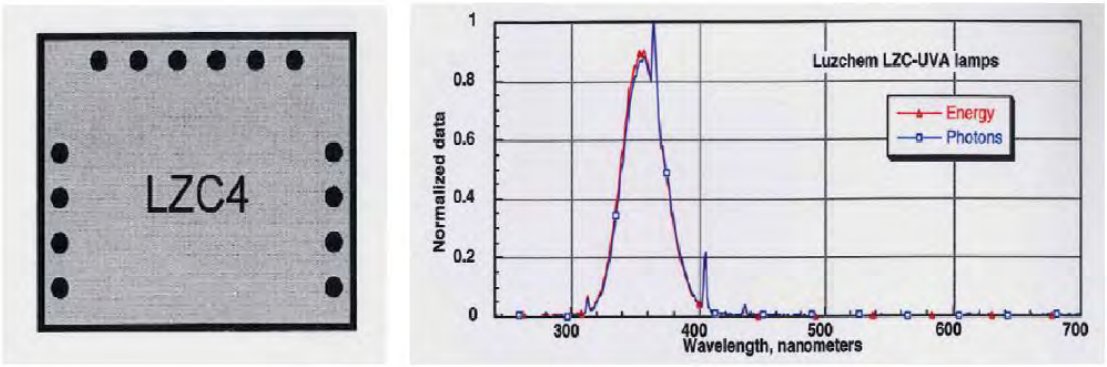

Figure 8.2. LZC4 UV/Vis photoreactor (left) and emission spectrum of LZC-UVA lamps (right).

- Selective irradiation by using a monochromator.

An oriel cornerstone 130 1/8m monochromator was used to generate monochromatic light (Figure 8.3), being the light source a 500 W Hg arc lamp in a proper lamp housing. The sample was placed in quatz cuvettes with a magnetic stirrer.

Figure 8.3. Oriel Cornerstone 130 1/8m monochromator.

APPENDIX A: Selected NMR spectra

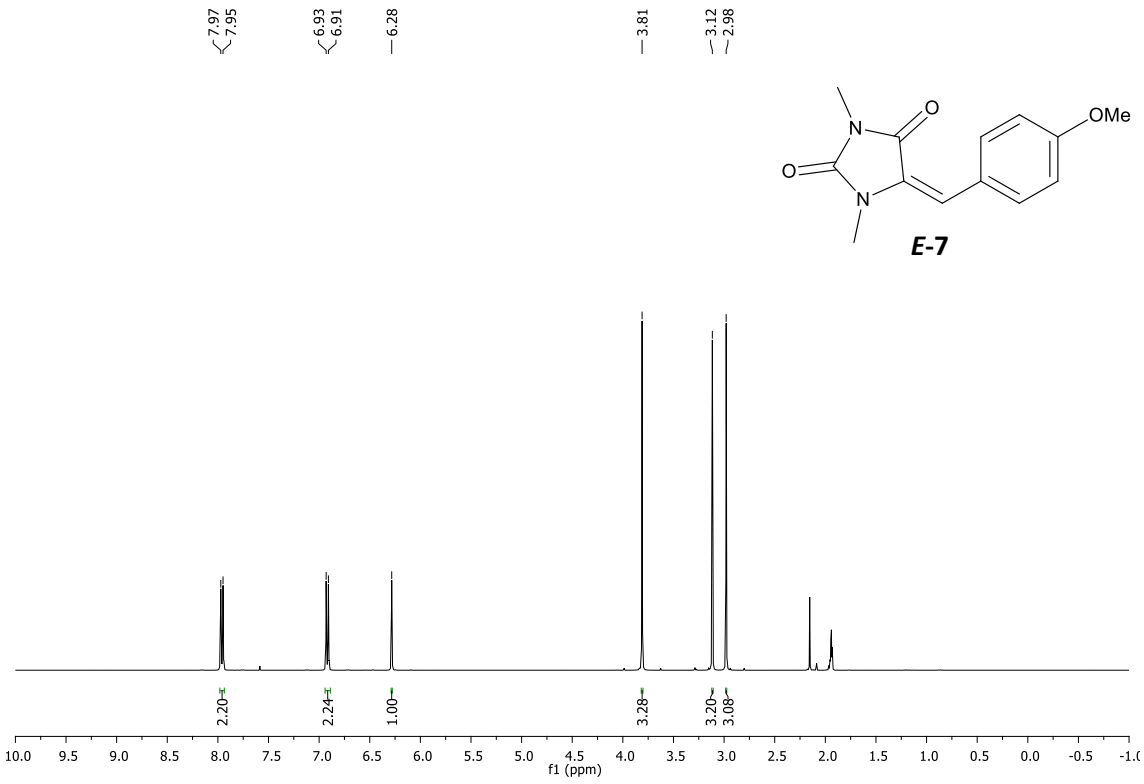
7.97
7.95
6.93
6.91
6.28
3.81
3.12
2.98
OMe
O
N
O
N
2.20
2.24
1.00
3.28
3.20
3.08
f1 (ppm)

***E*-7**

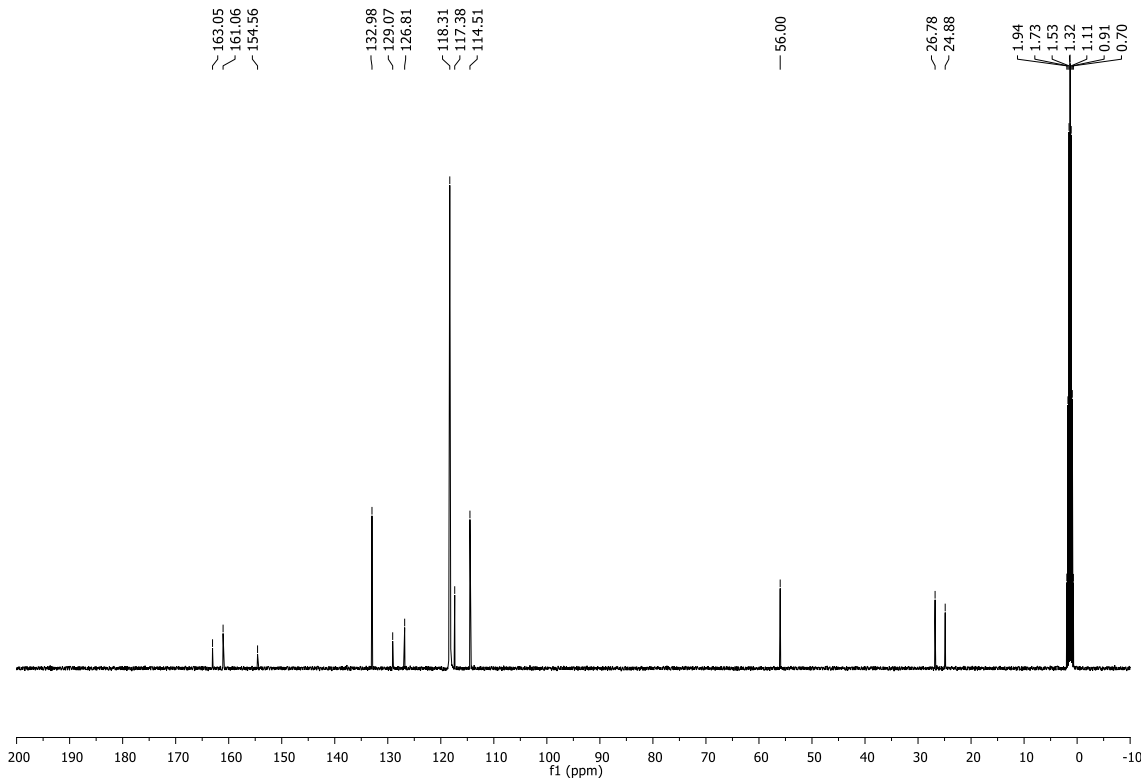
163.05
161.06
154.56
132.98
129.07
126.81
118.31
117.38
114.51
56.00
26.78
24.88
1.94
1.73
1.53
1.32
1.11
0.91
0.70
f1 (ppm)

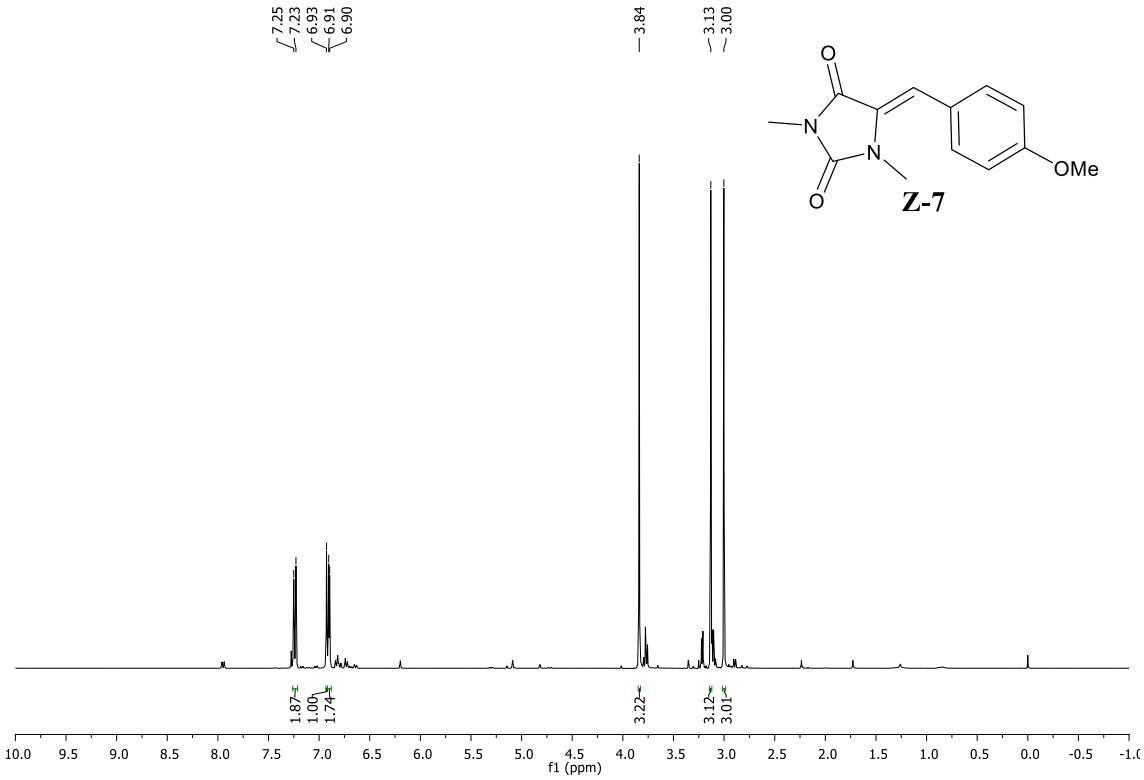
7.25
7.23
6.93
6.91
6.90
3.84
3.13
3.00
O
N
N
O
OMe
Z-7
1.87
1.00
1.74
3.22
3.12
3.01
10.0 9.5 9.0 8.5 8.0 7.5 7.0 6.5 6.0 5.5 5.0 4.5 4.0 3.5 3.0 2.5 2.0 1.5 1.0 0.5 0.0 -0.5
f1 (ppm)

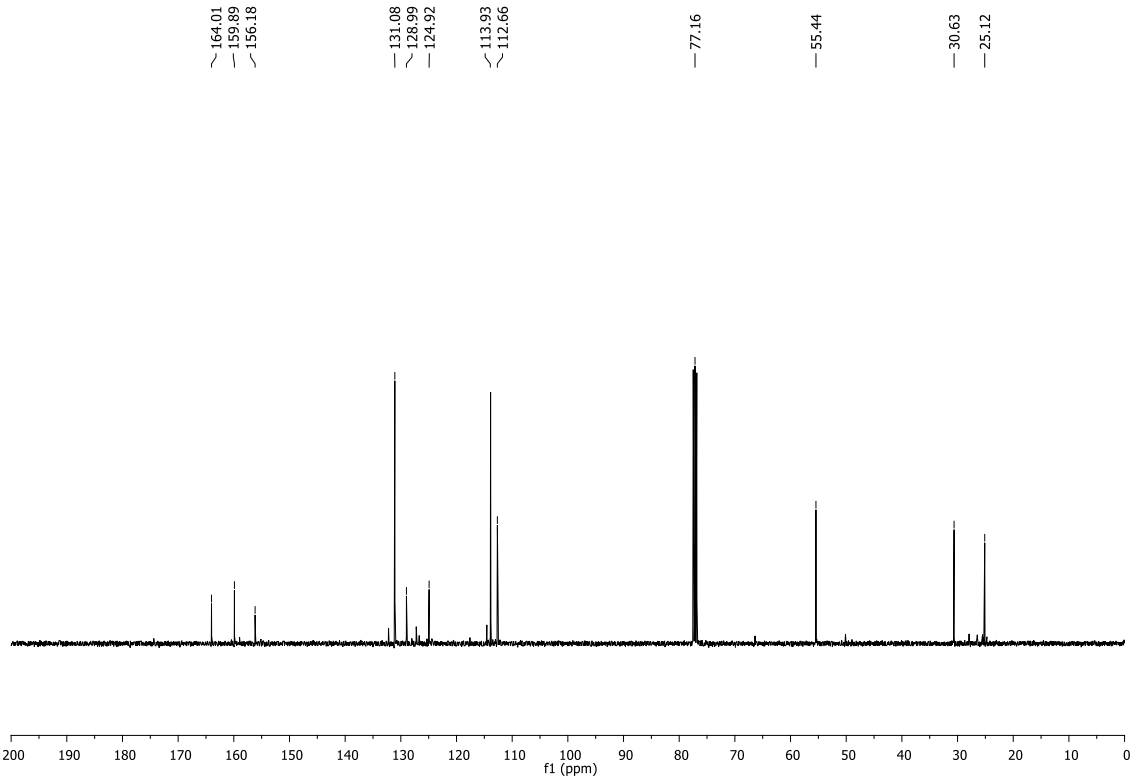
164.01
159.89
156.18
131.08
128.99
124.92
113.93
112.66
77.16
55.44
30.63
25.12
200 190 180 170 160 150 140 130 120 110 100 90 80 70 60 50 40 30 20 10 0
f1 (ppm)

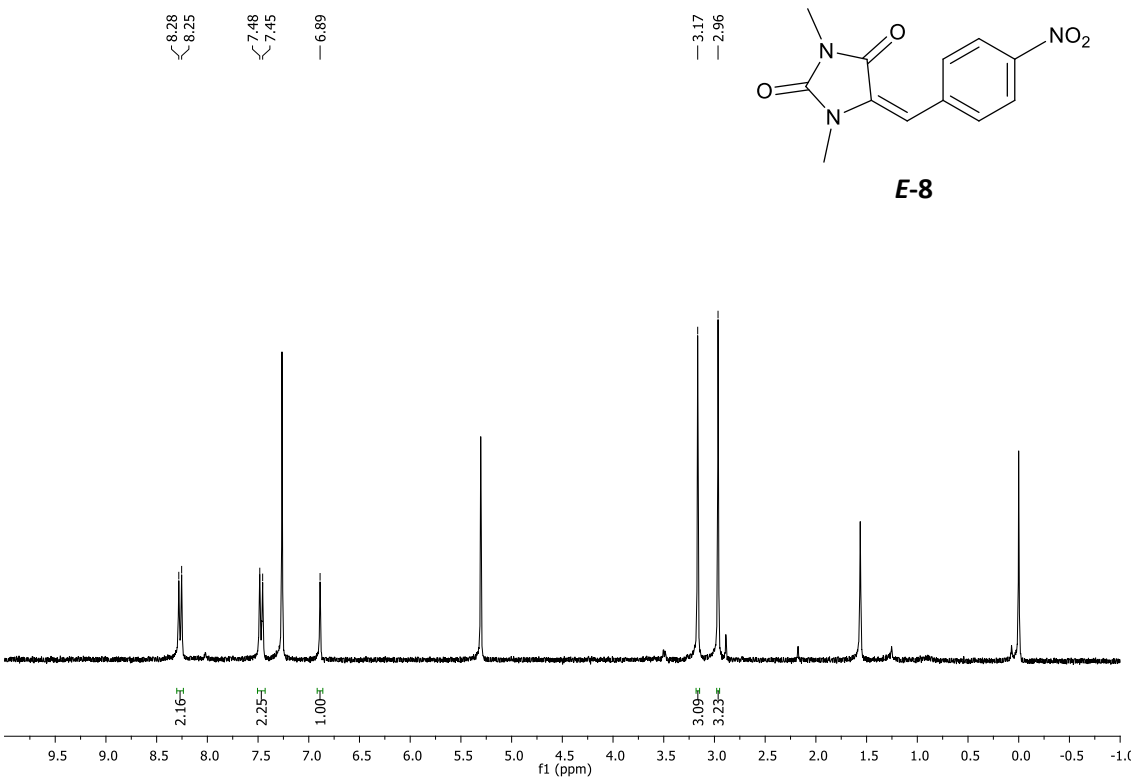
8.28
8.25
7.48
7.45
6.89
3.17
2.96
O
N
O
N
NO2
2.16
2.25
1.00
3.09
3.23
f1 (ppm)

***E*-8**

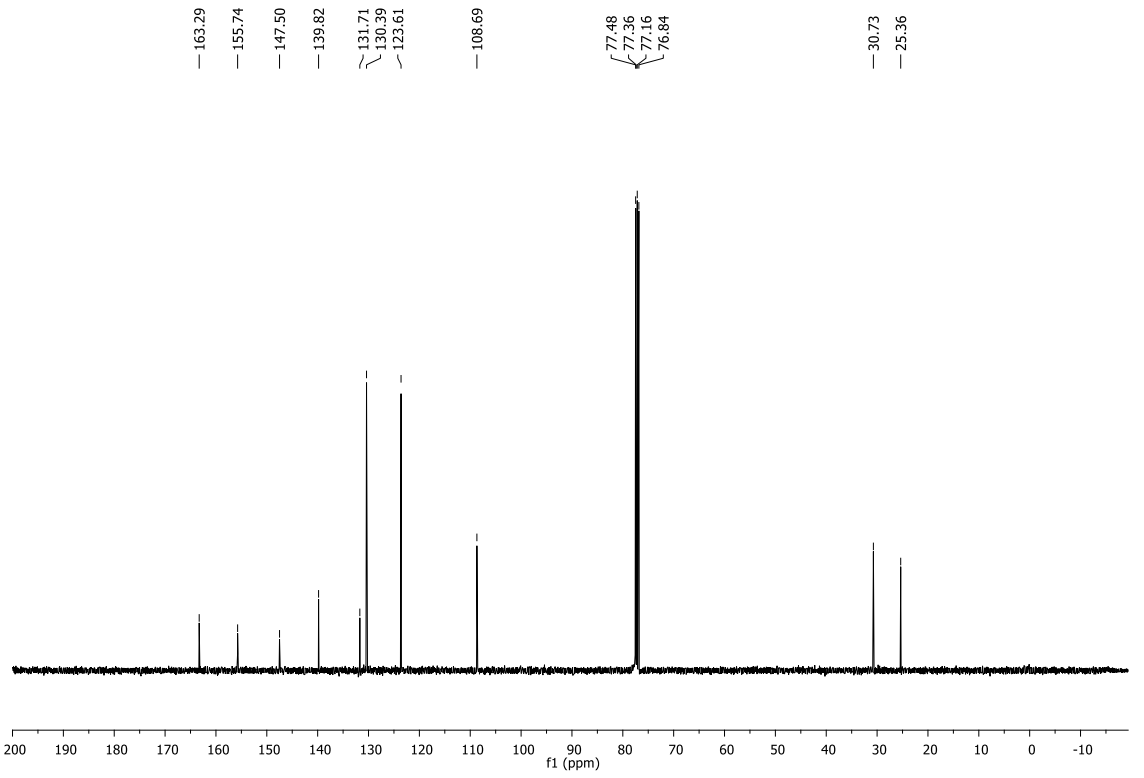
163.29
155.74
147.50
139.82
131.71
130.39
123.61
108.69
77.48
77.36
77.16
76.84
30.73
25.36
f1 (ppm)

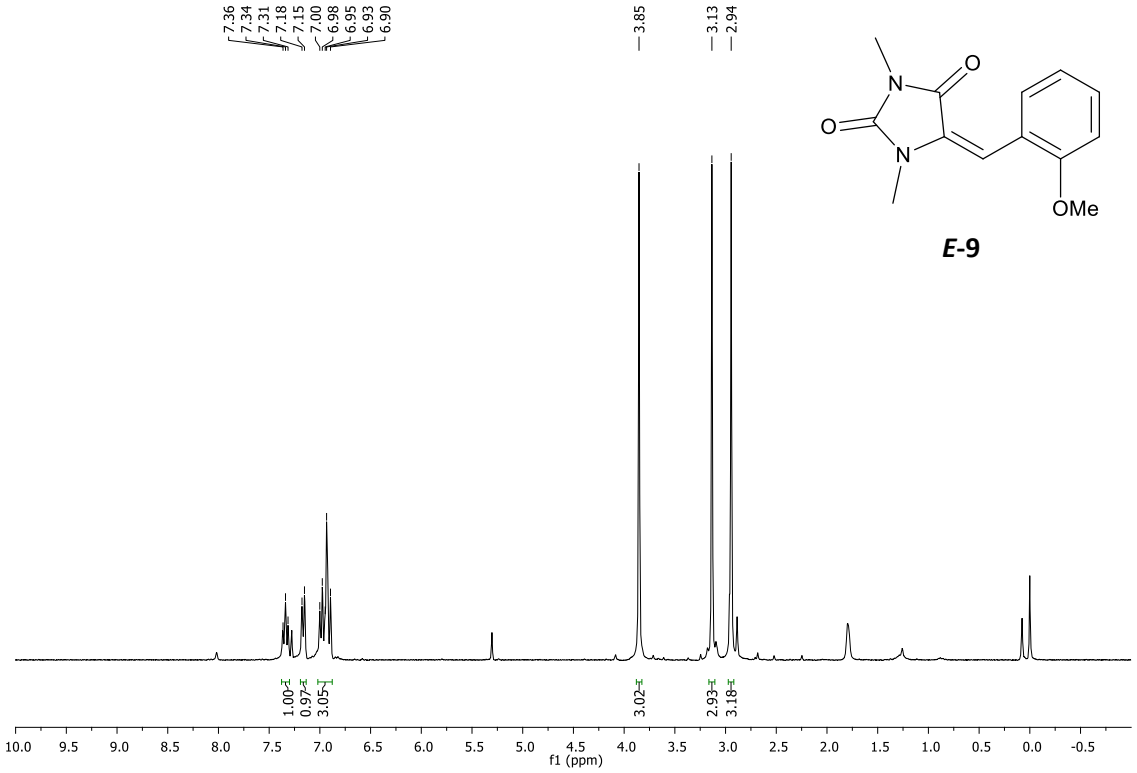
7.36
7.34
7.31
7.18
7.15
7.00
6.98
6.95
6.93
6.90
3.85
3.13
2.94
1.00
0.97
3.05
3.02
2.93
3.18
f1 (ppm)

N
O
O
N
OMe

***E*-9**

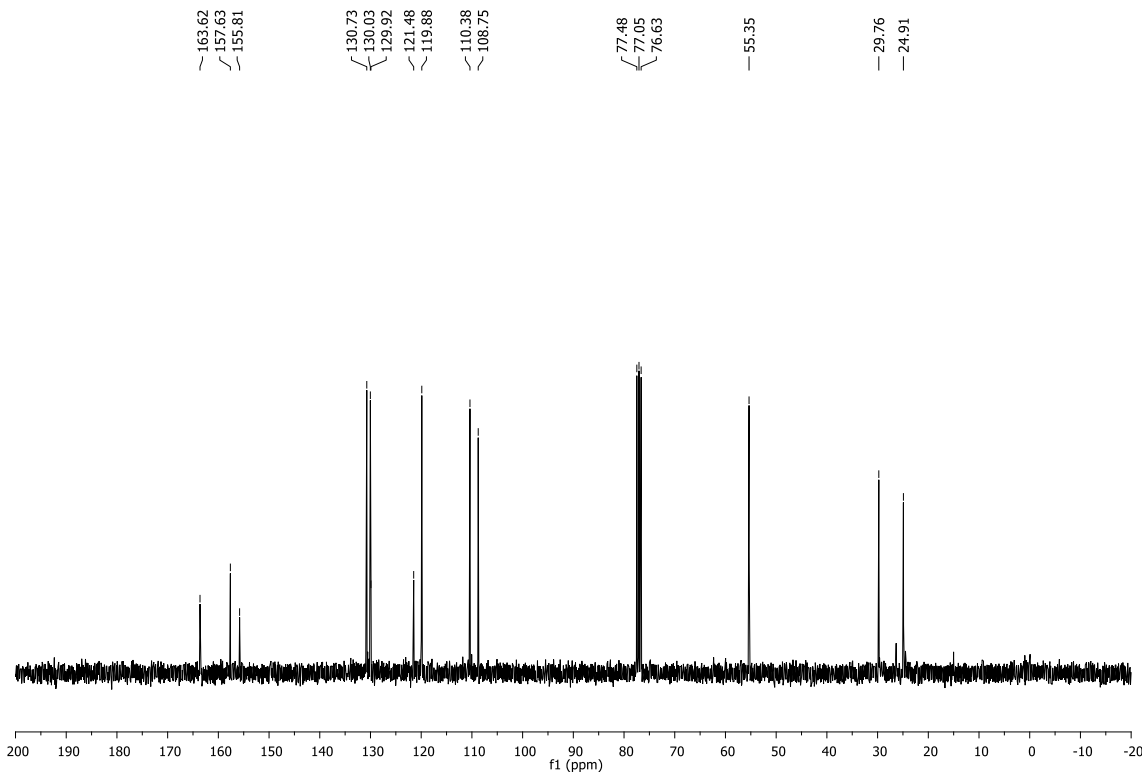
163.62
157.63
155.81
130.73
130.03
129.92
121.48
119.88
110.38
108.75
77.48
77.05
76.63
55.35
29.76
24.91
f1 (ppm)

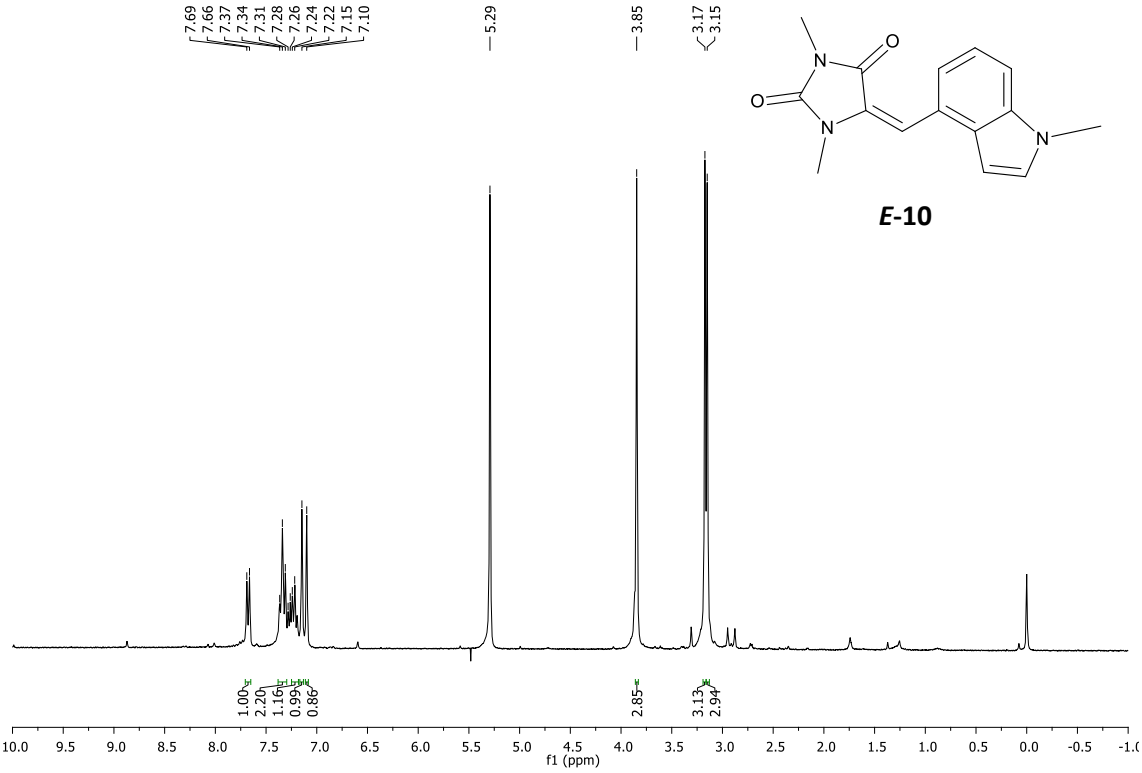
7.69
7.66
7.37
7.34
7.31
7.28
7.26
7.24
7.22
7.15
7.10
5.29
3.85
3.17
3.15
1.00
2.20
1.16
0.95
0.86
2.85
3.13
2.94
f1 (ppm)

***E*-10**

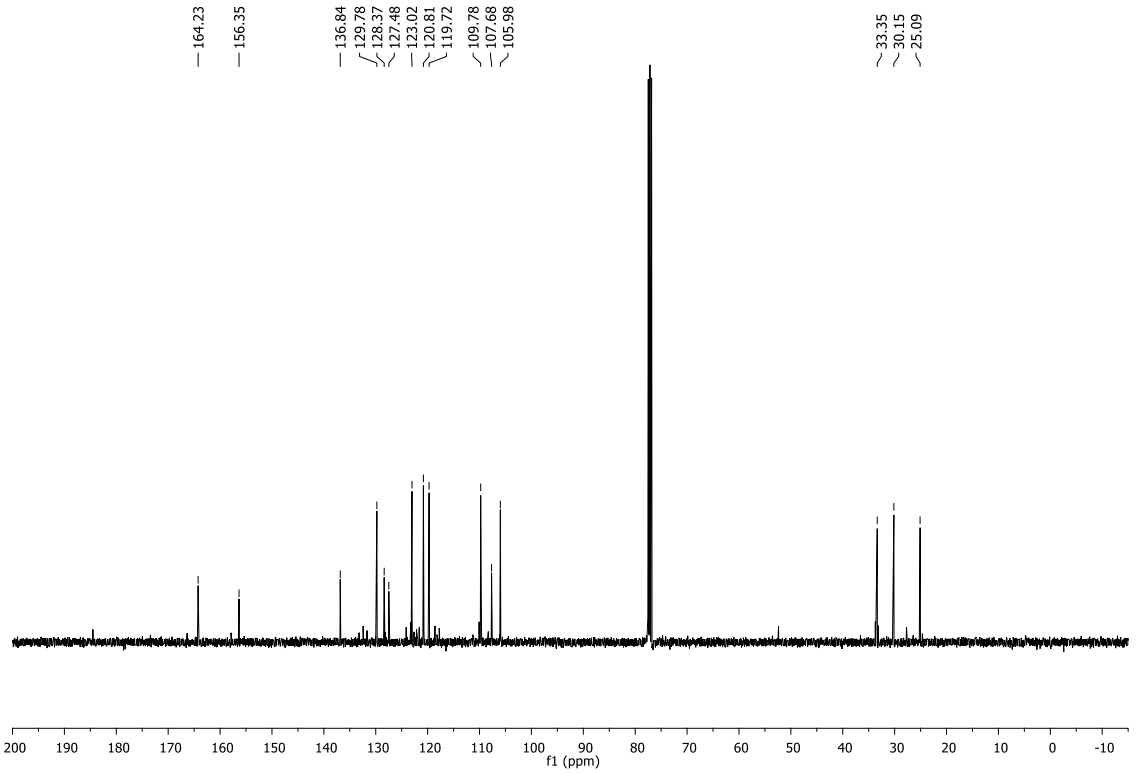
164.23
156.35
136.84
129.78
128.37
127.48
123.02
120.81
119.72
109.78
107.68
105.98
33.35
30.15
25.09
f1 (ppm)

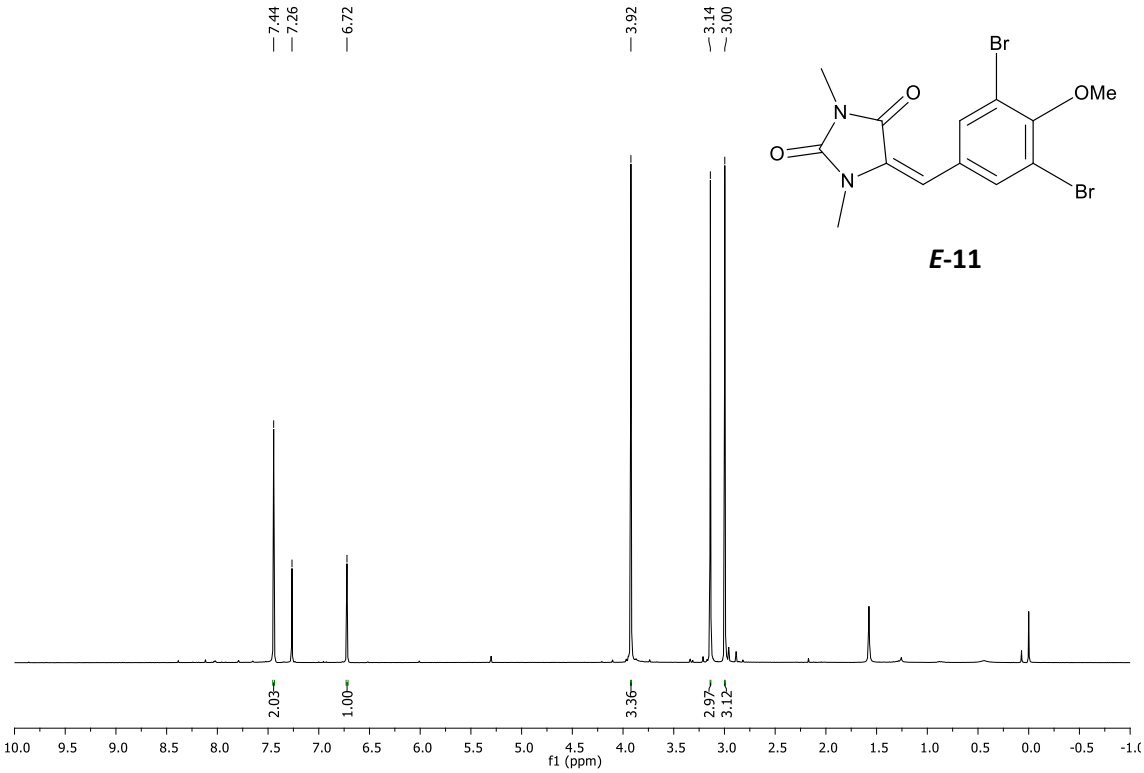
7.44
7.26
6.72
3.92
3.14
3.00
Br
OMe
Br
O
O
N
N
2.03
1.00
3.36
2.97
3.12
f1 (ppm)

***E*-11**

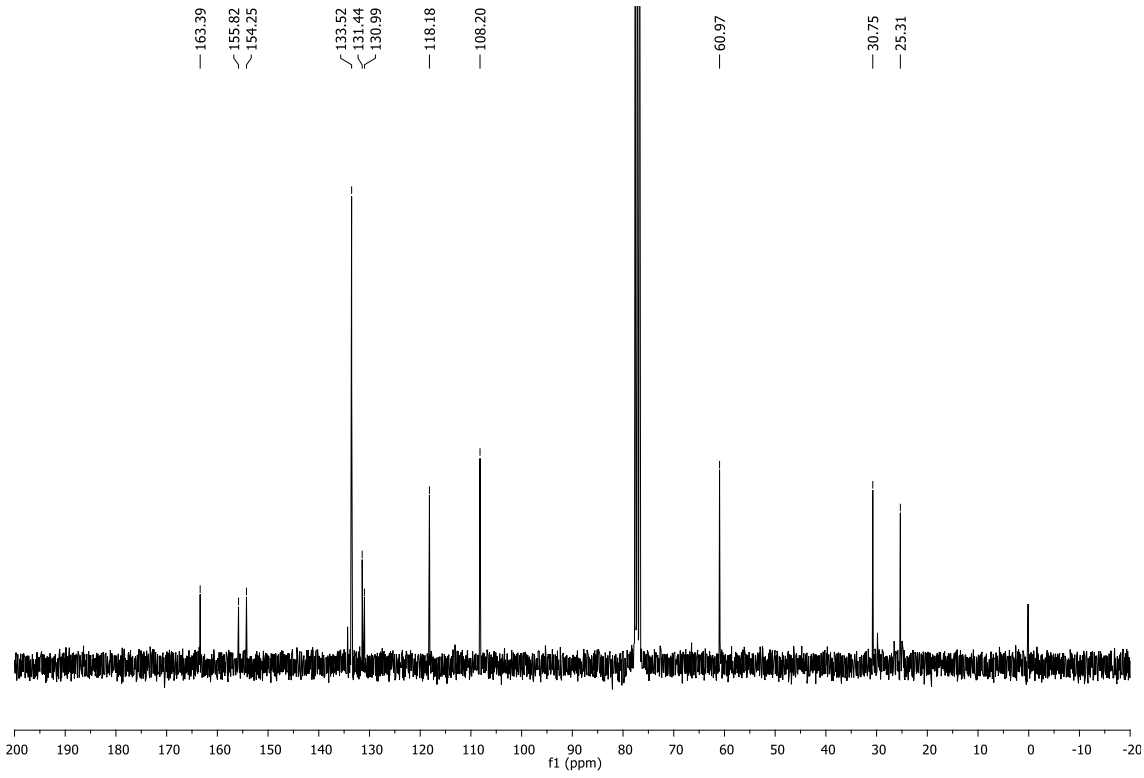
163.39
155.82
154.25
133.52
131.44
130.99
118.18
108.20
60.97
30.75
25.31
f1 (ppm)

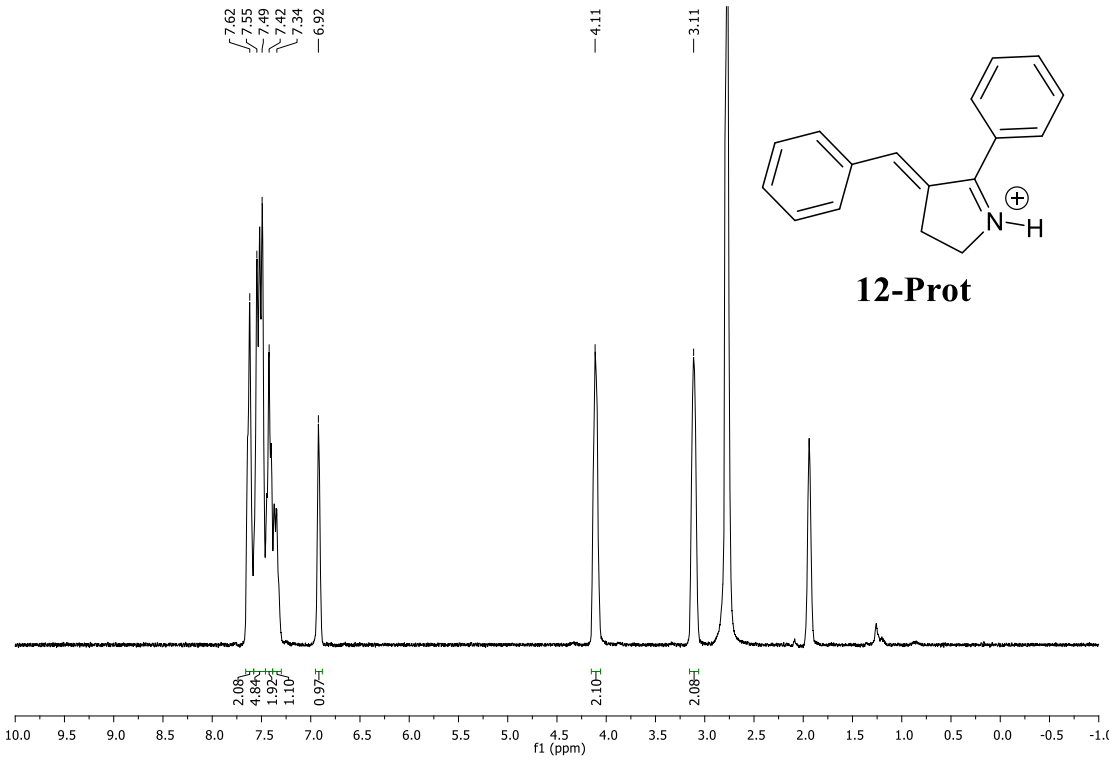
7.62
7.55
7.49
7.42
7.34
6.92
4.11
3.11
2.08
4.84
1.92
1.10
0.97
2.10
2.08
f1 (ppm)

N
H

12-Prot

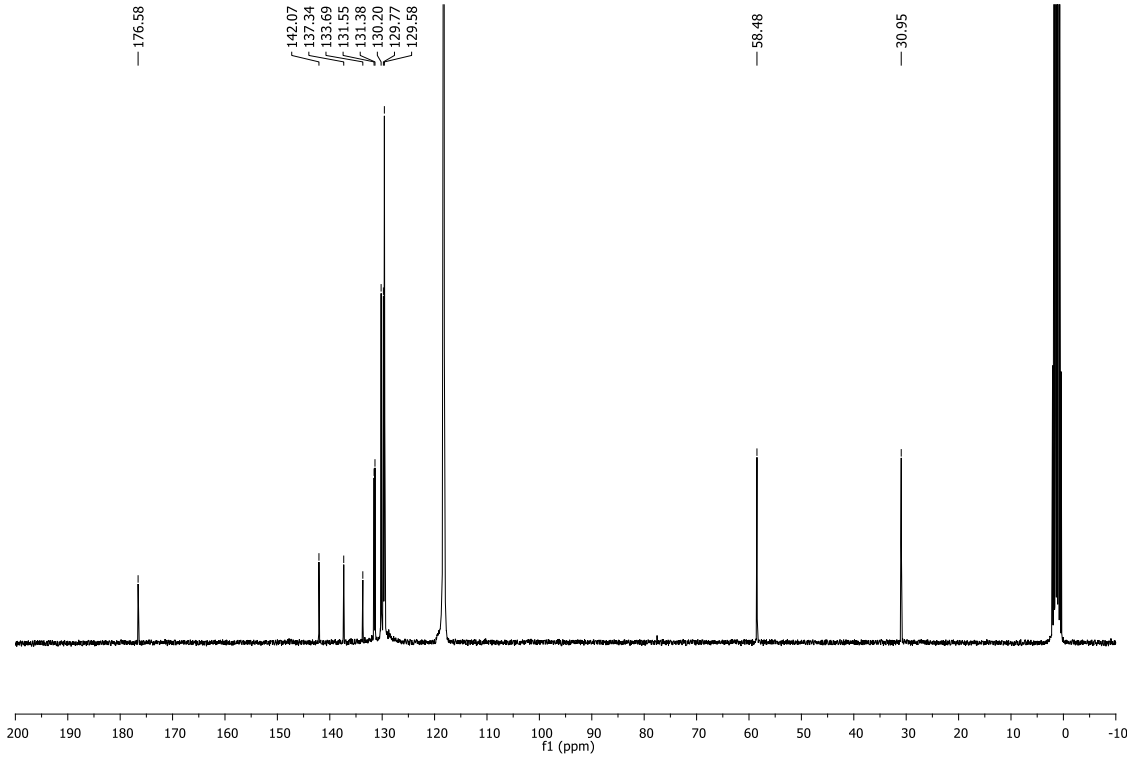
176.58
142.07
137.34
133.69
131.55
131.38
130.20
129.77
129.58
58.48
30.95
f1 (ppm)

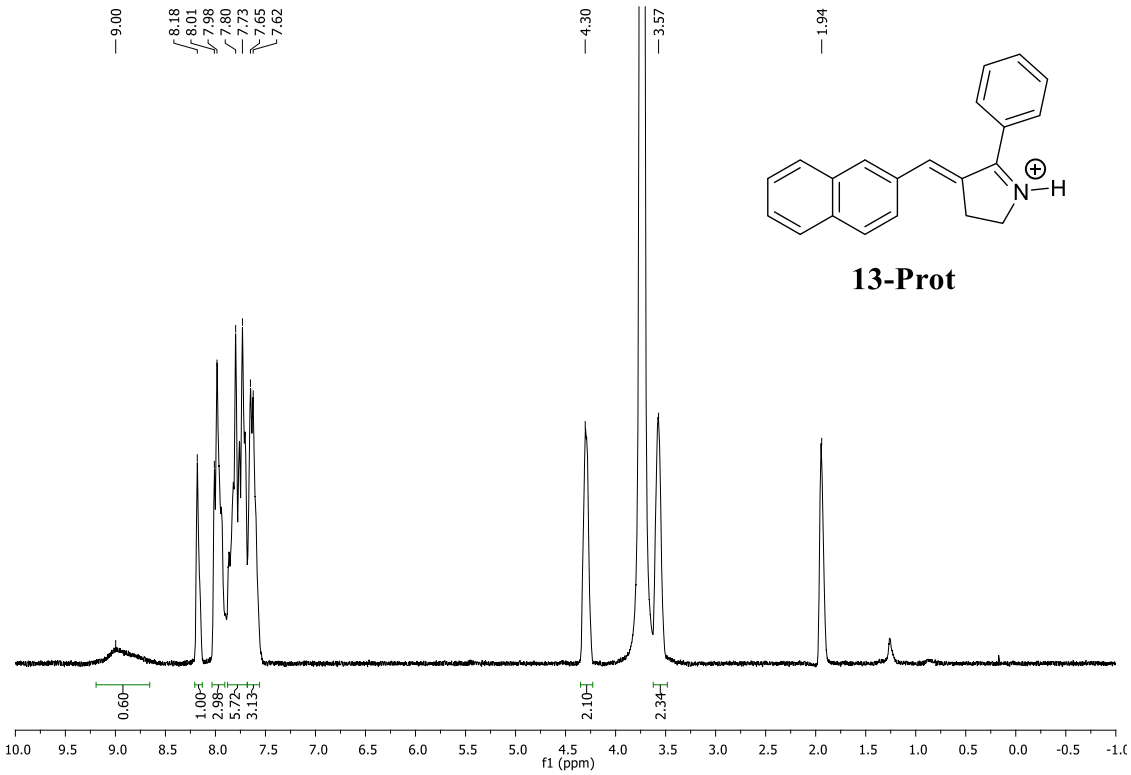
9.00
8.18
8.01
7.98
7.80
7.73
7.65
7.62
4.30
3.57
1.94
0.60
1.00
2.98
5.72
3.13
2.10
2.34
f1 (ppm)

13-Prot

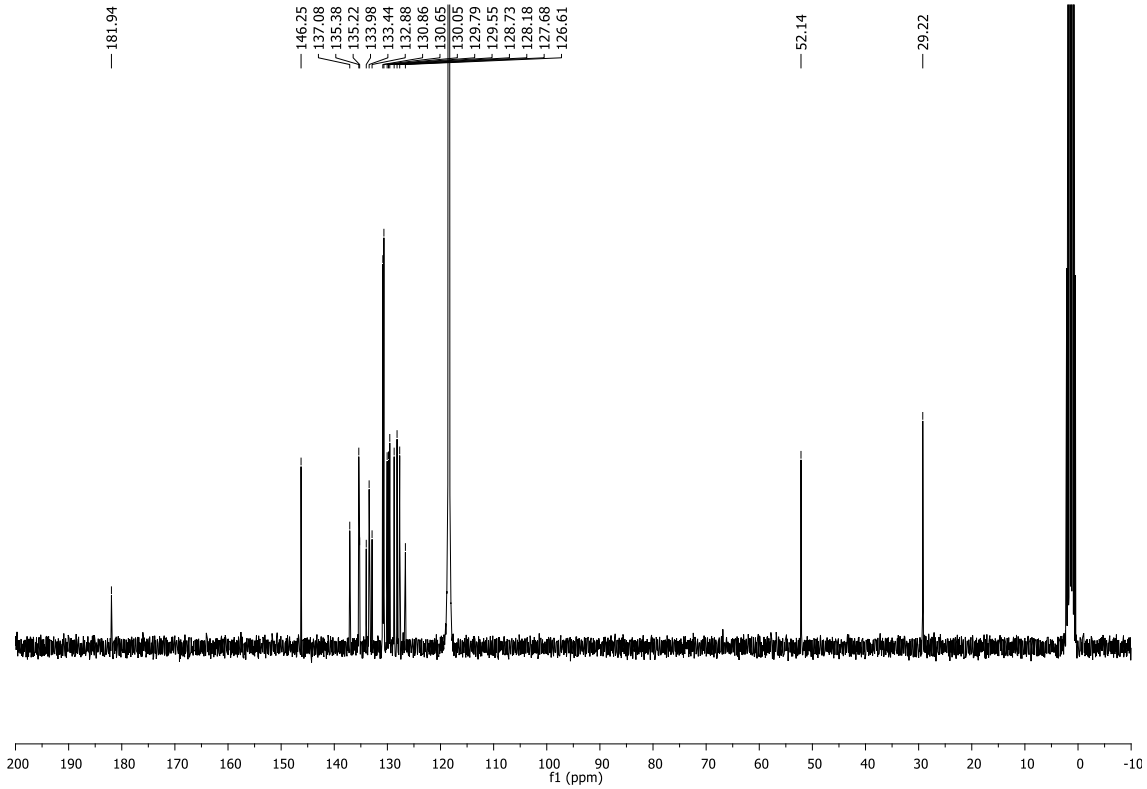
181.94
146.25
137.08
135.38
135.22
133.98
133.44
132.88
130.86
130.65
130.05
129.79
129.55
128.73
128.18
127.68
126.61
52.14
29.22
f1 (ppm)

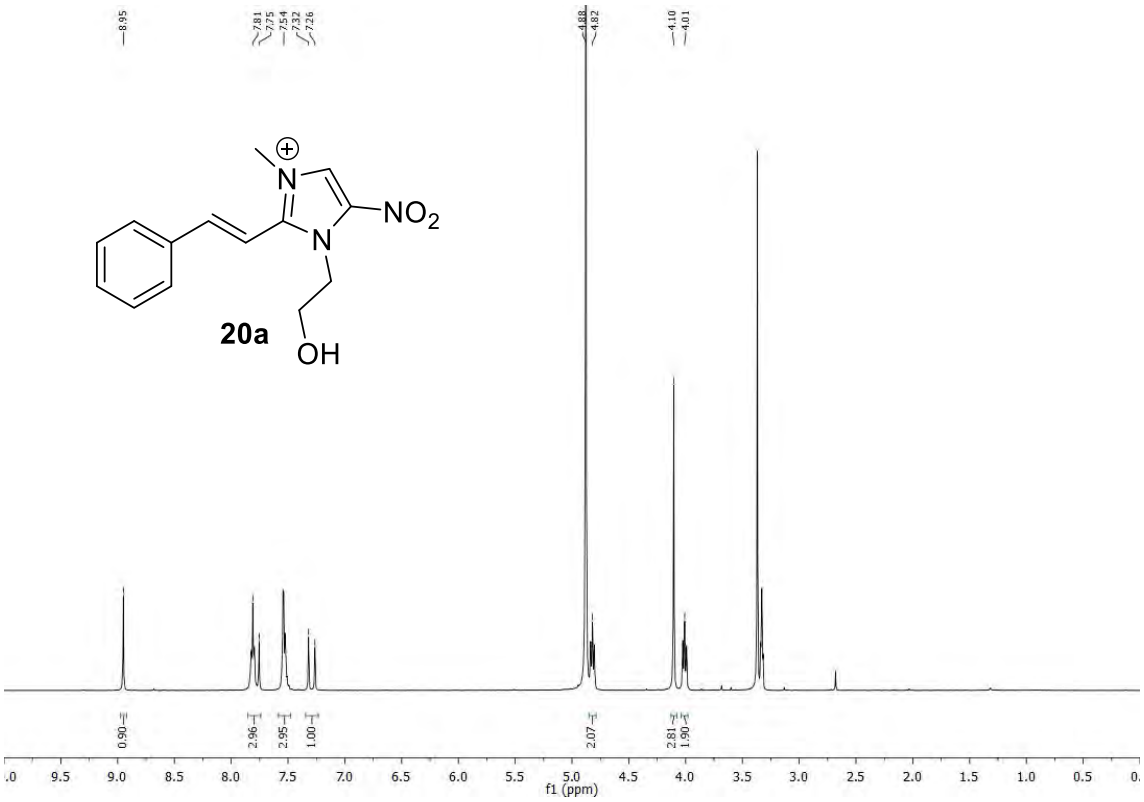
8.95
7.81
7.75
7.54
7.32
7.26
4.88
4.82
4.10
4.01
N
NO2
N
OH
20a
0.90
2.96
2.95
1.00
2.07
2.81
1.90
f1 (ppm)

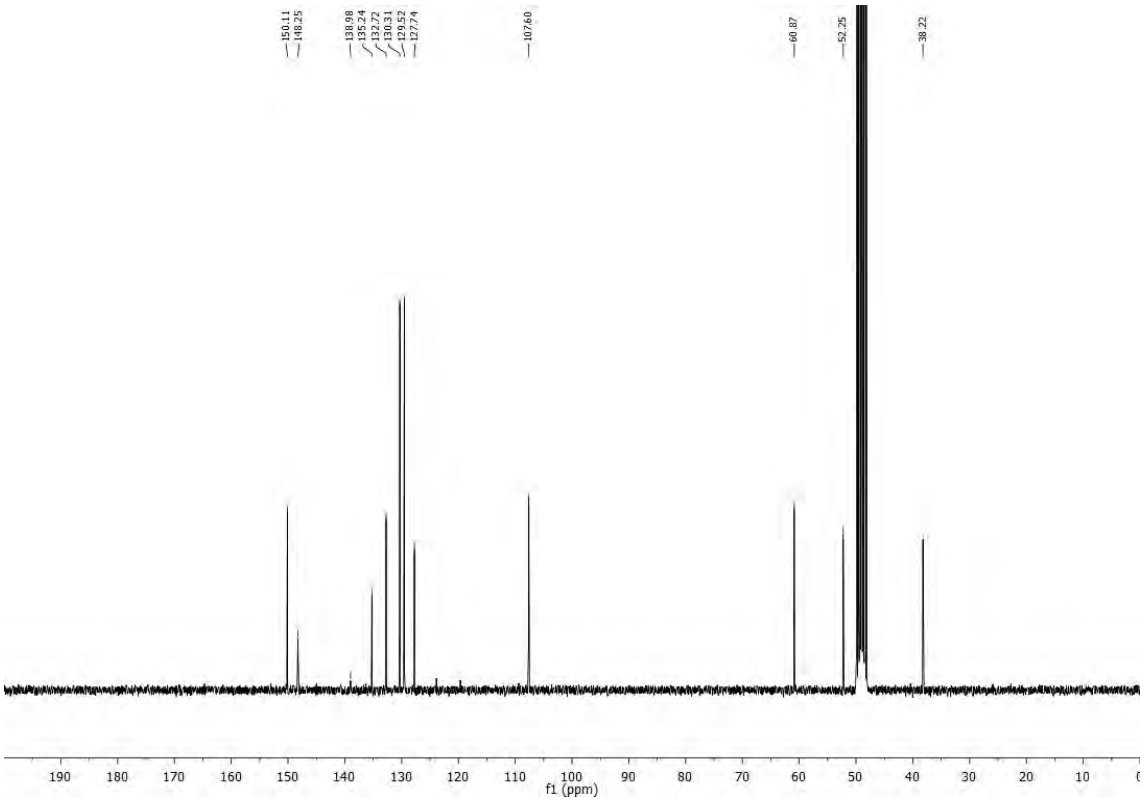
150.11
148.25
138.98
135.24
132.72
130.31
129.52
127.74
107.60
60.87
52.25
38.22
f1 (ppm)

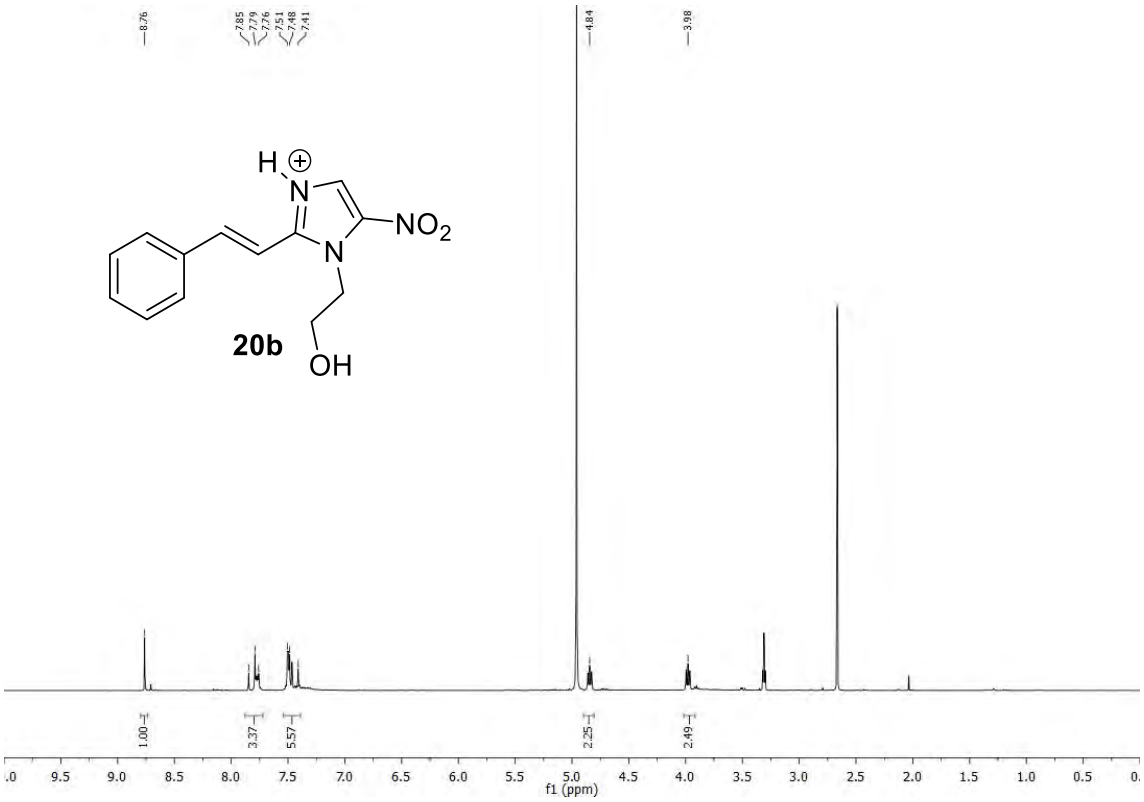
8.76
7.85
7.79
7.76
7.51
7.48
7.41
4.84
3.98
H
N
NO2
N
OH
20b
1.00
3.37
5.57
2.25
2.49
f1 (ppm)

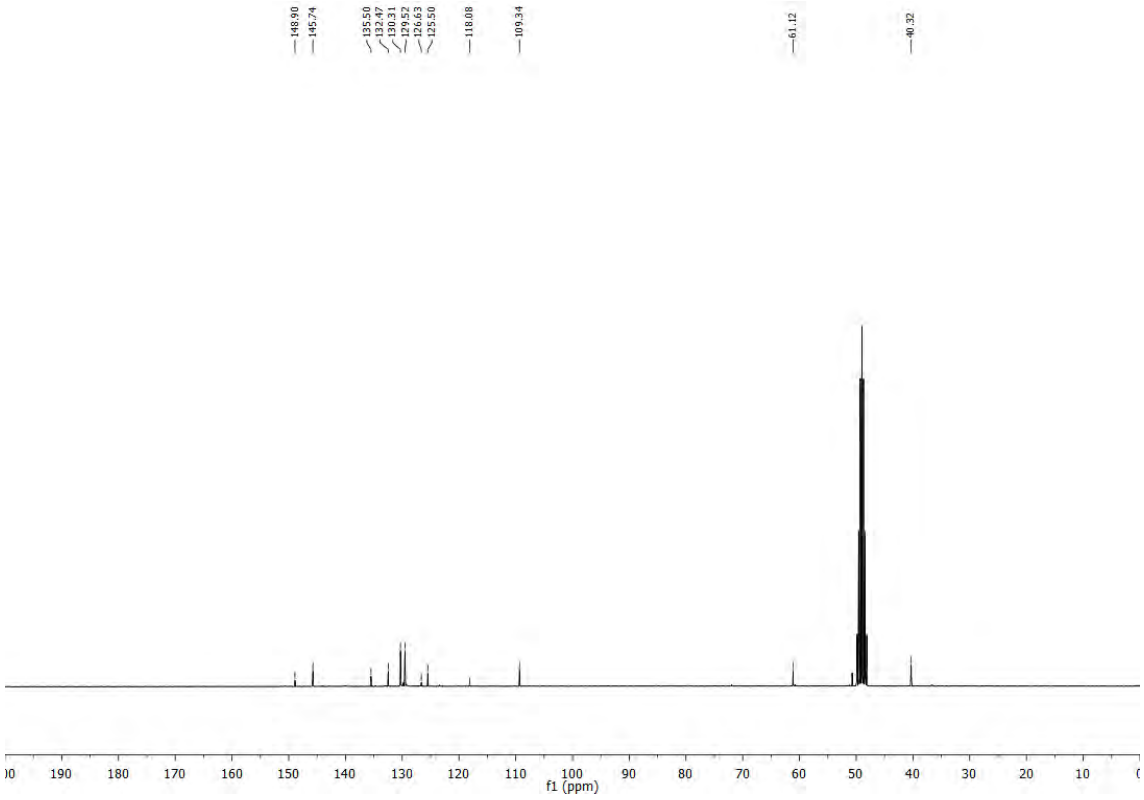
148.90
145.74
135.50
133.47
130.31
129.52
126.63
125.50
118.08
109.34
61.12
40.32
f1 (ppm)

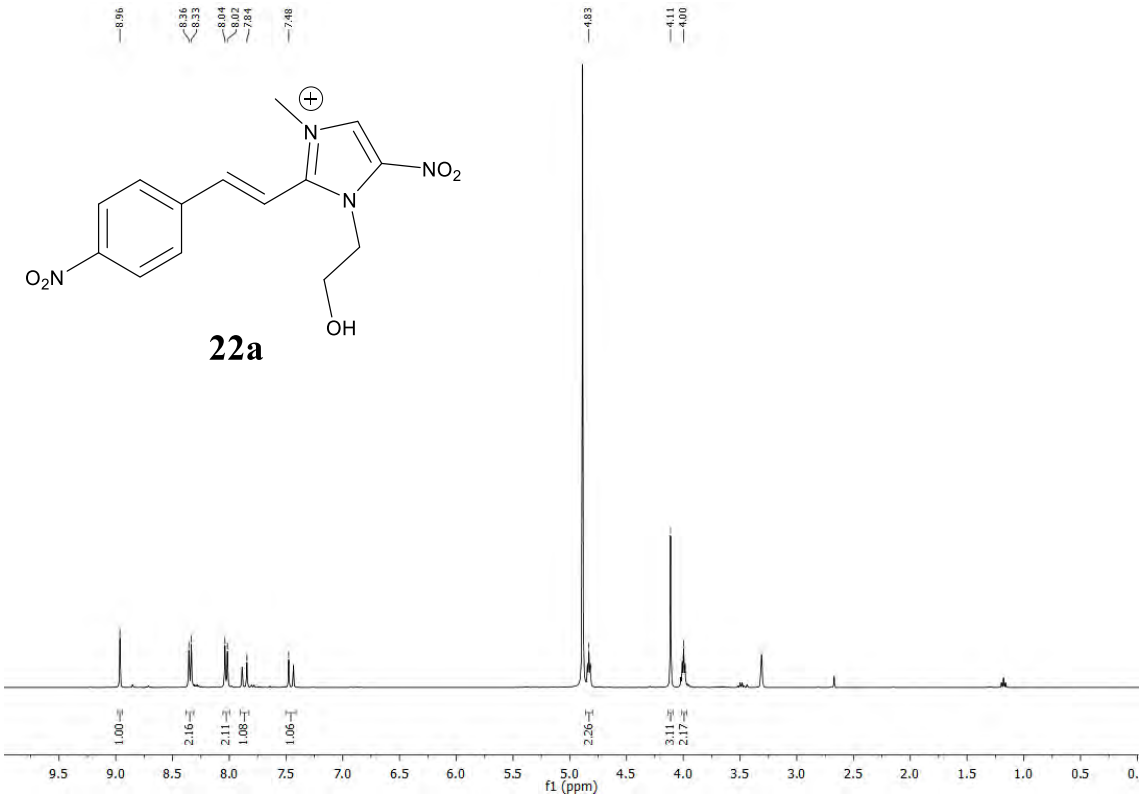
8.96
8.36
8.33
8.04
8.02
7.84
7.48
4.83
4.11
4.00
N
NO2
N
O2N
OH
1.00
2.16
2.11
1.08
1.06
2.26
3.11
2.17
f1 (ppm)

22a

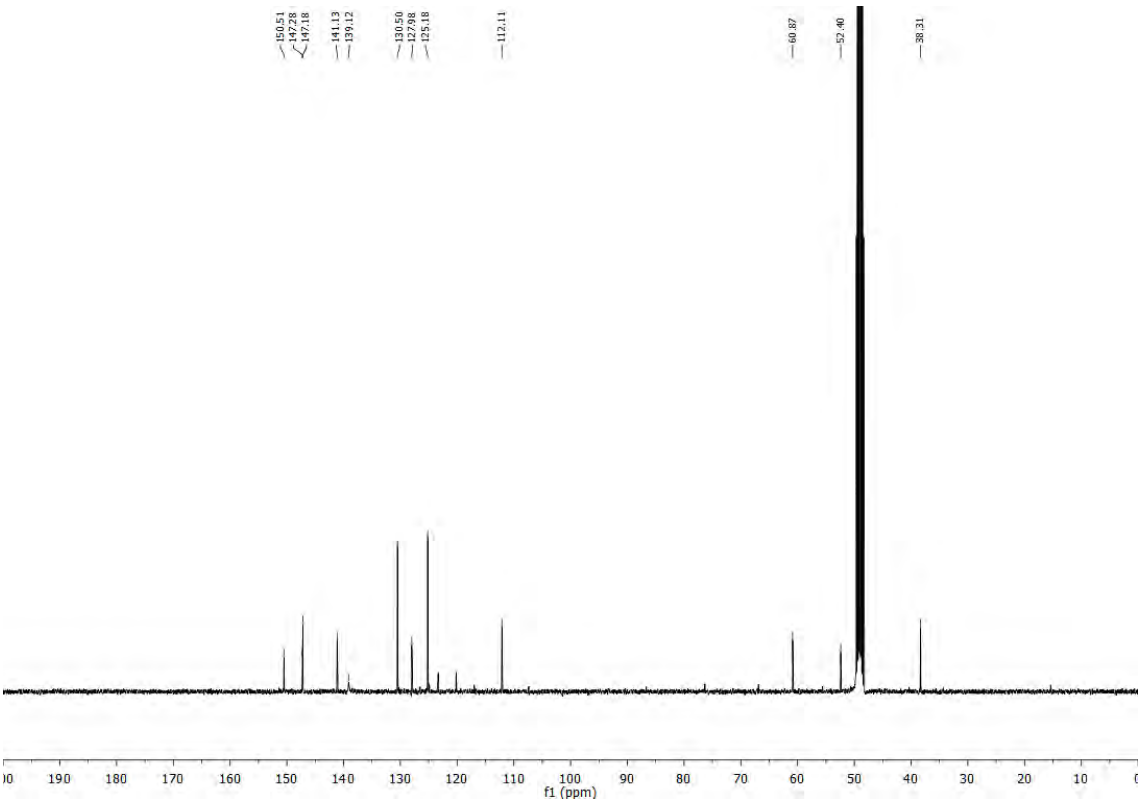
150.51
147.28
147.18
141.13
139.12
130.50
127.98
125.18
112.11
60.87
52.40
38.31
f1 (ppm)

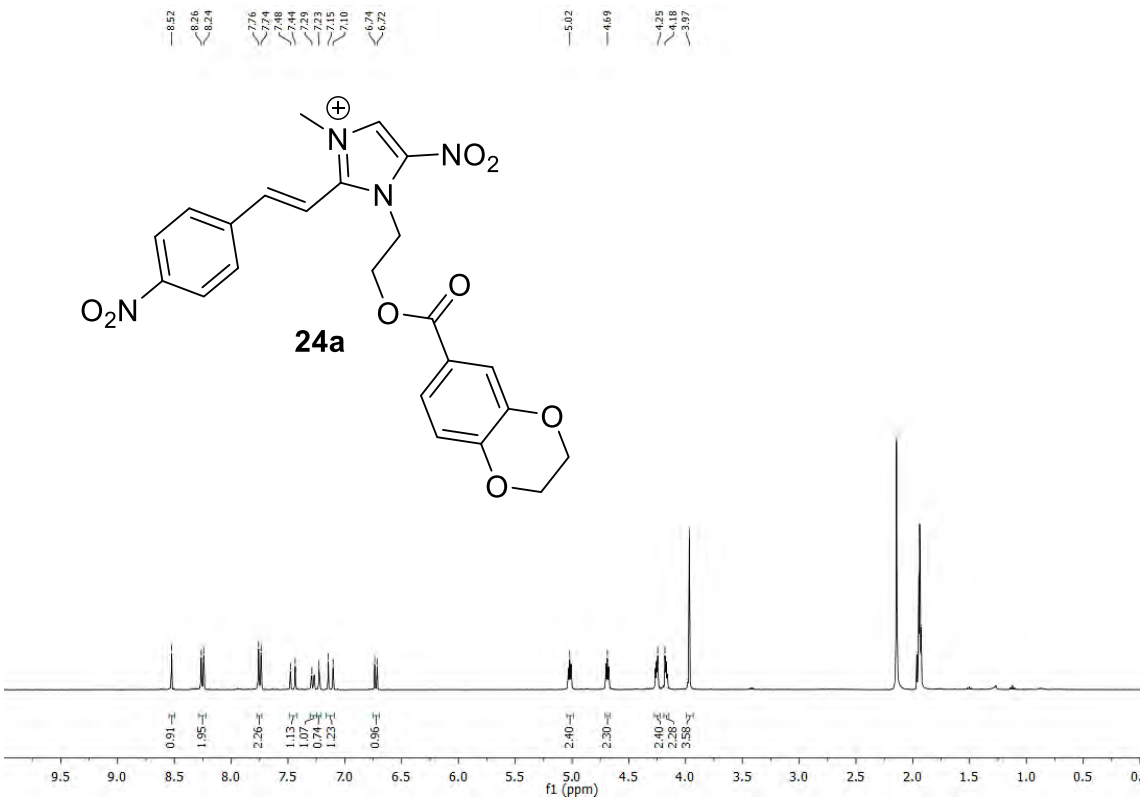
8.52
8.26
8.24
7.76
7.74
7.48
7.44
7.29
7.23
7.15
7.10
6.74
6.72
5.02
4.69
4.25
4.18
3.97
N
N
NO2
O2N
O
O
O
O
24a
0.91
1.95
2.26
1.13
1.07
0.74
1.23
0.96
2.40
2.30
2.40
2.28
3.58
9.5 9.0 8.5 8.0 7.5 7.0 6.5 6.0 5.5 5.0 4.5 4.0 3.5 3.0 2.5 2.0 1.5 1.0 0.5
f1 (ppm)

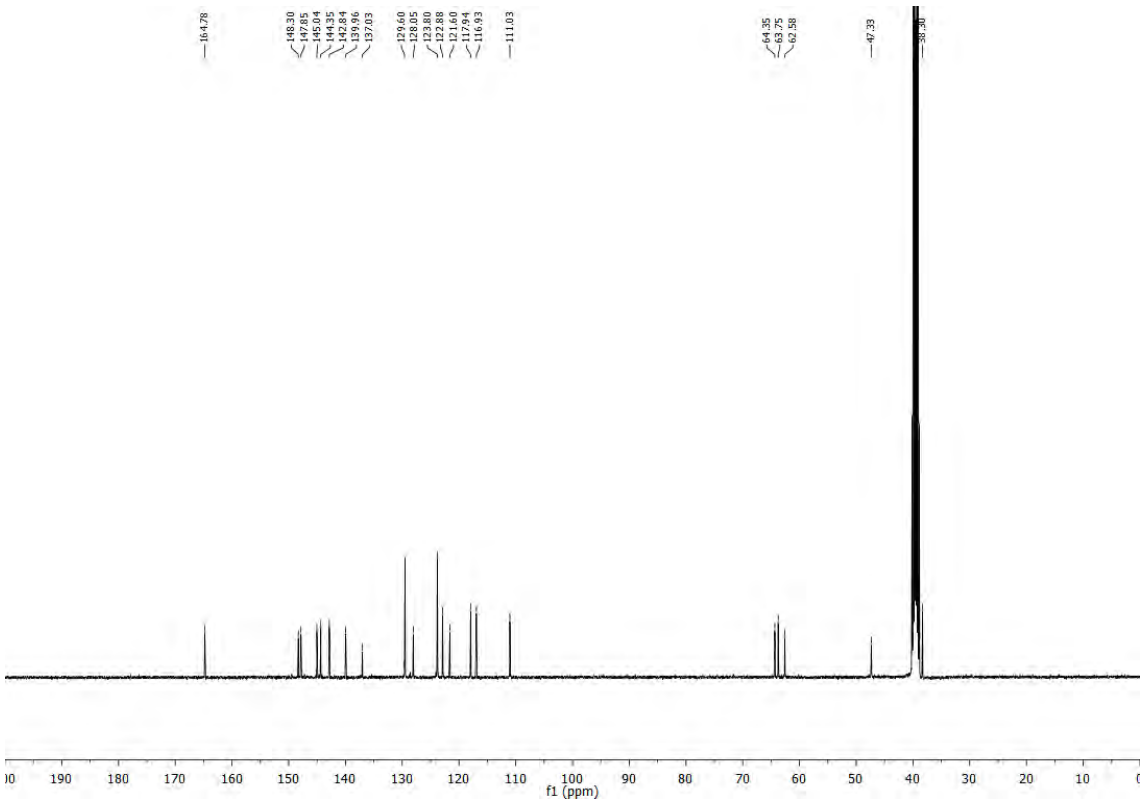
164.78
148.30
147.85
145.04
144.35
142.84
139.96
137.03
129.60
128.05
123.80
122.88
121.60
117.94
116.93
111.03
64.35
63.75
62.58
47.33
38.80
190 180 170 160 150 140 130 120 110 100 90 80 70 60 50 40 30 20 10
f1 (ppm)

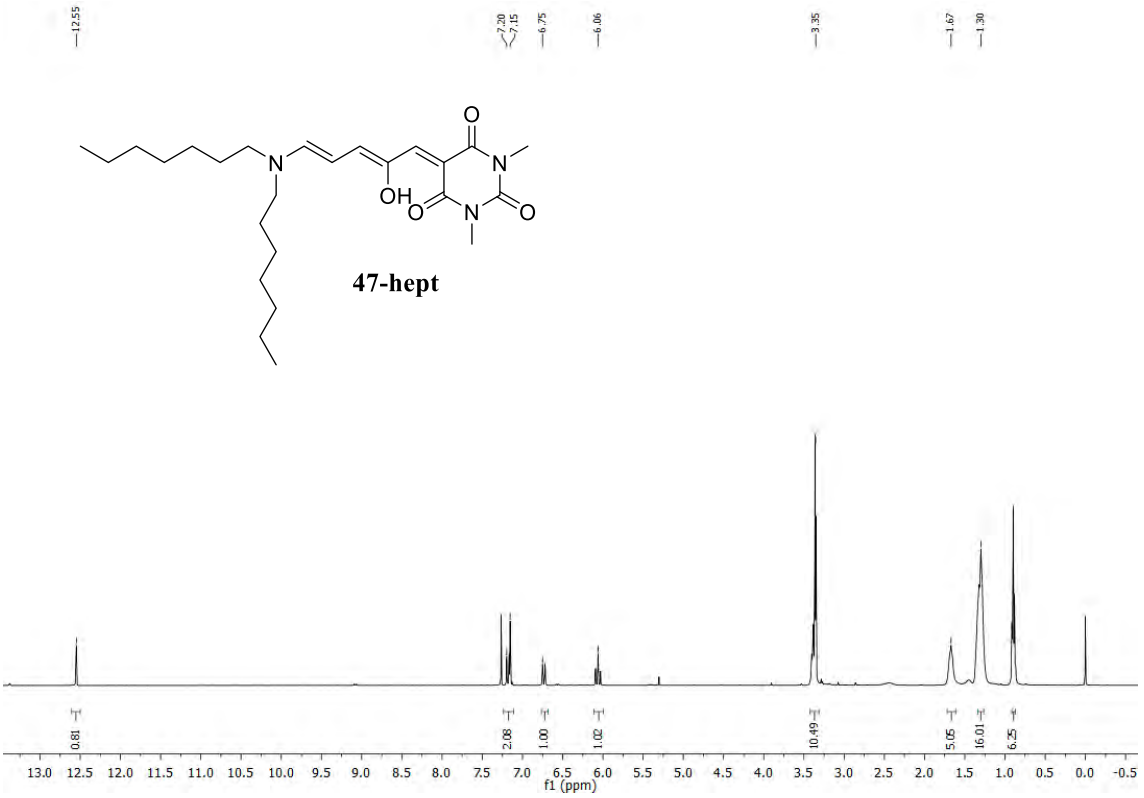
12.55
7.20
7.15
6.75
6.06
3.35
1.67
1.30
O
N
OH
O
N
O
N
0.81
2.08
1.00
1.02
10.49
5.05
16.01
6.25
f1 (ppm)

47-hept

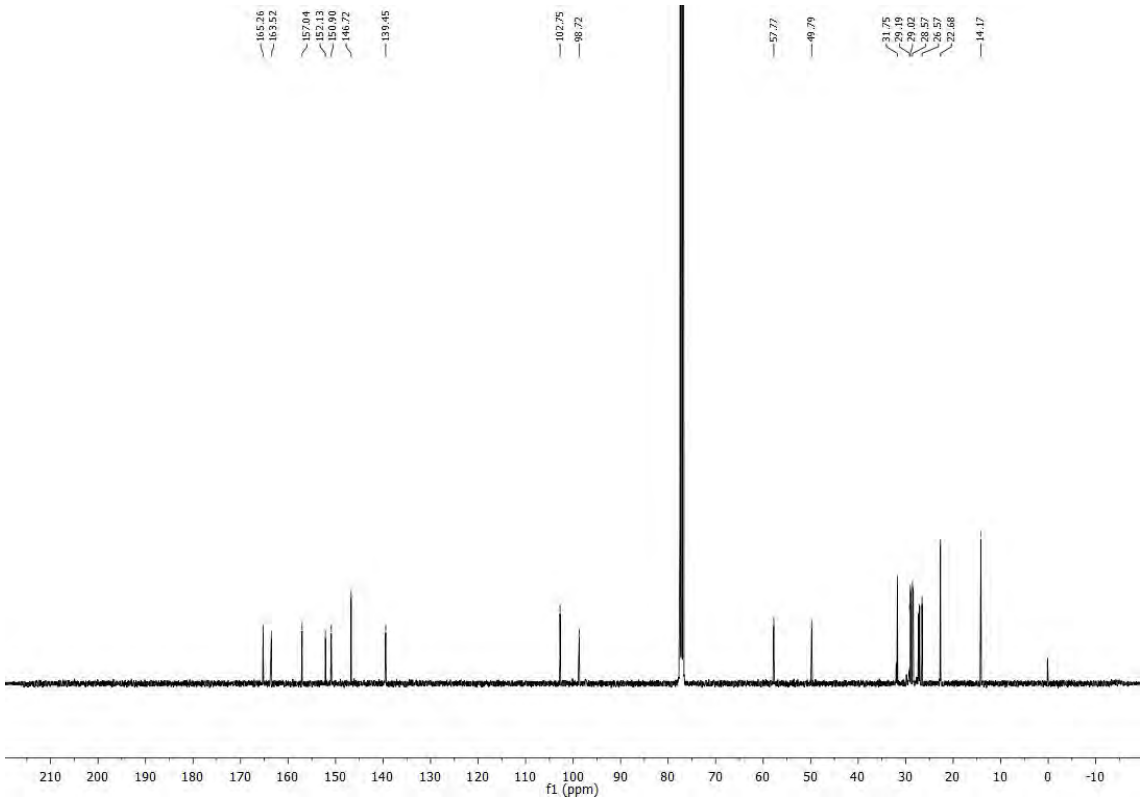
165.26
163.52
157.04
152.13
150.90
146.72
139.45
102.75
98.72
57.77
49.79
31.75
29.19
29.02
28.57
26.57
22.68
14.17
f1 (ppm)

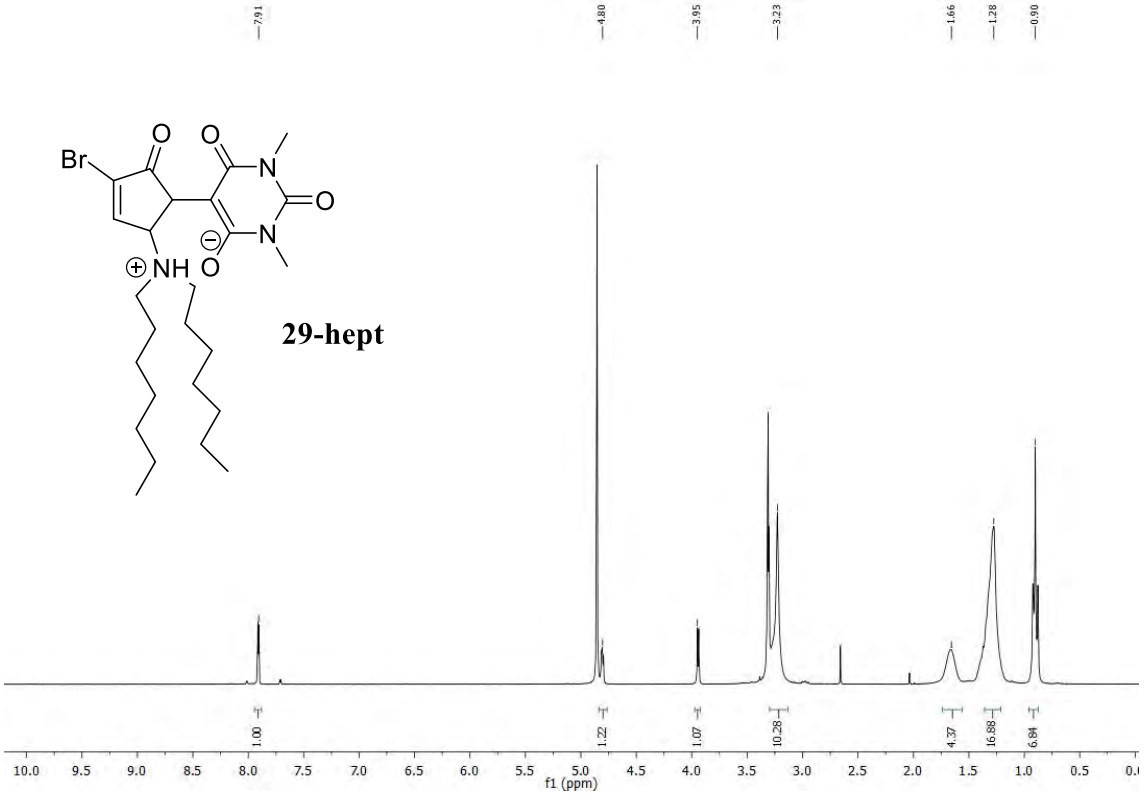
7.91
4.80
3.95
3.23
1.66
1.28
0.90
1.00
1.22
1.07
10.28
4.37
16.88
6.84
f1 (ppm)

29-hept

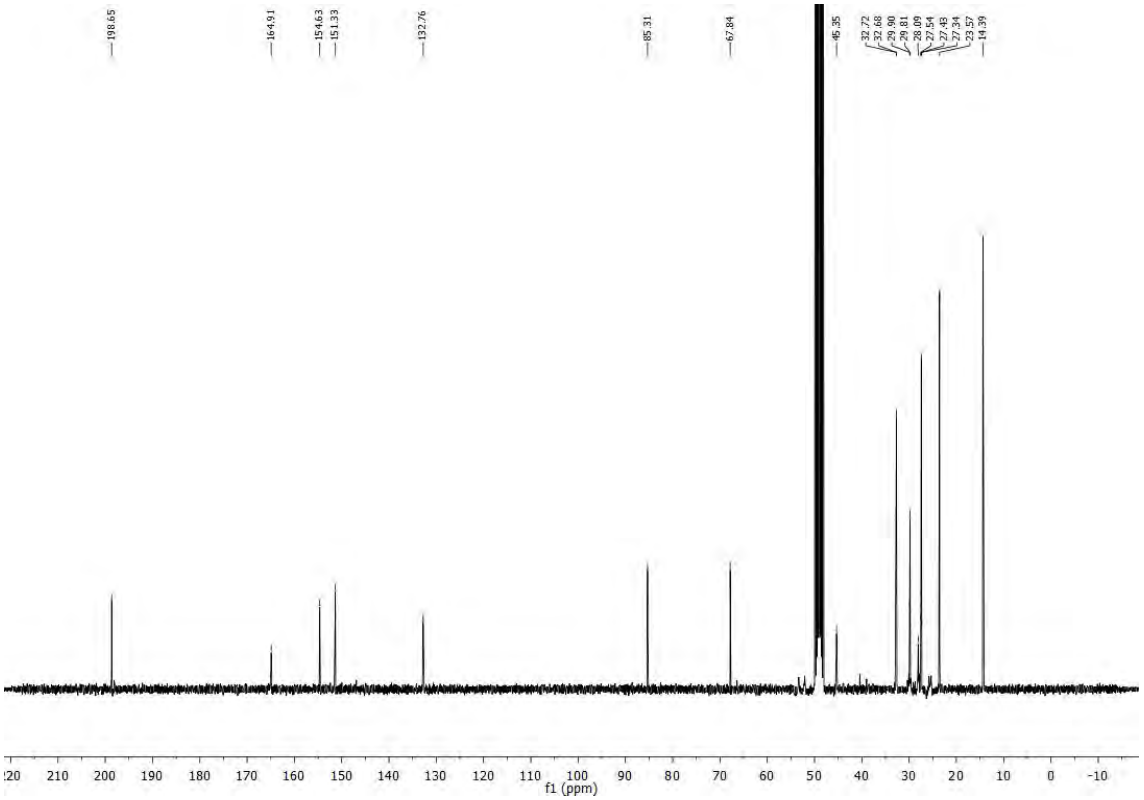
198.65
164.91
154.63
151.33
137.76
85.31
67.84
46.35
32.72
32.68
29.90
29.81
28.09
27.54
27.48
27.34
23.57
14.09
f1 (ppm)

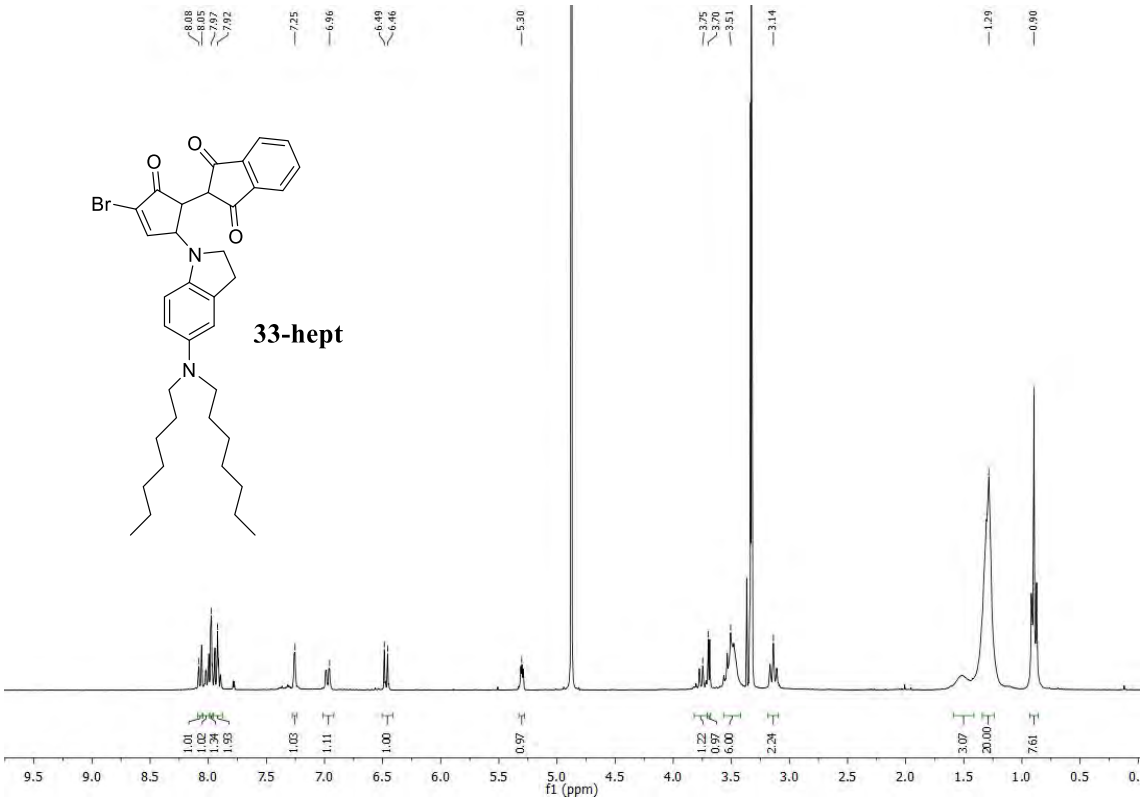
8.08
8.05
7.97
7.92
7.25
6.96
6.49
6.46
5.30
3.75
3.70
3.51
3.14
1.29
0.90
O
O
O
Br
N
N
33-hept
1.01
1.02
1.34
1.93
1.03
1.11
1.00
0.97
1.22
0.97
6.00
2.24
3.07
20.00
7.61
f1 (ppm)

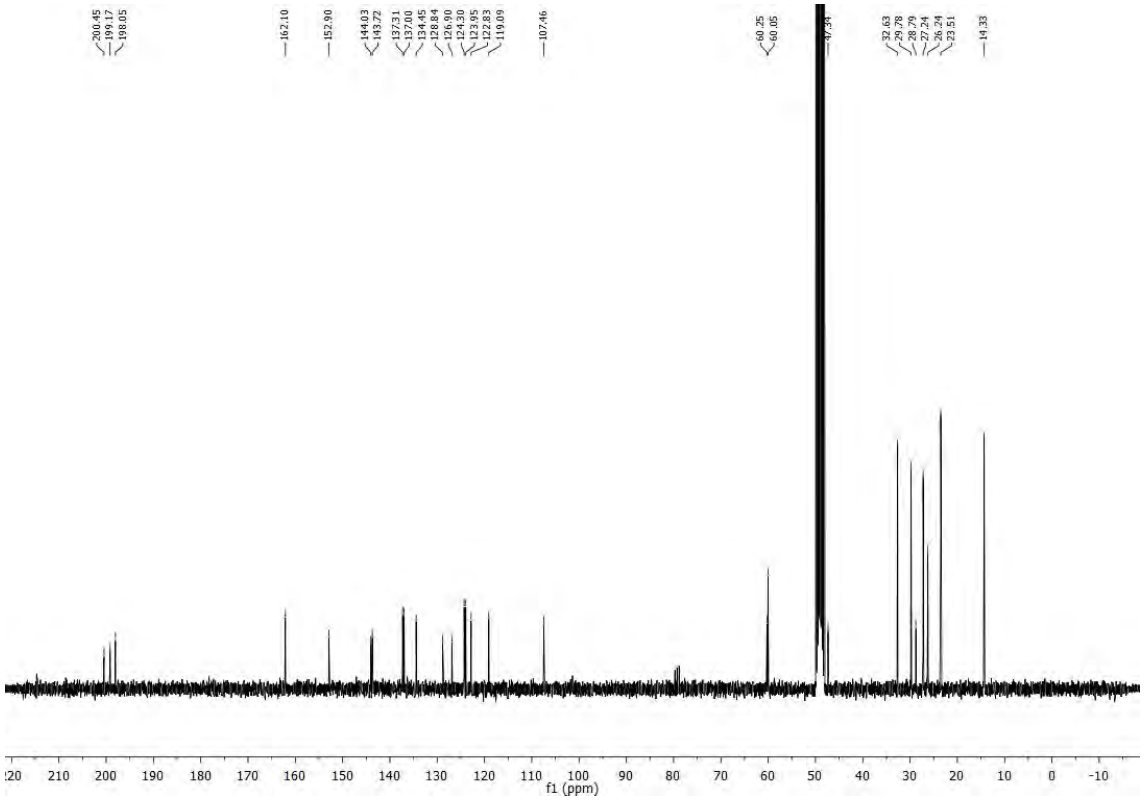
200.45
199.17
198.05
162.10
152.90
144.03
143.72
137.31
137.00
134.45
128.84
126.90
124.30
123.95
122.83
119.09
107.46
60.25
60.05
47.34
32.63
29.76
28.79
27.24
26.24
23.51
14.33
f1 (ppm)

APPENDIX B: X-Ray Diffraction data.

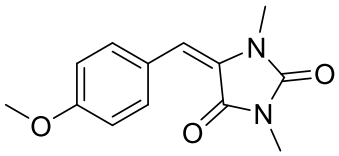

7

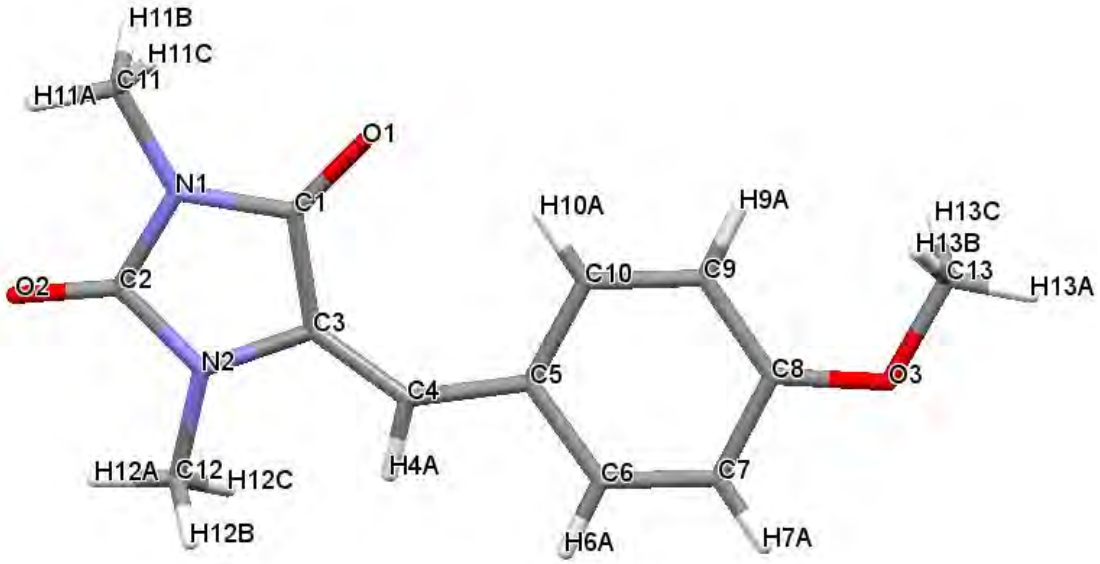

Empirical formula	C13 H14 N2 O3	
Formula weight	246.26	
Temperature	200(2) K	
Wavelength	1.54178 Å	
Crystal system	Monoclinic	
Space group	P2(1)/n	
Unit cell dimensions	a = 7.833 Å	a= 90°.
	b = 12.124 Å	b= 102.16
	c = 13.097 Å	g = 90°.
Volume	1215.9 $Å^3$	
Z	4	
Density (calculated)	1.345 Mg/m^3	
Absorption coefficient	0.801 mm^{-1}	
F(000)	520	
Crystal size	0.25 x 0.20 x 0.15 mm^3	
Theta range for data collection	6.92 to 68.36°.	
Index ranges	-9<=h<=7, -14<=k<=14, -15<=l<=15	
Reflections collected	7400	
Independent reflections	2212 [R(int) = 0.0184]	
Completeness to theta = 68.25°	98.8 %	
Absorption correction	Semi-empirical from equivalents	

Max. and min. transmission	0.8892 and 0.8248
Refinement method	Full-matrix least-squares on F^2
Data / restraints / parameters	2212 / 0 / 166
Goodness-of-fit on F^2	1.017
Final R indices [I>2sigma(I)]	R1 = 0.0428, wR2 = 0.1259
R indices (all data)	R1 = 0.0459, wR2 = 0.1310
Largest diff. peak and hole	0.225 and -0.234 e.Å^{-3}

Data collection: Kappa CCD

Refinement: HKL Scalepack (Otwinowski and Minor, 1997)

Program used for resolving the structure: SHELXS-97 (Sheldrick, 1997)

Program used for the refinement of the structure: SHELXS-97 (Sheldrick, 1997)

Atomic coordinates (x 10^4) and equivalent isotropic displacement parameters (Å^{2}x 10^3) for **7**.

U(eq) is defined as one third of the trace of the orthogonalized U^{ij} tensor.

	x	y	z	U(eq)
O(1)	2784(1)	6488(1)	4070(1)	54(1)
O(2)	7516(2)	7904(1)	2990(1)	64(1)
O(3)	467(2)	1227(1)	4367(1)	62(1)
N(1)	5019(2)	7455(1)	3594(1)	49(1)
N(2)	6606(2)	6109(1)	3145(1)	51(1)
C(1)	4138(2)	6507(1)	3755(1)	45(1)
C(2)	6509(2)	7226(1)	3214(1)	50(1)
C(3)	5188(2)	5587(1)	3452(1)	45(1)
C(4)	4988(2)	4486(1)	3415(1)	47(1)
C(5)	3714(2)	3729(1)	3692(1)	44(1)
C(6)	3939(2)	2611(1)	3469(1)	48(1)
C(7)	2843(2)	1805(1)	3698(1)	51(1)
C(8)	1465(2)	2085(1)	4164(1)	48(1)
C(9)	1204(2)	3188(1)	4389(1)	48(1)
C(10)	2314(2)	3995(1)	4153(1)	46(1)
C(11)	4443(2)	8568(1)	3757(1)	57(1)
C(12)	8038(2)	5546(2)	2837(2)	72(1)
C(13)	-922(2)	1471(2)	4882(2)	68(1)

Bond lengths [Å] and angles [°].

Bond lengths [Å]

Atom A-B	Distance (Å)
O(1)-C(1)	1.2160(18)
O(2)-C(2)	1.2164(18)
O(3)-C(8)	1.3601(18)
O(3)-C(13)	1.426(2)
N(1)-C(1)	1.3797(19)
N(1)-C(2)	1.3895(19)
N(1)-C(11)	1.4522(19)
N(2)-C(2)	1.362(2)
N(2)-C(3)	1.4086(18)
N(2)-C(12)	1.441(2)
C(1)-C(3)	1.488(2)
C(3)-C(4)	1.344(2)
C(4)-C(5)	1.457(2)
C(4)-H(4A)	0.9500
C(5)-C(10)	1.3965(19)
C(5)-C(6)	1.406(2)
C(6)-C(7)	1.375(2)
C(6)-H(6A)	0.9500
C(7)-C(8)	1.389(2)
C(7)-H(7A)	0.9500
C(8)-C(9)	1.394(2)
C(9)-C(10)	1.386(2)
C(9)-H(9A)	0.9500
C(10)-H(10A)	0.9500
C(11)-H(11A)	0.9800
C(11)-H(11B)	0.9800
C(11)-H(11C)	0.9800
C(12)-H(12A)	0.9800
C(12)-H(12B)	0.9800
C(12)-H(12C)	0.9800
C(13)-H(13A)	0.9800
C(13)-H(13B)	0.9800
C(13)-H(13C)	0.9800

bond angles [°]

Atom A-B-C	Angle
C(8)-O(3)-C(13)	117.48(12)
C(1)-N(1)-C(2)	111.92(12)
C(1)-N(1)-C(11)	124.77(13)
C(2)-N(1)-C(11)	123.26(13)
C(2)-N(2)-C(3)	111.63(12)
C(2)-N(2)-C(12)	123.22(13)
C(3)-N(2)-C(12)	125.10(13)
O(1)-C(1)-N(1)	124.61(13)
O(1)-C(1)-C(3)	130.25(13)
N(1)-C(1)-C(3)	105.13(12)
O(2)-C(2)-N(2)	127.41(15)
O(2)-C(2)-N(1)	125.98(15)
N(2)-C(2)-N(1)	106.61(12)
C(4)-C(3)-N(2)	121.86(13)
C(4)-C(3)-C(1)	133.43(13)
N(2)-C(3)-C(1)	104.69(12)
C(3)-C(4)-C(5)	134.20(13)
C(3)-C(4)-H(4A)	112.9
C(5)-C(4)-H(4A)	112.9
C(10)-C(5)-C(6)	117.13(13)
C(10)-C(5)-C(4)	127.19(13)
C(6)-C(5)-C(4)	115.68(12)
C(7)-C(6)-C(5)	121.90(14)
C(7)-C(6)-H(6A)	119.1
C(5)-C(6)-H(6A)	119.1
C(6)-C(7)-C(8)	120.10(14)
C(6)-C(7)-H(7A)	119.9
C(8)-C(7)-H(7A)	119.9
O(3)-C(8)-C(7)	115.53(13)
O(3)-C(8)-C(9)	125.18(13)
C(7)-C(8)-C(9)	119.29(14)
C(10)-C(9)-C(8)	120.21(13)
C(10)-C(9)-H(9A)	119.9
C(8)-C(9)-H(9A)	119.9
C(9)-C(10)-C(5)	121.36(13)

C(9)-C(10)-H(10A)	119.3
C(5)-C(10)-H(10A)	119.3
N(1)-C(11)-H(11A)	109.5
N(1)-C(11)-H(11B)	109.5
H(11A)-C(11)-H(11B)	109.5
N(1)-C(11)-H(11C)	109.5
H(11A)-C(11)-H(11C)	109.5
H(11B)-C(11)-H(11C)	109.5
N(2)-C(12)-H(12A)	109.5
N(2)-C(12)-H(12B)	109.5
H(12A)-C(12)-H(12B)	109.5
N(2)-C(12)-H(12C)	109.5
H(12A)-C(12)-H(12C)	109.5
H(12B)-C(12)-H(12C)	109.5
O(3)-C(13)-H(13A)	109.5
O(3)-C(13)-H(13B)	109.5
H(13A)-C(13)-H(13B)	109.5
O(3)-C(13)-H(13C)	109.5
H(13A)-C(13)-H(13C)	109.5
H(13B)-C(13)-H(13C)	109.5

Anisotropic displacement parameters ($Å^2 x\ 10^3$) for **7**.

The anisotropic displacement factor exponent takes the form: $-2\pi^2[\ h^2a^{*2}U^{11} + ... + 2\ h\ k\ a^*\ b^*\ U^{12}]$

	U^{11}	U^{22}	U^{33}	U^{23}	U^{13}	U^{12}
O(1)	53(1)	51(1)	64(1)	5(1)	24(1)	7(1)
O(2)	60(1)	57(1)	80(1)	16(1)	26(1)	-2(1)
O(3)	65(1)	48(1)	81(1)	-2(1)	33(1)	-4(1)
N(1)	51(1)	44(1)	53(1)	6(1)	15(1)	4(1)
N(2)	49(1)	51(1)	60(1)	7(1)	23(1)	3(1)
C(1)	47(1)	47(1)	43(1)	7(1)	11(1)	3(1)
C(2)	49(1)	52(1)	51(1)	10(1)	14(1)	1(1)
C(3)	44(1)	50(1)	45(1)	6(1)	14(1)	3(1)
C(4)	44(1)	51(1)	47(1)	2(1)	15(1)	7(1)
C(5)	45(1)	46(1)	40(1)	3(1)	9(1)	6(1)
C(6)	48(1)	50(1)	50(1)	-1(1)	16(1)	8(1)
C(7)	54(1)	44(1)	55(1)	-3(1)	15(1)	5(1)
C(8)	50(1)	45(1)	50(1)	2(1)	13(1)	1(1)

C(9)	47(1)	47(1)	51(1)	2(1)	17(1)	6(1)
C(10)	48(1)	44(1)	48(1)	2(1)	15(1)	7(1)
C(11)	64(1)	44(1)	65(1)	6(1)	16(1)	7(1)
C(12)	61(1)	61(1)	108(1)	14(1)	48(1)	8(1)
C(13)	62(1)	58(1)	92(1)	1(1)	36(1)	-5(1)

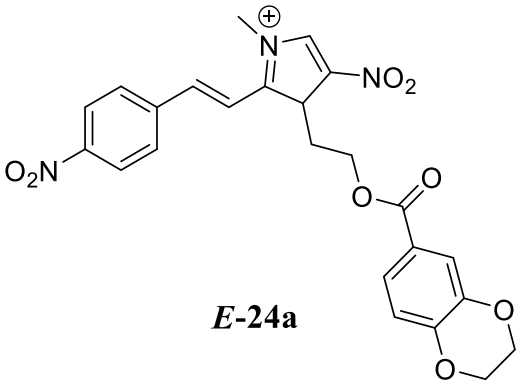

***E*-24a**

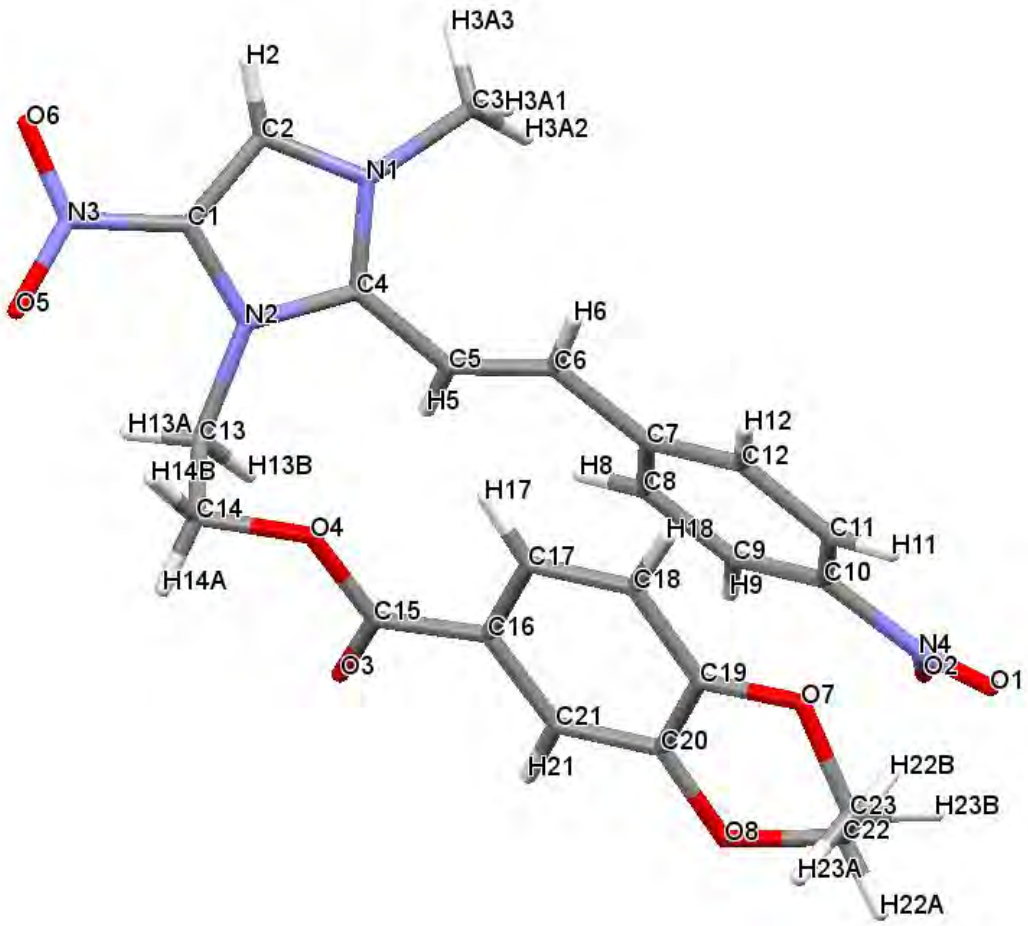

Empirical formula	C23 H21 B F4 N4 O8	
Formula weight	568.25	
Temperature	173(1) K	
Wavelength	0.71073 Å	
Crystal system	Monoclinic	
Space group	P 21/n	
Unit cell dimensions	a = 12.702 Å	α= 90°.
	b = 12.634 Å	β= 112.74°.
	c = 16.156 Å	γ= 90°.

Volume	2390.8 $Å^3$
Z	4
Density (calculated)	1.579 Mg/m^3
Absorption coefficient	0.139 mm^{-1}
F(000)	1168
Crystal size	0.2 x 0.1 x 0.1 mm^3
Theta range for data collection	2.114 to 25.682°.
Index ranges	-15<=h<=15, -15<=k<=15, -19<=l<=19
Reflections collected	25900
Independent reflections	4537 [R(int) = 0.0742]
Completeness to theta = 25.242°	99.8 %
Absorption correction	Semi-empirical from equivalents
Max. and min. transmission	1.0308 and 0.8957
Refinement method	Full-matrix least-squares on F^2
Data / restraints / parameters	4537 / 0 / 478
Goodness-of-fit on F^2	0.891
Final R indices [I>2sigma(I)]	R1 = 0.0535, wR2 = 0.1404
R indices (all data)	R1 = 0.0877, wR2 = 0.1646
Extinction coefficient	n/a
Largest diff. peak and hole	0.294 and -0.252 $e.Å^{-3}$

Data collection: Kappa CCD

Refinement: HKL Scalepack (Otwinowski and Minor, 1997)

Program used for resolving the structure: SHELXS-97 (Sheldrick, 1997)

Program used for the refinement of the structure: SHELXS-97 (Sheldrick, 1997)

Atomic coordinates (x 10^4) and equivalent isotropic displacement parameters ($Å^2$x 10^3) for ***E*-24a**.

U(eq) is defined as one third of the trace of the orthogonalized U^{ij} tensor.

	x	y	z	U(eq)
C(1)	9474(2)	5379(2)	6612(2)	34(1)
C(2)	8683(2)	5687(2)	5828(2)	37(1)
C(3)	6707(3)	6426(3)	5316(2)	45(1)
C(4)	7984(2)	5858(2)	6878(2)	31(1)
C(5)	7231(2)	6121(2)	7332(2)	32(1)
C(6)	6131(2)	5891(2)	7012(2)	31(1)
C(7)	5360(2)	6179(2)	7455(2)	28(1)
C(8)	5634(2)	6979(2)	8098(2)	33(1)
C(9)	4894(2)	7241(2)	8504(2)	35(1)

C(10)	3890(2)	6683(2)	8277(2)	33(1)
C(11)	3598(2)	5878(2)	7657(2)	34(1)
C(12)	4329(2)	5639(2)	7231(2)	33(1)
C(13)	9638(2)	5303(2)	8265(2)	36(1)
C(14)	9536(2)	4184(3)	8536(2)	41(1)
C(15)	7893(2)	4180(2)	8905(2)	41(1)
C(16)	6701(2)	3820(2)	8635(2)	36(1)
C(17)	6087(2)	3326(2)	7817(2)	35(1)
C(18)	4995(2)	2970(2)	7632(2)	37(1)
C(19)	4489(2)	3105(2)	8253(2)	37(1)
C(20)	5084(3)	3641(2)	9052(2)	40(1)
C(21)	6182(3)	3991(2)	9237(2)	40(1)
C(22)	3400(3)	3686(3)	9326(2)	49(1)
C(23)	3077(3)	2687(3)	8807(2)	51(1)
B(1)	6486(3)	3232(3)	5371(2)	45(1)
N(1)	7759(2)	5986(2)	5998(1)	33(1)
N(2)	9055(2)	5482(2)	7281(1)	31(1)
N(3)	10583(2)	4963(2)	6742(2)	41(1)
N(4)	3104(2)	6971(2)	8704(2)	40(1)
O(1)	2307(2)	6366(2)	8620(1)	48(1)
O(2)	3273(2)	7794(2)	9131(2)	55(1)
O(3)	8420(2)	4671(2)	9580(1)	56(1)
O(4)	8354(2)	3893(2)	8308(1)	40(1)
O(5)	11122(2)	4497(2)	7443(2)	51(1)
O(6)	10894(2)	5097(2)	6118(2)	55(1)
O(7)	3415(2)	2717(2)	8050(1)	47(1)
O(8)	4621(2)	3823(2)	9677(1)	50(1)
F(1A)	5922(3)	2930(3)	4481(2)	81(1)
F(2A)	6464(3)	2413(4)	5879(3)	83(1)
F(3A)	7602(2)	3490(2)	5479(2)	68(1)
F(4A)	5938(3)	4088(3)	5504(4)	103(2)
F(1B)	7251(6)	3680(5)	6222(5)	60(2)
F(2B)	6878(12)	2516(16)	5114(11)	201(10)
F(3B)	5765(12)	2608(12)	5765(7)	105(5)

Bond lengths [Å] and angles [°].

Bond lengths [Å]

Atom A-B	Distance (Å)
C(1)-C(2)	1.334(4)
C(1)-N(2)	1.384(3)
C(1)-N(3)	1.440(3)
C(2)-N(1)	1.359(3)
C(2)-H(2)	0.92(3)
C(3)-N(1)	1.473(4)
C(3)-H(3A1)	0.95(3)
C(3)-H(3A2)	1.00(4)
C(3)-H(3A3)	1.00(4)
C(4)-N(1)	1.347(3)
C(4)-N(2)	1.348(3)
C(4)-C(5)	1.451(4)
C(5)-C(6)	1.322(4)
C(5)-H(5)	0.81(3)
C(6)-C(7)	1.464(3)
C(6)-H(6)	0.94(3)
C(7)-C(12)	1.395(4)
C(7)-C(8)	1.394(4)
C(8)-C(9)	1.379(4)
C(8)-H(8)	0.96(3)
C(9)-C(10)	1.376(4)
C(9)-H(9)	0.90(3)
C(10)-C(11)	1.374(4)
C(10)-N(4)	1.463(3)
C(11)-C(12)	1.387(4)
C(11)-H(11)	0.9300
C(12)-H(12)	1.01(3)
C(13)-N(2)	1.489(3)
C(13)-C(14)	1.501(4)
C(13)-H(13A)	0.90(3)
C(13)-H(13B)	0.99(3)
C(14)-O(4)	1.448(3)
C(14)-H(14A)	0.94(3)
C(14)-H(14B)	0.97(3)

C(15)-O(3)	1.208(3)
C(15)-O(4)	1.357(3)
C(15)-C(16)	1.476(4)
C(16)-C(21)	1.388(4)
C(16)-C(17)	1.394(4)
C(17)-C(18)	1.377(4)
C(17)-H(17)	0.96(3)
C(18)-C(19)	1.395(4)
C(18)-H(18)	1.01(3)
C(19)-O(7)	1.364(3)
C(19)-C(20)	1.393(4)
C(20)-O(8)	1.370(3)
C(20)-C(21)	1.382(4)
C(21)-H(21)	0.97(3)
C(22)-O(8)	1.440(4)
C(22)-C(23)	1.483(5)
C(22)-H(22A)	0.98(4)
C(22)-H(22B)	1.08(4)
C(23)-O(7)	1.445(4)
C(23)-H(23A)	1.11(3)
C(23)-H(23B)	1.03(3)
B(1)-F(2B)	1.183(11)
B(1)-F(4B)	1.251(9)
B(1)-F(2A)	1.327(5)
B(1)-F(4A)	1.347(5)
B(1)-F(1A)	1.389(4)
B(1)-F(3A)	1.399(4)
B(1)-F(1B)	1.456(7)
B(1)-F(3B)	1.522(13)
N(3)-O(5)	1.224(3)
N(3)-O(6)	1.228(3)
N(4)-O(2)	1.220(3)
N(4)-O(1)	1.233(3)

bond angles (°)

Atom A-B-C	Angle (°)
C(2)-C(1)-N(2)	109.7(2)
C(2)-C(1)-N(3)	125.5(2)
N(2)-C(1)-N(3)	124.8(2)
C(1)-C(2)-N(1)	106.4(2)
C(1)-C(2)-H(2)	128.2(18)
N(1)-C(2)-H(2)	125.4(18)
N(1)-C(3)-H(3A1)	105.3(19)
N(1)-C(3)-H(3A2)	111.7(18)
H(3A1)-C(3)-H(3A2)	113(3)
N(1)-C(3)-H(3A3)	109.7(19)
H(3A1)-C(3)-H(3A3)	114(3)
H(3A2)-C(3)-H(3A3)	103(3)
N(1)-C(4)-N(2)	108.4(2)
N(1)-C(4)-C(5)	126.4(2)
N(2)-C(4)-C(5)	125.2(2)
C(6)-C(5)-C(4)	123.7(3)
C(6)-C(5)-H(5)	124.1(19)
C(4)-C(5)-H(5)	112.1(19)
C(5)-C(6)-C(7)	124.0(3)
C(5)-C(6)-H(6)	121.3(17)
C(7)-C(6)-H(6)	114.7(17)
C(12)-C(7)-C(8)	119.1(2)
C(12)-C(7)-C(6)	119.3(2)
C(8)-C(7)-C(6)	121.6(2)
C(9)-C(8)-C(7)	120.6(2)
C(9)-C(8)-H(8)	118.9(17)
C(7)-C(8)-H(8)	120.5(17)
C(10)-C(9)-C(8)	118.8(3)
C(10)-C(9)-H(9)	120(2)
C(8)-C(9)-H(9)	121(2)
C(11)-C(10)-C(9)	122.4(2)
C(11)-C(10)-N(4)	119.1(2)
C(9)-C(10)-N(4)	118.6(2)
C(10)-C(11)-C(12)	118.6(2)
C(10)-C(11)-H(11)	120.7

C(12)-C(11)-H(11)	120.7
C(11)-C(12)-C(7)	120.5(3)
C(11)-C(12)-H(12)	119.9(15)
C(7)-C(12)-H(12)	119.6(15)
N(2)-C(13)-C(14)	113.1(2)
N(2)-C(13)-H(13A)	108.6(16)
C(14)-C(13)-H(13A)	109.1(16)
N(2)-C(13)-H(13B)	108.4(14)
C(14)-C(13)-H(13B)	110.1(15)
H(13A)-C(13)-H(13B)	107(2)
O(4)-C(14)-C(13)	111.2(2)
O(4)-C(14)-H(14A)	110.1(17)
C(13)-C(14)-H(14A)	109.9(18)
O(4)-C(14)-H(14B)	106.0(18)
C(13)-C(14)-H(14B)	108.6(19)
H(14A)-C(14)-H(14B)	111(3)
O(3)-C(15)-O(4)	122.6(3)
O(3)-C(15)-C(16)	125.0(3)
O(4)-C(15)-C(16)	112.5(2)
C(21)-C(16)-C(17)	119.4(3)
C(21)-C(16)-C(15)	117.1(2)
C(17)-C(16)-C(15)	123.5(3)
C(18)-C(17)-C(16)	119.9(3)
C(18)-C(17)-H(17)	119.0(18)
C(16)-C(17)-H(17)	121.1(19)
C(17)-C(18)-C(19)	120.6(3)
C(17)-C(18)-H(18)	122.3(16)
C(19)-C(18)-H(18)	117.0(16)
O(7)-C(19)-C(18)	118.6(2)
O(7)-C(19)-C(20)	122.0(2)
C(18)-C(19)-C(20)	119.4(3)
O(8)-C(20)-C(21)	118.2(2)
O(8)-C(20)-C(19)	122.1(3)
C(21)-C(20)-C(19)	119.8(3)
C(16)-C(21)-C(20)	120.8(3)
C(16)-C(21)-H(21)	120.0(19)
C(20)-C(21)-H(21)	119.2(19)
O(8)-C(22)-C(23)	110.2(3)

O(8)-C(22)-H(22A)	111.2(19)
C(23)-C(22)-H(22A)	107(2)
O(8)-C(22)-H(22B)	110.3(18)
C(23)-C(22)-H(22B)	110.9(18)
H(22A)-C(22)-H(22B)	108(3)
O(7)-C(23)-C(22)	110.4(3)
O(7)-C(23)-H(23A)	105.4(16)
C(22)-C(23)-H(23A)	111.5(16)
O(7)-C(23)-H(23B)	107.5(17)
C(22)-C(23)-H(23B)	109.5(17)
H(23A)-C(23)-H(23B)	112(2)
F(2B)-B(1)-F(4B)	126.9(11)
F(2A)-B(1)-F(4A)	113.1(4)
F(2A)-B(1)-F(1A)	107.4(4)
F(4A)-B(1)-F(1A)	107.1(4)
F(2A)-B(1)-F(3A)	111.5(3)
F(4A)-B(1)-F(3A)	110.8(3)
F(1A)-B(1)-F(3A)	106.5(3)
F(2B)-B(1)-F(1B)	114.3(7)
F(4B)-B(1)-F(1B)	109.4(7)
F(2B)-B(1)-F(3B)	98.9(14)
F(4B)-B(1)-F(3B)	105.6(8)
F(1B)-B(1)-F(3B)	95.5(6)
C(4)-N(1)-C(2)	109.4(2)
C(4)-N(1)-C(3)	126.6(2)
C(2)-N(1)-C(3)	123.9(2)
C(4)-N(2)-C(1)	106.1(2)
C(4)-N(2)-C(13)	124.2(2)
C(1)-N(2)-C(13)	129.6(2)
O(5)-N(3)-O(6)	125.6(2)
O(5)-N(3)-C(1)	118.4(2)
O(6)-N(3)-C(1)	115.9(2)
O(2)-N(4)-O(1)	123.2(2)
O(2)-N(4)-C(10)	118.4(2)
O(1)-N(4)-C(10)	118.4(2)
C(15)-O(4)-C(14)	116.2(2)
C(19)-O(7)-C(23)	113.7(2)
C(20)-O(8)-C(22)	113.2(2)

Anisotropic displacement parameters ($Å^2 x\ 10^3$) for ***E*-24a**.

The anisotropic displacement factor exponent takes the form: $-2\pi^2[\ h^2a^{*2}U^{11} + ... + 2\ h\ k\ a^*\ b^*\ U^{12}]$.

	U^{11}	U^{22}	U^{33}	U^{23}	U^{13}	U^{12}
C(1)	31(1)	32(2)	47(2)	-7(1)	23(1)	-5(1)
C(2)	34(2)	41(2)	42(2)	-3(1)	22(1)	-6(1)
C(3)	38(2)	60(2)	39(2)	7(2)	18(1)	-1(2)
C(4)	26(1)	30(2)	39(1)	-2(1)	14(1)	-4(1)
C(5)	30(1)	36(2)	31(1)	-1(1)	14(1)	0(1)
C(6)	30(1)	30(2)	34(1)	2(1)	14(1)	1(1)
C(7)	25(1)	29(1)	30(1)	5(1)	11(1)	3(1)
C(8)	27(1)	38(2)	36(1)	-1(1)	13(1)	-3(1)
C(9)	36(2)	36(2)	33(1)	-3(1)	14(1)	2(1)
C(10)	31(1)	37(2)	34(1)	5(1)	17(1)	8(1)
C(11)	23(1)	39(2)	41(2)	1(1)	13(1)	0(1)
C(12)	29(1)	35(2)	37(1)	-2(1)	14(1)	1(1)
C(13)	26(1)	41(2)	41(2)	-4(1)	12(1)	-1(1)
C(14)	34(2)	42(2)	44(2)	1(1)	12(1)	2(1)
C(15)	43(2)	35(2)	39(2)	5(1)	11(1)	-3(1)
C(16)	44(2)	27(2)	36(1)	6(1)	14(1)	-2(1)
C(17)	43(2)	28(2)	35(1)	2(1)	16(1)	1(1)
C(18)	43(2)	33(2)	33(1)	-4(1)	12(1)	1(1)
C(19)	40(2)	34(2)	35(1)	2(1)	14(1)	-2(1)
C(20)	55(2)	36(2)	30(1)	2(1)	19(1)	-2(1)
C(21)	47(2)	40(2)	30(1)	-2(1)	11(1)	-8(1)
C(22)	54(2)	56(2)	43(2)	-1(2)	24(2)	-1(2)
C(23)	54(2)	59(2)	47(2)	-7(2)	26(2)	-10(2)
B(1)	44(2)	41(2)	44(2)	6(2)	11(2)	10(2)
N(1)	31(1)	38(1)	34(1)	1(1)	18(1)	-5(1)
N(2)	26(1)	31(1)	38(1)	-3(1)	15(1)	-4(1)
N(3)	33(1)	41(2)	55(2)	-12(1)	23(1)	-5(1)
N(4)	38(1)	48(2)	38(1)	5(1)	19(1)	7(1)
O(1)	38(1)	64(2)	51(1)	9(1)	26(1)	4(1)
O(2)	61(1)	57(2)	61(1)	-12(1)	38(1)	7(1)
O(3)	53(1)	69(2)	44(1)	-13(1)	17(1)	-20(1)
O(4)	37(1)	40(1)	41(1)	0(1)	15(1)	-4(1)
O(5)	36(1)	56(1)	60(1)	-3(1)	18(1)	8(1)

O(6)	47(1)	66(2)	67(1)	-10(1)	39(1)	-1(1)
O(7)	45(1)	59(1)	42(1)	-11(1)	21(1)	-13(1)
O(8)	56(1)	62(2)	36(1)	-8(1)	22(1)	-11(1)
F(1A)	94(2)	108(3)	36(1)	-6(2)	20(2)	-23(2)
F(2A)	63(2)	95(3)	81(3)	46(2)	17(2)	-6(2)
F(3A)	43(2)	60(2)	98(2)	15(2)	23(2)	1(1)
F(4A)	74(2)	67(2)	168(4)	-53(3)	48(3)	7(2)
F(1B)	71(5)	39(4)	53(4)	-3(3)	7(4)	-3(3)
F(2B)	127(10)	270(20)	157(13)	-142(14)	-3(10)	91(12)
F(3B)	109(9)	122(11)	60(6)	19(6)	5(7)	-54(9)
F(4B)	43(4)	92(9)	78(6)	47(7)	6(5)	9(5)

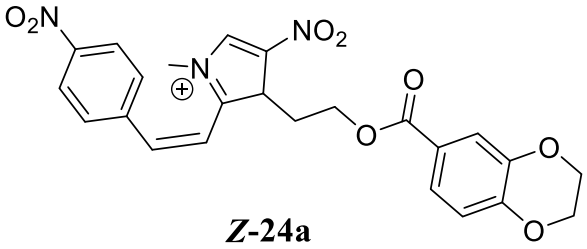

***Z*-24a**

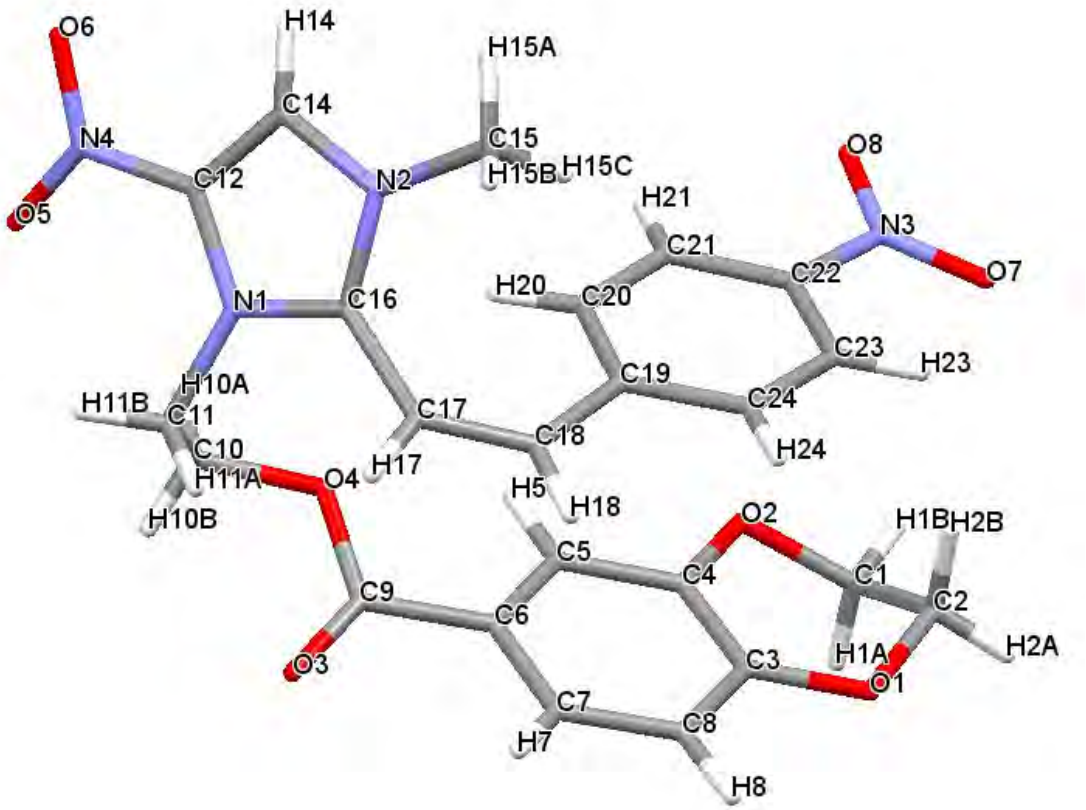

Empirical formula	C27 H31 B F4 N4 O9	
Formula weight	642.37	
Temperature	100(2) K	
Wavelength	0.71076 Å	
Crystal system	Monoclinic	
Space group	P 21/c	
Unit cell dimensions	a = 7.6248(4) Å	a= 90°.
	b = 30.4786(18) Å	b= 92.513(2)°.
	c = 12.6653(8) Å	g = 90°.
Volume	2940.5(3) $Å^3$	
Z	4	
Density (calculated)	1.451 Mg/m^3	
Absorption coefficient	0.124 mm^{-1}	
F(000)	1336	
Crystal size	? x ? x ? mm^3	

Theta range for data collection	2.756 to 25.681°.
Index ranges	-9<=h<=9, -37<=k<=37, -15<=l<=15
Reflections collected	54614
Independent reflections	5588 [R(int) = 0.0333]
Completeness to theta = 25.243°	99.8 %
Refinement method	Full-matrix least-squares on F^2
Data / restraints / parameters	5588 / 0 / 478
Goodness-of-fit on F^2	1.056
Final R indices [I>2sigma(I)]	R1 = 0.0620, wR2 = 0.1741
R indices (all data)	R1 = 0.0697, wR2 = 0.1827
Extinction coefficient	n/a
Largest diff. peak and hole	0.794 and -0.843 e.$Å^{-3}$

Data collection: Kappa CCD

Refinement: HKL Scalepack (Otwinowski and Minor, 1997)

Program used for resolving the structure: SHELXS-97 (Sheldrick, 1997)

Program used for the refinement of the structure: SHELXS-97 (Sheldrick, 1997)

Atomic coordinates (x 10^4) and equivalent isotropic displacement parameters ($Å^2$x 10^3) for **Z-24a**.

U(eq) is defined as one third of the trace of the orthogonalized U^{ij} tensor.

	x	y	z	U(eq)
C(1)	603(3)	2249(1)	4439(2)	23(1)
C(2)	1786(4)	2085(1)	3610(2)	26(1)
C(3)	4098(3)	2246(1)	4860(2)	18(1)
C(4)	3057(3)	2579(1)	5273(2)	16(1)
C(5)	3775(3)	2863(1)	6032(2)	15(1)
C(6)	5506(3)	2804(1)	6411(2)	15(1)
C(7)	6519(3)	2462(1)	6025(2)	17(1)
C(8)	5815(3)	2188(1)	5250(2)	20(1)
C(9)	6328(3)	3102(1)	7218(2)	16(1)
C(10)	6211(3)	3804(1)	8008(2)	17(1)
C(11)	7910(3)	4010(1)	7671(2)	18(1)
C(12)	7254(3)	4716(1)	6601(2)	18(1)
N(4)	6851(3)	5002(1)	7454(2)	28(1)
C(14)	7205(3)	4827(1)	5569(2)	19(1)
C(15)	7781(4)	4433(1)	3879(2)	26(1)
C(16)	7857(3)	4121(1)	5718(2)	16(1)
C(17)	8489(3)	3682(1)	5462(2)	18(1)

C(18)	7731(3)	3398(1)	4788(2)	18(1)
C(19)	6011(3)	3418(1)	4217(2)	17(1)
C(20)	4620(3)	3681(1)	4544(2)	18(1)
C(21)	3005(3)	3670(1)	4008(2)	18(1)
C(22)	2781(3)	3392(1)	3151(2)	19(1)
C(23)	4112(3)	3128(1)	2799(2)	22(1)
C(24)	5731(3)	3144(1)	3340(2)	21(1)
N(3)	1034(3)	3356(1)	2621(2)	23(1)
C(26)	11957(8)	4096(2)	9795(4)	89(2)
C(27)	10549(10)	4341(2)	10239(6)	109(2)
C(28)	7694(10)	4325(2)	10880(4)	92(2)
C(29)	6372(8)	4002(2)	11143(4)	91(2)
B(1)	2041(4)	4363(1)	6643(3)	24(1)
F(1)	1153(2)	4633(1)	7327(1)	35(1)
F(2)	1262(2)	4416(1)	5619(1)	33(1)
F(3)	1894(2)	3928(1)	6941(1)	29(1)
F(4)	3782(2)	4489(1)	6600(2)	40(1)
N(1)	7656(2)	4276(1)	6701(2)	16(1)
N(2)	7572(3)	4452(1)	5031(2)	17(1)
O(1)	3488(2)	1968(1)	4083(1)	25(1)
O(2)	1339(2)	2640(1)	4930(1)	21(1)
O(3)	7597(2)	3009(1)	7780(1)	22(1)
O(4)	5527(2)	3495(1)	7227(1)	15(1)
O(5)	6748(3)	4850(1)	8340(2)	39(1)
O(6)	6633(4)	5389(1)	7219(2)	46(1)
O(7)	749(3)	3045(1)	2021(2)	37(1)
O(8)	-72(3)	3632(1)	2820(2)	35(1)
O(9)	9097(6)	4091(1)	10298(3)	90(1)

Bond lengths [Å] and angles [°].

Bond lengths [Å]

Atom A-B	Distance (Å)
C(1)-O(2)	1.445(3)
C(1)-C(2)	1.501(4)
C(1)-H(1B)	0.92(3)
C(1)-H(1A)	0.95(3)
C(2)-O(1)	1.450(3)
C(2)-H(2A)	0.94(4)
C(2)-H(2B)	1.00(4)
C(3)-O(1)	1.366(3)
C(3)-C(8)	1.390(3)
C(3)-C(4)	1.404(3)
C(4)-O(2)	1.374(3)
C(4)-C(5)	1.387(3)
C(5)-C(6)	1.397(3)
C(5)-H(5)	0.96(3)
C(6)-C(7)	1.398(3)
C(6)-C(9)	1.484(3)
C(7)-C(8)	1.380(4)
C(7)-H(7)	0.87(3)
C(8)-H(8)	1.04(3)
C(9)-O(3)	1.209(3)
C(9)-O(4)	1.346(3)
C(10)-O(4)	1.446(3)
C(10)-C(11)	1.516(3)
C(10)-H(10A)	0.91(3)
C(10)-H(10B)	0.92(3)
C(11)-N(1)	1.479(3)
C(11)-H(11A)	0.95(3)
C(11)-H(11B)	0.95(3)
C(12)-C(14)	1.350(4)
C(12)-N(1)	1.381(3)
C(12)-N(4)	1.432(3)
N(4)-O(5)	1.221(3)
N(4)-O(6)	1.226(3)
C(14)-N(2)	1.365(3)

C(14)-H(14)	0.91(3)
C(15)-N(2)	1.476(3)
C(15)-H(15A)	0.9800
C(15)-H(15B)	0.9800
C(15)-H(15C)	0.9800
C(16)-N(2)	1.345(3)
C(16)-N(1)	1.346(3)
C(16)-C(17)	1.463(3)
C(17)-C(18)	1.330(4)
C(17)-H(17)	0.92(3)
C(18)-C(19)	1.471(3)
C(18)-H(18)	0.95(3)
C(19)-C(24)	1.399(3)
C(19)-C(20)	1.405(3)
C(20)-C(21)	1.380(4)
C(20)-H(20)	0.94(3)
C(21)-C(22)	1.383(3)
C(21)-H(21)	0.91(3)
C(22)-C(23)	1.383(4)
C(22)-N(3)	1.469(3)
C(23)-C(24)	1.386(4)
C(23)-H(23)	0.95(3)
C(24)-H(24)	0.94(3)
N(3)-O(8)	1.225(3)
N(3)-O(7)	1.227(3)
C(26)-C(27)	1.442(9)
C(26)-H(26A)	0.9800
C(26)-H(26B)	0.9800
C(26)-H(26C)	0.9800
C(27)-O(9)	1.348(8)
C(27)-H(27A)	0.9900
C(27)-H(27B)	0.9900
C(28)-C(29)	1.459(9)
C(28)-O(9)	1.506(7)
C(28)-H(28A)	0.9900
C(28)-H(28B)	0.9900
C(29)-H(29A)	0.9800
C(29)-H(29B)	0.9800

C(29)-H(29C)	0.9800
B(1)-F(4)	1.385(3)
B(1)-F(3)	1.385(3)
B(1)-F(1)	1.392(4)
B(1)-F(2)	1.412(4)

bond angles (°)

Atom A-B-C	Angle (°)
O(2)-C(1)-C(2)	110.0(2)
O(2)-C(1)-H(1B)	105.9(19)
C(2)-C(1)-H(1B)	107.7(19)
O(2)-C(1)-H(1A)	111.3(19)
C(2)-C(1)-H(1A)	105.9(19)
H(1B)-C(1)-H(1A)	116(3)
O(1)-C(2)-C(1)	110.3(2)
O(1)-C(2)-H(2A)	104(2)
C(1)-C(2)-H(2A)	111(2)
O(1)-C(2)-H(2B)	106(2)
C(1)-C(2)-H(2B)	110(2)
H(2A)-C(2)-H(2B)	115(3)
O(1)-C(3)-C(8)	117.5(2)
O(1)-C(3)-C(4)	122.5(2)
C(8)-C(3)-C(4)	119.9(2)
O(2)-C(4)-C(5)	118.5(2)
O(2)-C(4)-C(3)	121.7(2)
C(5)-C(4)-C(3)	119.7(2)
C(4)-C(5)-C(6)	119.8(2)
C(4)-C(5)-H(5)	122.3(19)
C(6)-C(5)-H(5)	117.7(19)
C(5)-C(6)-C(7)	120.2(2)
C(5)-C(6)-C(9)	121.5(2)
C(7)-C(6)-C(9)	118.3(2)
C(8)-C(7)-C(6)	119.8(2)
C(8)-C(7)-H(7)	119.6(18)
C(6)-C(7)-H(7)	120.6(18)
C(7)-C(8)-C(3)	120.4(2)
C(7)-C(8)-H(8)	122.0(17)

C(3)-C(8)-H(8)	117.6(17)
O(3)-C(9)-O(4)	123.7(2)
O(3)-C(9)-C(6)	124.4(2)
O(4)-C(9)-C(6)	111.90(19)
O(4)-C(10)-C(11)	111.31(19)
O(4)-C(10)-H(10A)	103.7(19)
C(11)-C(10)-H(10A)	110.8(19)
O(4)-C(10)-H(10B)	107.5(18)
C(11)-C(10)-H(10B)	109.4(18)
H(10A)-C(10)-H(10B)	114(3)
N(1)-C(11)-C(10)	112.21(19)
N(1)-C(11)-H(11A)	106.4(17)
C(10)-C(11)-H(11A)	110.6(18)
N(1)-C(11)-H(11B)	108.1(18)
C(10)-C(11)-H(11B)	110.9(18)
H(11A)-C(11)-H(11B)	109(3)
C(14)-C(12)-N(1)	109.2(2)
C(14)-C(12)-N(4)	125.5(2)
N(1)-C(12)-N(4)	125.2(2)
O(5)-N(4)-O(6)	125.2(2)
O(5)-N(4)-C(12)	119.1(2)
O(6)-N(4)-C(12)	115.7(2)
C(12)-C(14)-N(2)	106.0(2)
C(12)-C(14)-H(14)	131.7(17)
N(2)-C(14)-H(14)	122.3(17)
N(2)-C(15)-H(15A)	109.5
N(2)-C(15)-H(15B)	109.5
H(15A)-C(15)-H(15B)	109.5
N(2)-C(15)-H(15C)	109.5
H(15A)-C(15)-H(15C)	109.5
H(15B)-C(15)-H(15C)	109.5
N(2)-C(16)-N(1)	108.2(2)
N(2)-C(16)-C(17)	126.1(2)
N(1)-C(16)-C(17)	125.3(2)
C(18)-C(17)-C(16)	126.9(2)
C(18)-C(17)-H(17)	118.5(19)
C(16)-C(17)-H(17)	114.6(19)
C(17)-C(18)-C(19)	129.9(2)

C(17)-C(18)-H(18)	117(2)
C(19)-C(18)-H(18)	113.2(19)
C(24)-C(19)-C(20)	119.0(2)
C(24)-C(19)-C(18)	117.8(2)
C(20)-C(19)-C(18)	123.1(2)
C(21)-C(20)-C(19)	120.7(2)
C(21)-C(20)-H(20)	118.1(19)
C(19)-C(20)-H(20)	121.0(19)
C(20)-C(21)-C(22)	118.5(2)
C(20)-C(21)-H(21)	122(2)
C(22)-C(21)-H(21)	120(2)
C(21)-C(22)-C(23)	122.9(2)
C(21)-C(22)-N(3)	118.9(2)
C(23)-C(22)-N(3)	118.2(2)
C(22)-C(23)-C(24)	118.1(2)
C(22)-C(23)-H(23)	121(2)
C(24)-C(23)-H(23)	121(2)
C(23)-C(24)-C(19)	120.9(2)
C(23)-C(24)-H(24)	118.3(19)
C(19)-C(24)-H(24)	120.7(19)
O(8)-N(3)-O(7)	123.4(2)
O(8)-N(3)-C(22)	118.3(2)
O(7)-N(3)-C(22)	118.3(2)
C(27)-C(26)-H(26A)	109.5
C(27)-C(26)-H(26B)	109.5
H(26A)-C(26)-H(26B)	109.5
C(27)-C(26)-H(26C)	109.5
H(26A)-C(26)-H(26C)	109.5
H(26B)-C(26)-H(26C)	109.5
O(9)-C(27)-C(26)	110.9(6)
O(9)-C(27)-H(27A)	109.5
C(26)-C(27)-H(27A)	109.5
O(9)-C(27)-H(27B)	109.5
C(26)-C(27)-H(27B)	109.5
H(27A)-C(27)-H(27B)	108.1
C(29)-C(28)-O(9)	107.7(5)
C(29)-C(28)-H(28A)	110.2
O(9)-C(28)-H(28A)	110.2

C(29)-C(28)-H(28B)	110.2
O(9)-C(28)-H(28B)	110.2
H(28A)-C(28)-H(28B)	108.5
C(28)-C(29)-H(29A)	109.5
C(28)-C(29)-H(29B)	109.5
H(29A)-C(29)-H(29B)	109.5
C(28)-C(29)-H(29C)	109.5
H(29A)-C(29)-H(29C)	109.5
H(29B)-C(29)-H(29C)	109.5
F(4)-B(1)-F(3)	111.4(2)
F(4)-B(1)-F(1)	110.7(2)
F(3)-B(1)-F(1)	110.4(2)
F(4)-B(1)-F(2)	107.3(2)
F(3)-B(1)-F(2)	108.9(2)
F(1)-B(1)-F(2)	107.9(2)
C(16)-N(1)-C(12)	106.9(2)
C(16)-N(1)-C(11)	124.0(2)
C(12)-N(1)-C(11)	129.1(2)
C(16)-N(2)-C(14)	109.7(2)
C(16)-N(2)-C(15)	126.1(2)
C(14)-N(2)-C(15)	124.0(2)
C(3)-O(1)-C(2)	114.5(2)
C(4)-O(2)-C(1)	111.86(19)
C(9)-O(4)-C(10)	115.86(18)
C(27)-O(9)-C(28)	111.2(5)

Anisotropic displacement parameters ($Å^2 x\ 10^3$) for ***Z*-24a**.

The anisotropic displacement factor exponent takes the form: $-2\pi^2[\ h^2a^{*2}U^{11} + ... + 2\ h\ k\ a^*\ b^*\ U^{12}]$.

	U^{11}	U^{22}	U^{33}	U^{23}	U^{13}	U^{12}
C(1)	17(1)	28(1)	23(1)	-5(1)	-6(1)	-6(1)
C(2)	23(1)	32(2)	22(1)	-6(1)	-4(1)	-6(1)
C(3)	19(1)	19(1)	17(1)	-1(1)	2(1)	-5(1)
C(4)	12(1)	20(1)	15(1)	2(1)	-1(1)	-3(1)
C(5)	14(1)	16(1)	15(1)	2(1)	1(1)	-1(1)
C(6)	15(1)	16(1)	14(1)	4(1)	-1(1)	-4(1)
C(7)	12(1)	21(1)	19(1)	4(1)	1(1)	-1(1)
C(8)	18(1)	19(1)	22(1)	0(1)	5(1)	0(1)

C(9)	15(1)	19(1)	14(1)	4(1)	1(1)	-3(1)
C(10)	18(1)	19(1)	14(1)	-1(1)	-2(1)	-4(1)
C(11)	17(1)	21(1)	16(1)	2(1)	-4(1)	-4(1)
C(12)	14(1)	17(1)	23(1)	-2(1)	0(1)	-3(1)
N(4)	34(1)	22(1)	28(1)	-5(1)	2(1)	-4(1)
C(14)	14(1)	19(1)	24(1)	3(1)	1(1)	-1(1)
C(15)	38(2)	26(1)	16(1)	5(1)	4(1)	4(1)
C(16)	9(1)	20(1)	19(1)	1(1)	-1(1)	-3(1)
C(17)	14(1)	21(1)	18(1)	5(1)	1(1)	2(1)
C(18)	18(1)	17(1)	18(1)	4(1)	4(1)	2(1)
C(19)	18(1)	17(1)	15(1)	4(1)	3(1)	-1(1)
C(20)	19(1)	18(1)	16(1)	-1(1)	2(1)	-1(1)
C(21)	17(1)	19(1)	19(1)	0(1)	4(1)	2(1)
C(22)	17(1)	22(1)	16(1)	1(1)	0(1)	-1(1)
C(23)	23(1)	26(1)	18(1)	-5(1)	1(1)	0(1)
C(24)	19(1)	22(1)	21(1)	-3(1)	3(1)	3(1)
N(3)	19(1)	34(1)	17(1)	-2(1)	0(1)	0(1)
C(26)	83(4)	116(5)	67(3)	-12(3)	-3(3)	4(3)
C(27)	128(6)	97(5)	99(5)	-6(4)	-31(4)	-31(4)
C(28)	155(6)	86(4)	38(2)	-3(2)	16(3)	-1(4)
C(29)	97(4)	113(5)	61(3)	-12(3)	-3(3)	17(4)
B(1)	16(1)	24(1)	32(2)	2(1)	3(1)	-2(1)
F(1)	31(1)	33(1)	41(1)	-7(1)	7(1)	-4(1)
F(2)	28(1)	37(1)	33(1)	7(1)	-1(1)	-8(1)
F(3)	20(1)	25(1)	42(1)	8(1)	0(1)	-1(1)
F(4)	14(1)	43(1)	64(1)	13(1)	-1(1)	-7(1)
N(1)	10(1)	19(1)	18(1)	1(1)	-2(1)	-4(1)
N(2)	16(1)	19(1)	16(1)	3(1)	1(1)	0(1)
O(1)	22(1)	29(1)	25(1)	-11(1)	-1(1)	-2(1)
O(2)	14(1)	25(1)	23(1)	-5(1)	-5(1)	-1(1)
O(3)	19(1)	25(1)	21(1)	2(1)	-9(1)	1(1)
O(4)	13(1)	16(1)	16(1)	-1(1)	-2(1)	-2(1)
O(5)	66(2)	31(1)	22(1)	-5(1)	7(1)	-5(1)
O(6)	78(2)	21(1)	40(1)	-4(1)	10(1)	7(1)
O(7)	29(1)	43(1)	37(1)	-15(1)	-10(1)	1(1)
O(8)	22(1)	53(1)	32(1)	-11(1)	-3(1)	12(1)
O(9)	116(3)	97(3)	56(2)	1(2)	-10(2)	-19(2)

APPENDIX C: Computational study data

Cartesian coordinates of ***E-7***

6	-1.898704	-1.016877	-0.000089
7	-3.276095	-0.962694	0.000034
6	-1.447058	0.406225	-0.000060
7	-2.638884	1.157031	-0.000041
6	-3.751323	0.349459	-0.000041
8	-4.914071	0.691868	0.000054
8	-1.261820	-2.052527	-0.000013
6	-0.225872	0.975938	-0.000037
6	1.138500	0.457566	-0.000033
6	2.168835	1.405778	0.000026
6	3.509327	1.046073	0.000037
6	3.850220	-0.305339	-0.000013
6	2.837615	-1.269414	-0.000076
6	1.508126	-0.900476	-0.000086
8	5.120308	-0.778716	-0.000013
6	6.180891	0.152598	0.000103
6	-2.736938	2.593921	-0.000001
6	-4.131418	-2.127568	0.000121
1	-0.251574	2.063629	-0.000016
1	1.915866	2.462782	0.000066
1	4.268820	1.817961	0.000082
1	3.125068	-2.315285	-0.000116
1	0.738374	-1.660707	-0.000136
1	7.099103	-0.435081	0.000127
1	6.158188	0.787709	-0.893511
1	6.158077	0.787613	0.893782
1	-2.264080	3.019669	-0.891456
1	-3.797294	2.845541	-0.000005
1	-2.264094	3.019627	0.891480
1	-3.943843	-2.735760	0.887947

1	-5.162341	-1.774570	0.000185
1	-3.943965	-2.735795	-0.887707

Cartesian coordinates of ***Z*-7**

6	-2.767818	-1.173568	0.120261
7	-3.717290	-0.173262	0.056581
6	-1.453584	-0.470814	0.013046
7	-1.755953	0.888830	-0.124063
6	-3.131098	1.074845	-0.139308
8	-3.724764	2.115905	-0.308048
8	-2.978819	-2.359431	0.250743
6	-0.300981	-1.151666	0.054157
6	1.083663	-0.666156	0.104112
6	1.482794	0.375296	0.954907
6	2.800391	0.788454	1.012956
6	3.768396	0.164950	0.221890
6	3.399176	-0.890591	-0.610964
6	2.071345	-1.299007	-0.652096
8	5.031404	0.644762	0.344055
6	6.052229	0.040291	-0.421126
6	-0.880426	1.935927	-0.611392
6	-5.146901	-0.376758	0.119955
1	-0.444722	-2.229937	0.069298
1	0.750436	0.840511	1.606621
1	3.112391	1.587414	1.676632
1	4.131517	-1.402077	-1.223176
1	1.794884	-2.126384	-1.299333
1	6.970130	0.574568	-0.175430
1	6.171697	-1.019519	-0.166354
1	5.856965	0.132536	-1.496197
1	-0.294289	1.575465	-1.460940

1	-1.517053	2.763484	-0.924585
1	-0.194910	2.285682	0.162415
1	-5.313920	-1.446320	0.247658
1	-5.573212	0.170031	0.963835
1	-5.622887	-0.031542	-0.800464

Cartesian coordinates of **12**

6	8.009121	0.608931	3.716973
6	6.880906	-0.071352	3.212582
6	6.097642	-0.810926	4.124604
6	6.437839	-0.892728	5.472858
6	7.567404	-0.222289	5.951824
6	8.344863	0.532069	5.068429
6	6.453709	-0.045471	1.810690
6	7.141439	0.317367	0.704436
6	6.613310	0.236295	-0.680817
7	7.510494	0.366197	-1.602547
6	8.825027	0.559376	-0.972511
6	8.587757	0.737844	0.547069
6	5.190948	0.002112	-1.041214
6	4.877411	-0.873918	-2.093663
6	3.551703	-1.084001	-2.471136
6	2.518713	-0.412211	-1.809737
6	2.820336	0.470489	-0.769952
6	4.146800	0.673954	-0.383695
1	1.483368	-0.575034	-2.105528
1	7.834726	-0.280095	7.005762
1	5.818478	-1.476762	6.152045
1	5.213127	-1.332171	3.758905
1	8.615217	1.224761	3.062483
1	9.217466	1.071256	5.434416

1	5.440223	-0.410898	1.654329
1	8.731426	1.786528	0.841982
1	9.268884	0.135380	1.157547
1	4.372520	1.376806	0.414827
1	2.022266	1.005974	-0.257997
1	3.323581	-1.772876	-3.283155
1	5.684368	-1.390511	-2.608569
1	9.447059	-0.320580	-1.189497
1	9.325668	1.419031	-1.433168

Cartesian coordinates of **12-Prot**

6	0.037225	-0.116267	-0.007043
6	0.011272	-0.008768	1.395803
6	1.213710	0.157080	2.107474
6	2.425635	0.201069	1.422624
6	2.446996	0.098783	0.028217
6	1.253979	-0.052910	-0.683840
6	-1.265310	-0.039394	2.119273
6	-2.379002	-0.952069	1.941728
6	-3.502897	-0.468115	2.844961
6	-2.839974	0.611869	3.729312
7	-1.534008	0.813693	3.082443
6	-2.287880	-2.070088	1.170677
6	-3.274671	-3.103444	0.903742
6	-4.647084	-3.005685	1.225726
6	-5.517611	-4.051372	0.932275
6	-5.044515	-5.215204	0.316425
6	-3.691526	-5.325708	-0.019181
6	-2.820039	-4.279285	0.264330
1	-0.904690	1.582199	3.355438
1	3.395892	0.139064	-0.504482

1	-5.731006	-6.030259	0.092250
1	-3.318679	-6.225381	-0.505635
1	-1.766538	-4.364601	-0.001019
1	-5.047756	-2.107841	1.680626
1	-6.573092	-3.956997	1.181666
1	-1.322037	-2.249627	0.702631
1	-4.323566	-0.035130	2.259417
1	-3.919118	-1.279544	3.449471
1	-0.891702	-0.208371	-0.565434
1	1.268916	-0.119256	-1.770215
1	3.354854	0.313170	1.978323
1	1.198921	0.221345	3.194744
1	-2.680212	0.279413	4.761389
1	-3.384109	1.560083	3.748417

Cartesian coordinates of ***E*-24a** (C2Bb)

7	-4.044443	-2.626949	0.228661
6	-3.836282	-3.966375	0.092171
6	-2.876207	-1.969792	0.041362
7	-1.916633	-2.883924	-0.200672
6	-2.514830	-4.129000	-0.167825
7	-1.843331	-5.378315	-0.334513
6	-0.518838	-2.535160	-0.511167
6	0.332125	-2.525735	0.759324
8	1.583726	-1.888886	0.494994
6	1.601813	-0.542240	0.534216
8	0.590633	0.112925	0.725024
6	2.945652	0.029082	0.327458
6	4.067878	-0.783856	0.153400
6	5.317794	-0.214143	-0.028312
6	5.455520	1.183201	-0.022070

6	4.330432	1.991210	0.132791
6	3.081521	1.420902	0.307106
6	-2.619966	-0.545819	0.113712
6	-3.493958	0.402879	-0.258912
6	-3.248672	1.847780	-0.198754
6	-2.022738	2.395724	0.210352
6	-1.848514	3.768211	0.253969
6	-2.908735	4.589453	-0.114607
6	-4.131917	4.083135	-0.528693
6	-4.291712	2.706120	-0.569375
7	-2.725802	6.041446	-0.067296
8	-3.668593	6.753529	-0.390746
8	-1.638832	6.475724	0.293890
8	-0.619684	-5.377461	-0.378832
8	-2.551635	-6.371550	-0.410347
6	-5.339552	-2.042214	0.592813
8	6.394109	-1.038836	-0.197119
6	7.543740	-0.387374	-0.744392
6	7.791097	0.912650	-0.017567
8	6.663815	1.783593	-0.174459
1	-4.617610	-4.700121	0.208780
1	-0.140894	-3.251290	-1.235507
1	-0.535633	-1.550921	-0.974688
1	-0.181120	-2.006553	1.570508
1	0.578199	-3.539637	1.069649
1	3.982063	-1.863620	0.152709
1	4.462121	3.067545	0.125567
1	2.205498	2.044871	0.436922
1	-1.630290	-0.280515	0.471362
1	-4.463265	0.123725	-0.658943
1	-1.191824	1.758032	0.489552
1	-0.908024	4.202165	0.566693

1	-4.934546	4.751174	-0.811298
1	-5.240643	2.291376	-0.891696
1	-5.175779	-1.202337	1.265011
1	-5.869875	-1.719768	-0.302617
1	-5.917963	-2.807456	1.105132
1	7.383627	-0.207377	-1.813275
1	8.380251	-1.073726	-0.614380
1	8.648049	1.441750	-0.433789
1	7.956898	0.732713	1.049824